

**MODULATION OF THE ENDOGENOUS CANNABINOID
SYSTEM TO ATTENUATE INFLAMMATION IN
CENTRAL NERVOUS SYSTEM INJURY**

**A Dissertation
Submitted to
the Temple University Graduate Board**

**in Partial Fulfillment
of the Requirement for the Degrees of
DOCTOR OF PHILOSOPHY
DOCTOR OF MEDICINE**

**By
Zachary Wilmer Reichenbach
May 2015**

Examining Committee Members:

Dr. Ronald F. Tuma, Advisory Chair, Department of Molecular and Cellular Physiology
Dr. Rosario Scalia, Examining Chair, Department of Molecular and Cellular Physiology
Dr. Victor Rizzo, Department of Molecular and Cellular Physiology
Dr. Laurie Kilpatrick, Department of Molecular and Cellular Physiology
Dr. Sara Jane Ward, External Reader, Department of Pharmacology

UMI Number: 3604684

All rights reserved

INFORMATION TO ALL USERS

The quality of this reproduction is dependent upon the quality of the copy submitted.

In the unlikely event that the author did not send a complete manuscript and there are missing pages, these will be noted. Also, if material had to be removed, a note will indicate the deletion.



UMI 3604684

Published by ProQuest LLC (2013). Copyright in the Dissertation held by the Author.

Microform Edition © ProQuest LLC.

All rights reserved. This work is protected against unauthorized copying under Title 17, United States Code



ProQuest LLC.
789 East Eisenhower Parkway
P.O. Box 1346
Ann Arbor, MI 48106 - 1346

ABSTRACT

Modulation of the Endogenous Cannabinoid System to Attenuate Inflammation in Central Nervous System Injury

Zachary Wilmer Reichenbach

Degree: Doctor of Medicine

Doctor of Philosophy

Temple University, 2013

Doctoral Advisory Committee Chair: Ronald F. Tuma, Ph.D.

In non-pathological states the central nervous system maintains a degree of immunological privilege. When illness or injury occur, this privilege can be lost and the immune system drives pathology in the brain and spinal cord. More so, resident immune cells, the microglial, act as major effectors of this response. Cerebral ischemia, or stroke, is the fourth leading cause of death in developed nations. After the initial ischemia, the inflammatory response propagates further injury and cell death. Another affliction of the central nervous system, chronic pain and persistent use of the opioid analgesic, morphine, leads to tolerance and ineffectiveness of the drug. Currently, only one in three patients receive adequate pain relief from their pharmacological regimen. This loss of efficacy in morphine is also driven by an inflammatory response. Thus, a way to quell inflammation in both disease states could lead to better treatments for both disorders.

The endogenous cannabinoid system has two known receptors, CB₁ and CB₂. Both of these receptors have been intimately linked to inflammation and the activation or antagonism of the receptors can impart desired outcomes in modulating the immune response. Primarily the CB₁ receptor expression is on presynaptic terminals of neurons to modulate neuronal firing. The CB₂

receptor's expression predominates on immunological cells including microglial. However, some degree of expression exists with reports of neuronal CB₂ receptors and immunological CB₁ receptors. This makes pharmacological therapies targeted at both receptors ideal candidates in treating not only stroke and but also preventing the induction of morphine tolerance.

In the studies described here, we sought to investigate the role of the endogenous cannabinoid system in both stroke and as a way to prevent the induction of morphine tolerance. The results showed that CB₁ -/- CB₂ -/- receptor mice were able to maintain greater blood flow during cerebral ischemia. More so, CB₁ antagonism in a permanent occlusion of cerebral vessels showed a protective effect independent of the serotonin receptor. Lastly, a CB₂ agonist was able to limit the degree of tolerance that developed from chronic morphine therapy and also prevent hyperalgesia in addition to showing a reduction in pro-inflammatory cytokines. Acutely, this same agonist was found to antagonize the morphine receptor but this could be avoided if morphine was administered before the CB₂ agonist. In brief, the studies at hand show that the endogenous cannabinoid system can attenuate inflammation in central nervous system injury and shows great promise as a future therapeutic for clinical use.

ACKNOWLEDGEMENTS

So many people have been overwhelmingly supportive and understanding of this work that surely my gratitude cannot be adequately expressed in just words here. Without the guidance, help, and support of those around me, completing this research would not have been possible. My hope is that one day, this work will translate to clinical application that serves a patient in need.

First and foremost, I want to thank my advisor, Dr. Ronald F. Tuma. Dr. Tuma's expertise and knowledge exist as a benchmark for which I only hope to one day be able to begin to measure up to. His guidance and input have been tremendously valuable and this research would not have been possible without him. Further his manner of mentoring and supervision are also paramount. He provides guidance and leadership but in a way that the student is free to try new techniques and experiments while ultimately managing his own research. His leadership has greatly impacted my scientific thinking and developed my skills as a physician scientist. Almost as important, Dr. Tuma has not only helped develop me as a scientist but also as a person. He truly is a friend. Ron was there for multiple hardships in my personal life and I cannot imagine going through them without his guidance or while working for someone else.

I am also immensely grateful to Dr. Doina Ganea. She truly stands as an expert of immunology and also molecular biology. I want to thank her for her ongoing guidance as well as entertaining my numerous surprise visits at her door with questions or data to examine. In addition, I want to express my gratitude to Dr. Sara Jane Ward. Without her immense knowledge of behavioral studies and morphine tolerance, a lot of this work would not have been possible. Both of these scientists have been instrumental in my completion of this project and my development as a scientist.

I owe a multitude of appreciation to the members of my committee. Dr. Rosario Scalia, Dr. Victor Rizzo, and Dr. Laurie Kilpatrick. I wanted to thank them for their support and input throughout the years as well as apologize for any emails I may have sent them at 4am to schedule meetings. I would like to thank the Department of Cellular and Molecular Physiology for being supportive of my work and helping to impact my graduate education. Lastly, I want to say thank you to the Center for Substance Abuse Research under the direction of Dr. Ellen Unterwald. Dr. Unterwald's center truly carved out a home for us and our work in the Tuma lab. Also, a tremendously big thank you to Melva Smith and Lynn Heth who have been my savior on far too many occasions. Also, thank you to Dr. John Gaughan for his assistance with the biostatics of the Rhodamine studies.

My time in the laboratory has allowed me to meet and work with so many talented individuals that were always willing to help and teach. In Dr. Ganea's laboratory I want to thank Virginia Koceida, Sabina Adhikary, Fran Emig, Dr. Mario Skarica, Dr. Weimin Kong, and Dr. Jimmy Yen. Thank you guys for being so open to answering questions and teaching me. In my own laboratory I want to thank Dr. Ming Zhang, Dr. Hongbo Li, and Richard Ronca. Again, your guidance and help have been not only tremendously helpful but also inspiring. Hongbo in particular, this could not have been completed without you and I will be forever grateful for your assistance on so many occasions.

None of this would have been possible without an outside support system. I think it is appropriate to thank all the people that have put up with my tardiness, cancelled plans, complaints, and for just being there throughout the years. A huge thanks to Matthew Santiago, not only for being a great friend but for being an amazing Chief of Operations and keeping Temple University Emergency Medical Services running in my absence. Thank you for covering my shifts all the

nights I was late. Thank you to Rebecca Vallas for talking me through so many problems and providing some perspective. To this day, we may be the only people to have discussed cannabinoid receptor knockout mice at the Dunkin Donuts at Broad and Alleghany. And lastly, thank you to Nathan Carr-Whealy. I don't know where to begin other than to say you have been the voice of reason and thank you for so many late night dinner runs to rejuvenate. You always do that.

And most importantly, I want to thank my family. For without them and their love and support, I would have never completed this project. Thank you to my aunt Darlene for always making me laugh. Thank you to my brother, Kenneth for always listening to my problems and talking me through them. Your expertise in clinical stroke treatment has also been hugely helpful and inspiring to me. I want to thank you and your wife, Erin, for bringing the kids, Tyler and Makenna, to visit me on so many weekends in lab. Some of my favorite memories of lab will be your kids feeding my mice Fruit Loops and examining the big pickles hanging in the lobby of the medical school. Lastly, but certainly not least, thank you Mom and Dad. I do not know what I would have done without you guys. Thank you both for always being so understanding and supportive. Thank you for all my late night phone calls and for always making me feel better when lab didn't treat me the way I hoped it would. The dedication I watched you two put forth on so many projects growing up really inspired me to see this project through. And so many times throughout my life you looked at me and said, "Can do." I kept that in mind. Thank you.

DEDICATION

For quite some time I have been contemplating to whom this work should be dedicated. While many people have been so supportive, I kept coming back to the same answer. For that reason, I am dedicating my dissertation to my grandmother, Goldie Mae Oswald. Every weekend I would come home to visit and Gram would ask me, “How are your mice?” I think she was my biggest fan and would have loved to see me finish my research. It’s been three years since she passed away and I still miss her every day.



This photo was taken right around the time of Gram’s 90th birthday. Also, it was around the time that she suffered a stroke that left her unable to walk independently ever again. She passed away a few months later. Gram also had terrible osteoporosis and suffered numerous compression fractures of her spine. Due to the side effects and other health problems, she couldn’t take opioids for the chronic pain she had.

I really hope that one day these studies and this work will help someone like my grandmother. Miss you Gram.

“Someone told me that these hands could save a life or two. It still kills me to know that I could not save you.”—Last Breath by Ballyhoo

TABLE OF CONTENTS

	Page
ABSTRACT	ii
ACKNOWLEDGMENTS	iv
DEDICATION	vii
LIST OF TABLES	xiv
LIST OF FIGURES	xv
CHAPTER 1. THE ENDOGENOUS CANNABNOID SYSTEM AS A MEDIATOR OF INFLAMATTION IN CENTRAL NERVOUS SYSTEM INJURY	1
1.1 The Endogenous Cannabinoid System	1
1.2 The Endogenous Cannabinoid System and Its Effect on Inflammation	12
1.3 Cerebral Ischemia—An Inflammatory Pathology	18
1.4 The Endogenous Cannabinoid System in Cerebral Ischemia	26
1.5 Models of Cerebral Ischemia	31
1.6 Chronic Morphine Administration and Inflammation	32
1.7 Tristimulus Color Theory and Rhodamine 6G Applications	38
1.8 Works Cited	56
2. DEVELOPMENT OF 2 MODELS: NOVEL APPLICATION OF RHODAMINE 6G AND PHOTOTHROMBOTIC STROKE	85

2.1 Aims	85
2.2 Materials and Methods.....	85
2.2.1 Preparation of Rhodamine 6G	85
2.2.2 Administration of Rhodamine 6G for Injection Technique Studies	86
2.2.3 Preparation and Analysis of Blood Smears	86
2.2.4 Implant of Cranial Windows.....	87
2.2.5 Stimulation of Inflammation.....	88
2.2.6 Intravital Microscopy and Conversion to Still Images	88
2.2.7 Measurement of Leukocyte/Endothelial Interactions	89
2.2.8 Flow Cytometry	90
2.2.9 Statistical Analysis--Rhodamine.....	90
2.2.10 Photothrombotic Cerebral Ischemia	90
2.2.11 Visualization of Cranial Windows Following Photothrombotic Ischemia	91
2.2.12 Analysis of Flow in Cranial Windows Following Photothrombotic Ischemia and Statistical Analysis.....	91
2.3 Results.....	91
2.3.1 Effect of Injection Method on Leukocyte Luma in Peripheral Blood	91
2.3.2 Effect of Injection Method on Leukocyte HSL Lightness in Peripheral Blood	92

2.3.3 Effect of Injection Method on Leukocyte HSV Value in Peripheral Blood	93
2.3.4 Effect of Injection Method on Leukocyte HSI Intensity in Peripheral Blood	93
2.3.5 Effect of Injection Method on Leukocyte HSL and HSV Hue in Peripheral Blood	94
2.3.6 Effect of Injection Method on Leukocyte HSL Saturation in Peripheral Blood	94
2.3.7 Effect of Injection Method on Leukocyte HSV Saturation in Peripheral Blood	95
2.3.8 Effect of Injection Method on Leukocyte HSI Saturation in Peripheral Blood	96
2.3.9 Effect of Injection Method on Leukocyte Luma in Cranial Windows	97
2.3.10 Effect of Injection Method on Quantization of Rolling Leukocytes	97
2.3.11 Effect of Injection Method on Quantization of Adherent Leukocytes	98
2.3.12 Effect of Injection Method on Leukocyte Properties Examined by Flow Cytometry	99
2.3.13 Effect of Photothrombotic Ischemia on Pial Blood Flow	102
2.4 Discussion	102
2.5 Conclusions	129
2.6 Works Cited	132
2.7 Figures	135

3. MODULATION OF THE ENDOGENOUS CANNABINOID SYSTEM IN TWO STROKE MODELS	158
3.1 Specific Aims, Rational, and Hypothesis	159
3.2 Materials and Methods.....	159
3.2.1 Animals.....	159
3.2.2 Middle Cerebral Artery Occlusion and Reperfusion and Cerebral Blood Flow Monitoring	159
3.2.3 Infarct Volume Assessment	160
3.2.4 Neurological Evaluation	161
3.2.5 Photothrombotic Cerebral Ischemia	161
3.2.6 Preparation and Administration of SR14176A and WAY-100365	162
3.2.7 Statistical Analysis.....	162
3.3 Results.....	162
3.3.1 Transient Cerebral Ischemia in CB ₁ -/- and CB ₂ -/- Receptor Mice and the Effect on Infarct Size	162
3.3.2 Transient Cerebral Ischemia in CB ₁ -/- and CB ₂ -/- Receptor Mice and the Effect on Edema	163
3.3.3 Transient Cerebral Ischemia in CB ₁ -/- and CB ₂ -/- Receptor Mice and the Effect on Clinical Parameters	163
3.3.4 Transient Cerebral Ischemia in CB ₁ -/- and CB ₂ -/- Receptor Mice and the Effect on Regional Cerebral Blood Flow	163

3.3.5 Effect of SR141716A and WAY-100365 on Infarct Size in a Permanent Occlusion Model	164
3.3.6 Effect of SR141716A and WAY-100365 on Edema in a Permanent Occlusion Model	164
3.3.7 Effect of SR141716A and WAY-100365 on Clinical Parameters in a Permanent Occlusion Model	165
3.4 Discussion	165
3.5 Conclusions.....	174
3.6 Works Cited	176
3.7 Figures.....	181
4. UTILIZATION OF THE ENDOGENOUS CANNABINOID SYSTEM TO ATEENUATE INFLAMMATION ASSOCIATED WITH MORPHINE ADMINISTRATION	190
4.1 Specific Aims, Rational, and Hypothesis	190
4.2 Materials and Methods.....	191
4.2.1 Animals.....	191
4.2.2 Experimental Groups and Interactions.....	191
4.2.3 Measurement of Hot Plate Withdrawal Latency.....	191
4.2.4 Preparation and Dosing of O-1966, SR144528, and Morphine Sulfate	192
4.2.5 Quantitative Real Time Polymerase Chain Reaction (qRT-PCR).....	193
4.2.6 Statistical Analysis.....	194

4.3 Results.....	195
4.3.1 Effect of Chronic Morphine and O-1966 Treatment on the Development of Tolerance.....	195
4.3.2 Effect of Chronic Morphine and O-1966 Treatment on the Development of Hyperalgesia	196
4.3.3 Effect of Chronic Morphine and O-1966 on Inflammatory Gene Expression	197
4.3.4 Effect of O-1966 on Acute Morphine Administration.....	198
4.3.5 Effect of the Order of Administration on Morphine and O-1966.....	198
4.4 Discussion.....	198
4.5 Conclusions.....	206
4.6 Works Cited	208
4.7 Figures.....	212
5. CONCLUSIONS.....	222
5.1 Conclusions.....	222

LIST OF TABLES

Table	Page
Table 1, Fold Change in Chronic Morphine Administration.....	196
Table 2, Additive and Observed Effects of Morphine and O-1966	203

LIST OF FIGURES

Figures	Page
1. Eye Sensitivity to Light	82
2. Derivation of the RBG Tristimulus Space	83
3. Mathematical Diagram of Spectral Power Distributions	84
4. Peripheral Blood Smears.....	135
5. Luma of Peripheral Blood Smears.....	136
6. Lightness (HSL) of Peripheral Blood Smears	137
7. Value (HSV) of Peripheral Blood Smears	138
8. Intensity (HSI) of Peripheral Blood Smears	139
9. Hue of Peripheral Blood Smears.....	140
10. Saturation (HSL) of Peripheral Blood Smears	141
11. Saturation (HSV) of Peripheral Blood Smears	142
12. Saturation (HSI) of Peripheral Blood Smears.....	143
13. Cranial Window Images	144
14. Luma Cranial Windows	145
15. Rolling Leukocytes	146
16. Adherent Leukocytes	147
17. Flow Cytometry, Overall Leukocytes, Equal Rhodamine 6G Applied	148
18. Flow Cytometry, Leukocyte Subpopulations, Equal Rhodamine 6G Applied.....	149

19. Flow Cytometry, Leukocyte Subpopulations Quantified, Equal Rhodamine 6G Applied ...	150
20. Flow Cytometry, Overall Leukocytes, Increased IP Injection.....	151
21. Flow Cytometry, Leukocyte Subpopulations, Increased IP Injection	152
22. Flow Cytometry, Leukocyte Subpopulations Quantified, Increased IP Injection	153
23. Linear Regressions From 3 Hours to 8 Hours	154
24. Linear Regression of Luma in Cranial Windows	155
25. Blood Flow Following Photochemically Induced Cerebral Ischemia	156
26. Vessel Size	157
27. TTC Staining in Wild Type and Knockout Mice.....	181
28. Stroke Size in Wild Type and Knockout Mice	182
29. Edema in Wild Type and Knockout Mice	183
30. Clinical Parameters in Wild Type and Knockout Mice	184
31. Blood Flow in Wild Type and Knockout Mice	185
32. TTC Staining in Photothrombotic Studies	186
33. Stroke Size in Photothrombotic Studies	187
34. Edema in Photothrombotic Studies.....	188
35. Clinical Parameters in Photothrombotic Studies	189
36. Experimental Design for Chronic Morphine Administration	212
37. Dose Response Curves From Chronic Morphine Studies.....	213
38. Hyperalgesia From Chronic Morphine Administration	214

39. Molecular Analysis of Chronic Morphine Administration	215
40. GTP γ S Binding Study.....	216
41. Acute Interaction of Morphine and O-1966.....	217
42. Dose Equivalence Theory	218
43. Acute Morphine and O-1966 Interactions Depends on the Order of Administration	219
44. Proposed Signaling Pathway.....	220

CHAPTER 1

THE ENDOGENOUS CANNABINOID SYSTEM AS A MEDIATOR OF INFLAMMATION IN CENTRAL NERVOUS SYSTEM INJURY

1.1 The Endogenous Cannabinoid System

Only recently has the field of science begun to direct its attention to unraveling the endogenous cannabinoid system. However, the application of cannabinoids compounds have not been a new innovation. As early as the third millennium BC, the Chinese employed *Cannabis sativa* as an analgesic (1). For more than 3000 years, ancient India utilized the plant as an anxiolytic (2). The effects of elation and euphoria have been described in Charles Baudelaiare's book *Les Paradis Artificiels* in 1860 (3). In 1937, the United States outlawed the plant and drug extracts from it but as the 21st century arrived, several individual states began to allow for the administration of medical marijuana to alleviate symptoms associated with numerous ailments (2). The 2012 election also saw several states vote to decriminalize recreational use of the drug. Aside from the social and legal implications, research into the use of similar based compounds over the last 30 years has tremendously expanded and revealed the compelling evidence for the drug class's anti-inflammatory effects.

Interest in the field peaked in the early 1990s when two receptors were discovered and cloned (4). Both known receptors belong to the class of seven transmembrane domain receptors associated with small G proteins, the G-Protein Coupled Receptors (2, 4-9). The human receptors, named CB₁ and CB₂, share only 44% similarity between each other although in the transmembrane region it rises to 68% (4, 5, 9). Interspecies similarity and conservation remains high with human and mice receptors having 97% homology in regards to CB₁ and 82% for CB₂ (4, 5). Evidence also exists for the presence of non-CB₁, non-CB₂ receptors that bind similar compounds (5, 10).

CB₁ receptor expression predominately occurs in the mammalian brain to the extent that it is the most abundant receptor in mammalian neuronal tissue even surpassing that of other common neurotransmitter receptors such as dopamine, serotonin, and acetylcholine (2, 8). Expression is particularly high in the cerebellum, hippocampus, and basal ganglia (10). Newer studies have also indicated the existence of the CB₁ receptors in other locations such as the vasculature, immune cells, and the myocardium (2, 7, 11-13). The CB₂ receptor resides mainly on hematopoietic cells of the immune system but also has low expression in other peripheral areas such as the spleen, adrenal glands, heart, lung, prostate, uterus, pancreas and testis (4-8, 10, 14). In immune cells, mRNA levels of cannabinoid receptors are greatest for B cells, followed in decreasing succession by NK cells, neutrophils, CD8+ T cells, monocytes, and finally CD4+ T cells (14). Just as CB₁ receptors have expression in both neuronal and peripheral tissue, CB₂ receptors have been found in both the hematopoietic cells of the immune system and also in nervous tissue. Reports have indicated distribution of the CB₂ receptor in brainstem neurons as well as astrocytes and microglial cells (4, 15, 16). In fact, a study localizing CB₂ receptor expression found the receptor in cerebellum, hippocampus, cerebral cortex, striatum, and amygdala (4, 17). In short, CB₁ receptor expression dominates in the brain while CB₂ receptors have much greater distribution in the peripheral immune cells, however, both receptors can be located in other tissues.

In the central nervous system, the location of the CB₁ receptor occurs presynaptically and modulates neurotransmitter release (4, 18-22). Its location allows for one of the few examples of retrograde neurotransmission that modulates neuronal firing and release of more traditional neurotransmitters (4, 23). Of note is the ability of CB₁ receptor activation to suppress the release of GABA (γ -amino-butyric acid) and glutamate (19-21, 24).

Both receptors are GPCRs that associate with small G-Proteins. The CB₁ receptor has been shown to couple to G_i and G_o while the CB₂ receptor only couples to G_o (2, 25). Both the G_α and G_{βγ} subunits can produce intracellular effects including the regulation of adenylyl cyclase activity, the opening of ion channels, the activation of phosphatases, and the regulation of phospholipase activity among other actions (2, 4-7, 16, 26-30). Both receptors have been shown to have high constitutive activity independent of ligand activation (31, 32). The response to ligand activation on adenylyl cyclase activity, and consequently levels of cAMP, depends on the adenylyl cyclase isozyme present (2, 6, 26, 27, 33). By means of the G_{ia} or the G_{oa} subunit, cannabinoid activation leads to inhibition of adenylyl cyclase isoform 1, 5, 6 and 8 and a decrease in cAMP levels (2, 6, 26, 27, 33). In contrast the G_{βγ} subunit can stimulate the production of cAMP when adenylyl cyclase isoform 2, 4, and 7 are expressed (2, 26, 27, 33). The duration of incubation with CB₂ selective agonists can also produce variations in results on cAMP stimulation or inhibition (34). Short exposure inhibited cAMP production but long term exposure produced more cAMP (34). Thus, cannabinoid receptor action on cAMP levels depends on the adenylyl cyclase isozyme present in the tissue of question as well as the time for which agonists were applied.

Cannabinoid agonists can also modulate the activity of a number of ion channels. In general, activation of cannabinoid receptors inhibits voltage-gated Ca²⁺ channels but activates K⁺ channels (2, 35-37). Inhibition of the calcium currents occurs via inactivation of the N-type calcium channel and the effect is blocked by pertussis toxin which ultimately suggests a G_{ai} modulated mechanism (35, 38, 39). Studies have indicated that the CB₁ receptor allows a tonic inhibition of Ca²⁺ currents which can be enhanced by receptor activation or reversed with the highly selective CB₁ antagonist, SR141716A (40). The inhibition of calcium currents was not

confined to N-type calcium channels but was found in both L-type and Q-type channels as well (36, 37).

In contrast, other groups have demonstrated the ability of cannabinoid agonists to elevate intracellular calcium levels (6, 41, 42). Bash proposed that activation of the CB₁ receptor can stimulate G_s leading to the stimulation of adenylyl cyclase and increased cAMP which activates Protein Kinase A (PKA) and downstream L-Type Calcium channels thereby producing a transient rise in calcium (42). The study also found that calcium uptake was abolished at higher concentrations of agonist (1-10 nM versus 1 μM) (42). The discrepancy in calcium handling could be the result of the cell system studied, the adenylyl cyclase isoform present, and also the concentration and type of CB₁ agonist employed. As in multiple studies, all of these factors have generated different and even conflicting results. Additional studies have suggested that the change in calcium concentration does not involve voltage-gated calcium channels but rather is dependent on inositol triphosphate (IP₃) sensitive reservoirs (43).

On the other hand, cannabinoid agonists were shown to enhance inwardly rectifying potassium currents (37, 44, 45). Heteromultimers of GIRK1/GIRK4 and CB₁ receptors produced the greatest change in K⁺ currents when stimulated with a cannabinoid agonist but this was not replicated with CB₂ receptors (45). The effect was also reversible with SR141716A at GIRK1/GIRK4 complexes (45). In general, the action on potassium channels was thought to hyperpolarize neuronal cells. It should be noted that anandamide, an endogenous ligand may also activate the intracellular Transient Receptor Potential Vanilloid Subtype 1 Channel (TRPV1) and affect ion balance (22, 46, 47).

The activity of cannabinoids is pleiotropic and does more than just regulate cAMP, calcium currents, and potassium concentrations. In addition, cannabinoid receptor activation is also thought

to activate Phospholipase C (PLC) and Phospholipase D (PLD) (43, 48). More so, cannabinoid ligand activation of receptors has been shown to activate Phospholipase A₂ (48-50). The production of arachidonic acid has been shown to result from receptor binding and the activation of phospholipase A₂ (48-50). Therein lies an important link between the cannabinoid system and the notoriously eicosanoid inflammatory pathways.

Cannabinoids have also been shown to exert numerous effects on both kinase and phosphatase activity. Activation of the CB₁ receptor has been shown to activate Protein Kinase B (PKB) and Phosphatidylinositol-3-kinase (PI3K) pathway through a G_i or G_o dependent manner that could also be reversed with SR141716A (51, 52). In regards to phosphatases, activation of the CB₁ or CB₂ receptor in microglia induced Mitogen-Activated Protein Kinase Phosphatase-1 (MKP-1) to terminate Mitogen Activated Protein Kinase (MAP-K) signaling in Toll-Like Receptor 4 (TLR4) activated cells and attenuate microglial activation (28, 29). CB₁ activity has also been thought to regulate another phosphatase, Protein Phosphatase 2b (calcineuin) (2, 53). A study of CB₁ -/- mice in fear conditioning demonstrated an effect on the level of phosphorylated calcineuin (Protein Phosphatase 2b) in learning and memory (2, 53). The effects of cannabinoid receptor activation remain wide spread and comprehensive with the overall culmination aimed at affecting gene transcription distal to the signaling cascade through modulation of cAMP levels, ion concentrations, and the activity of phospholipases, kinases, and phosphatases.

Downstream from the receptor and through various mechanisms, the cannabinoid receptors act on multiple signal transduction cascades including p38 MAP Kinase, p42/44 MAP Kinase, and JUN-terminal Kinase (JNK) (2, 13, 54). A number of cannabinoid agonists including anandamide, 2-arachidonoylglycerol (2-AG), and Δ⁹-tetrahydrocannabinol, have been shown to activate p38 MAP Kinase (13, 54, 55). These studies also confirmed the activation of the JUN-terminal Kinase

with the exception of Derkinderen (13, 55, 56). Derkinderen's study was carried out in adult rat brains whereas the other studies have been performed on transfected cell lines which may lead to a tissue specific sensitivity of activation of JNK (13, 55, 56). An additional study showed that in microglial cell lines, CB₂ specific agonists would increase phosphorylation of JNK-1/2 but not p38 and the effect was pertussis sensitive and reversible with CB₂ antagonists (54). Examination of p42/p44 MAPK (Extracellular Signal-Regulated Kinase 1/2 (ERK1/2)) also showed that agonists acting at cannabinoid receptors would lead to activation, phosphorylation, and eventual gene transcription (50, 57, 58). Most studies examined the CB₁ receptor but the CB₂ receptor was shown to behave similarly with regard to p42/p44 MAPK phosphorylation and activation (59). In short, downstream of receptor activation evidence indicates that cannabinoid receptor activation results in phosphorylation and activation of signal transduction cascades.

In addition to signal transduction cascades, activation of the CB₁ receptor has also been shown to generate nitric oxide (NO) by utilization of a NO synthase (NOS) isoform as well as promote its release (60, 61). The release could be attenuated with the selective CB₁ antagonist, SR141716A (61). The effect of NO release by cannabinoid agonists was located in peripheral vascular tissue, namely umbilical vein endothelial cells and human arterial endothelial cells, and progressed through a calcium dependent mechanism (62, 63). In RAW264.7 macrophage cell line, Jeon revealed that activation of the CB₂ receptor inhibited cAMP accumulation, decreased binding to the cAMP Response Element (CRE), inhibited NF-κB, and overall prevented the activation of iNOS (64). A second study demonstrated that activation of either cannabinoid receptor in glial cells could suppress iNOS activity as well as generate Interleukin-1 Receptor Antagonist (IL-1ra) (65). The correlation between cannabinoid activity and decreased NO production demonstrates an

important link in the chain between cannabinoid effects and reduction of inflammation. However, different tissues may exhibit different responses to cannabinoid agonists and NO release.

Both known cannabinoid receptors have been shown to have high constitutive activity independent of ligand activation (5, 31, 32, 66). Chinese Hamster Ovary (CHO) cells transfected with the CB₁ receptor were shown to activate p42/p44 MAPK upon stimulation with a cannabinoid agonist and this effect could be blocked with SR141716A in a dose dependent manner (66). However, cells transfected with the CB₁ receptor exhibited levels of phosphorylated p42/p44 MAPK above wild type cells suggesting that the CB₁ receptor remains constitutively active (66). Treatment with SR141176A decreased p42/p44 phosphorylation levels below basal quantities, and thus, constitutes an inverse agonist (66). Katzung describes an inverse agonist as one that can “reduce receptor activity below basal levels observed in the absence of bound ligand”(67). These effects were pertussis sensitive indicating a mechanism involving the G_{αi} subunit (66). cAMP levels demonstrated a similar finding with CB₁ agonists decreasing intracellular levels of camp while the inverse agonist SR141716A increased levels beyond basal quantitates in wild type cells (66).

The fact that two different ligands could drive intracellular activity in two separate directions from the same receptor has enormous implications for selective signaling based on the ligand utilized. Howlett notes the importance of such findings stating that, “These ligand-selective G protein responses imply that multiple conformations of the receptor could be evoked by ligands in order to regulate individual G proteins” (33). She furthers the idea explaining, “The observation that a unique pattern of functional interactions is ligand specific [...] has great biological significance because it implies that ligands can direct cellular signal transduction pathways *via* one G_i subtype at the expense of inactivation of another” (33). Thus, different cannabinoid ligands

could facilitate different intracellular actions by association with specific and unique G proteins based on the confirmation of the receptor after ligand binding.

Di Marzo describes the complexity of the situation stating, “However, all CB₁ and CB₂ receptor antagonists tested so far in preclinical and clinical experimentation behave—in *in vitro* assays of functional activity—not as neutral antagonists but as inverse agonists” (22). He suggests that they destabilize a receptor conformation that preferentially couples to the G-protein even when an agonist is absent (22). A similar pattern with both p42/p44 MAPK and cAMP levels were found in CHO cells transfected with the CB₂ receptor and treated with the CB₂ antagonist SR144528 (5, 32, 68). Like SR141716A at the CB₁ receptor, SR144528 was found to be an inverse agonist at the CB₂ receptor and in a dose dependent manner abolished basal activity of autoreactive CB₂ receptors (5, 32, 68). At its basal state, the CB₂ receptor undergoes a phosphorylation in the sixth transmembrane domain at serine 352 that allows for its internalization (4, 32). Phosphorylation promotes G proteins to uncouple from the GPCR and increases the affinity of the GPCR for arrestin binding (32). SR144528 blocks further phosphorylation and contributes to receptor dephosphorylation as well as upregulation of CB₂ receptor expression on the cell surface (4, 32). Conversely, agonists promote phosphorylation at serine 352 which with time, desensitization and internalization (4).

Continued agonist stimulation of cannabinoid receptors leads to tolerance in both humans and animals models and implicitly involves receptor desensitization and internalization (5, 6, 69-71). Desensitization causes receptors to terminate signaling cascades as they become refractory to further agonist binding and prevent association with intracellular secondary messengers such as G proteins (5, 6, 69, 72). In reference to the CB₁ receptor, phosphorylation of Serine 317 in the third intracellular loop or Serine 426 and Serine 430 in the cytoplasmic tail allowed for

desensitization (5, 6, 70). A deletion of amino acid residues 418-439 prevented desensitization but did allow for internalization suggesting that phosphorylation of the serine residues at 426 and 430 were necessary for desensitization but not internalization (70). Studies of desensitization were carried out in *Xenopus* oocytes and desensitization was dependent on coexpression of G-Protein Receptor Kinase 3 (GRK3) and β-arrestin 2 (70). The phosphorylation of specific residues is achieved by GRK3 which allows for β-arrestin 2 binding and subsequent inhibition of interaction with G proteins to effectively block further signaling (70, 71).

Like the CB₁ receptor, the CB₂ receptor also relies on phosphorylation for desensitization (5, 32, 71). The CB₂ receptor's constitutive activity leads to phosphorylation of serine 352 which is increased by agonist binding (5, 32). Phosphorylation of the serine residue by agonist binding can last for up to 8 hours and leads to receptor desensitization (32). The exact mechanism of phosphorylation remains elusive but probably involves a GRK1 like kinase since the effect did not abolish with pertussis treatment therefore eliminating the activity of GRK2 and GRK3 in contrast to CB₁ desensitization (32). However, the selective CB₂ inverse agonist, SR144528, causes dephosphorylation of the receptor and allows the receptor to again be resensitized and activated by agonist binding (5, 32). In short, both known cannabinoid receptors have complex and tightly regulated methods to allow for desensitization.

Independent of desensitization, cannabinoid receptors also undergo internalization and ultimately either degradation or recycling back into the membrane (5, 6, 69-71, 73). Agonist activation of the CB₁ receptor leads to internalization and corresponds to the degree of receptor activation (69, 73). Treatment utilizing agonists with less agonist efficacy such as Δ⁹-THC or methanandamide did not generate as much internalization as the much more potent agonist Win 55,212-2 (69). Δ⁹-THC did cause greater desensitization and Wu speculates that this is due to the

lessened internalization such that internalization and recycling provide a means of resensitization (73). The effect of internalization was also blocked with the inverse agonist SR141716A (69). Like desensitization, the process of internalization did not rely on pertussis sensitive G proteins but did rely on phosphorylation (32, 69). However, studies of AtT20 cells suggest that the process is also dependent on clathrin-coated pits and caveolae/lipid rafts (69, 71, 73). The CB₁ receptor may also be degraded by lysosomal action particularly if co-localized with the lysosomal marker, Lysosome-associated Membrane Protein 1/2 (LAMP 1/2) (71, 74). Further, interaction between the CB₁ receptor and GPCR-associated Sorting Protein 1 (GASP1) after internalization promotes degradation by lysosomes and down regulation of cell surface expression (71, 74).

Internalization of CB₂ relies on amino acids 460-463 and truncated receptors lacking these residues fail to internalize (69). Upon entry into the cell by clathrin-coated pits, acidification of the endosomal vesicle, and dephosphorylation of the receptor allows for recycling back to the cell membrane (69, 71). Dephosphorylation is achieved by the activity of an okadaic acid sensitive phosphatase such as Protein Phosphatase 1 or Protein Phosphatase 2A (69). In short, desensitization and internalization exist as highly regulated processes to modulate activity of the cannabinoid receptors and serve as another point of regulation in signaling.

Of course the development of two specific receptors with downstream effectors and tightly regulated expression and activity would have been a waist of biological capital if the system was not designed with endogenous ligands for these receptors as well. Indeed, the receptors thus far described, and their concomitant ligands, compose the endogenous cannabinoid system. Cells release endocannabinoids immediately after synthesis as no compelling evidence exists for a storage mechanism in secretory vesicles (22). Increasing intracellular calcium either following depolarization or from intracellular stores initiates the synthetic process (2, 46). The actions of

endocannabinoids are paracrine in nature due to a high degree of lipophilicity and also because physiological conditions tend to inactivate them quickly (22, 46). To date, two known endocannabinoid ligands have been identified, anandamide (arachidonoyl ethanolamide, AEA) and 2-arachidonoylglycerol (2-AG) (2, 4, 6-8, 22, 46). In the adult brain, levels of 2-AG exist 2 orders of magnitude greater than levels of anandamide at basal state (2, 75). Levels of anandamide were found to be vary in different brain regions (75).

The synthesis of both compounds is a complex set of reactions involving multiple intermediates and enzymatic reactions. The initial precursor, phosphatidylethanolamine undergoes N-arachidoylation by both calcium sensitive and insensitive N-acyltransferases (NATs) (22, 46). The resulting product, N-arachidonoyl-phosphatidyl-ethanolamine (NArPE) can then enter any of four possible pathways to produce anandamide (22, 46). A direct route occurs by conversion by N-acyl-phosphatidylethanolamine-selective phosphodiesterase (NAPE-PLD) while other routes employ phospholipase C or lysophospholipase D (22, 46). Anandamide undergoes hydrolysis by Fatty Acid Amide Hydrolase (FAAH) to ethanolamine and arachidonic acid which may provide substrate for eicosanoid synthesis and link the endocannabinoid system to the inflammatory eicosanoid metabolic system (22, 46, 76). Studies indicate that FAAH remains localized to the membrane of cytosolic organelles (77).

2-AG is produced almost entirely by hydrolysis of diacylglycerols (DAG) by a *sn*-1-selective DAG lipase (DAGL) (22, 46). Two isoforms of DAGL exist with the nomenclature of DAGL- α and DAGL- β whereas DAGL- α predominates in adult nervous tissue and the β isoform in developing neuronal tissue (22, 46). 2-AG undergoes hydrolysis and degradation primarily by Monoacylglycerol Lipase (MAGL) but can also be converted by $\alpha\beta$ -hydrolase 6, $\alpha\beta$ -hydrolase 12, and FAAH (22, 46). The degradation of 2-AG is also closely linked to the eicosanoid system as

degradation of 2-AG may provide substrates for Cyclooxygenase-2 (COX-2) ultimately playing a role in inflammatory processes (22, 46). MAGL, unlike FAAH, is localized to presynaptic terminals and in particular those of GABAergic neurons (2, 77).

With regard to receptor binding, anandamide has the greater affinity for both CB₁ and CB₂ receptors while 2-AG has higher efficacy in regards to both receptors (8, 22). Pacher agrees that anandamide is a full agonist at CB₁ receptors but proposes that it has low efficacy and may even be an antagonist at CB₂ receptors (2). Basu credits anandamide with being a partial agonist at CB₂ (34). Pertwee notes that anandamide exists as a partial agonist with greater affinity for CB₁ than CB₂ and also greater efficacy at CB₁ than CB₂ whereas 2-AG is a full agonist at both receptors (8, 9, 75). Other studies have indicated that 2-AG is 3 times more potent than anandamide in terms of GTP γ S binding but anandamide could block 2-AG's potential to inhibit cAMP synthesis and act as an antagonist in this sense (78). Additionally, researchers have reported 2-AG as a full agonist at the CB₂ receptor and suspect that it is the natural ligand for this receptor (34). Basu notes the complexity of the research pointing out that different CB₂ ligands acting through the same receptor can generate vastly different results even in the same cellular environment (34). Variations among experimental design, animal model or cell line, and concentrations of endocannabinoids can all contribute to the varying results but the clear message exists that further research into the endocannabinoid system remains warranted.

1.2 The Endogenous Cannabinoid System and Its Effect on Inflammation

The location of CB₂ receptors on immune cells, and to a lesser extent CB₁ receptors on immune cells, has presented the opportunity for immunomodulation via receptor binding and indeed much research into the area has been conducted (25, 79, 80). Activity at the CB₂ receptor has been shown to affect the function of all immune cell types examined thus far (34). Many

processes in immune cell activation and the progression of inflammation are cAMP-dependent processes and activation of the cannabinoid receptor can block elevations in cAMP and preclude progression of signal transduction cascades (25, 79). In general, cannabinoids tend to quell immune responses and affect multiple avenues of the immune response. These include impairment of macrophage function, generation of an imbalance in the T-cell CD4+/CD8+ ratio, agitation in immunoglobulin production, down regulation of NK cell activity, attenuation of cytotoxic T cell activity, and also diminishment of rolling/adhesion of leukocytes (9, 25, 81-88).

On a more localized level, cannabinoid treatment was shown to decrease the production of inflammatory cytokines. Δ^9 -THC and WIN 55,212-2, both agonists at CB₁ and CB₂, were able to decrease production of TNF- α found in broncoalveolar lavage from mice treated with LPS as well as reduce neutrophil recruitment to the pleural cavity (25, 89). Anandamide was also shown to decrease TNF- α , IL-6, and IL-8 in a similar model (76). A comparable finding was found in peritoneal macrophages although activation of the cannabinoid receptor tended to not decrease TNF- α mRNA but rather TNF- α release (90, 91). WIN 55,212-2 and HU 201, a CB₁ agonist, were also shown to decrease TNF- α and IL-12 while increasing IL-10 levels in LPS treated animals although Smith demonstrated that the effect was CB₁ rather than CB₂ mediated (92). The production of TNF- α was also shown to be influenced by the concentration of the agonist utilized in the experimental conditions, particularly Δ^9 -THC (93). The CB₂ agonist, JWH-133 was also shown to decrease production of TNF- α , in addition to MIP-1 α and MIP-2 (94).

Depending on the cytokine in questions and the concentration of the drug varying effects could be found. Anandamide was shown to decrease production of both IL-6 and IL-8 at low concentrations (3-30 nM) but higher levels (0.3-3 μ M) were needed to decrease TNF- α , IFN- γ , and IL-4 (93). A similar pattern was seen when the marijuana component Δ^9 -THC was utilized in

the studies whereas 3nM decreased production of TNF- α , IL-6, and IL-8 while 3 μ M caused the production of all of these cytokines in addition to IFN- γ in human monocytes (93). In contrast to these findings, peritoneal macrophages also treated with Δ^9 -THC and LPS showed a decrease in IFN- γ production. (25, 95). CD4+ T cells stimulated with antigen and treated with a selective CB₂ agonist, JWH-133, also had decreased IFN- γ and IL-2 production (34, 96). Unfortunately, other studies with JWH-133 failed to show any effect on TNF, IL-1 β , or CXCL2 in a transient ischemic stroke model but did demonstrate other immuno-modulatory effects (97). In contrast, the same CB₂ agonist was able to attenuate production of IL-12p70 and IL-23 production in microglia stimulated with LPS and IFN γ (98). As discussed with the explanation of signal transduction pathways, alternating effects of cannabinoid activation should come as no surprise as the concentration of agonist, the cell type, and the experimental conditions seem to play a major role in outcomes and create a complex model of immune system regulation. Specifically, with regard to immune cells, the ligand, the activation status of the cell, and also the receptor could also vary and affect results (34).

In a model of polymicrobial sepsis, Csoka demonstrated that CB₂-/- mice generated less IL-10, IL-6, Macrophage inflammatory protein-2 (MIP-2), and also decreased NF- κ B activation which suggested that in sepsis, CB₂ receptor activation could contribute to mortality (99). However, in models of sterile inflammation such as ischemia and reperfusion, activation of the CB₂ receptor could upregulate IL-10 production and prove to be beneficial in the overall response (99). The findings of Csoka were in sharp contrast to Tschop where in the same model Tschop showed that CB₂-/- mice had increased IL-6, KC (CXCL1), Macrophage Inflammatory Protein-2 (MIP-2), neutrophil invasion, and overall bacteremia (100).

Activation of cannabinoid receptors was also shown to attenuate NO production by macrophages stimulated with LPS (64). The down regulation of NO production was shown to occur via a CB₂ dependent mechanism in this model and affect the ability of NF-κB and CRE to bind DNA (64). However, activity of cannabinoid agonists may not be limited only to the CB₁ or CB₂ receptor. The superoxide generation by fMLP stimulated neutrophils was shown to inhibited by cannabinoid activation but was not blocked by CB₁ or CB₂ specific agonists ultimately suggesting another site of cannabinoid action (101). In ischemia/reperfusion injury of the liver, CB₂ activation was also shown to decrease the myeloperoxidase activity of neutrophils and could be blocked by SR144528 (94). Δ⁹-THC at a concentration of 1-10 μM was shown to decrease production of IL-1α, IL-1β, IL-6, and TNF-α in rat microglial cells (102). However, when enantiomers of cannabinoid agonists were utilized in the same experiment, the same reductions in cytokine production were again found and could not be blocked with either CB₁ or CB₂ selective antagonists which suggests that the actions could be achieved through a non- CB₁ or non-CB₂ receptor in the microglia (25, 102).

Effects of cannabinoid based therapies were also seen in T cells in regards to activation and production of IL-2 (79). Δ⁹-THC, the CB₂ agonist, JWH015, and R(+)-methanandamide, a CB₁ agonist, were shown to induce a decrease in cAMP for up to one hour but after that period a refractory rebound of about 10 fold of cAMP levels were found and these levels remained elevated for as much as two days in Jurkat T lymphocytes (79). Treatment with Δ⁹-THC and JWH015 was shown to inhibit IL-2 mRNA production (79). Incubation of T cells with IL-4 caused up-regulation of expression of CB₁ receptors without affecting CB₂ expression and if such conditions were present, R(+)-methanandamide also inhibited IL-2 mRNA production (79, 103). The decrease in IL-2 production was shown to be a consequence of down-regulation of NF-κB and NFAT

transcription factors (76, 79). Further, treatment of T cells with cannabinoids prevented cell division and activation (76, 79). Inhibition of activation was thought to occur through a stable phosphorylation of Tyrosine 505 of Leukocyte-specific Protein Tyrosine Kinase (LcK) (79).

Cannabinoid agents have also been shown to have a tremendous impact on cellular migration and neutrophil function (34, 97, 104, 105). In a study of neutrophil migration across endothelial cells, the ECV304 cell line, WIN 55,212-2 was shown to both inhibit neutrophil migration as well as IL-8 release from endothelial cells (104). The treatment did not affect the number of receptors for CXC1 or CXC2 on neutrophils or the neutrophil's ability to respond to IL-8 (104). JWH-133 was shown to inhibit neutrophil migration to CXCL2 and this effect was lost in CB₂-/- mice which confers the mechanism may be dependent on the CB₂ receptor (97). The decrease in migration was attributed to enhanced phosphorylation of p38 but not p44/42 or JNK (97). However, both CB₁ and CB₂ antagonists were unable to block the effect in the Nilsson study which again suggests a site distinct from the two identified cannabinoid receptors that may modulate activity (104). In a model of mouse peritonitis, neutrophil migration as well as the production of KC (CXCL1), Macrophage Inflammatory Protein-2 (MIP-2), and Monocyte Chemoattractant Protein-1 (MCP-1) were all decreased with cannabinoid receptor agonists and this effect could be blocked with SR141716A (105). Additionally, among other outcomes, anandamide has been also shown to cause cell rounding, a loss of motility, and decreased chemotaxis to IL-1 in macrophages (106). In brief, cannabinoids seems to affect cellular migration through multiple mechanisms.

Other groups have also suggested a site distinct from the CB₁ and CB₂ receptor for affecting neutrophil migration (107). Anandamide but not 2-AG was shown to inhibit neutrophil migration in response to the bacterial wall component, fMLP (107). Interestingly, SR141716A was able to

attenuate the anandamide induced reduction on migration but the effect was enhanced when SR144528 was added (107). In addition to evidence presented from other cannabinoid like compounds, the authors concluded that there is in fact a site distinct from the CB₁ and CB₂ receptors that binds cannabinomimetic drugs and decreases migration (107). The constitutive activity of the CB₂ receptor may compete with this effect and thus antagonism of the receptor may enhance the inhibition on migration (107). However, experimental conditions in this study utilized fMLP while the previously described studies employed chemokines such as CXCL2 and TNF α /IL8 (97, 104, 107). Regardless of the experimental design, enough evidence has been presented to conclude that cannabinoid based therapies impart an effect on neutrophil migration.

In addition to reducing migration by inflammatory leukocytes, cannabinoid agonists had been shown to decrease adhesion molecules (81, 82, 94). In models of cerebral ischemia and reperfusion, the CB₂ agonist, O-1966, was shown to decrease expression of Mac-1(Macrophage-1 antigen, heterodimer of CD11b and CD18) and ICAM-1 (Intracellular Adhesion Molecule 1) expression compared to vehicle treated controls (81, 82). Similar findings were demonstrated in hepatic ischemia and reperfusion but included VCAM-1 (Vascular Cell Adhesion Molecule 1) in addition to a reduction in ICAM-1 expression with the CB₂ receptor agonist JWH133 (94).

Despite sometimes conflicting reports, several conclusions can be drawn from the work of researchers in the field of immunology and cannabinoid receptor pharmacology. First of all, immune cells express the cannabinoid receptors (14). The activation, or blockade, of such receptors produces profound effects on the immunological response to injury and inflammation. The effects seen downstream depend on the nature of the experimental system, the agonist utilized, and also the concentration of that agonist. Any variation in these parameters can generate vastly different results and outcomes among studies. Overall, cannabinomimetic pharmaceuticals remain

an enticing and promising avenue of research in regards to quelling inflammatory states in various disease models.

1.3 Cerebral Ischemia—An Inflammatory Pathology

To tell someone that the prevalence of cerebral ischemia, or stroke, in 2010 in the United States hovered around 2.8% would be accurate but tend to underestimate the severity of the problem (108). A more accurate depiction would include that diagnosed stroke afflicted 795,000 Americans over the age of 20 in 2010 (108). This translates to a stroke occurring every 40 seconds in the United States, a stroke killing someone every 4 minutes, and ultimately stroke remains the #4 cause of death (108). Predictions suggest that by 2030, an increase of 21.9% in stroke incidence will occur (108). More so, experts estimate that anywhere from 6% to 28% of patients suffered from an undiagnosed silent stroke not included in prevalence and incidence data (108-110). The risk of stroke increases with age (108). Over 70% of individuals who suffer from a stroke are over 65 years of age and about 30% are over the age of 80 (108, 111, 112).

Surviving the cerebral ischemia does not translate to full recovery. Three months after the onset of acute symptoms, 15-30% of stroke survivors are permanently disabled and 20% require institutional care which make stroke one of the leading causes of permanent disability (108, 111, 113, 114). The Framingham Heart Study listed more specifics in regards to deficits in patients over 65 years of age 6 months after a stroke noting the incidence of the following as such: 50% hemiparesis, 30% unable to walk without assistance, 46% cognitive defects, 35% depression, 19% aphasia, 26% dependent in activities of daily living, 26% institutionalized in a skilled nursing facility, and 22% bladder incontinence (108, 115).

The cost of acute treatment and care as well as ongoing rehabilitation and long term care is staggering. The direct medical cost of stroke care in 2009 was \$22.8 billion dollars and when indirect costs added were added in, the cost rose to \$38.6 billion (108). The total cost of stroke from 2005 to 2050 is projected to be \$2.2 trillion dollars (108, 116). Despite the tremendous impact cerebral ischemia has on the patient both physically and monetarily, there exists only one FDA approved therapeutic for treatment (111, 117). Tissue Plasminogen Activator (tPA) is the only treatment but a mere 7% of stroke patients meet criteria to receive it (111, 117, 118).

Further understanding into the basic pathophysiology of cerebral ischemia remains essential for enhancing any attempts at the production of novel therapeutics. Prior to exploring any original methodologies of treatment, first a firm foundation in current knowledge of the effects of cerebral ischemia at the cellular level should be established. Evidence will be presented to show that cerebral ischemia exists as two pathological insults to neuronal tissue in first an ischemic attack and then a reperfusion injury (111, 117, 119-121). Both injuries lead to an inflammatory response and attenuation of this inflammation could prove to be beneficial (36, 111, 114, 119). The endogenous cannabinoid system remains a promising target for such anti-inflammatory therapy (81, 82, 97, 119, 122, 123).

The brain comprises only 1-2% of an individuals' body weight but yet receives 15% of cardiac output and utilizes 20% of the total body oxygen consumption (121). Cerebral blood flow is approximately 50 mL/min per 100 grams of neuronal tissue but varies depending on the brain region (121). Thus, the brain is exquisitely sensitive to any deprivation in oxygen or glucose (121, 124). When flow to the brain is interrupted, cerebral ischemia ensues and the clinical manifestations thereof are referred to as a stroke (121, 124). Stroke may arise as a result of hypoxia/ischemia resulting from a profound global reduction in pO₂ or an interruption of flow to

cerebral tissue by a blockage (108, 121, 124). Ischemic insult implies a depletion of both oxygen and metabolites as would occur in a blockage of a vessel (121, 125). Hemorrhage or rupture of a blood vessel may also lead to stroke (121, 124). In terms of etiology, 87% of strokes are ischemic, 10% are the result of intracerebral hemorrhage, and 3% from subarachnoid hemorrhage (108).

Ischemic strokes typically arise as a result of thrombotic or embolic occlusions (121, 124). The majority of thrombotic occlusions result from atherosclerosis (121). Narrowing of an atherosclerotic artery can lead directly to an interruption of blood flow or a ruptured plaque may generate emboli distal to the initial lesion to preclude blood flow (121, 124). The origin of the middle cerebral artery, the origin of the posterior cerebral artery, and the basilar/vertebral transition tend to be more prone to such events (121, 124). An occlusion in a particular vessel, as well as the location within that vessel, dictate the clinical signs and symptoms a patient may present (121, 124). Signs and symptoms may include hemiparesis, aphasia, altered mental status/confusion, dizziness, paresthesia, incontinence, changes in vision, high blood pressure, respiratory distress, nausea/vomiting, seizures, unequal pupillary responses, and/or headache (126).

In stroke pathophysiology, the first phase encompasses an ischemic set of reactions. Pyramidal cells of the Sommer sector (CA1) of the hippocampus, Purkinje cells of the cerebellum, and the pyramidal neurons of the neocortex tend to be most easily perturbed by ischemic insult (121, 127). The ischemic cascade in neuronal tissue proceeds like that in various other organs with some additional considerations. In ischemia, the mitochondria remain some of the first to feel the effects of oxygen and metabolite depletion and consequently oxidative phosphorylation decreases or stops completely depending on the severity of the nutrient deprivation (121, 127). As oxidative phosphorylation slows, ATP stores become depleted and cellular metabolic pathways

switch to anaerobic glycolysis ultimately producing acidic conditions intracellularly (121). Reactive oxygen species are also produced by this transition (121, 127).

More so, the depletion of ATP prevents Na^+ pumps from functioning and ions begin to accumulate in the cytoplasm (121). Na^+ and Ca^{2+} accumulate with water and K^+ exits the cell but the cells continue to swell (121). Membrane integrity begins to decrease (121). Eventually the cell surpasses a point from which it cannot recover and cell death, dissolution of the cell, and necrosis ensue (121). The resulting demise and release of intracellular material such as proteases and hydrolytic enzymes accelerates and further insults surrounding tissue (121). For neuronal tissue, the process begins after about 4 minutes of energy deprivation and permanent effects take hold around the 6 minute mark (126).

In addition, neuronal tissue has the added risk of excitotoxicity as a result of ischemia (121, 124, 125). During ischemia, neurons release excitatory amino acid neurotransmitters such as glutamate that can cause overstimulation and prolonged opening of membrane channels such as *N*-methyl-*D*-aspartate (NMDA) and kainite receptors (121, 124). Stimulation of such channels leads to added influxes of Na^+ and Ca^{2+} (121, 124). Additional Ca^{2+} influx can further stimulate intracellular release of Ca^{2+} from intracellular stores (124). In the extracellular space, accumulation of K^+ also promotes depolarization and firing of neurons with the effect of even more transmitter release (124, 125). The overabundance of intracellular Ca^{2+} tends to activate proteases, phospholipases, endonucleases, and other enzymes as well as promote further cellular swelling, membrane compromise, and death (121, 124, 128). This phenomenon seems to be more prevalent in the penumbral region or area where blood flow is 15-40% of normal flow than in the ischemic core where blood flow drops to below 15% (119, 124). Initiation of apoptosis as a means of cellular death is also prevalent in the penumbral region (127).

The injured brain tissue initiates an inflammatory response within minutes of the onset of ischemia which includes the production of inflammatory cytokines, leukocyte recruitment to the brain, compromise of the blood-brain barrier, and activation of resident immunological cells (81, 82, 117, 127, 129-131). Many of these sequelae result from the induction of pro-inflammatory genes via transcription factors such as NF-κB (117, 130, 132). Injured neurons, glial cells, and endothelium produce such inflammatory signaling molecules as IL-1 β , IL-6, and TNF α as well as chemokines (117, 129, 130, 132, 133). These cytokines are intimately involved in the upregulation of cell adhesion molecules such as ICAM-1, VCAM-1, and E-selectin which promote leukocyte infiltration into the brain (130).

Ischemia alters cellular morphology in both the ischemic core and penumbral region (117, 129). The lack of oxygen and metabolites activates resident microglia to proliferate and transform to an amoeboid shape with a loss of ramified morphology (117, 129, 131). Microglial respond as early as 4-6 hours after the onset of ischemia and their activity peaks between 2 and 3 days post stroke (117). Proliferation of microglia peak at 2-3 days as well (114). Until approximately day 3, the microglial cells remain the most prevalent in the ischemic hemisphere (130). Microglial may exacerbate injury by producing reactive oxygen and nitrogen species or may have a protective role in becoming phagocytic (131). Activated microglia are the primary source of TNF- α (123, 134).

Endothelium has constitutively expressed receptors in place for the tethering of immunological cells as part of the body's surveillance system and ischemia both upregulates these as well as promotes the expression of others (129). Leukocytes also express these receptors, such as L-selectin, at basal conditions (129). Selectins promote a process known as rolling that reduces the velocity of leukocytes in circulation (129). Inflammatory cytokines can promote endothelial

cells to express P-selectin and well as E-selectin (129). P-selectin expression was found to increase during ischemia while E-selectin levels reached a maximum at 24 hours after the onset of ischemia (128, 129, 131, 135-137). The process of firm adhesions succeeds rolling in the vasculature (111, 129). Leukocytes also constitutively express firm adhesion molecules such as CD11b/CD18, also known as Leukocyte Function Associated Antigen-1 (LFA-1), and Very-Late-Antigen-4 Complex (VLA-4) (129). Endothelial cells utilize ICAM-1 to bind LFA-1 and VCAM-1 for VLA-4 (129). ICAM-1 and VCAM-1 generally have low levels of expression on endothelial cells but undergo enhanced expression with inflammatory cytokines (111, 129, 138). Adherent leukocytes may contribute to further microvasculature dysfunction by prevention of cerebral blood flow (81, 82, 120, 139).

Ischemic injury is also associated with production of chemokines such as IL-8 for neutrophils, MCP-1 for monocytes, RANTES, LTB-4, KC (CXCL1), and Macrophage Inflammatory Protein-2 (CXCL2) (140-142). The production of chemokines recruits leukocytes from the periphery to extravasate into the cerebral tissue (129). Microglia, already present, and macrophages begin to increase noticeably by as early as 12 hours although differentiation between the two remains difficult due to a common lineage (130). However, Schilling notes that in his study of transient cerebral ischemia in GFP mice, hematopoietic macrophages did not appear in significant numbers until day 3 after ischemia (114, 143). In addition to a multitude of proinflammatory cytokines, infiltrated macrophages are believed to produce IL-23 which then stimulates TCR γ δ T cells to produce IL-17 (122). IL-17 promotes apoptosis of neuronal cells in the penumbral region (122).

Blood derived monocytes/macrophages also enter the ischemic tissue from peripheral circulation (117). Since microglia originate from monocytes and share common surface markers,

differentiation between activated resident microglia and migrated peripheral monocytes remains difficult without complex immunological experimental design (117, 130). Activated microglia and infiltrating macrophages produce inflammatory cytokines, particularly IL-1, and activate neighboring endothelium to promote rolling and adhesion (16, 28, 138, 144-146).

Neutrophils appeared in small amounts after 12 hours and predominated in the neuronal tissue by day 3 (130). The neutrophils remain one of the earliest cells to infiltrate the injured brain and peak between days 1 and 3 (114, 147). In a model of ischemia and reperfusion in mice, on day 3 the percentage of hematopoietic cells in the ischemic hemisphere looked like: 34% microglia, 39% neutrophil, 27% macrophage, dendritic cell, NK cell, and lymphocyte (130). Neutrophils contribute to neuronal injury in a number of fashions including the production of ROS (superoxide by NADPH oxidase and hypochlorous acid by MPO), the release of proinflammatory cytokines such as IL-1 β , IL-6, and TNF- α , and also the release of elastase and MMPs, particularly MMP-9 (114). Lastly, neutrophils enhance the expression of adhesion molecules such as (LFA-1, CD11b/CD18, PSGL-1, L-selectin) (114). Changes in the post ischemic brain promote cell entry and cell entry promotes changes in the post ischemic brain. Unfortunately, each step amplifies itself and promotes a destructive cyclic pattern.

Lymphocytes also infiltrate injured brain tissue (130). By day 3 post ischemia, equal numbers of T and B lymphocytes were present in the ischemic hemisphere but tended to gravitate towards the ischemic border rather than the core (123, 130). Studies of both photochemical thrombotic stroke and transient ischemia confirmed this time course (114, 147, 148). T cells appear to be the major source of IFN- γ (123). Rag1 $^{-/-}$ mice seem to be protected from stroke suggesting a role of T cells in the pathophysiology (149). However, studies with T cells lacking

costimulatory molecules were not protected which implies that the adaptive immune arm of T cell functions are not a prominent feature of the T cell's role in stroke progression (149).

CD4-/CD8- T cells were present as early as day 1 but CD4+ T cells were not found until day 3 in an ischemia/reperfusion model (130). The presence of both CD4+ and CD8+ T cells have been shown to exacerbate stroke compared to mice lacking these cells (114, 150). However, different subsets of CD4+ cells may exert varying effects (114, 151). CD4+ TH1 cells may contribute to injury by producing IL-2, IL-12, IFN- γ , and TNF- α while on the other hand CD4+ TH2 cells may mitigate damage through IL-4, IL-5, IL-10, and IL-13 production (114, 151). Double negative T cells have been surmised to have a regulatory role in maintaining self-tolerance and downregulating immune response (130). Data also suggests that CD4+CD25+Foxp3+ cells, T_{reg} , play a role about 7 days after ischemia and provide protection and attempt to attenuate damage (123). T_{reg} cells decrease inflammatory cytokines through an IL-10 dependent manner (123).

NKT cells and dendritic cells also tend to increase on day 3 but not NK cells (130). NKT cells exist as a type of T cell that has an $\alpha\beta$ -T cell receptor in association with NK type markers such as NK 1.1 (130, 152, 153). Reports on the function of NKT cells vary as some suggest an anti-inflammatory purpose and others suggest the promotion of inflammation (130, 153). Dendritic cells on day 3 were primarily of myeloid origin and had high levels of MHC II expression but only mild expression of CD80 which may lead to anergy and prevent full activation among T cells (130, 154). Ultimately, the presence of dendritic cells may be a built in safety mechanism to control the inflammatory response.

Ischemia and the subsequent inflammation also promotes the expression of Matrix Metalloproteinase (MMP) (128). MMPs are a family of more than 20 zinc endopeptidases (128, 155). MMP-2 and MMP-9 exist as gelatinases that target the collagen IV and laminin of the

neuronal basal lamina and degrade the integrity of the Blood-Brain Barrier (BBB) (128, 156). Upstream activation of MAP Kinases can lead to transcription of MMPs (128). MMP-9 can also be activated by S-nitrosylation of the catalytic site directly by nitric oxide (128). Neutrophils contain granules of MMP-9 that are rapidly released but further synthesis can be initiated by neutrophils as well as mononuclear cells (155). Neurons, astrocytes, microglia, and endothelial cells are also capable of expressing MMPs (111, 156). Levels of MMP-9 in the ischemic hemisphere were found to be elevated within 3 hours of permanent cerebral ischemia (111, 157). Loss of the BBB, precipitated by MMPs, leads to vasogenic edema and potentially hemorrhage following a stroke (111, 156). The induction of MMPs contributes to leukocyte invasion into the neuronal tissue. Likewise, the arrival of proinflammatory leukocytes generate more MMPs. Like cytokines and infiltrating peripheral leukocytes, the process is cyclic and overall promotes inflammation, BBB breakdown, and extravasation of blood derived hematopoietic cells. The key to effective stroke treatment exists in an ability to reduce inflammatory processes

1.4 The Endogenous Cannabinoid System in Cerebral Ischemia

The endogenous cannabinoid system undergoes a number of changes in response to cerebral ischemia and these responses may also be utilized for therapeutic purposes with specific pharmacological agents (119). A number of researchers reported increases in both anandamide (AEA) and 2-AG in response to permanent and transient ischemia (119, 158-161). In a study in rats, 5 hours after permanent occlusion, a 12 fold increase in anandamide was found in the ipsilateral hemisphere (119, 158). A subsequent rise in precursors to anandamide was also found (158). The anandamide and precursor levels were measured in the striatum and cortex (158). Another study reported a rise in anandamide but not 2-AG as early as 30 minutes after the onset of ischemia (159). The changes in anandamide levels seen in the striatum were further increased

when reperfusion was permitted (160). Two hours of ischemia with 1 hour of reperfusion produced more anandamide in the ipsilateral striatum than did occlusion alone (160). These changes were partnered with both a decrease in degrading enzyme, FAAH, and also an increase in the synthesis enzyme, N-acylphosphatidylethanolamine (NAPE)-hydrolyzing phospholipase D (NAPE-PLD) (160). A second reperfusion study showed a rise in anandamide, although not statistically significant, with twenty minutes of ischemia and reperfusion (162). Increases in anandamide have also been confirmed in a human patient with a large vessel stroke (163). Longer increments of ischemia tend to increase the level of anandamide found in the ipsilateral neuronal tissue (119). In contrast, Degn's study with permanent occlusion in mice failed to show a rise in anandamide following ischemia but there was a significant rise in 2-AG 4 hours after the onset of ischemia (161). Regardless of the study referenced, it appears that the endocannabinoid system undergoes alterations as a result of ischemia.

Changes in levels of endogenous cannabinoid ligands are met with changes in receptor expression (82, 119, 164, 165). Several studies have indicated a rise in CB₁ receptor expression following cerebral ischemia (82, 119, 164). The rise was reported as early as 1-2 hours after ischemia (82, 164). Changes in CB₂ receptor expression took longer with no rise indicated until 24 hours in one study and 3 days in a second (82, 165). The pharmacological activation, blockade, or genetic ablation of these receptors impacts stroke outcomes and remains a viable target for novel therapies. There is relatively firm consensus that activation of the CB₂ receptor provides protection following an ischemic event but conflicting reports abound on the outcome following activation or antagonism of the CB₁ receptor.

Activation of the CB₁ receptor with WIN 55,212-2 produced smaller infarct volumes in a permanent cerebral ischemia and this effect was blocked with SR141716A (119, 166). However,

the blockade of the receptors alone did not make the infarct volume worse (166). A study of CB₁ -/- mice demonstrated higher mortality and increased infarct volumes in the knock-out mice compared to wild type controls (119, 167). This also supported the notion that activation of the CB₁ receptor could be beneficial and protective (119). Multiple hypothesis were put forth to explain the protective effect of CB₁ receptor activation. CB₁ receptor activation is thought to protect against glutamate-induced excitotoxicity possibly by decreasing calcium transients (119).

A second thought focused on the ability of CB₁ receptor activation to induce hypothermia (119, 168). In a study of permanent cerebral ischemia, rats administered the CB₁ agonist HU-210 had body temperatures approximately 6°C lower than vehicle treated rats and lower stroke volumes at 24 hours (119, 168). Lastly, there remains some evidence that activation of the CB₁ receptor could decrease edema (119). Hillard describes the consequences of edema stating that “edema results in an expansion of brain volume resulting in an increase in intracranial pressure which can damage cells directly through compression and indirectly by impairment of cerebral perfusion” (119). 2-AG administered after traumatic head injury reduced edema and the effect could be blocked with SR141716A administration (119, 169). Δ⁹-THC also decreased edema in a chemically induced excitotoxic injury (119, 170). The decrease in edema may stem from an ability of CB₁ receptor activation to decrease system blood pressure (119, 171).

On the other hand, a number of studies have shown that blockade of the CB₁ receptor provides a degree of neuroprotection by decreasing infarct volumes and improving neurological scores (158-160). A permanent occlusion model in rats showed protection when SR141716A was provided (158). Two studies of transient occlusions with reperfusion also showed a protective effect in SR141176A with decreased infarct fractions (159, 160). Our laboratory also has shown

repeatedly a protective effect in SR141716A with lower infarct volumes and improved neurological findings (82, 172, 173). Several mechanisms may exist for this protective effect.

One protective effect of CB₁ blockade may derive from enhanced GABA signaling and aversion to excitotoxicity (119). Several studies have shown that CB₁ receptors maintain a presynaptic location and activation thereof decreases GABA release (19, 20, 119, 174). The theory therefore hypothesizes that antagonism of the receptor would lead to increased GABA release (119). Increased GABA signaling has been shown to be protective in ischemia/reperfusion injury by activating Akt signaling and inhibiting JNK, bcl-2, and c-jun phosphorylation (175). In one study, hippocampal neurons were shown to decrease release of GABA with cannabinoid agonists and the effect could be blocked with SR141716A (19). However, SR141716A alone did not produce any alterations in GABA signaling (19). The precise mechanism of the cannabinoid GABA axis in ischemia reperfusion has not been studied directly but warrants further examination. Another study has shown that cannabinoid activation of CB₁ receptors in astrocytes increases the release of glutamate, thus exacerbating excitotoxic injury (119, 176). Pharmacological antagonism could mitigate this damaging effect (119).

Another potential benefit of antagonizing the CB₁ receptor may stem from enhanced autoregulation and coupling of the neurovascular unit (119). The neurovascular unit exists as a tightly regulated barrier and includes cerebral vasculature, endothelial cells, neurons, astrocytes, and basal lamina (119, 128, 177). Several studies have indicated the presence of CB₁ receptors in cerebral vasculature and activation thereof relaxes cerebral blood vessels and decreases vascular resistance (36, 178). Blockade of the CB₁ receptor could prevent this relaxation. Dilated vasculature may seem beneficial during periods of ischemia but it may also contribute to an inability to autoregulate and provide blood flow to areas with the most demand (119). Studies in

our laboratory have shown that CB₁ blockade in conjunction with CB₂ receptor activation increases blood flow and arteriolar diameter through the ischemic core during the period of occlusion (82, 173). Thus, CB₁ receptor blockade may help to maintain the neurovascular coupling and promote blood flow to ischemic areas ultimately preserving more neuronal tissue (119).

The CB₂ receptor has also been shown to be protective in cerebral ischemia and reperfusion when it is activated (81, 82, 97, 172). First of all, activation of the CB₂ receptor has been shown to decrease lymphocyte migration and well as production of chemokines, inflammatory cytokines, and adhesion molecules (34, 94, 97). CB₂ agonists have also been shown to inhibit neutrophil migration and invasion following cerebral ischemia reperfusion (97). With direct visualization of pial blood vessels, CB₂ agonists have also been shown to decrease rolling and adhesion of leukocytes in venules and arterioles after the onset of reperfusion (82). Lastly, mice lacking the CB₂ receptor had significantly larger infarct volumes and more adverse neurological scores following an ischemia reperfusion injury (81). In brief, activation of the CB₂ receptor tends to quell inflammation that is associated with cerebral ischemia and the subsequent reperfusion injury.

Stroke may exist as one of the most devastating afflictions to befall an individual. Its rapid onset and malignant consequences make it a challenging situation for a clinician to manage not only from a medical standpoint but also as the interface between the patient and the bewildered next of kin. Individuals that survive the stroke face a hard road of rehabilitation as they learn to navigate the neurological consequences cast upon them. Indeed, stroke has fallen to the #4 killer of Americans according to the most recent data, but we have also listed predictions here that the number of strokes occurring will continue to rise and place an outstanding toll on our society (108). At its core, stroke is an inflammatory pathology that unleashes a vicious and self-perpetuating cycle of neuronal inflammation, blood-brain barrier breakdown, and lymphocyte infiltration. The

endogenous cannabinoid system stands as a way to effectively modify and arrest some of these adverse sequelae. It seems that via blockade of the CB₁ receptor and activation of the CB₂ receptor, brain tissue can be saved that effectively translates to improved neurological outcomes (82). However, the endogenous cannabinoid system remains an enigma unto itself with different researchers publishing varying reports. Thus, here we set out to explore the effect of stroke in mice that lacked both cannabinoid receptors. We hypothesized that based on single knockout studies, the injury would be much greater. To our surprise, that was not the finding here which further confounds our knowledge of cannabinoids and stroke. Regardless, the investigation of cannabinoid based therapies in cerebral ischemia warrants further study.

1.5 Models of Cerebral Ischemia

The Middle Cerebral Artery Occlusion/Reperfusion (MCAO/R) through the internal carotid is the most widely used method and provides the advantage of closely mimicking human stroke (179). Sutures can be left in place for variable periods of time and the technique does not require a craniotomy (179). However, premature reperfusion and subarachnoid hemorrhage remains complications of the procedure (179, 180). Damage to brain regions will be widespread and may produce complex motor, sensory, autonomic, and cognitive defects depending on the time of occlusion (179).

The technique can also lead to substantial variations in the volume of damage within and between strains of mice (179). C57Bl/6 mice are much more susceptible to neurological damage than other strains because of deficiencies in collateral flow from the posterior communicating artery (PCA) (179). Both histology and high resolution MRI revealed that C57Bl/6 mice had either unilateral or lacked both PCAs (181, 182). When present it was typically less than 1/3 the diameter of the basilar artery (181, 182). There also exists a sharp correlation between occlusion time and

infarct size as increasing the time of occlusion from 15 minutes to 30 minutes produced a fivefold increase in infarct volumes (179, 183).

In other studies, a photothrombotic method of inducing cerebral ischemia was employed. Rose Bengal was injected into the peritoneal cavity and irradiated through an intact skull to produce singlet oxygen, focal endothelial damage, platelet activation, and simultaneous microvascular occlusion (179, 184). Utilization of light through an intact skull allows for stereotactic placement of the light to ultimately produce highly standardized strokes in both size and location (179). Unlike the filamentous method, photochemical stroke has less penumbra (179). More so, this method induces both vasogenic (extracellular) and cytotoxic (intracellular) edema simultaneously which differs slightly from stroke progression in humans (179). Despite these drawbacks, the method remains easily implemented and produces consistent results that have generated much insight into stroke pathophysiology (179).

1.6 Chronic Morphine Administration and Inflammation

Just as cerebral ischemia exists as an inflammatory pathology in the central nervous system, the chronic administration of morphine produces many of the same downstream and deleterious sequelae. Chronic morphine administration has been shown to initiate inflammation and act through many of the same cytokines as cerebral ischemia. Thus, just as we hypothesized that modulation of the cannabinoid system could be protective in stroke, we sought to explore its utility in attenuating inflammation with chronic morphine administration. More so, inflammation associated with morphine administration leads to the development of tolerance and hyperalgesia. We wanted to explore if cannabinoid modulation employed here could alleviate these effects as well.

Morphine came into practice as an analgesic in 1803 when Sertüner isolated it and named it after Morpheus, the Greek God of dreams (67). Unfortunately, in current therapeutic regiments, 2/3 of patients receive little to no relief from their prescribed pain medication (185). This is particularly true of patients suffering from neuropathic pain which Raghavendra describes as “pain associated with severe, chronic sensory disturbances characterized by spontaneous pain, increased responsiveness to painful stimuli (hyperalgesia), and pain perceived in response to normally non-noxious stimuli (allodynia)” (186).

There exists 3 types of opioid receptors, μ , δ , and κ but the vast majority of analgesic therapeutics are targeted at the μ receptor (67). Morphine is a full agonist at the μ receptor (67). The μ receptor is a G Protein Coupled Receptor that induces 2 primary changes in the cell upon activation including the closure of Ca^{2+} channels on presynaptic terminals and the opening of K^+ channels on postsynaptic neurons (67, 187, 188). The overall effect is to produce hyperpolarization of the neuron and reduce firing and therefore transmission of pain signals and neurotransmitters (67, 188). The μ receptor signals through $\text{G}_{i/o}$ mechanisms and also inhibits the production of cAMP (187, 189). The μ receptor has also been shown to be associated with the TRPV1 and also Substance P receptor (67).

μ receptors are located on both primary pain afferents and pain transmission neurons in the dorsal horn of the spinal cord as well as on the terminals of pain sensing neurons in the periphery (67). Their location imparts effects on both spinal and supra-spinal processes (187). However, utilization of such drugs is not without side effect. Common side effects of opioid usage include sedation, respiratory depression, constipation, and the development of tolerance, hyperalgesia, and allodynia (67, 190).

G Protein Coupled Receptors have been shown to form homo and heterodimers with each other and impact receptor function and signaling (191). μ receptors have been shown to dimerize with CB₁ receptors with implications on signaling which occurs through common G protein (189, 192). Studies have shown that activation of both receptors produces attenuation of signaling in individual receptors alone (189). This may be due to competition for G proteins or may result from allosteric modulation of the receptors (189). Other studies have indicated that cannabinoid agonists activate far fewer, by several fold, numbers of G proteins than μ receptors and the authors attributed this to be different intrinsic abilities of the receptors to couple to the G proteins (193).

The interaction between the opioid and cannabinoid signaling system remains an area of intense research. Studies have revealed that administration of agonists for both systems has multiple downstream effects including enhanced antinociceptive actions (188). Δ^9 -THC and CP-55,940 was also shown to increase the efficacy of morphine in antinociceptive effects (194-197). CP-55,940 was shown to generate analgesia in animals tolerant to morphine, but not naïve animals (196). However, in animals tolerant to CP-55,940, morphine lost its analgesic effect (196). Further, administration of cannabinoid agonists also increased the production and release of endogenous opioids (188, 198). More specifically, Δ^9 -THC has been shown to promote the release of dynorphin A while CP-55,940 augments the release of dynorphin B (199, 200). On the other hand, administration of morphine has been shown to affect the level of endogenous cannabinoids by lowering the levels of 2-AG but not anandamide (188). Repeated application of Δ^9 -THC also causes an increase in proenkephalin gene expression, activation of μ receptors, and a downregulation of CB₁ receptors (201).

Chronic treatment with morphine and other opioid agonists leads to states of tolerance and decreased efficacy of morphine (190, 196, 202). In such states, higher levels of morphine are

required to reach effective pain relief. Chronic treatment with morphine has been shown to upregulate adenylyl cyclase levels (202). Prolonged treatment with morphine has also been shown to increase expression of the CB₁ and CB₂ receptors (203, 204). A link between the opioid and cannabinoid system exists as treatment with both anandamide and Δ⁹-THC have been shown to diminish signs of opioid dependence (201, 205). CP-55,940 has also been shown to prevent the induction of morphine tolerance and preserve efficacy in a chronic treatment regimen (190).

Another avenue in which chronic administration of morphine promotes tolerance exists in the activation of glial cells and subsequent inflammation (186, 206-209). Numerous studies in which morphine was administered chronically showed that microglia were activated in response to such administrations (186, 207, 209). Glial activation parallels the frequency of opioid treatment and the process produces a gradually opposing course that contributes to morphine tolerance (206, 210). The method of activation may come from morphine directly binding μ receptors, by binding TLR-4 on microglia, or by substances released from afferent pain fibers such as Substance P (206, 209). Glial activation seems to be a prerequisite for the development of tolerance as methods that block such activation thwart the onset of tolerance and hyperalgesia (207, 209, 210). In addition to inflammatory stimuli, including morphine, neurotransmitters released from neurons may activate glial cells in neuron-to-glia signaling (210).

Activated glial amplify pain signals and also generate multiple inflammatory cytokines (206, 209, 210). Morphine activation of microglial produces IL-1β, TNF-α, and IL-6 (186, 209-211). Hutchinson refers to them as the “linchpin in glial enhancement of pain” (206). Such cytokines may increase pain signaling by activating receptors on neurons and increasing neuronal excitability and synaptic strength through increased conductivity (210, 212). These cytokines also further contribute to the development of hypersensitivity and tolerance (207, 209). They can block

the effects of morphine injections within as little as 5 minutes (210, 213). Therapies aimed at blocking IL-1 β were shown to prevent hypersensitivity and prevent tolerance (211). The same was true of not only IL-1 β , but also TNF- α and IL-6 (186). Particularly interesting is the ability of morphine to activate microglia through TLR-4 receptors ultimately contributing to inflammation and hypersensitivity (206, 214). Studies have also shown that acute exposure to morphine has resulted in both transcriptional and translational upregulation of TLR-4 (206). The blockade of TLR-4 receptors reduces neuropathic pain and also potentiates morphine analgesia (206). Additionally, administration of morphine was shown to generate the production and release of GRO/KC (CXCL1), Macrophage Inflammatory Protein-1 α (MIP-1 α), and Monocyte Chemoattractant Protein-1 (MCP-1) in the spinal cord as well (213).

Thus, the administration of morphine activates microglia which produce inflammatory cytokines (206). Inflammatory cytokines block the effect of morphine and further activate microglial (213). The inflammation contributes to increased pain which mandates increasing doses of morphine (209). As more morphine is administered, the process amplifies with more inflammation (209). Eventually, for efficacious pain relief, very high doses of morphine must be implemented and thus tolerance has developed (190). Thereby, blocking the activation of microglia could prove to be a successful therapeutic strategy to prevent the onset of opioid tolerance (209). CB₂ receptor activation in microglia induced Mitogen-Activated Protein Kinase Phosphatase-1 (MKP-1) to terminate Mitogen Activated Protein Kinase (MAP-K) signaling in TLR-4 activated cells and attenuated microglial activation (28, 29). Cannabinoid agonists have been shown to preclude microglial production of numerous other cytokines as well (102).

CB₂ agonists have been shown to prevent the induction of hyperalgesia and provide mechanisms to directly produce analgesia (215, 216). The application of CB₂ selective agonists

have been shown to prevent the activation of microglia (215, 216). In a model of chronic morphine administration, selective CB₂ agonists also attenuated the production of IL-1 β and TNF- α in conjunction with prevention of hyperalgesia and allodynia (215). The thermal hyperalgesia and mechanical allodynia in this study could be produced if a selective CB₂ antagonist was given with the CB₂ agonist (215).

Aside from preventing the activation of microglia, CB₂ receptor activation may be working directly on neuronal cells as several authors speculate that the CB₂ receptor is in fact expressed here (215, 217-220). Beltramo references an electrophysiological study that shows CB₂ activation decreases C-fiber mediated activity in spinal cord neurons (218). Further, gene studies have shown CB₂ to be present in the Dorsal Root Ganglia and therefore part of the nociceptive pathway (218, 221). Intranasal but not intravenous administration of CB₂ agonists were also shown to block cocaine seeking behavior (217). This administration technique favors the notion that the CB₂ receptor has a neuronal location as well as a peripheral one (217). However, non-discriminate receptor binding may account for this finding. Immunohistochemistry and molecular techniques have also shown CB₂ receptors to be located on sensory afferents in the dorsal horn of injured nerves (221, 222). The presence of both CB₁ and CB₂ has also been confirmed by flow cytometry on Dorsal Root Ganglion but some controversy remains in regards to the accuracy of the antibodies utilized (223).

However, evidence for an antinociceptive action of CB₂ activation abounds. Numerous studies have shown that activation of said receptor decreases thermal pain, inflammatory hyperalgesia, and c-fos expression (218, 224-226). Studies have shown that CB₂ activation inhibits nociception through cAMP inhibition but does not rely on the μ receptor (221). However, CB₂ activation can generate and promote the release of the endogenous opioid, β -endorphin, which

may contribute to its analgesic effect (227). Win 55,212-2 produces analgesia but the effect is lost in CB₂ -/- mice (228). Thus, the CB₂ receptor may provide a tonic level of activity that sets the sensory threshold for pain modulation (228). To further complicate the situation, studies have shown that anandamide in combination with palmitoylethanolamide decrease pain but either SR141716A or SR144528 can block this effect and both CB₁ and CB₂ receptors are implicated in inflammatory hypersensitivity (229-231). In short, the benefits of a highly selective CB₂ agonist could preclude the onset of tolerance and hyperalgesia not only by blocking microglial activation but also through a number of other neuronal mechanisms that would promote the efficacy of opioid therapy (206, 210, 218).

1.7 Tristimulus Color Theory and Rhodamine 6G Applications

To further some of our studies, we sought to develop a novel method of administering Rhodamine 6G for visualization through a cranial window. Intravital microscopy would prove to be invaluable in understanding some of the mechanistic details behind the photothrombotic stroke. Further, the development of a simplified method to inject Rhodamine 6G could prove beneficial in additional studies later if our laboratory sought to pursue quantification of rolling and adherent leukocytes in either the cerebral ischemia or chronic morphine administration models of pathology.

The blood-brain barrier (BBB) stands as a specialized system of endothelial cells and tight junctions that line the blood vessels supplying blood to the brain. Glial processes and basal lamina, in addition to these endothelial cells, form the BBB and in nonpathological states, provide a reliable and effective barrier to limit transport both into and out of the nervous tissue (232). The BBB endothelial cells differ from other endothelial cells in two important aspects. First of all, BBB endothelial cells have few endocytic vesicles to limit transport of substances into the brain (232). Secondly, tight junctions adjoin BBB endothelial cells to limit paracellular transports (232).

Thus, for most molecules, transport into the brain remains prohibited. The exception lies with small, lipophilic, non-ionized particles with a molecular mass less than 180 Da (232, 233).

However, in pathological states, the integrity of the BBB becomes compromised. Traumatic brain injury, multiple sclerosis, infection, and cerebral ischemia all reduce the ability of the BBB to limit transport into and out of the CNS. In all of these pathologies, peripheral leukocytes enter the brain through weakened and insulted BBB (111, 114, 234-237). The process of leukocyte extravasation begins with rolling and adhesion of leukocytes to the endothelial cells (238). The capability to follow leukocyte rolling and adhesion in pial blood vessels allows for real time quantization of inflammatory processes. Intavital microscopy allows for such visualization and has been employed by scientists to study the process in both stroke and experimental autoimmune encephalomyelitis (EAE) (81, 82).

Leukocytes, but not erythrocytes, contain mitochondria which facilitates the application of epi-illuminescence intravital fluorescence microscopy for evaluation of rolling and adhesion (239). Rhodamine dyes positively charged at physiological pH, including Rhodamine 123, 6G, and 3B stain mitochondria (240, 241). Uncharged rhodamines for example, Rhodamine B, 19, 110, and 116, or negatively charged dyes, such as fluorescein, lack this ability (241). Platelets also contain mitochondria (239) and will take up rhodamine dyes. Thus, clear visualization of platelets and leukocytes can be easily achieved with administration of positively charged rhodamine dyes.

Rhodamine has traditionally been administered through intravenous access as demonstrated by multiple scientists (81, 82, 242). Intravenous access in a rodent, and in particular a mouse, poses multiple difficulties and drawbacks. First of all, most intravenous access requires some degree of surgical skill regardless of the injection site. Whether it is the tail, facial, femoral, saphenous, popliteal, or jugular vein, the technician must be able to cannulate the lumen of the

vein. At the present time, there is no universal method to quantify researcher performance regarding the injections of animals or to verify the administration of experimental compounds (243). The tail vein in mice is very small such that consistent and dependable injections are difficult to perform (243). Further, Groman reported that in a study of tail vein injection success, 40% of injections were improperly administered and considered a failure (243). This study looked at 3 technicians, 2 of which had extensive experience in tail vein injections (243). Those 2 technicians had a combined failure rate of 25% while a third technician only achieved successful injections 30% of the time (243). Such errors in administering compounds could skew preliminary data and drive research into an erroneous direction.

The efficacy of injections into a femoral, saphenous, or popliteal vein of a mouse has not been studied but the site of injection itself poses multiple drawbacks. While researchers probably succeed in cannulating this vessel more than 60% of the time, especially if performed under microscopy, the site of injection has its own set of particular disadvantages. Mice that require kinematic outcome assessments including but not limited to gait analysis by Basso, Beattie, and Bresnahan (BBB) or Basso Mouse Scale (BMS) motor analysis could be complicated by any incisions made to the inner thigh (242).

Extensive dissection of the neck to access the jugular vein could also damage structures affecting gait including descending spinal tracts and muscle attachments on both the ventral surface of the animal and in the neck (242). Additionally, dissection is confounded by multiple vascular and neural microstructures located in the area. Permanent nerve damage, vascular injury, and hemorrhaging remain paramount complications of such surgical endeavors. Lastly, dissection of the neck in a small vertebrate such as a mouse requires extensive training and practice on the part of the technician.

The facial vein stands as a surgical access point for intravenous injection that alleviates many of these complications (242). It mandates a much simpler dissection than that of the vasculature of the neck and also should not interfere with gait and mobility (242). However, since the incision for facial vein injection extends from the external auditory meatus to the ipsilateral canthus, there is a possibility that damage to the eye could occur. Improper closing of the skin could also pull a skin tag over the posterior portion of the eye. These repercussions could affect gait as well as cognitive and memory testing, especially a test like novel-object that relies on heavy visual cues for the animal to respond. Like all other intravenous access sites, entering the connective tissue around the vein without cannulation still exist as a concern (242).

As mentioned, access to the femoral, jugular, and facial veins all require surgery and technical skill to gain competency in administering injections and this competency must be consistent to ensure repeatable experiments. Surgery poses obvious complications in bleeding, infection, and the requirement of anesthesia. Anesthetics can induce significant bradycardia as well as fluctuations in respiratory rate leading to breathing problems commonly associated with surgical procedures and sedation (244, 245). The implementation of anesthesia containing alpha-2-adrenergic agents, such as xylazine, induces considerable bradycardia than can last as long as 5 hours (245). Other reports have suggested that a combinations of ketamine and xylazine lead to fluctuations in multiple physiological parameters including respiratory rates, blood pressure, and body temperature (246). Salivary secretions can build up during periods of anesthesia and increase mortality rate (245). Repeated administrations of anesthesia for longer studies or observations augment these associated risks. More so, the effect of anesthesia varies among animals as a result of the animal's age, endocrine/metabolic status, overall health, nutritional status, sex, and even body temperature (247). Thus, a method to administer rhodamine that alleviated these risks but

also provided reliable and effective delivery to allow for epi-illuminescence intravital fluorescence microscopy would be highly advantageous especially in lengthy studies that historically would have required multiple doses of anesthesia.

Intraperitoneal injection satisfied the objectives of relieving the adverse side effects associated with surgical intravenous access. To our knowledge, no one had examined the efficacy of intraperitoneal rhodamine. Morrey had successfully utilized the intraperitoneal route to administer fluorescein and Manenko employed it in an administration of Evans Blue Stain (248, 249). In a model of intracerebral hemorrhage, after 3 hours of circulation time, there was no statistical difference in the amount of Evans Blue Stain in circulation or in the brain whether it had been administered intravenously or intraperitoneally (249).

The peritoneum presents a large absorptive area in the abdominal cavity (247). As long as the needle is placed below the umbilicus and directed approximately 45° cephalad, little danger exists of piercing abdominal viscera (247). The American Association of Laboratory Animal Science Learning Library recommends inserting the needle along an imaginary line drawn just above the knee, near the midline on the right side of the animal (250). Injecting on the right side avoids accidentally hitting the cecum on the left and the small intestines, situated more so on the right, remain far less likely to be punctured by a needle (250). AALAS recommends entering at a 30° angle to a depth of 5mm and adds that as an extra precaution, aspiration of the needle should be performed to ascertain that the researcher has not struck a blood vessel, intestines, or the urinary bladder. Striking these organs remains a risk of intraperitoneal injection but following the prescribed instructions significantly decreases that risk and the benefit to risk ratio of intraperitoneal injection far outweighs intravenous access.

Much of what is absorbed through intraperitoneal injection enters portal circulation and therefore may undergo hepatic deactivation and metabolism (247). No reports of rhodamine undergoing hepatic metabolism were located in a review of literature. Further, even if rhodamine did succumb to some degree of hepatic metabolism and inactivation, enough might still be functional to make it as useful as an intravenous administration of rhodamine. Therefore, experiments were designed to determine if rhodamine could be administered through the peritoneum and if so, if its effectiveness *in vivo* would deviate from the intravenous method. Experiments needed to be designed to discover if intraperitoneal rhodamine could deliver enough rhodamine to circulation to adequately stain leukocytes for visual detection by the researcher.

Two types of cells account for vision. Scotopic or night-time viewing relies on rod cells and the photosensitive pigment rhodopsin while vision in well-lit conditions, or photopic vision, utilizes cone cells within the retina of the eye (251). In typical light conditions, the cones account for almost all visual information (252). The cone cells also allow an individual to see color vision because of opsins in the outer membrane that have sensitivities that vary according to the wavelength of light being received (251). Perceived color vision comes from the relative contribution of cells excited according to these different spectral sensitivities (251). The peak spectral sensitivity varies according to different authors but blue cones (β) generally peak around 430nm, green cones (γ) around 530, and red cones (ρ) at approximately 560 (251, 253). The maximal spectral sensitivity in the blue range remains the most debated because measurements in these cells are greatly complicated by the fact that products of bleaching absorb blue light in variable amounts but do not create proportional color responses (253). Thus all perceived colors can be created by mixing varying amounts of excitation in specific red, green, or blue sensitive rod cells and thus lays the foundation for Young-Helmholtz Trichromacy Theory (251).

It should be noted that the spectral sensitivity curves for each specific rod overlap such that no green rod can be excited without exciting a corresponding red or blue rod, Figure 1 (253). This overlapping provides the basis for good detection of changes in hue, or the deviation from pure color throughout the visual spectrum (253-256). However, the overall effect of stimulation by Red, Green, and Blue light (R, G, B) can be defined according to a rod's spectral sensitivity to yield

$$\rho = \rho_R + \rho_G + \rho_B$$

$$\gamma = \gamma_R + \gamma_G + \gamma_B$$

$$\beta = \beta_B + \beta_G$$

where ρ = the overall contribution of perceived vision from ρ sensitive rods, ρ_R represents light received by the eye in the range sensitive to ρ rods, ρ_G light received by the eye in both the range of ρ and γ sensitive rods, and ρ_B light received by the eye in both the range of ρ and β sensitive rods (253). A similar pattern exists for γ and β equations. Neuroscience makes note that the β rods do in fact overlap with the ρ rods as opposed to Hunt. If that approach is taken, the final formula should be corrected to include the contribution of the red spectrum, β_R .

Thus, the eye can integrate perceived light by means of varying the amount of three signals. The signals exist analogous to the luminance and color-difference signals used in color television, the R, G, and B, signals and while this is not the case in all animals, current findings suggest it to be true in human vision (253). Expressed light from the source can also be described as a set of three values or vectors in three-dimensional space, the tristimulus values, R, G, and B (257). There exists no coincidence that evolution has produced eyes and neural circuitry that interpret light as a means of three different stimuli and science has developed a method to describe light by three stimuli. For the remainder of the discussion, customary nomenclature of the letter Q, as described

by Wyszecki, will represent an arbitrary color stimulus, while R, G, and B represent the fixed primary stimuli (257).

Rather than a single wavelength, light is a continuous mixture of all the wavelengths across the visible spectrum and perceived color becomes a function of the spectral distribution of amplitude of each wavelength (252). Chromaticity, or color without regard to the intensity of the light, becomes delineated by the shape of the distribution (252). When examining a chromaticity, the amplitude or absolute power level creates the sensation known as intensity (252). Color stimuli are assumed to be uniquely defined by their respective absolute spectral radiant power distributions $\{P_\lambda d\lambda\}$ (257). A specific color stimuli, Q, can be defined as:

$$Q = \{P_\lambda d\lambda\}_Q$$

where P = the power at wavelength λ and $d\lambda$ equals the wavelength of emitted light. The absolute spectral radiant power distributions of the primary stimuli can be denoted by:

$$R = \{\rho P_\lambda d\lambda\}_R$$

$$G = \{\gamma P_\lambda d\lambda\}_G$$

$$B = \{\beta P_\lambda d\lambda\}_B$$

where ρ, γ, β exist as positive constant factors and while related to the cone's sensitivity functions, are not a direct substitution here (257). P_λ equals the power at a certain wavelength and $d\lambda$ signifies the wavelength in question similar to the first equation. The color stimulus, Q, can now be defined as

$$Q = R_Q R + G_Q G + B_Q B$$

where R_Q, G_Q , and B_Q , are scalar multipliers and measured in terms of the assigned respective units of the primary stimuli R, G, and B (257). The unit vectors R, G, and B define space and share a common origin but are orthogonal to each other (257). Vector Q can be calculated from the other

3 vectors given that it has the same origin and its components' lengths correspond to the value of the R_Q , G_Q , and B_Q , Figure 2 (257). R_Q , G_Q , and B_Q , thus, constitute the tristimulus values

The idea that a color stimulus can be formed by 3 primary stimuli, R,G, and B can be expanded to accommodate varying wavelengths of emitted light. The previous relationship, $Q = \{P_\lambda d\lambda\}_Q$ can be considered an additive mixture of a set of stimuli Q_i with spectral power distributions $Q = \{P_\lambda d\lambda\}_{Qi}$ confined to n wavelength intervals of width $(\Delta\lambda)_i$ where $i = 1$ to n (257). The width of the wavelengths intervals may vary as constant width is not a required stipulation, but λ will span the visible spectrum from $\lambda_a = 360$ nm, near the maximal sensitivity of β cones in the blue colors, to $\lambda_b = 830$ nm in the red spectrum and sensitivity of ρ cones(257). Thus for each stimulus:

$$Q_i = R_{Qi}R + G_{Qi}G + B_{Qi}B$$

such that R_{Qi} , G_{Qi} , and B_{Qi} are still tristimulus values of an additive mixture of any stimuli, Q_i (257). The additive mixture of all stimuli Q_i ($i = 1$ to n) must therefore constitute the original stimulus Q , in a manner that:

$$Q = \sum_{i=1}^n Q_i = (\sum_{i=1}^n R_{Qi})R + (\sum_{i=1}^n G_{Qi})G + (\sum_{i=1}^n B_{Qi})B \quad (257).$$

It should be clear that the tristimulus values have now been defined as follows to allow for multiple inputs:

$$R_Q = \sum_{i=1}^n R_{Qi}$$

$$G_Q = \sum_{i=1}^n G_{Qi}$$

$$B_Q = \sum_{i=1}^n B_{Qi}$$

The argument can further be made and shown that the number, n , of wavelengths can be increased and their widths $(\Delta\lambda)_i$ decreased to the point where the width approaches zero (257).

$$\lim_{||(\Delta\lambda)_i|| \rightarrow 0} \sum_{i=1}^n P_{\lambda i} * (\Delta\lambda)_i = P$$

Here $\|(\Delta\lambda)_{i=k}\|$ represents the width of the largest wavelength interval ($i = k$). $P_{\lambda i}$ equals the radiant power at wavelength λ_i located anywhere within the wavelength interval $(\Delta\lambda)_i$ (257). In the equation, the limit P of the sum is the area under the curve defined by the spectral concentration of P_{λ} of radiant power from the wavelengths of visible light beginning with λ_a and ending with λ_b , Figure 3 (257).

Bounding the limits of radiant power to the visible spectrum $[\lambda_a, \lambda_b]$, where $a = 360$ nm and $b = 830$ nm as previously described, allows for the equation to be simplified to an integral:

$$\lim_{\|(\Delta\lambda)_{i=k}\| \rightarrow 0} \sum_{i=1}^n P_{\lambda i} * (\Delta\lambda)_i = \int_{\lambda_a}^{\lambda_b} P_{\lambda} d\lambda \quad (257)$$

Providing that the researcher desires to divide the spectrum into equal widths allows the substitution of $(\Delta\lambda)_i = \Delta\lambda$ so that the equation in terms of the limit simplifies to

$$\lim_{(\Delta\lambda) \rightarrow 0} \sum_{i=1}^n P_{\lambda i} * \Delta\lambda = \int_{\lambda_a}^{\lambda_b} P_{\lambda} d\lambda = P \quad (257)$$

where λ_i stands as the central wavelength in the interval $\Delta\lambda$. The value of $P_{\lambda} d\lambda$ constitutes the radiant power in the wavelength of width $d\lambda$ centered at wavelength λ and also represents the monochromatic stimulus of wavelength λ (257). Lastly for each monochromatic stimulus, the relationship

$$Q_{\lambda} = R_{\lambda}R + G_{\lambda}G + B_{\lambda}B$$

must hold true given the previously derived equations and equalities (257). Thus, for any wavelength of light in the visible spectrum, R_{λ} , G_{λ} , and B_{λ} represent the tristimulus values of a spectral power distribution or visible light source.

Therefore, it has been shown for any source emitting light in the visible spectrum, that light can be described as three vectors comprising the Red, Green, and Blue components of that light. The digital imaging software available in the laboratory allowed for the collection of images,

conversion to multichannel attributes, and finally analysis of each of the Red, Green, and Blue signals. Utilizing this approach would allow quantization of differences in visual characteristics associated with identifying rhodamine labeled cells with the different dye delivery methods implemented. From this point on, the Red, Green, and Blue tristimulus values will be simply denoted by the letters R, G, and B without subscripts. The values of R, G, and B range from 0 to 255. Lower case r, g, and b will imply that the R, G, and B signals were normalized to the range [0,1].

The first parameter examined looked at a quantity called Luma. Poynton defines luminance according to the Commission Internationale de L'Eclairage (CIE) as “the radiant power weighted by a spectral sensitivity function that is characteristic of vision” (258, 259). In regards to the magnitude of luminance, it is proportional to the physical power of the stimuli and in that context seemingly like intensity, but intensity does not take into account the spectral composition as it relates to human vision like luminance does (258). Smith reverberates this notion adding that luminance measures the brightness perceived by a human observing radiant energy and it also takes into account both the signal and the perceptions of the observer (260).

In video imaging, images undergo a gamma correction to adjust for changes in non-linear voltage feeding cathode tubes displaying the Red, Green, and Blue outputs to video monitors (258, 260). Light output from a receiver cathode-ray is approximately proportional to the cube of the applied voltage (253). If logarithm of tube luminance is plotted against the logarithm of applied voltage, the slope of the line obtained is 2.8 ± 0.3 or the accepted index of what is referred to as gamma correction for color receivers (253). Gamma correction is considered a nonlinear distortion and produces a nearly standardized noise sensitivity throughout the color scale (261). Thus, to account for this gamma correction in performing calculations, Poynton argues that the calculation

of luminance from video monitors should appropriately be called luma, not luminance, and denoted Y' due to its nonlinear relationship (258). To calculate luma from Red, Green, and Blue signals in accordance with the National Television System Committee (NTSC), Poynton provides the formula

$$Y' = 0.299R + 0.587G + 0.114B$$

where Y' = Luma, and R, G, and B represent tristimulus values (258). Other researchers have used the same formula to convert to a quantity called gray scale instead of luma (262, 263). Smith argues that color monitors should be considered linear devices since an RGB monitor is assumed to contain a gamma-correction table for each cathode and thus, the correction is applied before the signal is received by the viewer (260). He asserts that the formula for NTSC luminance is

$$L_n = Y = 0.30R + 0.59G + 0.11B$$

where L_n = luminance (260). It looks much like Poynton's formula for non-linear NTSC luma calculations. Haifa investigated utilization of a basic office scanner to quantify electrophoresis gels (254). Of interest is a quantity that he also called gray scale. He converted R, G, and B signals to gray scale and pointed out that in the literature this was not a standardized process, but in the most often employed method, gray scale was set equal to the luminance of the color (254). Linear Red, Green, and Blue signals were obtained and utilized in the equation

$$\text{Gray} = 0.3R + 0.59G + 0.11B$$

with no processing or modifications made to the Red, Green, or Blue signals output from the receiver (254). In accordance with the notion that gray scale equals luminance or luma, black and white television sets only receive only that signal as viewing black and white television remains a matter of observing differences in the luminance (260).

To avoid confusion of the term luminance with other quantities having the same name, the attribute will be termed luma and utilize the formula

$$Y' = 0.299R + 0.587G + 0.114B$$

since it stood in close agreement with other published literature. As a point of comparison, Poynton listed the formula for calculating CIE Luminance, with linear Red, Green, and Blue signals as

$$Y = 0.2126R + 0.7152G + 0.722B \quad (258)$$

The largest difference for any of the three tristimulus values is in the Green value and a difference of 0.1282 from the non-linear formula. Rhodamine has an excitation wavelength of approximately 480 nm and an emission wavelength of 504 nm which does place it close to the green maximal sensitivity of 530 (251, 264, 265). Since the tristimulus values collected range from 0 to 255, at most, the difference in the two formulas would present green as having a difference of 32.69. A difference in luminance of approximately 33 would be unnoticeable and would be imparted on both the intravenous and intraperitoneal groups simultaneously. Ultimately using Poynton's formula for linear attributes would not affect the comparison between the two methods of administration. In short, despite Poynton's assertion that luma should be calculated as non-linear quantities of Red, Green, and Blue stimulus values, and Smith's argument that the values collected have already been corrected to linear quantities, they have utilized the same formulas as did Haifa, Mahmoud-Ghoneim, and Blinn (254, 258, 260, 262, 263).

The Red, Green, and Blue tristimulus values define a color space that can be converted into the HSV, HSL, or HSI color space through mathematic calculation. The HSV and HSL system exist as device independent systems to relay color information and therefore need no calibration on the equipment projecting and receiving the signal (259). The theory behind the development

of these color spaces refers to the originally proposed theory that the Red, Green, and Blue Color Space is composed of three vectors orthogonal to each other. While the collection of Red, Green, and Blue tristimulus values ranges from 0 to 255, the values here will be normalized to 1 such that $r, g, b \in [0,1]$ and the corners of a cube have the coordinates $[0,1] \times [0,1] \times [0,1]$ (259). A new axis will be placed between the points $(0,0,0)$ and $(1,1,1)$ that will form the center of a cylinder and this new axis will be referred to as the achromatic axis along which lie shades of gray such that $R = G = B$ along the achromatic axis (259).

The HSV (hue, saturation, and value) and HSL (hue, saturation, and lightness) color spaces are represented by this cylinder (252, 254, 260). They, in addition to the HSI color space, are more akin to an observer's perception of color than other color spaces (255, 256). The outer circumference represents hue, the radius saturation, and the height of the cylinder value or lightness (254). In each model, hue refers to the pure color or dominant wavelength , and exists as a dimension with points on it normally referred to by basic colors such as red or yellow (253, 254, 256, 260). Hue actually refers to an angle measurement that is measured starting at the direction corresponding to pure red and moves through yellow, blue, and finally back to red as a full revolution through 360° is reached (259, 266). A vector is projected towards $(1,0,0)$, the pure red, while a second vector to the color observed but perpendicular to the achromatic axis and hue is considered the angle between the two (259, 266). Measurements of hue rely on the fact that primary colors are arranged in their natural order with even distancing between them and their compliments around the outer circumference (252). Since the function to calculate hue is non-continuous, points of discontinuity prove problematic as human vision has the tendency to enhance such variations in brightness for any of the three retinal receptor systems (252). These

discontinuities demonstrate Mach binding or the illusion of overly light or dark areas (252). To calculate hue, the following set of functions was employed:

$$h = \begin{cases} \left[60^\circ \times \frac{g-b}{\max-\min} \right] \text{mod}360^\circ, & \text{if } \max = r \\ \left[\left(60^\circ \times \frac{b-r}{\max-\min} \right) + 120^\circ \right] \text{mod}360^\circ, & \text{if } \max = g \\ \left[\left(60^\circ \times \frac{r-g}{\max-\min} \right) + 240^\circ \right] \text{mod}360^\circ, & \text{if } \max = b \end{cases}$$

where h = hue, r, g , and b = R, G, and B normalized to the range [0,1] respectively, \max = the maximal tristimulus value, and \min = the minimum tristimulus value (254). The calculations for hue in the HSV and HSL system do not differ (254). In the HSI Color Model, the formula for calculating hue is

$$\alpha = r - 0.5 \times (g + b)$$

$$\beta = [(\sqrt{3})/2] \times (g - b)$$

$$h = \arctan (\beta/\alpha)$$

where r , g , and b equal the tristimulus values normalized to [0,1] (256).

In the HSV model, the V refers to a quantity called Value. This is the height along the achromatic axis ranging from 0 = black to 1 = white and it measures a departure of hue from black (252, 260). The calculations for which are:

$$v = \max$$

where v =value and \max = the maximal tristimulus value normalized to the range [0,1]. In the HSL model, L refers to lightness. Joblove correlates lightness to intensity and notes that it is defined by the height along the vertical or achromatic axis as well (252). Alternatively, lightness may refer to brightness and intensity although depending on the author's usage, brightness tends to refer to self-luminous objects and lightness to non-self-luminous objects (260). As opposed to value, lightness ranges from black = 0 to white = 0.5 (254, 259). The formula to calculate lightness is

$$l = \frac{1}{2}(\max + \min)$$

where l = lightness, \max = the maximal tristimulus value, and \min = the minimal tristimulus value also normalized to the range [0,1] (254). Another dimension very similar to v and l could also be calculated. The HSI system imposes equal weights on the tristimulus values and defines this as intensity.

$$I = (1/3) \times (r + g + b)$$

where I = intensity and r , g , and b are the R, G, and B tristimulus values normalized to [0,1] respectively (256, 259).

The S in the HSV, HSL, and HSI model refers to a quantity called saturation. Saturation measures the departure of a hue from achromatic, white or gray (260). More so, it represents the purity of a color which varies from pure color at full saturation to a gray equivalent (254, 256). In both the HSL and HSV models, saturation defines the radial component of the cylinder (252). Any vector with fixed lightness or value that has the longest projected color vector will have a maximum saturation of 1 or pure color, while achromatic tones have a saturation of 0 (266). It should be noted, however, that saturation depends on the lightness function chosen and consequently varies in HSL system (259). In the HSL system, saturation is calculated as follows:

$$s = \begin{cases} 0, & \text{if } \max = \min \\ (\max - \min) / (\max + \min) = (\max - \min) / (2l), & \text{if } l \leq 0.5 \\ (\max - \min) / [2 - (\max + \min)] = (\max - \min) / (2 - 2l), & \text{if } l \geq 0.5 \end{cases}$$

where s = saturation, \max = maximal tristimulus value, \min = minimum tristimulus value, and l equals lightness (254). The tristimulus values are normalized to the range [0,1]. In the HSV system, the formula changes to

$$s = \begin{cases} 0, & \text{if } \max = 0 \\ (\max - \min) / \max = 1 - \left(\frac{\min}{\max} \right), & \text{otherwise} \end{cases}$$

where s = saturation, max = the maximal tristimulus value, and min = the minimum tristimulus value normalized to [0,1] (254). In the HSI system the method is slightly more straight forward and defined as

$$\alpha = r - 0.5 \times (g + b)$$

$$\beta = [(\sqrt{3})/2] \times (g - b)$$

$$s = \sqrt{(\alpha^2 + \beta^2)}$$

where r, g, and b equal the tristimulus values normalized to [0,1] (256).

An understanding of these attributes as they pertain to rhodamine in an in vivo system could prove to be hugely beneficial to other researchers. Currently a number of laboratories are working to write computer algorithms to analyze a myriad of images remotely collected from patients. For instance, Li has studied the usefulness of the HSI system to analyze images from wireless capsule endoscopy with images of the gastrointestinal tract in hopes of decreasing the amount of physician time required for review of such clinical studies (256). Other researchers are exploring an analysis of light microscopic images in the detection of liver fibrosis from such attributes as HSI (262, 267). To our knowledge, no one has ever characterized properties such as luma, hue, value, lightness, or saturation in utilizing in vivo administration of Rhodamine 6G. A characterization of Rhodamine 6G in terms of these physical parameters may allow for computer based algorithms to detect rhodamine stained cells and enhance in vivo tracking with greater precision and less time by the researcher.

To effectively measure these parameters and determine if any differences among the administration techniques existed, an understanding of the nature of light in both the way a radiant body transmits it as well as the way an observer perceives it would be needed to accomplish such a task. Here it has been detailed in the ways in which the eye can detect different colors as a matter

of cone cell sensitivity. A justification for describing light by a set of three values comprising red, green, and blue components has also been provided and paralleled to the eyes' sensitivity. Further, the acquisition of these tristimulus values allows for calculating the aforementioned qualities that would allow the experiment to describe any differences in the effect of administration route of Rhodamine 6G *in vivo*.

In short, a method to administer rhodamine without surgery and anesthesia would greatly facilitate intravital microscopy as it would decrease adverse reactions to medication, surgical complications, and require less skill on the part of the technician overall reducing errors in experimentation. The first experiments explored basic principles of colorimetry comparing the administration methods. After taking peripheral blood and preparing slides, a number of parameters including luma, value, intensity, hue, and lastly saturation were able to be quantified and evaluated over the course of 8 hours. Next, cranial windows were implanted and the luma, measured through the window, was accessed among each group. Both techniques delivered enough rhodamine to easily allow for visual detection of cells. Rolling and adhered cells were also quantified to see if the administration techniques would affect the number of visible cells. Finally, flow cytometry was employed to obtain a very precise snapshot of staining efficacy and fluorescent signal.

1.8 Works Cited

1. Mechoulam R. *Cannabinoids as therapeutic agents*. Boca Raton, Fla.: CRC Press; 1986.
2. Pacher P, Bátkai S, Kunos G. The endocannabinoid system as an emerging target of pharmacotherapy. *Pharmacol Rev*. 2006;58(3):389-462. doi: 10.1124/pr.58.3.2.
3. Iversen LL. *The science of marijuana*. Oxford ; New York: Oxford University Press; 2000.
4. Lutz B. Molecular biology of cannabinoid receptors. *Prostaglandins Leukot Essent Fatty Acids*. 2002;66(2-3):123-42. doi: 10.1054/plef.2001.0342.
5. Abood ME. Molecular biology of cannabinoid receptors. *Handb Exp Pharmacol*. 2005;(168):81-115.
6. Howlett AC. Cannabinoid receptor signaling. *Handb Exp Pharmacol*. 2005;(168):53-79.
7. Tuma RF, Steffens S. Targeting the endocannabinoid system to limit myocardial and cerebral ischemic and reperfusion injury. *Curr Pharm Biotechnol*. 2012;13(1):46-58.
8. Pertwee RG, Ross RA. Cannabinoid receptors and their ligands. *Prostaglandins Leukot Essent Fatty Acids*. 2002;66(2-3):101-21. doi: 10.1054/plef.2001.0341.
9. Sánchez AJ, García-Merino A. Neuroprotective agents: cannabinoids. *Clin Immunol*. 2012;142(1):57-67. doi: 10.1016/j.clim.2011.02.010.
10. Begg M, Pacher P, Bátkai S, Osei-Hyiaman D, Offertáler L, Mo FM, et al. Evidence for novel cannabinoid receptors. *Pharmacol Ther*. 2005;106(2):133-45. doi: 10.1016/j.pharmthera.2004.11.005.
11. Golech SA, McCarron RM, Chen Y, Bembry J, Lenz F, Mechoulam R, et al. Human brain endothelium: coexpression and function of vanilloid and endocannabinoid receptors. *Brain Res Mol Brain Res*. 2004;132(1):87-92. doi: 10.1016/j.molbrainres.2004.08.025.
12. Mestre L, Íñigo PM, Mecha M, Correa FG, Hernangómez-Herrero M, Loría F, et al. Anandamide inhibits Theiler's virus induced VCAM-1 in brain endothelial cells and reduces

leukocyte transmigration in a model of blood brain barrier by activation of CB(1) receptors. *J Neuroinflammation*. 2011;8:102. doi: 10.1186/1742-2094-8-102.

13. Liu J, Gao B, Mirshahi F, Sanyal AJ, Khanolkar AD, Makriyannis A, et al. Functional CB1 cannabinoid receptors in human vascular endothelial cells. *Biochem J*. 2000;346 Pt 3:835-40.

14. Bouaboula M, Rinaldi M, Carayon P, Carillon C, Delpech B, Shire D, et al. Cannabinoid-receptor expression in human leukocytes. *Eur J Biochem*. 1993;214(1):173-80.

15. Van Sickle MD, Duncan M, Kingsley PJ, Mouihate A, Urbani P, Mackie K, et al. Identification and functional characterization of brainstem cannabinoid CB2 receptors. *Science*. 2005;310(5746):329-32. doi: 10.1126/science.1115740.

16. Färber K, Kettenmann H. Physiology of microglial cells. *Brain Res Brain Res Rev*. 2005;48(2):133-43. doi: 10.1016/j.brainresrev.2004.12.003.

17. Gong JP, Onaivi ES, Ishiguro H, Liu QR, Tagliaferro PA, Brusco A, et al. Cannabinoid CB2 receptors: immunohistochemical localization in rat brain. *Brain Res*. 2006;1071(1):10-23. doi: 10.1016/j.brainres.2005.11.035.

18. Herkenham M, Lynn AB, de Costa BR, Richfield EK. Neuronal localization of cannabinoid receptors in the basal ganglia of the rat. *Brain Res*. 1991;547(2):267-74.

19. Katona I, Sperlágh B, Sík A, Käfalvi A, Vizi ES, Mackie K, et al. Presynaptically located CB1 cannabinoid receptors regulate GABA release from axon terminals of specific hippocampal interneurons. *J Neurosci*. 1999;19(11):4544-58.

20. Hájos N, Katona I, Naiem SS, MacKie K, Ledent C, Mody I, et al. Cannabinoids inhibit hippocampal GABAergic transmission and network oscillations. *Eur J Neurosci*. 2000;12(9):3239-49.

21. Katona I, Sperlágh B, Maglóczky Z, Sántha E, Köfalvi A, Czirják S, et al. GABAergic interneurons are the targets of cannabinoid actions in the human hippocampus. *Neuroscience*. 2000;100(4):797-804.

22. Di Marzo V. Targeting the endocannabinoid system: to enhance or reduce? *Nat Rev Drug Discov*. 2008;7(5):438-55. doi: 10.1038/nrd2553.

23. Elphick MR, Egertová M. The neurobiology and evolution of cannabinoid signalling. *Philos Trans R Soc Lond B Biol Sci.* 2001;356(1407):381-408. doi: 10.1098/rstb.2000.0787.
24. Sokal DM, Benetti C, Girlanda E, Large CH. The CB1 receptor antagonist, SR141716A, prevents high-frequency stimulation-induced reduction of feedback inhibition in the rat dentate gyrus following perforant path stimulation *in vivo*. *Brain Res.* 2008;1223:50-8. doi: 10.1016/j.brainres.2008.05.065.
25. Berdyshev EV. Cannabinoid receptors and the regulation of immune response. *Chem Phys Lipids.* 2000;108(1-2):169-90.
26. Rhee MH, Bayewitch M, Avidor-Reiss T, Levy R, Vogel Z. Cannabinoid receptor activation differentially regulates the various adenylyl cyclase isoforms. *J Neurochem.* 1998;71(4):1525-34.
27. Rhee MH, Nevo I, Avidor-Reiss T, Levy R, Vogel Z. Differential superactivation of adenylyl cyclase isoforms after chronic activation of the CB(1) cannabinoid receptor. *Mol Pharmacol.* 2000;57(4):746-52.
28. Eljaschewitsch E, Witting A, Mawrin C, Lee T, Schmidt PM, Wolf S, et al. The endocannabinoid anandamide protects neurons during CNS inflammation by induction of MKP-1 in microglial cells. *Neuron.* 2006;49(1):67-79. doi: 10.1016/j.neuron.2005.11.027.
29. Rivest S. Cannabinoids in microglia: a new trick for immune surveillance and neuroprotection. *Neuron.* 2006;49(1):4-8. doi: 10.1016/j.neuron.2005.12.004.
30. Mukhopadhyay S, Shim JY, Assi AA, Norford D, Howlett AC. CB(1) cannabinoid receptor-G protein association: a possible mechanism for differential signaling. *Chem Phys Lipids.* 2002;121(1-2):91-109.
31. Bouaboula M, Poinot-Chazel C, Bourrié B, Canat X, Calandra B, Rinaldi-Carmona M, et al. Activation of mitogen-activated protein kinases by stimulation of the central cannabinoid receptor CB1. *Biochem J.* 1995;312 (Pt 2):637-41.
32. Bouaboula M, Dussossoy D, Casellas P. Regulation of peripheral cannabinoid receptor CB2 phosphorylation by the inverse agonist SR 144528. Implications for receptor biological responses. *J Biol Chem.* 1999;274(29):20397-405.

33. Howlett AC. Efficacy in CB1 receptor-mediated signal transduction. *Br J Pharmacol.* 2004;142(8):1209-18. doi: 10.1038/sj.bjp.0705881.
34. Basu S, Dittel BN. Unraveling the complexities of cannabinoid receptor 2 (CB2) immune regulation in health and disease. *Immunol Res.* 2011;51(1):26-38. doi: 10.1007/s12026-011-8210-5.
35. Mackie K, Hille B. Cannabinoids inhibit N-type calcium channels in neuroblastoma-glioma cells. *Proc Natl Acad Sci U S A.* 1992;89(9):3825-9.
36. Gebremedhin D, Lange AR, Campbell WB, Hillard CJ, Harder DR. Cannabinoid CB1 receptor of cat cerebral arterial muscle functions to inhibit L-type Ca²⁺ channel current. *Am J Physiol.* 1999;276(6 Pt 2):H2085-93.
37. Mackie K, Lai Y, Westenbroek R, Mitchell R. Cannabinoids activate an inwardly rectifying potassium conductance and inhibit Q-type calcium currents in AtT20 cells transfected with rat brain cannabinoid receptor. *J Neurosci.* 1995;15(10):6552-61.
38. Pan X, Ikeda SR, Lewis DL. Rat brain cannabinoid receptor modulates N-type Ca²⁺ channels in a neuronal expression system. *Mol Pharmacol.* 1996;49(4):707-14.
39. Caulfield MP, Brown DA. Cannabinoid receptor agonists inhibit Ca current in NG108-15 neuroblastoma cells via a pertussis toxin-sensitive mechanism. *Br J Pharmacol.* 1992;106(2):231-2.
40. Pan X, Ikeda SR, Lewis DL. SR 141716A acts as an inverse agonist to increase neuronal voltage-dependent Ca²⁺ currents by reversal of tonic CB1 cannabinoid receptor activity. *Mol Pharmacol.* 1998;54(6):1064-72.
41. Sugiura T, Kodaka T, Kondo S, Tonegawa T, Nakane S, Kishimoto S, et al. 2-Arachidonoylglycerol, a putative endogenous cannabinoid receptor ligand, induces rapid, transient elevation of intracellular free Ca²⁺ in neuroblastoma x glioma hybrid NG108-15 cells. *Biochem Biophys Res Commun.* 1996;229(1):58-64. doi: 10.1006/bbrc.1996.1757.
42. Bash R, Rubovitch V, Gafni M, Sarne Y. The stimulatory effect of cannabinoids on calcium uptake is mediated by Gs GTP-binding proteins and cAMP formation. *Neurosignals.* 2003;12(1):39-44. doi: 68915.

43. Netzeband JG, Conroy SM, Parsons KL, Gruol DL. Cannabinoids enhance NMDA-elicited Ca²⁺ signals in cerebellar granule neurons in culture. *J Neurosci*. 1999;19(20):8765-77.
44. Henry DJ, Chavkin C. Activation of inwardly rectifying potassium channels (GIRK1) by co-expressed rat brain cannabinoid receptors in *Xenopus* oocytes. *Neurosci Lett*. 1995;186(2-3):91-4.
45. McAllister SD, Griffin G, Satin LS, Abood ME. Cannabinoid receptors can activate and inhibit G protein-coupled inwardly rectifying potassium channels in a *xenopus* oocyte expression system. *J Pharmacol Exp Ther*. 1999;291(2):618-26.
46. Di Marzo V, Petrosino S. Endocannabinoids and the regulation of their levels in health and disease. *Curr Opin Lipidol*. 2007;18(2):129-40. doi: 10.1097/MOL.0b013e32803dbdec.
47. Niforatos W, Zhang XF, Lake MR, Walter KA, Neelands T, Holzman TF, et al. Activation of TRPA1 channels by the fatty acid amide hydrolase inhibitor 3'-carbamoylbiphenyl-3-yl cyclohexylcarbamate (URB597). *Mol Pharmacol*. 2007;71(5):1209-16. doi: 10.1124/mol.106.033621.
48. Burstein S, Budrow J, Debatis M, Hunter SA, Subramanian A. Phospholipase participation in cannabinoid-induced release of free arachidonic acid. *Biochem Pharmacol*. 1994;48(6):1253-64.
49. Shivachar AC, Martin BR, Ellis EF. Anandamide- and delta9-tetrahydrocannabinol-evoked arachidonic acid mobilization and blockade by SR141716A [N-(Piperidin-1-yl)-5-(4-chlorophenyl)-1-(2,4-dichlorophenyl)-4-methyl-1H-pyrazole-3-carboximide hydrochloride]. *Biochem Pharmacol*. 1996;51(5):669-76.
50. Wartmann M, Campbell D, Subramanian A, Burstein SH, Davis RJ. The MAP kinase signal transduction pathway is activated by the endogenous cannabinoid anandamide. *FEBS Lett*. 1995;359(2-3):133-6.
51. Gómez del Pulgar T, Velasco G, Guzmán M. The CB1 cannabinoid receptor is coupled to the activation of protein kinase B/Akt. *Biochem J*. 2000;347(Pt 2):369-73.
52. Gómez Del Pulgar T, De Ceballos ML, Guzmán M, Velasco G. Cannabinoids protect astrocytes from ceramide-induced apoptosis through the phosphatidylinositol 3-kinase/protein kinase B pathway. *J Biol Chem*. 2002;277(39):36527-33. doi: 10.1074/jbc.M205797200.

53. Cannich A, Wotjak CT, Kamprath K, Hermann H, Lutz B, Marsicano G. CB1 cannabinoid receptors modulate kinase and phosphatase activity during extinction of conditioned fear in mice. *Learn Mem.* 2004;11(5):625-32. doi: 10.1101/lm.77904.
54. Merighi S, Gessi S, Varani K, Simioni C, Fazzi D, Mirandola P, et al. Cannabinoid CB(2) receptors modulate ERK-1/2 kinase signalling and NO release in microglial cells stimulated with bacterial lipopolysaccharide. *Br J Pharmacol.* 2012;165(6):1773-88. doi: 10.1111/j.1476-5381.2011.01673.x.
55. Derkinderen P, Ledent C, Parmentier M, Girault JA. Cannabinoids activate p38 mitogen-activated protein kinases through CB1 receptors in hippocampus. *J Neurochem.* 2001;77(3):957-60.
56. Rueda D, Galve-Roperh I, Haro A, Guzmán M. The CB(1) cannabinoid receptor is coupled to the activation of c-Jun N-terminal kinase. *Mol Pharmacol.* 2000;58(4):814-20.
57. Davis MI, Ronesi J, Lovinger DM. A predominant role for inhibition of the adenylate cyclase/protein kinase A pathway in ERK activation by cannabinoid receptor 1 in N1E-115 neuroblastoma cells. *J Biol Chem.* 2003;278(49):48973-80. doi: 10.1074/jbc.M305697200.
58. Valjent E, Pagès C, Hervé D, Girault JA, Caboche J. Addictive and non-addictive drugs induce distinct and specific patterns of ERK activation in mouse brain. *Eur J Neurosci.* 2004;19(7):1826-36. doi: 10.1111/j.1460-9568.2004.03278.x.
59. Bouaboula M, Poinot-Chazel C, Marchand J, Canat X, Bourrié B, Rinaldi-Carmona M, et al. Signaling pathway associated with stimulation of CB2 peripheral cannabinoid receptor. Involvement of both mitogen-activated protein kinase and induction of Krox-24 expression. *Eur J Biochem.* 1996;237(3):704-11.
60. Fimiani C, Liberty T, Aquirre AJ, Amin I, Ali N, Stefano GB. Opiate, cannabinoid, and eicosanoid signaling converges on common intracellular pathways nitric oxide coupling. *Prostaglandins Other Lipid Mediat.* 1999;57(1):23-34.
61. Stefano GB, Salzet B, Salzet M. Identification and characterization of the leech CNS cannabinoid receptor: coupling to nitric oxide release. *Brain Res.* 1997;753(2):219-24.
62. Fimiani C, Mattocks D, Cavani F, Salzet M, Deutsch DG, Pryor S, et al. Morphine and anandamide stimulate intracellular calcium transients in human arterial endothelial cells: coupling to nitric oxide release. *Cell Signal.* 1999;11(3):189-93.

63. Maccarrone M, Bari M, Lorenzon T, Bisogno T, Di Marzo V, Finazzi-Agrò A. Anandamide uptake by human endothelial cells and its regulation by nitric oxide. *J Biol Chem.* 2000;275(18):13484-92.
64. Jeon YJ, Yang KH, Pulaski JT, Kaminski NE. Attenuation of inducible nitric oxide synthase gene expression by delta 9-tetrahydrocannabinol is mediated through the inhibition of nuclear factor- kappa B/Rel activation. *Mol Pharmacol.* 1996;50(2):334-41.
65. Molina-Holgado F, Pinteaux E, Moore JD, Molina-Holgado E, Guaza C, Gibson RM, et al. Endogenous interleukin-1 receptor antagonist mediates anti-inflammatory and neuroprotective actions of cannabinoids in neurons and glia. *J Neurosci.* 2003;23(16):6470-4.
66. Bouaboula M, Perrachon S, Milligan L, Canat X, Rinaldi-Carmona M, Portier M, et al. A selective inverse agonist for central cannabinoid receptor inhibits mitogen-activated protein kinase activation stimulated by insulin or insulin-like growth factor 1. Evidence for a new model of receptor/ligand interactions. *J Biol Chem.* 1997;272(35):22330-9.
67. Katzung BG. Basic & clinical pharmacology. 9th ed. New York: Lange Medical Books/McGraw Hill; 2004.
68. Bouaboula M, Desnoyer N, Carayon P, Combes T, Casellas P. Gi protein modulation induced by a selective inverse agonist for the peripheral cannabinoid receptor CB2: implication for intracellular signalization cross-regulation. *Mol Pharmacol.* 1999;55(3):473-80.
69. Hsieh C, Brown S, Derleth C, Mackie K. Internalization and recycling of the CB1 cannabinoid receptor. *J Neurochem.* 1999;73(2):493-501.
70. Jin W, Brown S, Roche JP, Hsieh C, Celver JP, Kovoor A, et al. Distinct domains of the CB1 cannabinoid receptor mediate desensitization and internalization. *J Neurosci.* 1999;19(10):3773-80.
71. Smith TH, Sim-Selley LJ, Selley DE. Cannabinoid CB1 receptor-interacting proteins: novel targets for central nervous system drug discovery? *Br J Pharmacol.* 2010;160(3):454-66. doi: 10.1111/j.1476-5381.2010.00777.x.
72. Reiter E, Lefkowitz RJ. GRKs and beta-arrestins: roles in receptor silencing, trafficking and signaling. *Trends Endocrinol Metab.* 2006;17(4):159-65. doi: 10.1016/j.tem.2006.03.008.

73. Wu DF, Yang LQ, Goschke A, Stumm R, Brandenburg LO, Liang YJ, et al. Role of receptor internalization in the agonist-induced desensitization of cannabinoid type 1 receptors. *J Neurochem*. 2008;104(4):1132-43. doi: 10.1111/j.1471-4159.2007.05063.x.
74. Martini L, Waldhoer M, Pusch M, Kharazia V, Fong J, Lee JH, et al. Ligand-induced down-regulation of the cannabinoid 1 receptor is mediated by the G-protein-coupled receptor-associated sorting protein GASP1. *FASEB J*. 2007;21(3):802-11. doi: 10.1096/fj.06-7132com.
75. Schmid HH, Schmid PC, Berdyshev EV. Cell signaling by endocannabinoids and their congeners: questions of selectivity and other challenges. *Chem Phys Lipids*. 2002;121(1-2):111-34.
76. Parolaro D, Massi P, Rubino T, Monti E. Endocannabinoids in the immune system and cancer. *Prostaglandins Leukot Essent Fatty Acids*. 2002;66(2-3):319-32. doi: 10.1054/plef.2001.0355.
77. Gulyas AI, Cravatt BF, Bracey MH, Dinh TP, Piomelli D, Boscia F, et al. Segregation of two endocannabinoid-hydrolyzing enzymes into pre- and postsynaptic compartments in the rat hippocampus, cerebellum and amygdala. *Eur J Neurosci*. 2004;20(2):441-58. doi: 10.1111/j.1460-9568.2004.03428.x.
78. Gonsiorek W, Lunn C, Fan X, Narula S, Lundell D, Hipkin RW. Endocannabinoid 2-arachidonyl glycerol is a full agonist through human type 2 cannabinoid receptor: antagonism by anandamide. *Mol Pharmacol*. 2000;57(5):1045-50.
79. Börner C, Smida M, Höllt V, Schraven B, Kraus J. Cannabinoid receptor type 1- and 2-mediated increase in cyclic AMP inhibits T cell receptor-triggered signaling. *J Biol Chem*. 2009;284(51):35450-60. doi: 10.1074/jbc.M109.006338.
80. Cabral GA, Raborn ES, Griffin L, Dennis J, Marciano-Cabral F. CB2 receptors in the brain: role in central immune function. *Br J Pharmacol*. 2008;153(2):240-51. doi: 10.1038/sj.bjp.0707584.
81. Zhang M, Adler MW, Abood ME, Ganea D, Jallo J, Tuma RF. CB2 receptor activation attenuates microcirculatory dysfunction during cerebral ischemic/reperfusion injury. *Microvasc Res*. 2009;78(1):86-94. doi: 10.1016/j.mvr.2009.03.005.
82. Zhang M, Martin BR, Adler MW, Razdan RJ, Kong W, Ganea D, et al. Modulation of cannabinoid receptor activation as a neuroprotective strategy for EAE and stroke. *J Neuroimmune Pharmacol*. 2009;4(2):249-59. doi: 10.1007/s11481-009-9148-4.

83. Ramirez SH, Haskó J, Skuba A, Fan S, Dykstra H, McCormick R, et al. Activation of cannabinoid receptor 2 attenuates leukocyte-endothelial cell interactions and blood-brain barrier dysfunction under inflammatory conditions. *J Neurosci.* 2012;32(12):4004-16. doi: 10.1523/JNEUROSCI.4628-11.2012.
84. McCoy KL, Matveyeva M, Carlisle SJ, Cabral GA. Cannabinoid inhibition of the processing of intact lysozyme by macrophages: evidence for CB2 receptor participation. *J Pharmacol Exp Ther.* 1999;289(3):1620-5.
85. Wallace JM, Tashkin DP, Oishi JS, Barbers RG. Peripheral blood lymphocyte subpopulations and mitogen responsiveness in tobacco and marijuana smokers. *J Psychoactive Drugs.* 1988;20(1):9-14.
86. Schatz AR, Koh WS, Kaminski NE. Delta 9-tetrahydrocannabinol selectively inhibits T-cell dependent humoral immune responses through direct inhibition of accessory T-cell function. *Immunopharmacology.* 1993;26(2):129-37.
87. Klein TW, Newton C, Friedman H. Inhibition of natural killer cell function by marijuana components. *J Toxicol Environ Health.* 1987;20(4):321-32. doi: 10.1080/15287398709530986.
88. Klein TW, Kawakami Y, Newton C, Friedman H. Marijuana components suppress induction and cytolytic function of murine cytotoxic T cells in vitro and in vivo. *J Toxicol Environ Health.* 1991;32(4):465-77. doi: 10.1080/15287399109531496.
89. Berdyshev E, Boichot E, Corbel M, Germain N, Lagente V. Effects of cannabinoid receptor ligands on LPS-induced pulmonary inflammation in mice. *Life Sci.* 1998;63(8):PL125-9.
90. Zheng ZM, Specter S, Friedman H. Inhibition by delta-9-tetrahydrocannabinol of tumor necrosis factor alpha production by mouse and human macrophages. *Int J Immunopharmacol.* 1992;14(8):1445-52.
91. Zheng ZM, Specter SC. Delta-9-tetrahydrocannabinol suppresses tumor necrosis factor alpha maturation and secretion but not its transcription in mouse macrophages. *Int J Immunopharmacol.* 1996;18(1):53-68.
92. Smith SR, Terminelli C, Denhardt G. Effects of cannabinoid receptor agonist and antagonist ligands on production of inflammatory cytokines and anti-inflammatory interleukin-10 in endotoxemic mice. *J Pharmacol Exp Ther.* 2000;293(1):136-50.

93. Berdyshev EV, Boichot E, Germain N, Allain N, Anger JP, Lagente V. Influence of fatty acid ethanolamides and delta9-tetrahydrocannabinol on cytokine and arachidonate release by mononuclear cells. *Eur J Pharmacol.* 1997;330(2-3):231-40.
94. Bátkai S, Osei-Hyiaman D, Pan H, El-Assal O, Rajesh M, Mukhopadhyay P, et al. Cannabinoid-2 receptor mediates protection against hepatic ischemia/reperfusion injury. *FASEB J.* 2007;21(8):1788-800. doi: 10.1096/fj.06-7451com.
95. Blanchard DK, Newton C, Klein TW, Stewart WE, Friedman H. In vitro and in vivo suppressive effects of delta-9-tetrahydrocannabinol on interferon production by murine spleen cells. *Int J Immunopharmacol.* 1986;8(7):819-24.
96. Maresz K, Pryce G, Ponomarev ED, Marsicano G, Croxford JL, Shriver LP, et al. Direct suppression of CNS autoimmune inflammation via the cannabinoid receptor CB1 on neurons and CB2 on autoreactive T cells. *Nat Med.* 2007;13(4):492-7. doi: 10.1038/nm1561.
97. Murikinati S, Jüttler E, Keinert T, Ridder DA, Muhammad S, Waibler Z, et al. Activation of cannabinoid 2 receptors protects against cerebral ischemia by inhibiting neutrophil recruitment. *FASEB J.* 2010;24(3):788-98. doi: 10.1096/fj.09-141275.
98. Correa F, Docagne F, Mestre L, Clemente D, Hernangómez M, Loría F, et al. A role for CB2 receptors in anandamide signalling pathways involved in the regulation of IL-12 and IL-23 in microglial cells. *Biochem Pharmacol.* 2009;77(1):86-100. doi: 10.1016/j.bcp.2008.09.014.
99. Csóka B, Németh ZH, Mukhopadhyay P, Spolarics Z, Rajesh M, Federici S, et al. CB2 cannabinoid receptors contribute to bacterial invasion and mortality in polymicrobial sepsis. *PLoS One.* 2009;4(7):e6409. doi: 10.1371/journal.pone.0006409.
100. Tschöp J, Kasten KR, Nogueiras R, Goetzman HS, Cave CM, England LG, et al. The cannabinoid receptor 2 is critical for the host response to sepsis. *J Immunol.* 2009;183(1):499-505. doi: 10.4049/jimmunol.0900203.
101. Kraft B, Wintersberger W, Kress HG. Cannabinoid receptor-independent suppression of the superoxide generation of human neutrophils (PMN) by CP55 940, but not by anandamide. *Life Sci.* 2004;75(8):969-77. doi: 10.1016/j.lfs.2004.02.007.
102. Puffenbarger RA, Boothe AC, Cabral GA. Cannabinoids inhibit LPS-inducible cytokine mRNA expression in rat microglial cells. *Glia.* 2000;29(1):58-69.

103. Börner C, Bedini A, Höllt V, Kraus J. Analysis of promoter regions regulating basal and interleukin-4-inducible expression of the human CB1 receptor gene in T lymphocytes. *Mol Pharmacol.* 2008;73(3):1013-9. doi: 10.1124/mol.107.042945.
104. Nilsson O, Fowler CJ, Jacobsson SO. The cannabinoid agonist WIN 55,212-2 inhibits TNF-alpha-induced neutrophil transmigration across ECV304 cells. *Eur J Pharmacol.* 2006;547(1-3):165-73. doi: 10.1016/j.ejphar.2006.07.016.
105. Smith SR, Denhardt G, Terminelli C. The anti-inflammatory activities of cannabinoid receptor ligands in mouse peritonitis models. *Eur J Pharmacol.* 2001;432(1):107-19.
106. Stefano GB, Salzet M, Rialas CM, Mattocks D, Fimiani C, Bilfinger TV. Macrophage behavior associated with acute and chronic exposure to HIV GP120, morphine and anandamide: endothelial implications. *Int J Cardiol.* 1998;64 Suppl 1:S3-13.
107. McHugh D, Tanner C, Mechoulam R, Pertwee RG, Ross RA. Inhibition of human neutrophil chemotaxis by endogenous cannabinoids and phytocannabinoids: evidence for a site distinct from CB1 and CB2. *Mol Pharmacol.* 2008;73(2):441-50. doi: 10.1124/mol.107.041863.
108. Go AS, Mozaffarian D, Roger VL, Benjamin EJ, Berry JD, Borden WB, et al. Executive summary: heart disease and stroke statistics--2013 update: a report from the American Heart Association. *Circulation.* 2013;127(1):143-52. doi: 10.1161/CIR.0b013e318282ab8f.
109. Vermeer SE, Longstreth WT, Koudstaal PJ. Silent brain infarcts: a systematic review. *Lancet Neurol.* 2007;6(7):611-9. doi: 10.1016/S1474-4422(07)70170-9.
110. Das RR, Seshadri S, Beiser AS, Kelly-Hayes M, Au R, Himali JJ, et al. Prevalence and correlates of silent cerebral infarcts in the Framingham offspring study. *Stroke.* 2008;39(11):2929-35. doi: 10.1161/STROKEAHA.108.516575.
111. Lakhan SE, Kirchgessner A, Hofer M. Inflammatory mechanisms in ischemic stroke: therapeutic approaches. *J Transl Med.* 2009;7:97. doi: 10.1186/1479-5876-7-97.
112. Russo T, Felzani G, Marini C. Stroke in the very old: a systematic review of studies on incidence, outcome, and resource use. *J Aging Res.* 2011;2011:108785. doi: 10.4061/2011/108785.
113. Donnan GA, Fisher M, Macleod M, Davis SM. Stroke. *Lancet.* 2008;371(9624):1612-23. doi: 10.1016/S0140-6736(08)60694-7.

114. Jin R, Yang G, Li G. Inflammatory mechanisms in ischemic stroke: role of inflammatory cells. *J Leukoc Biol.* 2010;87(5):779-89. doi: 10.1189/jlb.1109766.
115. Kelly-Hayes M, Beiser A, Kase CS, Scaramucci A, D'Agostino RB, Wolf PA. The influence of gender and age on disability following ischemic stroke: the Framingham study. *J Stroke Cerebrovasc Dis.* 2003;12(3):119-26. doi: 10.1016/S1052-3057(03)00042-9.
116. Brown DL, Boden-Albala B, Langa KM, Lisabeth LD, Fair M, Smith MA, et al. Projected costs of ischemic stroke in the United States. *Neurology.* 2006;67(8):1390-5. doi: 10.1212/01.wnl.0000237024.16438.20.
117. Kriz J. Inflammation in ischemic brain injury: timing is important. *Crit Rev Neurobiol.* 2006;18(1-2):145-57.
118. Caswell J. Stroke Connection: Winter 2013. *Stroke Connection:* American Heart Association; 2013.
119. Hillard CJ. Role of cannabinoids and endocannabinoids in cerebral ischemia. *Curr Pharm Des.* 2008;14(23):2347-61.
120. Muir KW, Tyrrell P, Sattar N, Warburton E. Inflammation and ischaemic stroke. *Curr Opin Neurol.* 2007;20(3):334-42. doi: 10.1097/WCO.0b013e32813ba151.
121. Kumar V, Abbas AK, Fausto N, Robbins SL, Cotran RS. Robbins and Cotran pathologic basis of disease. 7th ed. Philadelphia: Elsevier Saunders; 2005.
122. Shichita T, Sugiyama Y, Ooboshi H, Sugimori H, Nakagawa R, Takada I, et al. Pivotal role of cerebral interleukin-17-producing gammadeltaT cells in the delayed phase of ischemic brain injury. *Nat Med.* 2009;15(8):946-50. doi: 10.1038/nm.1999.
123. Liesz A, Suri-Payer E, Veltkamp C, Doerr H, Sommer C, Rivest S, et al. Regulatory T cells are key cerebroprotective immunomodulators in acute experimental stroke. *Nat Med.* 2009;15(2):192-9. doi: 10.1038/nm.1927.
124. McPhee SJ, Ganong WF. Pathophysiology of Disease An Introduction to Clinical Medicine. 5th ed. New York2006.
125. Choi D. Stroke. *Neurobiol Dis.* 2000;7(5):552-8. doi: 10.1006/nbdi.2000.0354.

126. Limmer D, Adams BL, Dickinson ET. Emergency care. 9th ed. Upper Saddle River, NJ: Brady/Prentice Hall Health; 2001.
127. Lo EH, Dalkara T, Moskowitz MA. Mechanisms, challenges and opportunities in stroke. *Nat Rev Neurosci*. 2003;4(5):399-415. doi: 10.1038/nrn1106.
128. Lo EH, Moskowitz MA, Jacobs TP. Exciting, radical, suicidal: how brain cells die after stroke. *Stroke*. 2005;36(2):189-92. doi: 10.1161/01.STR.0000153069.96296.fd.
129. Stoll G, Jander S, Schroeter M. Inflammation and glial responses in ischemic brain lesions. *Prog Neurobiol*. 1998;56(2):149-71.
130. Gelderblom M, Leypoldt F, Steinbach K, Behrens D, Choe CU, Siler DA, et al. Temporal and spatial dynamics of cerebral immune cell accumulation in stroke. *Stroke*. 2009;40(5):1849-57. doi: 10.1161/STROKEAHA.108.534503.
131. Yilmaz G, Granger DN. Leukocyte recruitment and ischemic brain injury. *Neuromolecular Med*. 2010;12(2):193-204. doi: 10.1007/s12017-009-8074-1.
132. O'Neill LA, Kaltschmidt C. NF-kappa B: a crucial transcription factor for glial and neuronal cell function. *Trends Neurosci*. 1997;20(6):252-8.
133. Vila N, Castillo J, Dávalos A, Chamorro A. Proinflammatory cytokines and early neurological worsening in ischemic stroke. *Stroke*. 2000;31(10):2325-9.
134. Gregersen R, Lambertsen K, Finsen B. Microglia and macrophages are the major source of tumor necrosis factor in permanent middle cerebral artery occlusion in mice. *J Cereb Blood Flow Metab*. 2000;20(1):53-65. doi: 10.1097/00004647-200001000-00009.
135. Okada Y, Copeland BR, Mori E, Tung MM, Thomas WS, del Zoppo GJ. P-selectin and intercellular adhesion molecule-1 expression after focal brain ischemia and reperfusion. *Stroke*. 1994;25(1):202-11.
136. Haring HP, Berg EL, Tsurushita N, Tagaya M, del Zoppo GJ. E-selectin appears in nonischemic tissue during experimental focal cerebral ischemia. *Stroke*. 1996;27(8):1386-91; discussion 91-2.

137. Zhang R, Chopp M, Zhang Z, Jiang N, Powers C. The expression of P- and E-selectins in three models of middle cerebral artery occlusion. *Brain Res.* 1998;785(2):207-14.
138. Cannella B, Raine CS. The adhesion molecule and cytokine profile of multiple sclerosis lesions. *Ann Neurol.* 1995;37(4):424-35. doi: 10.1002/ana.410370404.
139. Mori E, del Zoppo GJ, Chambers JD, Copeland BR, Arfors KE. Inhibition of polymorphonuclear leukocyte adherence suppresses no-reflow after focal cerebral ischemia in baboons. *Stroke.* 1992;23(5):712-8.
140. Barone FC, Feuerstein GZ. Inflammatory mediators and stroke: new opportunities for novel therapeutics. *J Cereb Blood Flow Metab.* 1999;19(8):819-34. doi: 10.1097/00004647-199908000-00001.
141. McColl BW, Rothwell NJ, Allan SM. Systemic inflammatory stimulus potentiates the acute phase and CXC chemokine responses to experimental stroke and exacerbates brain damage via interleukin-1- and neutrophil-dependent mechanisms. *J Neurosci.* 2007;27(16):4403-12. doi: 10.1523/JNEUROSCI.5376-06.2007.
142. Frangogiannis NG. Chemokines in ischemia and reperfusion. *Thromb Haemost.* 2007;97(5):738-47.
143. Schilling M, Besselmann M, Müller M, Strecker JK, Ringelstein EB, Kiefer R. Predominant phagocytic activity of resident microglia over hematogenous macrophages following transient focal cerebral ischemia: an investigation using green fluorescent protein transgenic bone marrow chimeric mice. *Exp Neurol.* 2005;196(2):290-7. doi: 10.1016/j.expneurol.2005.08.004.
144. Graeber MB, Li W, Rodriguez ML. Role of microglia in CNS inflammation. *FEBS Lett.* 2011;585(23):3798-805. doi: 10.1016/j.febslet.2011.08.033.
145. Liu W, Tang Y, Feng J. Cross talk between activation of microglia and astrocytes in pathological conditions in the central nervous system. *Life Sci.* 2011;89(5-6):141-6. doi: 10.1016/j.lfs.2011.05.011.
146. Griffin WS. Inflammation and neurodegenerative diseases. *Am J Clin Nutr.* 2006;83(2):470S-4S.

147. Stevens SL, Bao J, Hollis J, Lessov NS, Clark WM, Stenzel-Poore MP. The use of flow cytometry to evaluate temporal changes in inflammatory cells following focal cerebral ischemia in mice. *Brain Res.* 2002;932(1-2):110-9.
148. Jander S, Kraemer M, Schroeter M, Witte OW, Stoll G. Lymphocytic infiltration and expression of intercellular adhesion molecule-1 in photochemically induced ischemia of the rat cortex. *J Cereb Blood Flow Metab.* 1995;15(1):42-51. doi: 10.1038/jcbfm.1995.5.
149. Kleinschmitz C, Schwab N, Kraft P, Hagedorn I, Dreykluft A, Schwarz T, et al. Early detrimental T-cell effects in experimental cerebral ischemia are neither related to adaptive immunity nor thrombus formation. *Blood.* 2010;115(18):3835-42. doi: 10.1182/blood-2009-10-249078.
150. Yilmaz G, Arumugam TV, Stokes KY, Granger DN. Role of T lymphocytes and interferon-gamma in ischemic stroke. *Circulation.* 2006;113(17):2105-12. doi: 10.1161/CIRCULATIONAHA.105.593046.
151. Arumugam TV, Granger DN, Mattson MP. Stroke and T-cells. *Neuromolecular Med.* 2005;7(3):229-42. doi: 10.1385/NMM:7:3:229.
152. Miyake S, Yamamura T. NKT cells and autoimmune diseases: unraveling the complexity. *Curr Top Microbiol Immunol.* 2007;314:251-67.
153. Grisieri T, Beaudoin L, Novak J, Mars LT, Lepault F, Liblau R, et al. Invariant NKT cells exacerbate type 1 diabetes induced by CD8 T cells. *J Immunol.* 2005;175(4):2091-101.
154. Mahnke K, Bedke T, Enk AH. Regulatory conversation between antigen presenting cells and regulatory T cells enhance immune suppression. *Cell Immunol.* 2007;250(1-2):1-13. doi: 10.1016/j.cellimm.2008.01.004.
155. Cuzner ML, Opdenakker G. Plasminogen activators and matrix metalloproteases, mediators of extracellular proteolysis in inflammatory demyelination of the central nervous system. *J Neuroimmunol.* 1999;94(1-2):1-14.
156. Asahi M, Wang X, Mori T, Sumii T, Jung JC, Moskowitz MA, et al. Effects of matrix metalloproteinase-9 gene knock-out on the proteolysis of blood-brain barrier and white matter components after cerebral ischemia. *J Neurosci.* 2001;21(19):7724-32.

157. Park KP, Rosell A, Foerch C, Xing C, Kim WJ, Lee S, et al. Plasma and brain matrix metalloproteinase-9 after acute focal cerebral ischemia in rats. *Stroke*. 2009;40(8):2836-42. doi: 10.1161/STROKEAHA.109.554824.
158. Berger C, Schmid PC, Schabitz WR, Wolf M, Schwab S, Schmid HH. Massive accumulation of N-acylethanolamines after stroke. Cell signalling in acute cerebral ischemia? *J Neurochem*. 2004;88(5):1159-67.
159. Muthian S, Rademacher DJ, Roelke CT, Gross GJ, Hillard CJ. Anandamide content is increased and CB1 cannabinoid receptor blockade is protective during transient, focal cerebral ischemia. *Neuroscience*. 2004;129(3):743-50. doi: 10.1016/j.neuroscience.2004.08.044.
160. Amantea D, Spagnuolo P, Bari M, Fezza F, Mazzei C, Tassorelli C, et al. Modulation of the endocannabinoid system by focal brain ischemia in the rat is involved in neuroprotection afforded by 17beta-estradiol. *FEBS J*. 2007;274(17):4464-775. doi: 10.1111/j.1742-4658.2007.05975.x.
161. Degn M, Lambertsen KL, Petersen G, Meldgaard M, Arntmann A, Clausen BH, et al. Changes in brain levels of N-acylethanolamines and 2-arachidonoylglycerol in focal cerebral ischemia in mice. *J Neurochem*. 2007;103(5):1907-16. doi: 10.1111/j.1471-4159.2007.04892.x.
162. Franklin A, Parmentier-Batteur S, Walter L, Greenberg DA, Stella N. Palmitoylethanolamide increases after focal cerebral ischemia and potentiates microglial cell motility. *J Neurosci*. 2003;23(21):7767-75.
163. Schäbitz WR, Giuffrida A, Berger C, Aschoff A, Schwaninger M, Schwab S, et al. Release of fatty acid amides in a patient with hemispheric stroke: a microdialysis study. *Stroke*. 2002;33(8):2112-4.
164. Jin KL, Mao XO, Goldsmith PC, Greenberg DA. CB1 cannabinoid receptor induction in experimental stroke. *Ann Neurol*. 2000;48(2):257-61.
165. Ashton JC, Rahman RM, Nair SM, Sutherland BA, Glass M, Appleton I. Cerebral hypoxia-ischemia and middle cerebral artery occlusion induce expression of the cannabinoid CB2 receptor in the brain. *Neurosci Lett*. 2007;412(2):114-7. doi: 10.1016/j.neulet.2006.10.053.
166. Nagayama T, Sinor AD, Simon RP, Chen J, Graham SH, Jin K, et al. Cannabinoids and neuroprotection in global and focal cerebral ischemia and in neuronal cultures. *J Neurosci*. 1999;19(8):2987-95.

167. Parmentier-Batteur S, Jin K, Mao XO, Xie L, Greenberg DA. Increased severity of stroke in CB1 cannabinoid receptor knock-out mice. *J Neurosci*. 2002;22(22):9771-5.
168. Leker RR, Gai N, Mechoulam R, Ovadia H. Drug-induced hypothermia reduces ischemic damage: effects of the cannabinoid HU-210. *Stroke*. 2003;34(8):2000-6. doi: 10.1161/01.STR.0000079817.68944.1E.
169. Panikashvili D, Simeonidou C, Ben-Shabat S, Hanus L, Breuer A, Mechoulam R, et al. An endogenous cannabinoid (2-AG) is neuroprotective after brain injury. *Nature*. 2001;413(6855):527-31. doi: 10.1038/35097089.
170. van der Stelt M, Veldhuis WB, Bär PR, Veldink GA, Vliegenthart JF, Nicolay K. Neuroprotection by Delta9-tetrahydrocannabinol, the main active compound in marijuana, against ouabain-induced in vivo excitotoxicity. *J Neurosci*. 2001;21(17):6475-9.
171. Mendizábal VE, Adler-Graschinsky E. Cannabinoids as therapeutic agents in cardiovascular disease: a tale of passions and illusions. *Br J Pharmacol*. 2007;151(4):427-40. doi: 10.1038/sj.bjp.0707261.
172. Zhang M, Martin BR, Adler MW, Razdan RK, Ganea D, Tuma RF. Modulation of the balance between cannabinoid CB(1) and CB(2) receptor activation during cerebral ischemic/reperfusion injury. *Neuroscience*. 2008;152(3):753-60. doi: 10.1016/j.neuroscience.2008.01.022.
173. Zhang M, Mahadevan A, Amere M, Li H, Ganea D, Tuma RF. Unique Effects of Compounds Active at Both Cannabinoid and Serotonin Receptors During Stroke. *Translational Stroke Research*. 2012;3(3):348-56.
174. Varma N, Carlson GC, Ledent C, Alger BE. Metabotropic glutamate receptors drive the endocannabinoid system in hippocampus. *J Neurosci*. 2001;21(24):RC188.
175. Xu J, Li C, Yin XH, Zhang GY. Additive neuroprotection of GABA A and GABA B receptor agonists in cerebral ischemic injury via PI-3K/Akt pathway inhibiting the ASK1-JNK cascade. *Neuropharmacology*. 2008;54(7):1029-40. doi: 10.1016/j.neuropharm.2008.01.014.
176. Navarrete M, Araque A. Endocannabinoids mediate neuron-astrocyte communication. *Neuron*. 2008;57(6):883-93. doi: 10.1016/j.neuron.2008.01.029.

177. Mehta SL, Manhas N, Raghbir R. Molecular targets in cerebral ischemia for developing novel therapeutics. *Brain Res Rev.* 2007;54(1):34-66. doi: 10.1016/j.brainresrev.2006.11.003.
178. Wagner JA, Járai Z, Bátkai S, Kunos G. Hemodynamic effects of cannabinoids: coronary and cerebral vasodilation mediated by cannabinoid CB(1) receptors. *Eur J Pharmacol.* 2001;423(2-3):203-10.
179. Carmichael ST. Rodent models of focal stroke: size, mechanism, and purpose. *NeuroRx.* 2005;2(3):396-409. doi: 10.1602/neurorx.2.3.396.
180. Schmid-Elsaesser R, Zausinger S, Hungerhuber E, Baethmann A, Reulen HJ. A critical reevaluation of the intraluminal thread model of focal cerebral ischemia: evidence of inadvertent premature reperfusion and subarachnoid hemorrhage in rats by laser-Doppler flowmetry. *Stroke.* 1998;29(10):2162-70.
181. Yang G, Kitagawa K, Matsushita K, Mabuchi T, Yagita Y, Yanagihara T, et al. C57BL/6 strain is most susceptible to cerebral ischemia following bilateral common carotid occlusion among seven mouse strains: selective neuronal death in the murine transient forebrain ischemia. *Brain Res.* 1997;752(1-2):209-18.
182. Beckmann N. High resolution magnetic resonance angiography non-invasively reveals mouse strain differences in the cerebrovascular anatomy in vivo. *Magn Reson Med.* 2000;44(2):252-8.
183. McColl BW, Carswell HV, McCulloch J, Horsburgh K. Extension of cerebral hypoperfusion and ischaemic pathology beyond MCA territory after intraluminal filament occlusion in C57Bl/6J mice. *Brain Res.* 2004;997(1):15-23.
184. Watson BD, Dietrich WD, Busto R, Wachtel MS, Ginsberg MD. Induction of reproducible brain infarction by photochemically initiated thrombosis. *Ann Neurol.* 1985;17(5):497-504. doi: 10.1002/ana.410170513.
185. Sindrup SH, Jensen TS. Efficacy of pharmacological treatments of neuropathic pain: an update and effect related to mechanism of drug action. *Pain.* 1999;83(3):389-400.
186. Raghavendra V, Rutkowski MD, DeLeo JA. The role of spinal neuroimmune activation in morphine tolerance/hyperalgesia in neuropathic and sham-operated rats. *J Neurosci.* 2002;22(22):9980-9.

187. Dhawan BN, Cesselin F, Raghbir R, Reisine T, Bradley PB, Portoghesi PS, et al. International Union of Pharmacology. XII. Classification of opioid receptors. *Pharmacol Rev.* 1996;48(4):567-92.
188. Viganò D, Rubino T, Parolari D. Molecular and cellular basis of cannabinoid and opioid interactions. *Pharmacol Biochem Behav.* 2005;81(2):360-8. doi: 10.1016/j.pbb.2005.01.021.
189. Rios C, Gomes I, Devi LA. mu opioid and CB1 cannabinoid receptor interactions: reciprocal inhibition of receptor signaling and neuritogenesis. *Br J Pharmacol.* 2006;148(4):387-95. doi: 10.1038/sj.bjp.0706757.
190. Fischer BD, Ward SJ, Henry FE, Dykstra LA. Attenuation of morphine antinociceptive tolerance by a CB(1) receptor agonist and an NMDA receptor antagonist: Interactive effects. *Neuropharmacology.* 2010;58(2):544-50. doi: 10.1016/j.neuropharm.2009.08.005.
191. Rios CD, Jordan BA, Gomes I, Devi LA. G-protein-coupled receptor dimerization: modulation of receptor function. *Pharmacol Ther.* 2001;92(2-3):71-87.
192. Hojo M, Sudo Y, Ando Y, Minami K, Takada M, Matsubara T, et al. mu-Opioid receptor forms a functional heterodimer with cannabinoid CB1 receptor: electrophysiological and FRET assay analysis. *J Pharmacol Sci.* 2008;108(3):308-19.
193. Sim LJ, Selley DE, Xiao R, Childers SR. Differences in G-protein activation by mu- and delta-opioid, and cannabinoid, receptors in rat striatum. *Eur J Pharmacol.* 1996;307(1):97-105.
194. Smith FL, Cichewicz D, Martin ZL, Welch SP. The enhancement of morphine antinociception in mice by delta9-tetrahydrocannabinol. *Pharmacol Biochem Behav.* 1998;60(2):559-66.
195. Manzanares J, Corchero J, Romero J, Fernández-Ruiz JJ, Ramos JA, Fuentes JA. Pharmacological and biochemical interactions between opioids and cannabinoids. *Trends Pharmacol Sci.* 1999;20(7):287-94.
196. Viganò D, Rubino T, Vaccani A, Bianchetti S, Marmorato P, Castiglioni C, et al. Molecular mechanisms involved in the asymmetric interaction between cannabinoid and opioid systems. *Psychopharmacology (Berl).* 2005;182(4):527-36. doi: 10.1007/s00213-005-0114-4.

197. Tham SM, Angus JA, Tudor EM, Wright CE. Synergistic and additive interactions of the cannabinoid agonist CP55,940 with mu opioid receptor and alpha2-adrenoceptor agonists in acute pain models in mice. *Br J Pharmacol.* 2005;144(6):875-84. doi: 10.1038/sj.bjp.0706045.
198. Williams IJ, Edwards S, Rubo A, Haller VL, Stevens DL, Welch SP. Time course of the enhancement and restoration of the analgesic efficacy of codeine and morphine by delta9-tetrahydrocannabinol. *Eur J Pharmacol.* 2006;539(1-2):57-63. doi: 10.1016/j.ejphar.2006.04.003.
199. Houser SJ, Eads M, Embrey JP, Welch SP. Dynorphin B and spinal analgesia: induction of antinociception by the cannabinoids CP55,940, Delta(9)-THC and anandamide. *Brain Res.* 2000;857(1-2):337-42.
200. Pugh G, Mason DJ, Combs V, Welch SP. Involvement of dynorphin B in the antinociceptive effects of the cannabinoid CP55,940 in the spinal cord. *J Pharmacol Exp Ther.* 1997;281(2):730-7.
201. Corchero J, Romero J, Berrendero F, Fernandez-Ruiz J, Ramos JA, Fuentes JA, et al. Time-dependent differences of repeated administration with Delta9-tetrahydrocannabinol in proenkephalin and cannabinoid receptor gene expression and G-protein activation by mu-opioid and CB1-cannabinoid receptors in the caudate-putamen. *Brain Res Mol Brain Res.* 1999;67(1):148-57.
202. Ammer H, Schulz R. Chronic morphine treatment increases stimulatory beta-2 adrenoceptor signaling in A431 cells stably expressing the mu opioid receptor. *J Pharmacol Exp Ther.* 1997;280(1):512-20.
203. Rubino T, Tizzoni L, Viganò D, Massi P, Parolaro D. Modulation of rat brain cannabinoid receptors after chronic morphine treatment. *Neuroreport.* 1997;8(15):3219-23.
204. Lim G, Wang S, Mao J. Central glucocorticoid receptors modulate the expression of spinal cannabinoid receptors induced by chronic morphine exposure. *Brain Res.* 2005;1059(1):20-7. doi: 10.1016/j.brainres.2005.08.002.
205. Vela G, Ruiz-Gayo M, Fuentes JA. Anandamide decreases naloxone-precipitated withdrawal signs in mice chronically treated with morphine. *Neuropharmacology.* 1995;34(6):665-8.
206. Hutchinson MR, Bland ST, Johnson KW, Rice KC, Maier SF, Watkins LR. Opioid-induced glial activation: mechanisms of activation and implications for opioid analgesia, dependence, and reward. *ScientificWorldJournal.* 2007;7:98-111. doi: 10.1100/tsw.2007.230.

207. Raghavendra V, Tanga FY, DeLeo JA. Attenuation of morphine tolerance, withdrawal-induced hyperalgesia, and associated spinal inflammatory immune responses by propentofylline in rats. *Neuropsychopharmacology*. 2004;29(2):327-34. doi: 10.1038/sj.npp.1300315.
208. Song P, Zhao ZQ. The involvement of glial cells in the development of morphine tolerance. *Neurosci Res*. 2001;39(3):281-6.
209. Watkins LR, Milligan ED, Maier SF. Glial activation: a driving force for pathological pain. *Trends Neurosci*. 2001;24(8):450-5.
210. Milligan ED, Watkins LR. Pathological and protective roles of glia in chronic pain. *Nat Rev Neurosci*. 2009;10(1):23-36. doi: 10.1038/nrn2533.
211. Johnston IN, Milligan ED, Wieseler-Frank J, Frank MG, Zapata V, Campisi J, et al. A role for proinflammatory cytokines and fractalkine in analgesia, tolerance, and subsequent pain facilitation induced by chronic intrathecal morphine. *J Neurosci*. 2004;24(33):7353-65. doi: 10.1523/JNEUROSCI.1850-04.2004.
212. Stellwagen D, Malenka RC. Synaptic scaling mediated by glial TNF-alpha. *Nature*. 2006;440(7087):1054-9. doi: 10.1038/nature04671.
213. Hutchinson MR, Coats BD, Lewis SS, Zhang Y, Sprunger DB, Rezvani N, et al. Proinflammatory cytokines oppose opioid-induced acute and chronic analgesia. *Brain Behav Immun*. 2008;22(8):1178-89. doi: 10.1016/j.bbi.2008.05.004.
214. Tanga FY, Nutile-McMenamy N, DeLeo JA. The CNS role of Toll-like receptor 4 in innate neuroimmunity and painful neuropathy. *Proc Natl Acad Sci U S A*. 2005;102(16):5856-61. doi: 10.1073/pnas.0501634102.
215. Tumati S, Largent-Milnes TM, Keresztes A, Ren J, Roeske WR, Vanderah TW, et al. Repeated morphine treatment-mediated hyperalgesia, allodynia and spinal glial activation are blocked by co-administration of a selective cannabinoid receptor type-2 agonist. *J Neuroimmunol*. 2012;244(1-2):23-31. doi: 10.1016/j.jneuroim.2011.12.021.
216. Ashton JC, Glass M. The cannabinoid CB₂ receptor as a target for inflammation-dependent neurodegeneration. *Curr Neuropharmacol*. 2007;5(2):73-80.
217. Xi ZX, Peng XQ, Li X, Song R, Zhang HY, Liu QR, et al. Brain cannabinoid CB₂ receptors modulate cocaine's actions in mice. *Nat Neurosci*. 2011;14(9):1160-6. doi: 10.1038/nn.2874.

218. Beltramo M, Bernardini N, Bertorelli R, Campanella M, Nicolussi E, Fredduzzi S, et al. CB2 receptor-mediated antihyperalgesia: possible direct involvement of neural mechanisms. *Eur J Neurosci*. 2006;23(6):1530-8. doi: 10.1111/j.1460-9568.2006.04684.x.
219. Atwood BK, Mackie K. CB2: a cannabinoid receptor with an identity crisis. *Br J Pharmacol*. 2010;160(3):467-79. doi: 10.1111/j.1476-5381.2010.00729.x.
220. Liu QR, Pan CH, Hishimoto A, Li CY, Xi ZX, Llorente-Berzal A, et al. Species differences in cannabinoid receptor 2 (CNR2 gene): identification of novel human and rodent CB2 isoforms, differential tissue expression and regulation by cannabinoid receptor ligands. *Genes Brain Behav*. 2009;8(5):519-30. doi: 10.1111/j.1601-183X.2009.00498.x.
221. Anand U, Otto WR, Sanchez-Herrera D, Facer P, Yangou Y, Korchev Y, et al. Cannabinoid receptor CB2 localisation and agonist-mediated inhibition of capsaicin responses in human sensory neurons. *Pain*. 2008;138(3):667-80. doi: 10.1016/j.pain.2008.06.007.
222. Wotherspoon G, Fox A, McIntyre P, Colley S, Bevan S, Winter J. Peripheral nerve injury induces cannabinoid receptor 2 protein expression in rat sensory neurons. *Neuroscience*. 2005;135(1):235-45. doi: 10.1016/j.neuroscience.2005.06.009.
223. Ross RA, Coutts AA, McFarlane SM, Anavi-Goffer S, Irving AJ, Pertwee RG, et al. Actions of cannabinoid receptor ligands on rat cultured sensory neurones: implications for antinociception. *Neuropharmacology*. 2001;40(2):221-32.
224. Malan TP, Ibrahim MM, Deng H, Liu Q, Mata HP, Vanderah T, et al. CB2 cannabinoid receptor-mediated peripheral antinociception. *Pain*. 2001;93(3):239-45.
225. Quartilho A, Mata HP, Ibrahim MM, Vanderah TW, Porreca F, Makriyannis A, et al. Inhibition of inflammatory hyperalgesia by activation of peripheral CB2 cannabinoid receptors. *Anesthesiology*. 2003;99(4):955-60.
226. Nackley AG, Makriyannis A, Hohmann AG. Selective activation of cannabinoid CB(2) receptors suppresses spinal fos protein expression and pain behavior in a rat model of inflammation. *Neuroscience*. 2003;119(3):747-57.
227. Ibrahim MM, Porreca F, Lai J, Albrecht PJ, Rice FL, Khodorova A, et al. CB2 cannabinoid receptor activation produces antinociception by stimulating peripheral release of endogenous opioids. *Proc Natl Acad Sci U S A*. 2005;102(8):3093-8. doi: 10.1073/pnas.0409888102.

228. Ibrahim MM, Rude ML, Stagg NJ, Mata HP, Lai J, Vanderah TW, et al. CB2 cannabinoid receptor mediation of antinociception. *Pain*. 2006;122(1-2):36-42. doi: 10.1016/j.pain.2005.12.018.
229. Calignano A, La Rana G, Giuffrida A, Piomelli D. Control of pain initiation by endogenous cannabinoids. *Nature*. 1998;394(6690):277-81. doi: 10.1038/28393.
230. Clayton N, Marshall FH, Bountra C, O'Shaughnessy CT. CB1 and CB2 cannabinoid receptors are implicated in inflammatory pain. *Pain*. 2002;96(3):253-60.
231. Jaggar SI, Hasnie FS, Sellaturay S, Rice AS. The anti-hyperalgesic actions of the cannabinoid anandamide and the putative CB2 receptor agonist palmitoylethanolamide in visceral and somatic inflammatory pain. *Pain*. 1998;76(1-2):189-99.
232. Rubin LL, Staddon JM. The cell biology of the blood-brain barrier. *Annu Rev Neurosci*. 1999;22:11-28. doi: 10.1146/annurev.neuro.22.1.11.
233. Kroll RA, Neuwelt EA. Outwitting the blood-brain barrier for therapeutic purposes: osmotic opening and other means. *Neurosurgery*. 1998;42(5):1083-99; discussion 99-100.
234. Lustig S, Danenberg HD, Kafri Y, Kobiler D, Ben-Nathan D. Viral neuroinvasion and encephalitis induced by lipopolysaccharide and its mediators. *J Exp Med*. 1992;176(3):707-12.
235. Kenne E, Erlandsson A, Lindbom L, Hillered L, Clausen F. Neutrophil depletion reduces edema formation and tissue loss following traumatic brain injury in mice. *J Neuroinflammation*. 2012;9:17. doi: 10.1186/1742-2094-9-17.
236. Bauer M, Brakebusch C, Coisne C, Sixt M, Wekerle H, Engelhardt B, et al. Beta1 integrins differentially control extravasation of inflammatory cell subsets into the CNS during autoimmunity. *Proc Natl Acad Sci U S A*. 2009;106(6):1920-5. doi: 10.1073/pnas.0808909106.
237. Kawakami N, Bartholomäus I, Pesic M, Mues M. An autoimmunity odyssey: how autoreactive T cells infiltrate into the CNS. *Immunol Rev*. 2012;248(1):140-55. doi: 10.1111/j.1600-065X.2012.01133.x.
238. Goldsby RA, Kindt TJ, Osborne BA, Kuby J. Kuby immunology. 4th ed. New York: W.H. Freeman; 2000.

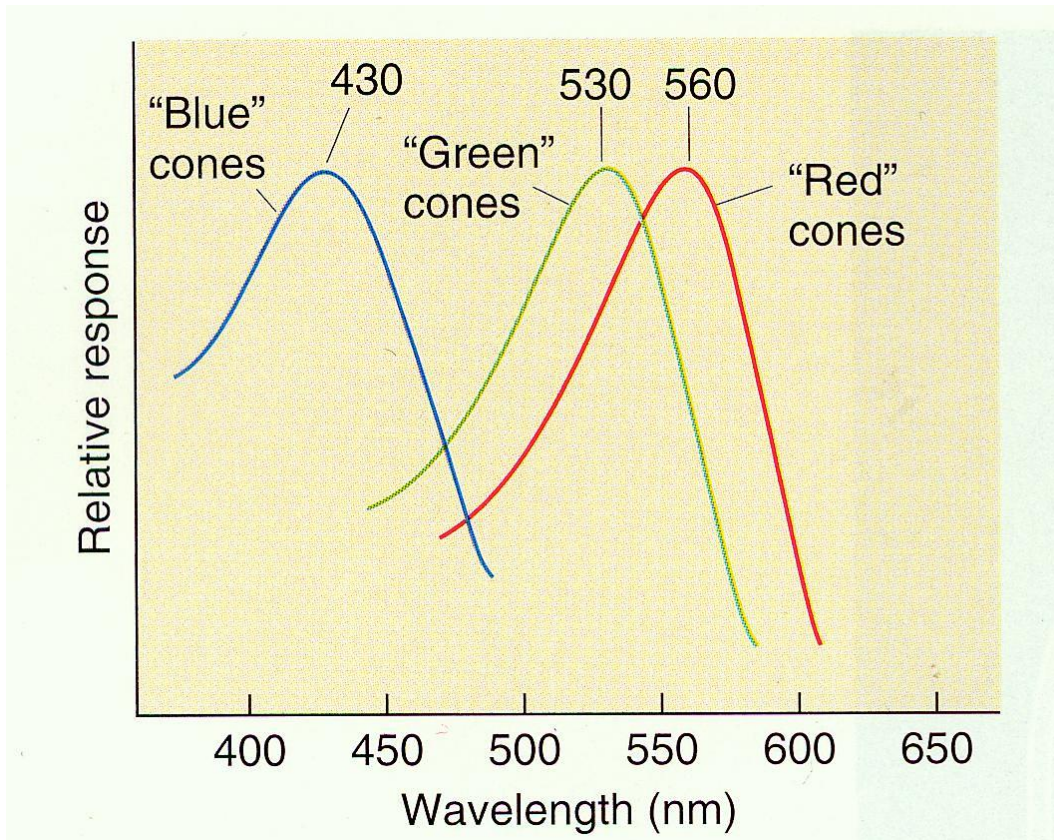
239. Ross MH, Pawlina W. Histology : a text and atlas : with correlated cell and molecular biology. 5th ed. Baltimore, MD: Lippincott Williams & Wilkins; 2006.
240. Gear AR. Rhodamine 6G. A potent inhibitor of mitochondrial oxidative phosphorylation. *J Biol Chem*. 1974;249(11):3628-37.
241. Johnson LV, Walsh ML, Chen LB. Localization of mitochondria in living cells with rhodamine 123. *Proc Natl Acad Sci U S A*. 1980;77(2):990-4.
242. Levene HB, Zhang M, Erb CJ, Jallo JI, Loftus CM, Tuma RF. Method to perform IV injections on mice using the facial vein. *J Neurosci Methods*. 2007;164(2):304-7. doi: 10.1016/j.jneumeth.2007.05.007.
243. Groman EV, Reinhardt CP. Method to quantify tail vein injection technique in small animals. *Contemp Top Lab Anim Sci*. 2004;43(1):35-8.
244. Stoenica L, Senkov O, Gerardy-Schahn R, Weinhold B, Schachner M, Dityatev A. In vivo synaptic plasticity in the dentate gyrus of mice deficient in the neural cell adhesion molecule NCAM or its polysialic acid. *Eur J Neurosci*. 2006;23(9):2255-64. doi: 10.1111/j.1460-9568.2006.04771.x.
245. Olson ME, Vizzutti D, Morck DW, Cox AK. The parasympatholytic effects of atropine sulfate and glycopyrrolate in rats and rabbits. *Can J Vet Res*. 1994;58(4):254-8.
246. Cox AK, Morck DW, Olson ME. Evaluation of detomidine and ketamine-detomidine for anesthesia in laboratory rats. *Contemp Top Lab Anim Sci*. 1994;33(2):52-5.
247. Barnes CD, Eltherington LG. Drug dosage in laboratory animals, a handbook. Rev. and enl. ed. Berkeley,: University of California Press; 1973.
248. Morrey JD, Olsen AL, Siddharthan V, Motter NE, Wang H, Taro BS, et al. Increased blood-brain barrier permeability is not a primary determinant for lethality of West Nile virus infection in rodents. *J Gen Virol*. 2008;89(Pt 2):467-73. doi: 10.1099/vir.0.83345-0.
249. Manaenko A, Chen H, Kammer J, Zhang JH, Tang J. Comparison Evans Blue injection routes: Intravenous versus intraperitoneal, for measurement of blood-brain barrier in a mice hemorrhage model. *J Neurosci Methods*. 2011;195(2):206-10. doi: 10.1016/j.jneumeth.2010.12.013.

250. AALAS Learning Library Animal Care and Use in Research and Education. 2005 [4/17/2012].
251. Bear MF, Connors BW, Paradiso MA. Neuroscience : exploring the brain. 3rd ed. Philadelphia, PA: Lippincott Williams & Wilkins; 2007.
252. Joblove GH, Greenberg D, editors. Color Spaces for Computer Graphics. SIGGRAPH '78 Proceedings on Computer Graphics and Interactive Techniques 1978; New York.
253. Hunt RWG. The reproduction of colour. 6th ed. Chichester, West Sussex, England ; Hoboken, NJ: John Wiley & Sons; 2004.
254. Haifa BA, Bacarea V, Iacob O, Calinici T, Schiopu A. Comparison between Digital Image Processing and Spectrophotometric Measurements Methods. Application in Electrophoresis Interpretation. Applied Medical Informatics. 2011;28(1):29-36.
255. Yu C-H, Chen S-Y. Universal Colour Quantisation for Different Colour Spaces IEE Proceedings Vision, Image & Signal Processing 2006;153(4):445-55.
256. Li B, Meng MQ. Computer-based detection of bleeding and ulcer in wireless capsule endoscopy images by chromaticity moments. Comput Biol Med. 2009;39(2):141-7. doi: 10.1016/j.combiomed.2008.11.007.
257. Wyszecki Gn, Stiles WS. Color science : concepts and methods, quantitative data and formulae. 2nd ed. New York: Wiley; 1982.
258. Poynton C. Color FAQ - Frequently Asked Questions Color. 2006 [cited 2012 December 15, 2012]; Available from: <http://www.poynton.com/PDFs/ColorFAQ.pdf>.
259. Hanbury A. The Taming of the Hue, Saturation, and Brightness Colour Space. 7th Computer Vision Winter Workshop. 2002:234-43.
260. Smith AR. Color Gamut Transform Pairs. SIGGRAPH 78 Conference Proceedings. 1978:12-9. doi: 10.1145/800248.807361.
261. Schreiber WF. Fundamentals of electronic imaging systems : some aspects of image processing. 3rd ed. Berlin ; New York: Springer-Verlag; 1993.

262. Mahmoud-Ghoneim D. Optimizing automated characterization of liver fibrosis histological images by investigating color spaces at different resolutions. *Theor Biol Med Model.* 2011;8:25. doi: 10.1186/1742-4682-8-25.
263. Blinn JF. NTSC: Nice Technology, Super Color. *IEEE Computer Graphics and Applications.* 1993;13(2):17-23.
264. Vives G, Guerrero JM, Godoy J, Khatua S, Wang YP, Kiappes JL, et al. Synthesis of fluorescent dye-tagged nanomachines for single-molecule fluorescence spectroscopy. *J Org Chem.* 2010;75(19):6631-43. doi: 10.1021/jo101468u.
265. Forbes MW, Jockusch RA. Gas-phase fluorescence excitation and emission spectroscopy of three xanthene dyes (rhodamine 575, rhodamine 590 and rhodamine 6G) in a quadrupole ion trap mass spectrometer. *J Am Soc Mass Spectrom.* 2011;22(1):93-109. doi: 10.1007/s13361-010-0017-4.
266. Levkowitz H, Herman GT. GLHS: A Generalized Lightness, Hue, and Saturation Color Model. *CVGIP: Graphical Models and Image Processing.* 1993;55(No. 4, July):271-85.
267. van Der Laak JA, Pahlplatz MM, Hanselaar AG, de Wilde PC. Hue-saturation-density (HSD) model for stain recognition in digital images from transmitted light microscopy. *Cytometry.* 2000;39(4):275-84.

1.9 Figures

Figure 1, Eye Sensitivity to Light



Sensitivity of ρ , γ , and β cones as they relate to wavelength. Note that no green (γ) cone can be excited without subsequent excitation of a red (ρ) or blue (β) cone. Hunt does not indicate β cones overlap with ρ cones in his text. (251)

Figure 2, Derivation of the RGB Tristimulus Space

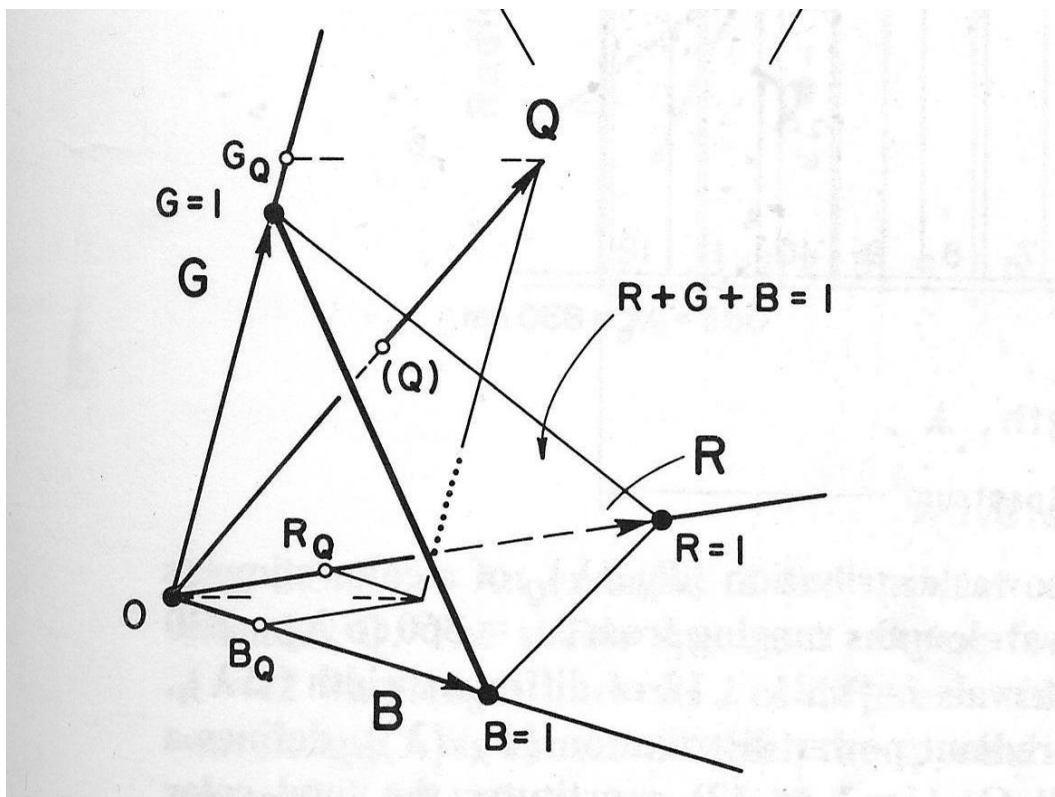


Diagram of the R, G, B color space. Primary stimuli R, G, and B share a common origin indicated 0. A spectral power distribution, Q, exists as a tristimulus vector with components of length R_Q , G_Q , and B_Q , the tristimulus values. (257)

Figure 3, Mathematical Diagram of Spectral Power Distributions

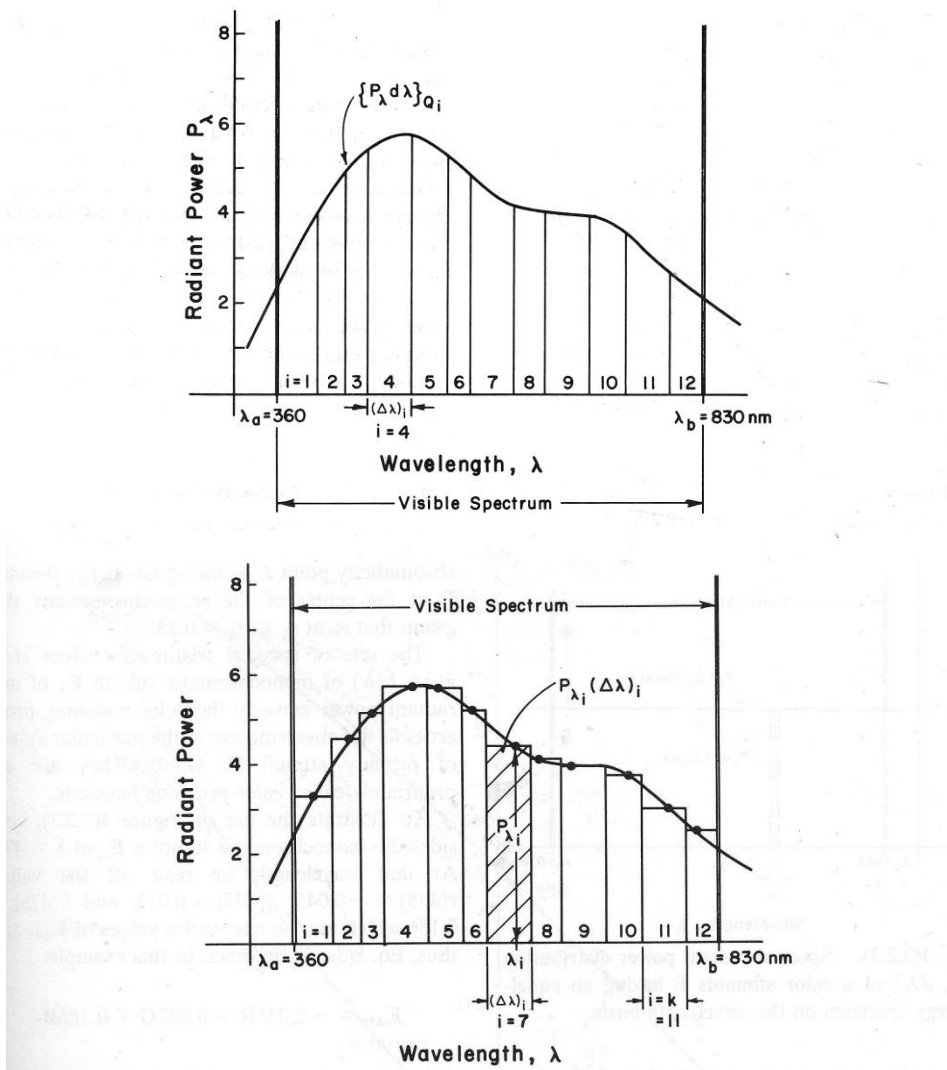


Diagram of a spectral power distribution with mathematical notation corresponding to derivation.

(257)

CHAPTER 2

DEVELOPMENT OF 2 MODELS: NOVEL APPLICATION OF RHODAMINE 6G AND PHOTOTHROMBOTIC STROKE

2.1 Aims

1. Develop a novel method to administer Rhodamine 6G that would alleviate the need for surgical manipulation and anesthesia.
2. Characterize and quantify physical characteristics of any differences in administration techniques in the application methods of Rhodamine 6G.
3. Develop a repository of physical parameters among the 2 techniques over the course of 8 hours to facilitate development of automated detection algorithms.
4. Apply Rhodamine 6G findings to synthesize a method for characterizing pial blood flow in a photothrombotic stroke within 24 hours of injury.

2.2 Materials and Methods

2.2.1 Preparation of Rhodamine 6G

5mg of Rhodamine 6G (Sigma) was dissolved in 1 mL of 0.9% normal saline solution to produce 0.5% rhodamine solution. The solution was dissolved 1:10 with 0.9% normal saline to produce 0.05% rhodamine. This was done each day to ensure that the rhodamine was fresh and not subject to light degradation or oxidation prior to use. (81)

2.2.2 Administration of Rhodamine 6G for Injection Technique Studies

The freshly prepared 0.05% rhodamine was administered in an amount of 100 uL except for the last set of flow cytometry studies in which 200 uL was administered intraperitoneally. For intravenous administration, the animal was anesthetized with a mixture of ketamine (100 mg/mL) and xylazine (20mg/mL) mixed (1:1 by volume) at a dose of 1 mL/kg.

In accordance with approved institutional animal standards and after the depth of anesthesia was confirmed by a lack of toe pinch response, the skin over the inner thigh was shaved and prepped for surgery by swabbing with isopropyl alcohol. A 1 cm incision was made to visualize the popliteal and saphenous veins. Under light microscopy, a 30 gauge needle was advanced into the lumen of the vein at a distal location. Upon injection of rhodamine, displacement of blood in the vessel confirmed entry and placement of the needle. A return of venous flow was also confirmed to ensure adequate delivery. Pressure was applied until bleeding stopped and the skin was closed with staples.

For intraperitoneal injection, the needle was inserted at a 30° angle on an imaginary line drawn across the abdomen just above the knees of the mice. The needle was inserted along this line on the right side of the midline to a depth of 5mm. Aspiration was performed prior to injection of Rhodamine 6G to ensure proper placement (250).

2.2.3 Preparation and Analysis of Blood Smears

After injection of Rhodamine 6G, a vein was compromised to cause bleeding. The tail vein or saphenous vein was utilized for such purpose. A drop of blood was placed on a slide and then smeared across it with a second slide that had been blunted. Slides were transferred to the microscope in a closed box to prevent photo bleaching.

An Olympus BX51 fluorescent microscope equipped with an Olympus DP70 camera was utilized to view the slides at 200x. Basic light microscopy was utilized to confirm the quality of the smear and presence of the cells. An image was collected and then the microscope was switched to fluorescent mode. A TRITC filter was utilized. Using the Olympus MicroSuite Biological Suite, the exposure time was set to 100 msec. Background light was kept constant among images and fluorescent images corresponding to the previously collected light microscopy images were obtained from a live video feed. At least 5 fields of view were analyzed with at least 10 cells in each field.

The images were saved as JPEG files and using the same software, converted to multichannel images. After confirming fluorescent activity corresponding to genuine cells, the cells were defined as Regions of Interest. Then the Regions of Interest were measured utilizing a function to provide Average Intensity reported as the R, G, and B tristimulus values. These values were employed as previously described for colorimetric calculations.

2.2.4 Implant of Cranial Windows

Animals were anesthetized with a mixture of ketamine (100 mg/mL) and xylazine (20mg/mL) mixed (1:1 by volume) at a dose of 1 mL/kg. The head was shaved and positioned in a stereotactic holder. The skin over the right cortical hemisphere was swabbed with isopropyl alcohol twice and then removed. The periosteum was also removed. A 4mm diameter circular craniotomy was performed using an electric high speed drill (Fine Science Tools) over the right parietal cortex. It was bounded anteriorly by the coronal suture, medially by the sagittal suture, laterally by the attachment of the temporal muscle, and posteriorly by the lambdoid suture. The window was positioned in the middle of the sagittal suture to include some terminal branches of the middle cerebral artery. Sterile isotonic saline was dripped over the cranium to avoid thermal

injury of the cortex. The dura was also removed and exposed brain kept moist with the saline as well. A 5mm diameter coverglass was then implanted over the exposed brain and an airtight seal formed with Nexaband Quick Seal. The coverglass provided adequate mechanical protection from infection or contamination. A recovery period of 4 days was provided between the implant of the windows and the examination of rhodamine application (81, 82).

2.2.5 Stimulation of Inflammation

Lipopolysaccharide (LPS) from *E. coli* O111:B4 (Calbiochem) was dissolved in 1XPBS to a concentration of 1 µg/mL. The LPS was injected intraperitoneally at a concentration of 5 mg/kg in each animal at the time of Rhodamine 6G administrations.

2.2.6 Intravital Microscopy and Conversion to Still Images

Mice were anesthetized with a mixture of ketamine (100 mg/mL) and xylazine (20mg/mL) mixed (1:1 by volume) at a dose of 1 mL/kg. After a lack of toe pinch response, the surface of the window was visualized under a dissecting scope. Any debris on the window was removed and the animal was fixed in a stereotactic head holder. A x20 water-immersion objective (WI 20, 0.4; Olympus, Tokyo, Japan), an Olympus BX10 epi-illuminescence microscope (Olympus, Tokyo, Japan), an image intensifier (Ceniisys Image Intensifier, Dage-MTI, Michigan City, IN, USA), a TRITC filter, and a monitor (12VM968; Audiotronics, North Hollywood, CA, USA) were employed to gain a final total magnification of x660. The microscope was equipped with a digital camera (Cooke 1600, Cooke Corporation, Romulus, Michigan) and utilized for image acquisition. Only one image was collected at each time point to prevent photo-bleaching and phototoxicity by the mercury lamp although attempts were made to find the same vessel each time. Post capillary venules for examined for the purpose of Rhodamine 6G studies. The collection time was limited

to 30 seconds. The images were displayed on a computer monitor and recorded by Camware software at a video frame rate of 30 frames/sec and saved as mpeg files. (81, 82)

The files were then opened in Windows Media Player Classic. This software allowed for the collection of snapshots of the video images to produce JPEG files. The JPEG images were then opened in Olympus MicroSuite Biological Suite and converted to multichannel images. As before, Regions of Interest were identified and then analyzed with the Average Intensity function to collect R, G, and B tristimulus values.

2.2.7 Measurement of Leukocyte/Endothelial Interactions

Leukocyte and endothelial interactions were accessed every hour for 8 hours following the injection of Rhodamine 6G and LPS. Attempts were made to locate the same vessel with each viewing. The number of rolling leukocytes was considered to be the total number of leukocytes moving at a significantly slower rate than the midline velocity of blood cells. They were counted as they passed an arbitrary line drawn perpendicular to the long axis of the vessel for 30 seconds. This count was repeated 3 times for each vessel with the arbitrary line repositioned each time. The average of the 3 counts was reported and normalized to 1 minute with results reported as the number of rolling leukocytes/minute.

Adherent leukocytes were defined as the total number of leukocytes that were firmly attached to the endothelium and did not change position during the course of 30 seconds of observation. Adherent leukocytes were reported as the number of cells/mm². The vascular surface area for each vessel was calculated to accomplish this by utilizing ImageJ software (NIH). (81, 82, 172)

2.2.8 Flow Cytometry

4 hours after the administration of Rhodamine 6G, a lancet was utilized to perforate the facial vein of the mice and a few drops of blood were collected in 1 mL of PBS containing heparin (750 ng/mL). The samples were centrifuged and resuspended in 2 mL RBC Lysis Buffer (eBioscience Inc, San Diego, California). Cells were again centrifuged, the supernatant removed, and the cells resuspended in 1 mL 1X PBS. A second wash was performed and finally the cells resuspended in 200 µL 1X PBS. The samples were analyzed with a BD FACSCalibur flow cytometer and analysis performed with Cell Quest Pro software.

2.2.9 Statistical Analysis--Rhodamine

All of the data, except for flow cytometry studies, were analyzed with analysis of variance for repeated measures with Bonferroni correction for multiple comparisons. Flow cytometry studies were subjected to a Student's t-Test. Data is reported as the mean ± the standard error of the mean. A p-value <0.05 was used for statistical significance.

2.2.10 Photothrombotic Cerebral Ischemia

Four days prior to ischemia, cranial windows were implanted in the mice as described in 2.2.4 with the exception that the removed bone flap was placed in 0.9% saline and kept at 4°C. On the day of ischemia, mice were anesthetized with a mixture of ketamine (100 mg/mL) and xylazine (20 mg/mL) mixed (1:1 by volume) at a dose of 1 mL/kg. The bone flap was laid back into place over the window. Mice were maintained at 36.5° to 37.5° C throughout the procedure. 0.1 mL of Rose Bengal (Sigma Aldrich), 10 mg/mL dissolved in 0.9% saline, was injected intraperitoneally. The head was shaved and skin and periosteum over the right parietal bone removed. The head was secured in place and a cold light source positioned over the bone flap. 5

minutes after the injection of dye, the light source was activated for 20 minutes and temperature monitored.

2.2.11 Visualization of Cranial Windows Following Photothrombotic Ischemia

The medial aspect of the thigh was shaved and skin retracted to expose the saphenous vein. 0.1 mL of 0.05% Rhodamine 6G was injected into the vessel. The window was visualized as described in section 2.2.6 with the difference that 3 videos were obtained approximately 1 hour after the onset of ischemia. Both post capillary venules and pre capillary arterioles were examined.

2.2.12 Analysis of Flow in Cranial Windows Following Photothrombotic Ischemia and Statistical Analysis

Vessels were characterized as having blood flow or stasis/no flow. The number of vessels was tabulated. Vessel width was also measured using ImageJ Software (NIH). Vessels with flow were compared to vessels with no flow by means of a Student's t-Test. Data is reported as the mean \pm the standard error of the mean. A p-value <0.05 was used for statistical significance.

2.3 Results

2.3.1 Effect of Injection Method on Leukocyte Luma in Peripheral Blood, Figure 4 and 5

Intravenous injection of Rhodamine 6G analyzed for luma of leukocytes at one hour showed an average value of 152.34 ± 3.82 . This value decreased to 134.95 ± 4.98 at 2 hours, 131.34 ± 5.62 at 3 hours, and 111.52 ± 4.74 at 4 hours. A small increase to 112.31 ± 4.18 was observed at 5 hours and then the luma continued to decrease to 88.28 ± 5.21 at 6 hours, 79.23 ± 4.51 at 7 hours, and finally 75.86 ± 7.27 at 8 hours. The change from 1 hour to every other time point except 2 hours was statistically significant with p values all < 0.001 . Intraperitoneal injection

produced a luma value of 119.23 ± 7.46 at one hour which decreased to 99.83 ± 5.54 at 2 hours. The value rose to 135.27 ± 5.76 at 3 hours, to 136.00 ± 7.04 at 4 hours, and to 141.85 ± 4.83 at 5 hours. The value again dropped to 102.92 ± 7.91 at 6 hours and but rose to 121.12 ± 8.19 at 7 hours. The final luma recorded at 8 hours was 72.25 ± 6.30 . The change in luma among time points that were injected intraperitoneally were statistically significant from 1 hour compared to 2 hours and 8 hours ($p < 0.001$). At no time point did the luma from intravenously injected rhodamine group reach statistical significance when compared to the intraperitoneally injected group at that same time point.

2.3.2 Effect of Injection Method on Leukocyte HSL Lightness in Peripheral Blood, Figure 6

When lightness was examined in peripheral leukocytes, the intravenous value at one hour was found to be 0.46 ± 0.01 . The value decreased to 0.44 ± 0.01 at 2 hours, to 0.42 ± 0.01 at 3 hours, and to 0.38 ± 0.01 at 4 hours. A small rise at 5 hours produced a value of 0.39 ± 0.01 , while at 6 hours the lightness value measured 0.33 ± 0.01 . Lightness was found to be 0.35 ± 0.02 at 7 hours and finally 0.24 ± 0.02 at 8 hours. No statistically significant change was found during the period of observation. Findings for intraperitoneal injections were similar with an initial lightness value of 0.40 ± 0.02 at 1 hour with a decrease to 0.36 ± 0.02 at 2 hours. The lightness measured 0.45 ± 0.02 at 3 hours, 0.43 ± 0.02 at 4 hours, and 0.45 ± 0.01 at 5 hours, and dropped to 0.35 ± 0.02 at 6 hours. Seven hours saw a rise to 0.41 ± 0.02 with a final decrease to 0.29 ± 0.02 at 8 hours. Like the intravenous injection, there was no statistically significant change among time points in the intraperitoneal group and overall no statistically different lightness values between the two groups at any corresponding time point.

2.3.3 Effect of Injection Method on Leukocyte HSV Value in Peripheral Blood, Figure 7

An intravenous injection of Rhodamine 6G produced an HSV value measurement in peripheral leukocytes of 0.79 ± 0.01 at 1 hour, 0.74 ± 0.02 at 2 hours, 0.72 ± 0.02 at 3 hours, 0.66 ± 0.03 at 4 hours, and 0.68 ± 0.01 at 5 hours. A greater decrease was seen at 6 hours as the measure of value at that point was only 0.56 ± 0.02 but it rose to 0.60 ± 0.02 at 7 hours and ended at 0.41 ± 0.03 at 8 hours. There was no statistically significant change from the 1 hour time point to any other time point. When administered intraperitoneally, the value measure was 0.70 ± 0.03 at 1 hour but dropped to 0.61 ± 0.02 at 2 hours and rose again to 0.74 ± 0.02 at 3 hours. At 4 hours, the measurement of value dropped slightly to 0.72 ± 0.02 and then rose to 0.77 ± 0.01 at 5 hours. At 6 hours the measure of value was 0.59 ± 0.03 , then climbed to 0.67 ± 0.03 at 7 hours, and finally 0.49 ± 0.03 at 8 hours. Like the intravenous group, there was no statistically different measure among the intraperitoneal group. Over all 8 hours, there was no statistically significant difference between the methods of injection at any matched time point.

2.3.4 Effect of Injection Method on Leukocyte HSI Intensity in Peripheral Blood, Figure 8

The measured intensity of intravenously injected Rhodamine 6G when examined in leukocytes smeared onto a slide at 1 hour was 0.50 ± 0.01 which decreased to 0.46 ± 0.1 at 2 hours, and 0.44 ± 0.02 at 3 hours. The decrease in intensity continued at 4 hours reaching an intensity of 0.39 ± 0.01 , 0.39 ± 0.1 at 5 hours, and 0.31 ± 0.02 at 6 hours. The intensity rose slightly at 7 hours reaching 0.34 ± 0.02 and finally ended at 0.22 ± 0.02 at 8 hours. There was no statistically significant difference among any of the time points. When the Rhodamine 6G was injected into the peritoneum, the initial intensity was 0.41 ± 0.02 at 1 hour and dropped to 0.35 ± 0.02 at 2 hours. The intensity climbed to 0.47 ± 0.02 at 3 hours, and registered 0.46 ± 0.02 at 4 hours and 0.48 ± 0.01 at 5 hours. The intensity was 0.35 ± 0.02 at 6 hours, 0.42 ± 0.03 at 7 hours, and finally 0.26

± 0.02 at 8 hours. No statistically significant difference could be identified between time points in the intraperitoneal group or when both groups were compared to each other at matching time points.

2.3.5 Effect of Injection Method on Leukocyte HSV and HSL Hue in Peripheral Blood,

Figure 9

Both intravenously injected and intraperitoneally injected groups underwent measurements to determine the hue at each time point. In the intravenous group, hue was found to be $40.73^\circ \pm 1.12^\circ$ at 1 hour and dropped to $34.57^\circ \pm 1.57^\circ$ at 2 hours. A small rise to $35.51^\circ \pm 1.49^\circ$ was found at 3 hours but at 4 hours it again dropped to $31.03^\circ \pm 1.41^\circ$. At 5 hours, the hue was $28.89^\circ \pm 1.28^\circ$, $19.61^\circ \pm 1.63^\circ$ at 6 hours, $22.59^\circ \pm 2.02^\circ$ at 7 hours, and $12.56^\circ \pm 1.75^\circ$ at 8 hours. There was no statistically significant difference among the time points measured. In the intraperitoneal group the hue at 1 hour was found to be $28.58^\circ \pm 2.22^\circ$ while at 2 hours it was only $23.09^\circ \pm 1.61^\circ$. At 3 hours a rise in hue was noted as it reached $34.15^\circ \pm 1.84^\circ$ and continued to rise to $35.76^\circ \pm 1.88^\circ$ at 4 hours, and finally $36.04^\circ \pm 1.65^\circ$ at 5 hours. Over the last time points, recorded measurements of hue included $24.21^\circ \pm 2.09^\circ$ at 6 hours, $30.15^\circ \pm 2.54^\circ$ at 7 hours, and $15.30^\circ \pm 1.86^\circ$ at 8 hours. No statistically significant difference was discovered among the different time points in the group and overall no statistically significant difference existed between the two groups at coinciding time points.

2.3.6 Effect of Injection Method on Leukocyte HSL Saturation in Blood Smears, Figure 10

In the intravenous group, HSL saturation was measured in peripheral leukocytes. At 1 hour the saturation was found to be 0.74 ± 0.01 and it dropped to 0.71 ± 0.01 at 2 hours. The saturation rose again to 0.74 ± 0.01 at 3 hours and had the same value of 0.74 ± 0.01 at 4 hours. It remained

relatively constant as it rose to 0.76 ± 0.01 at 5 hours and registered 0.74 ± 0.01 at 6 hours, 0.75 ± 0.01 at 7 hours, and ended at 0.77 ± 0.01 at 8 hours. The differences among the time points were not statistically significant. The saturation measurements in the intraperitoneal group were very similar. At one hour the saturation was 0.72 ± 0.02 and 0.73 ± 0.01 at 2 hours. At 3 hours the saturation was 0.73 ± 0.02 , 0.71 at 4 hours, and 0.72 ± 0.01 at 5 hours. The trend continued, ultimately producing saturation measurements of 0.74 ± 0.01 at 6 hours, 0.70 ± 0.02 at 7 hours, and finally 0.77 ± 0.02 at 8 hours. No statistically significant differences were found among the different time points in the intraperitoneal group nor were the differences among the two groups at matching time points statistically different.

2.3.7 Effect of Injection Method on Leukocyte HSV Saturation in Peripheral Blood, Figure 11

The HSV saturation of leukocytes was also measured in both the injection groups. In the intravenously injected rhodamine group, the saturation was found to be 0.83 ± 0.004 at 1 hour, 0.81 ± 0.01 at 2 hours, 0.84 ± 0.003 at 3 hours, 0.85 ± 0.003 at 4 hours, and 0.86 ± 0.004 at 5 hours. For the 3 remaining time points, the saturation measurements held relatively constant with a measure of 0.85 ± 0.01 at 6 hours, 0.85 ± 0.01 at 6 hours, and finally 0.86 ± 0.01 at 8 hours. When comparing the time points in the intravenous group, the differences among them lacked statistical significance. The saturation for the intraperitoneal group was similar with a value of 0.85 ± 0.01 at 1 hour, 0.83 ± 0.01 at 2 hours, and 0.76 ± 0.04 at 3 hours. As the experiment progressed, the saturation was found to be 0.81 ± 0.01 at 4 hours, 0.83 ± 0.01 at 5 hours, 0.84 ± 0.01 at 6 hours, 0.81 ± 0.01 at 7 hours, and ultimately, 0.86 ± 0.01 at 8 hours. Like the intravenous group, comparisons at different time points in the intraperitoneal group failed to return any statistically

significant differences. The same was true of comparisons made between the groups at corresponding time points.

2.3.8 Effect of Injection Method on Leukocyte HSI Saturation in Peripheral Blood, Figure 12

The HSI saturation overall showed a different pattern than the HSV or HSL saturation in leukocytes. While the HSV and HSL saturations remained relatively constant throughout the 8 hours, the HSI calculation for saturation showed an overall decrease over the time period and exhibited a pattern more reminiscent of HSV value or HSL lightness. The initial saturation of the intravenous group at 1 hour was 0.59 ± 0.09 followed by 0.53 ± 0.11 at 2 hours and 0.54 ± 0.11 at 3 hours. At the halfway point, 4 hours, the value of the saturation in the intravenous group was 0.49 ± 0.10 and it continued to 0.51 ± 0.08 at 5 hours. Then it dropped to 0.43 ± 0.13 at 6 hours, 0.46 ± 0.14 at 7 hours, and finally it reached the lowest measurement at 8 hours with 0.32 ± 0.16 . The differences between the time points did not reach statistical significance. In the intraperitoneal group, the value at 1 hour measured 0.53 ± 0.13 , at 2 hours, 0.45 ± 0.13 , and at 3 hours, 0.54 ± 0.14 . At 4 hours the HSI saturation was found to be 0.52 ± 0.13 and then 0.57 ± 0.07 at 5 hours, 0.44 ± 0.16 at 6 hours, 0.48 ± 0.13 at 7 hours, and finally 0.38 ± 0.14 at 8 hours. Like the intravenous group, among the different time points the differences were not found to be statistically significant. More importantly, at matched time points between the intravenous and intraperitoneal group, no statistically significant difference was found either.

2.3.9 Effect of Injection Method on Leukocyte Luma in Cranial Windows, Figure 13 and

14

When the luma of leukocytes was analyzed through the cranial window, the value in the intravenous group at 1 hour was found to be 189.48 ± 5.55 . The value dropped to 170.12 ± 5.15 at 2 hours and continued to fall to 134.59 ± 6.78 at 3 hours. It rose again at 4 hours reaching a value of 172.81 ± 3.97 and fell to 139.51 ± 5.99 at 5 hours. The final 3 hours were more stable with a value of 152.99 ± 3.37 at 6 hours, 153.54 ± 3.91 at 7 hours, and ultimately 156.48 ± 3.90 at 8 hours. The difference from 1 hour to every other time point was statistically significant within the intravenous group. In the intraperitoneal group, the luma at 1 hour was 143.40 ± 5.18 , 103.50 ± 4.88 at 2 hours, 129.86 ± 2.84 at 3 hours, and 127.70 ± 2.87 at 4 hours. At later time points, the luma reached values of 114.99 ± 3.43 at 5 hours, 125.40 ± 2.74 at 6 hours, 112.65 ± 3.86 at 7 hours, and finally 113.67 ± 3.61 at 8 hours. The difference in luma measurements among the intraperitoneal group showed a statistically significant difference from the measurement at 1 hour and every other time point except 3 and 4 hours. However, at each matched time point, the difference in the groups did not reach statistical significance.

2.3.10 Effect of Injection Method on Quantization of Rolling Leukocytes, Figure 15

Rolling leukocytes were assessed through the cranial windows every hour for 8 hours. In the intravenous group, 42.73 ± 11.44 cells/min were observed rolling at 1 hour. At 2 hours, the number of rolling leukocytes was 42.10 ± 10.04 cells/min and 62.37 ± 11.05 cells/min at 3 hours. The number of rolling leukocytes dropped to 35.80 ± 4.67 cells/min at 4 hours and then was 50.58 ± 11.62 cells/min at 5 hours. The final 3 hours of observation showed leukocytes rolling at 44.32 ± 9.91 cells/min at 6 hours, 40.06 ± 9.55 cells/min at 7 hours, and to 37.56 ± 13.17 cells/min at 8 hours. Among the intravenous group, there existed no statistically significant difference among

the different time points. The intraperitoneal group exhibited 80.18 ± 32.66 cells/min at 1 hour and 38.25 ± 10.79 cells/min at 2 hours. Rolling in the intraperitoneal group was found to be 47.33 ± 14.97 cells/min at 3 hours, 38.87 ± 18.62 cells/min at 4 hours, and 59.02 ± 23.51 cells/min at 5 hours. The final 3 time points evaluated showed 55.45 ± 16.14 cells/min at 6 hours, 59.91 ± 26.98 cells/min at 7 hours, and finally 70.48 ± 25.23 cells/min at 8 hours. Within the intraperitoneal group, the 1 hour time point demonstrated a statistically significant difference among every other time point except 8 hours. It should be noted that within the intraperitoneal group, 2 of the mice showed very high rolling and adhesion at 1 hour.

When the 2 methods of injection were compared to one another, only at 1 hour was a statistically significant difference found. The intraperitoneal group showed a greater amount of rolling but supported the hypothesis that intraperitoneal rhodamine would be as efficacious as intravenous rhodamine in detecting rolling leukocytes.

2.3.11 Effect of Injection Method on Quantization of Adherent Leukocytes, Figure 16

Adherent leukocytes were also evaluated between the 2 injection methods. In the intravenous group, at 1 hour 731.87 ± 124.09 cells/mm were found adhered compared to 631.39 ± 58.46 cells/mm at 2 hours. The number of adhered cells rose again at 3 hours reaching 773.52 ± 79.07 cells/mm and 835.20 ± 103.82 cells/mm at 4 hours. The number of adhered cells at 5 hours was 1445.55 ± 606.58 cells/mm, 1052.54 ± 70.57 cells/mm at 6 hours, 1195.75 ± 187.61 cells/mm at 7 hours, and 1050.93 ± 113.12 cells/mm at 8 hours. Within the intravenous group, a statistically significant difference was found between 1 hour and 5, 6, 7, and 8 hours. In the intraperitoneal group, adhered cells were 496.75 ± 153.21 cells/mm at 1 hour, 533.49 ± 57.03 cells/mm at 2 hours, and 1042.07 ± 54.83 cells/mm at 3 hours. At 4 hours the number of adhered cells/mm was 983.78 ± 110.78 , at 5 hours, 1305.40 ± 404.14 cells/mm, and at 6 hours 1476.1 ± 106.47 cells/mm. At

the final time points, 1101.70 ± 210.99 cells/mm were found adhered at 7 hours and 1074.94 ± 138.26 cells/mm at 8 hours. Within the intraperitoneal group, a statistically significant difference was found between 1 hour and all other time points except for 2 hours.

As in the rolling data, 2 of the mice in the intraperitoneal group displayed high rolling and adhesion at 1 hour ultimately raising the overall mean for the 1 hour time point. In comparing the groups a statistically significant difference was found between the intraperitoneal and intravenous methods at 1 hour and also at 6 hours. At 1 hour, the intravenous group showed only a slightly higher number of adhered cells (731.87 IV vs 496.75 IP). At 6 hours, the intraperitoneal group showed a greater number of adhered cells with 1476.10 versus 1052.54 in the intravenous group.

2.3.12 Effect of Injection Method on Leukocyte Properties Examined by Flow Cytometry

Blood was extracted from both the intravenous group and the intraperitoneal group 4 hours after injection and analyzed utilizing flow cytometry. When an equal dose was administered in both methods, overall staining of leukocytes in the intravenous group was $85.88\% \pm 1.70\%$ while in the intraperitoneal group it was $73.28\% \pm 5.84\%$, Figure 17. This difference was not statistically significant. The fluorescent mean of the intravenous group was found to be 450.29 ± 173.46 compared to 119.182 ± 72.76 in the intraperitoneal group, Figure 17. This difference was statistically significant, $p = 0.0123$. Lastly, the geometric mean was analyzed and found to be 308.15 ± 98.85 in the intravenous group compared to 100.308 ± 36.25 in the intraperitoneal group, Figure 17. This difference was also found to be statistically significant, $p = 0.0085$.

Cells were then gated to differentiate lymphocytes (T cells, B cells, and natural killer cells) and monocytes from granulocytes (basophils, eosinophils, and neutrophils), Figure 18. In mice administered rhodamine intravenously, the rhodamine stained $72.77\% \pm 9.83\%$ of lymphocytes

and monocytes (agranulocytes), Figure 19. In the intraperitoneal group, only $54.90\% \pm 17.00\%$ of agranulocytes were stained, Figure 19. This difference was not statistically significant. However, the differences were statistically significant for the fluorescent mean and geometric mean of agranulocytes among the injection methods. The mean fluorescent value of agranulocytes injected with intravenous rhodamine was 495.68 ± 177.51 versus 138.774 ± 38.76 in the intraperitoneal group ($p = 0.012$), Figure 19. The geometric mean of intravenously injected mice was 316.96 ± 107.81 and in the intraperitoneal group it was only 100.76 ± 24.40 ($p = 0.0155$), Figure 19.

Like the lymphocytes and monocytes, when the granulocytes were studied, significant differences were found between the fluorescent mean and the geometric mean but not the percentage of overall stained granulocytes. The fluorescent mean is simply the arithmetic mean of the population while the geometric mean is the summation of the log of the means (268). The geometric mean is preferred for populations that may be skewed in such that the fluorescent mean is more readily distorted by outliers in data (268). Both have been included here for completeness. The intravenously injected mice showed $99.84\% \pm 0.08\%$ of their granulocytes stained while the intraperitoneal group had $94.30\% \pm 7.63\%$ stained, Figure 19. The mean fluorescent value of intravenous rhodamine stained granulocytes was 471.24 ± 58.42 versus 184.73 ± 100.88 in the intraperitoneal group ($p = 0.0465$), Figure 19. Lastly, the geometric mean of the granulocytes was 397.99 ± 95.74 in the intravenous group and 148.53 ± 74.54 in the intraperitoneal group ($p=0.0263$), Figure 19.

Since the fluorescent mean and geometric mean of agranulocytes and granulocytes were lower with the intraperitoneal method, the amount of rhodamine injected intraperitoneally was doubled and compared to the original dose of intravenous rhodamine. In this study, intravenous

rhodamine stained $79.89\% \pm 5.79\%$ of all leukocytes compared to $85.62\% \pm 6.40\%$ of leukocytes from mice given a double dose intraperitoneally, Figure 20. The fluorescent mean was 387.35 ± 44.15 in the intravenous group and 365.58 ± 80.49 in the intraperitoneal group, Figure 20. Lastly, the geometric mean was 268.09 ± 30.47 in the intravenous group compared to 269.44 ± 53.54 in the intraperitoneal group, Figure 20. None of these parameters reached statistical significance when the differences were examined.

The significant difference among the lymphocyte and monocyte values were also erased when the amount of rhodamine administered through the peritoneum was doubled. Intravenous administration of rhodamine stained $70.80\% \pm 5.30\%$ of agranulocytes while intraperitoneal administration stained $79.67\% \pm 6.13$, Figure 21 and 22. The fluorescent mean in the intravenous group was 397.18 ± 101.94 versus 288.04 ± 108.68 in the intraperitoneal group, Figure 22. The geometric mean was found to be 240.51 ± 55.67 in the intravenous group and 192.55 ± 68.85 in the intraperitoneal group, Figure 22. None of these differences reached statistical significance.

Little change was seen when the intraperitoneal dose of rhodamine was doubled versus intravenously injected dye when granulocytes were examined. The percentage of stained granulocytes in the intravenous group was $99.84\% \pm 0.15\%$ and compared to $99.79\% \pm 0.19\%$ in the intraperitoneal group, Figure 22. The fluorescent mean was 370.45 ± 110.53 in the intravenous group and 485.76 ± 285.75 in the intraperitoneal group, Figure 22. This was the only time that the fluorescent mean of the intraperitoneal group achieved a higher value than in the intravenous group. The same trend was seen for the geometric mean in which the value for intravenous mice was 313.93 ± 88.90 but rose to 424.50 ± 244.38 in the intraperitoneal group, Figure 22. The statistically significant difference originally seen in the granulocytes fluorescent mean and

geometric mean was not observed when the amount of rhodamine injected intraperitoneally was doubled.

2.3.13 Effect of Photothrombotic Ischemia on Pial Blood Flow

After establishing a more complete understanding of Rhodamine 6G for use in visualization of cranial windows the technique was put forth in the study of cerebral ischemia. Initially we had hoped to employ the intraperitoneal administration method for the stroke studies. However, when we employed the photothrombotic stroke induced by Rose Bengal the risk of Rhodamine 6G oxidizing and contributing to vascular injury became a concern. Ultimately for examination of the cranial window after photothrombotic stroke, we reverted back to intravenous administration to eliminate incubation time and circumvent any further or contributing photogenic injury to vessels.

When flow was examined approximately 1 hour after the onset of ischemia, 0.89 ± 0.35 vessels/animal had flow compared to 6.0 ± 1.054 vessels/animal that had no flow, Figure 25. This translated to $15.54\% \pm 8.02\%$ of vessels with flow compared to $84.46\% \pm 8.02\%$ of vessels without flow, Figure 25. This difference was statistically significant. Of the vessels that had flow, the average vessel diameter was $49.97 \mu\text{m} \pm 8.31 \mu\text{m}$ while vessels that did not show blood flow had an average diameter of $35.58 \mu\text{m} \pm 3.29 \mu\text{m}$, Figure 26. This difference was not statistically different.

2.4 Discussion

Our studies here have allowed us to determine that injections of Rhodamine 6G into the peritoneal cavity exists as a technique as efficacious as traditional intravenous injections. However, the added benefit of reducing surgical risk and complications has been achieved. More

so, over the course of 8 hours, we were able to characterize the physical properties of in vivo Rhodamine 6G administration.

Visual responses to light emitting bodies can be influenced and polluted by the presence of other visual stimuli immediately neighboring the spatiotemporal field of the retinal receptors (261). To achieve maximum retinal sensitivity, the eyes of the observer should be fully adapted to the dark environment such that the visual mechanisms of the eye have adjusted to the surroundings (261, 269). If the luminance of the background and surroundings remain low enough to prevent any significant number of photosensitive rhodopsin from activating in the eye, then the eye's ability to detect light remains at its completely dark adapted level (261). To ensure this, both the collection and analysis of images were performed in the dark after adequate time for adaptation to occur. Leukocytes containing Rhodamine 6G emit light when excited with appropriate wavelengths of fluorescent light, but enough rhodamine must be present in the cell for the cell to stand out from the background.

In these cases, the light elicits a response from the eye of the observer when an average of 5 to 14 photo receptors undergo activation and stimulation by a photon (261). In such a case a target becomes detectable and discernible when its luminance exceeds statistical fluctuation in the luminance of the background (261). Schrieber defines this contrast as

$$C = (\Delta L)/L$$

where C = contrast and L = Luminance (261). Adding limitations to this yields

$$C_{\min} = (\Delta L_{\min})/L = (\Delta N_{\min})/N$$

where N = the number of photons emitted during a detection interval (261). This contrast must be at least 1% to 3% from the background to meet the minimal detection threshold (261).

For the rhodamine staining to be efficacious, cells would have to take up enough rhodamine to stand out from the unstained background such that an observer could identify them. Of course, this would depend on the amount of rhodamine that actually entered circulation and ultimately each leukocyte. The 1% to 3% minimum contrast in luminance that allows for detection of a light emitting body from background is called the Weber-Fechner Fraction (261). Both injection methods have been shown to create enough contrast in the background to allow for detection of leukocytes up to eight hours and among the methods, there was no difference in the luma measurements of leukocytes.

Luma measurements exist as quantities proportional to the radiant power of an emitting body but calculations of such take into account the perception and visual capacities of the observer (252, 254, 258, 260). The magnitude of luminance remains proportional to physical power and in a sense represents the intensity of a body emitting light, but intensity fails to also takes into account the effect and nature of human vision (258, 260). Likewise, Smith describes the quantity as brightness perceived by observing the radiant energy and further characterizes it as a psychophysical adjustment to both the emitting device and the observers' perceptions as he interprets R, G, and B signals (260). This explains the emphasis calculations give the green component of the tristimulus signal since human vision remains most sensitive in the green portion of the spectrum where γ photoreceptors undergo activation (253). When examining the luma of peripheral leukocytes in the blood smears of the two groups, the most obvious and important conclusion to draw from the data lies in the fact that at each time point, there exists no statistically significant difference between the intravenous and the intraperitoneal group, Figure 5.

Despite the fact that over the first 2 hours, the intravenous group produced greater luma values, no visible difference could be detected in comparison to the intraperitoneal group as the

differences lacked statistical significance. More so, we had no difficulty in discerning and identifying leukocytes with either method. However, at three hours, the values were found to be essentially equal and the intraperitoneal group remained relatively constant up to 5 hours while the intravenous group continued to decrease in luma of the leukocytes. From 3 hours onward, the intraperitoneal group had higher luma values in the cells than the intravenous group. Compared to the luma values recorded at 1 hour in the intravenous group, aside from the 2 hour time point, all the other time points in the intravenous group were significantly different from the original intravenous luma measure at 1 hour. However, this was not the case in the intraperitoneal treated mice where compared to 1 hour, only the 2 hour and 8 hour time point were significantly different from the original measurement at 1 hour.

If a line of best fit were applied to both groups, the intravenous group would have a formula such that $\text{luma} = -11.219x + 161.22$, where x represents the time in hours. The correlation coefficient for this line was 0.9684. If a similar linear regression was applied to the intraperitoneal group, the formula found was $\text{luma} = -3.733x + 132.86$ with a correlation coefficient of only 0.1531. The low index of correlation here stems from the fact that in the intraperitoneal group the luma values rose to 3 hours, remained constant to 5 hours, and then decreased. The slopes of these 2 lines reached statistical significance in examining their differences ($p = <0.0001$).

However, if the linear regression was only applied to the time points from 3 hours to 8 hours, a different situation becomes apparent, Figure 23. The formula for the line of best fit for the intravenous group does not change substantially and becomes $\text{luma} = -11.391x + 158.1$. The correlation coefficient drops to 0.6449 since the time points at 5 hours and 7 hours are slightly higher than would be expected and the expected values at 1 and 2 hours are not in the calculation to counteract this. However, in the intraperitoneal group, the formula becomes $\text{luma} = -11.379x$

+ 139.58 with a correlation coefficient of 0.9374. Now the linear regression produces lines with slopes essentially equal to one another and not significantly different.

This leads to the conclusion that intraperitoneally injected rhodamine stains leukocytes such that they remain equally identifiable to intravenously treated mice at 1 hour based on leukocyte luma values. However, the maximal luma for intraperitoneal rhodamine will not be reached until approximately 3 hours. It is plausible that sufficient diffusion occurs at 1 hour but for the rhodamine to achieve a maximal impact, diffusion requires up to 3 hours. It also continues up to 5 hours producing nearly constant values from 3 to 5 hours suggesting that the diffusion continues at a constant rate up to 5 hours. After 5 hours the majority of rhodamine probably has left the peritoneal cavity and diffusion into circulation slows as the leukocyte luma values continue to decrease through the 8 hour time point. At this point, it may be possible to see cumulative effects of hepatic metabolism and deactivation (247).

Likewise, the intravenous rhodamine reaches a maximal luma in 1 hour and continues to decrease over the next 8 hours although both methods allow for visualization of leukocytes up to 8 hours. The peak at 1 hour in intravenous administration seems plausible as all of the Rhodamine 6G was injected directly into the blood stream and from that point on would only face metabolism and clearance from circulation. In line with this reasoning, the value of the leukocyte luma is most likely dependent on the concentration of rhodamine in the vasculature system at any given time. Therefore, based on luma measures, no advantage exists in intravenous injections over intraperitoneal injections. Each method produces enough staining and dye uptake to allow for detection of cells from their unstained background.

When the HSL lightness was examined in the leukocytes, a very similar pattern appeared in the data. Lightness refers to the height along the achromatic axis in the cylindrical HSL color

system and can alternatively be called brightness and intensity although it should not be confused with the HSI intensity described later (252, 259). White has a lightness of 0.5 and black scores a 0 (254, 259).

Like luma, when the groups were compared at matching time points, there was no statistically significant difference among the intraperitoneal group and the intravenous group. Likewise, in either group, there was no statistically significant difference from all the time points compared to the measurements at 1 hour within groups, Figure 6. While the luma measurements were designed to take into account the perception of the observer based on cells in the eye, the lightness utilizes a simple average of the maximal and minimal tristimulus signals. This quantity does not produce a bias based on visual perceptions. It is best employed when the objective is to distinguish colors by their brightness (260). Since experiments revealed that cells were in fact identifiable up through 8 hours, we wanted to comprehensively examine physical parameters. First of all, this would allow for the detection of any differences in the injection methods as well as characterize the physical properties of Rhodamine 6G *in vivo* over the course of 8 hours. Lastly, conversion to gray scales and comparisons of brightness lacks a uniform consensus on a standardized procedure and thus we explored multiple avenues to do so (254).

Again, the maximal lightness values for the intraperitoneal group were found at 3 hours and they remained constant up to 5 hours before decreasing. The intravenous group immediately peaked at 1 hour and continued to decrease over the 8 hour time course. When examining the linear regression from 3 hours to 8 hours, again, the slopes were found to be very similar and only differed by a rate of 0.0017 lightness/hour suggesting that the rhodamine was eliminated and cleared at an equal rate regardless of the injection method ultimately producing an equal decrease in lightness, Figure 23. Like luma, this supported the idea that maximal diffusion takes up to 3

hours for intraperitoneal rhodamine application but for every time point, no difference in the lightness of leukocytes existed between the rhodamine injected intravenously versus the rhodamine injected intraperitoneally. More so, this measure of lightness showed that in either injection method, the lightness did not significantly change over the course of 8 hours within groups. However, differences were noted in the luma of leukocytes within groups but not between groups. This most likely stems from the fact that the luma calculations build in biases of human visual perception and these biases reveal statistically significant decreases over 8 hours.

HSV value and HSI intensity also demonstrated these same findings, Figure 7 and 8. Like lightness, value refers to the height along the achromatic axis in the cylindrical HSV color system ranging from 0 at black to 1 at white (252, 260). Simply put, it measures a deviation from black (252, 260). In the peripheral blood smears or intravital images, the background appears black so a departure from this black towards white would allow for detection of rhodamine stained cells. Value exists as the quantity of the maximal tristimulus measurement for a given light source (254, 260). For the leukocytes examined in the blood smears, the maximal tristimulus measurement always came from the Red component. The HSV value would be utilized when equal weight should be attributed to pure hues, for example, as in a painting program (260). It seems that HSL lightness would be a more accurate methodology for quantifying the amount of light and ability to detect cells but HSV Value has been included here as well for completeness and also as a novel endeavor to characterize the colorimetric properties of Rhodamine 6G *in vivo*. In fact, several new studies have delved into the use of HSL, HSV, and HSI color systems for analysis of medical imaging and thus identifying parameters associated with rhodamine could prove useful in other applications such as the development of computerized algorithms for image analysis (256, 262, 267).

More so, the HSI color space also imitates human color perception and should generate results more aligned to vision as perceived by an observer (256). According to Li, intensity shows the lightness of a color ranging from black to white but this should not be confused with HSL lightness as they are calculated very differently (256). HSI intensity calculations attribute equal weight to each of the 3 tristimulus measurements and simply take an average of them (256).

When the HSV value was examined it produced a pattern similar to both luma and HSL lightness. Again, the data shows an even decrease from 1 hour to 8 hours in the intravenous group with the intraperitoneal group obtaining a maximal value at 5 hours although it remained relatively constant from 3 hours to 5 hours. When the linear regression from 3 hours to 8 hours was examined, the slopes were nearly equal (differing only by 0.0086 value/hour) supporting the idea that elimination of rhodamine and its decrease in value occurs at an equal rate between both groups, Figure 23. More so, it supports the notion that intraperitoneal diffusion of rhodamine takes approximately 3 hours for it to reach peak effect and that the value calculated depends on the amount of rhodamine in the vasculature.

HSI intensity nearly mirrored this same pattern supporting the above findings. In the peripheral blood smears, the red component always achieved the maximal measurement with a moderate contribution from green and almost no blue component. While Li contends that HSI color space mimics human color perception, it appears that luma more closely approximates this as it places emphasis on the green component to mimic cone cell sensitivity (253, 256). Despite the discrepancy, the findings were quite similar to the luma calculations. Again, intravenous injection achieved a maximal intensity at 1 hour and decreased over 8 hours with intraperitoneal injections reaching maximal intensity at 5 hours, although it was only slightly higher than at 3 hours and relatively stable from 3 to 5 hours. It appears that in this color space, the findings

support the idea that intraperitoneal injection requires about 3 hours for diffusion to occur fully and this process continues up to 5 hours. Meanwhile, the slope of a linear regression applied from 3 hours to 8 hours showed no significant difference in slope between the 2 methods (a difference of 0.0024 intensity/hour between slopes) that shows elimination and decrease in intensity signal occurs at an equal rate in the 2 methods, Figure 23.

In terms of saturation, two patterns were found in the data pertaining to peripheral leukocytes in blood smears. Saturation represents the purity of a hue with pure color having a value of 1 (260, 266). As saturation decreases and approaches 0, more gray infiltrates the hue and its color becomes less vivid (260, 266). Cells with unsaturated values would be hard to differentiate against a black background and thus provides the impetus for examining this quality. HSL saturation calculations rely on the HSL lightness quantity calculated whereas HSV saturation only on the tristimulus measures (254, 259). Despite this dependence, both HSL and HSV saturation returned nearly constant results. HSL saturation hovered just about 0.7 while HSV saturation averaged just above 0.8. The HSV and HSL saturation measurements of leukocytes had no statistically significant difference among the time points within the two groups or between the two groups at any time point in particular.

The trend in both color systems demonstrates that both methods of injection produce nearly identical levels of saturation. More so, both methods of injection yield nearly saturated hues (approximately 0.8 in the HSV system and 0.7 in the HSL system). Lastly, in terms of saturation, the 3 hours for maximal diffusion to occur in the intraperitoneal injection system do not play a factor. Nearly saturated tones were achieved at 1 hour in both injection groups which also leads to the conclusion that saturation remains independent of the concentration of rhodamine in the

HSV and HSL system at any given time in contrast to luma, lightness, value, and intensity which all depend on the rhodamine present in the blood vessels, Figure 10 and 11.

In contrast, the HSI saturation in leukocytes returned results that very much looked like the pattern found for luma, lightness, value, and intensity, Figure 12. In calculating the HSI saturation it becomes apparent that the number under the radical sign approaches r^2 and essentially the saturation equals r or the quantity of the red tristimulus vector normalized to [0,1] for this data set. The calculation for HSV value remains simply the maximal tristimulus quantity collected and in the peripheral blood smears that always came from the red component. Thus, the trend for HSI intensity should be reflective of the HSV value. Like the HSV value results, the HSI saturation showed that intravenous rhodamine peaked at 1 hour and decreased over the course of 8 hours but did not change significantly within this group. Intraperitoneal rhodamine took 5 hours to reach maximal saturation, although it did not change substantially from a near maximum at 3 hours, suggesting that in terms of HSI intensity, diffusion time and concentration both contribute to the saturation measurement of leukocytes. However, within the group of mice receiving intraperitoneal rhodamine there was no statistically significant difference among time points. Likewise, there was no significant difference between the two groups suggesting that despite the time needed for the intraperitoneal diffusion, at any time point, saturation in one group versus the other does not differ significantly.

Like the luma, lightness, value and intensity quantities examined, a linear regression applied from 3 hours onward produced lines of best fit with nearly parallel slopes. The slopes differed only by 0.0064 saturation/hour indicating that HSI saturation decreases at the same rate in both intravenously and intraperitoneally injected rhodamine, Figure 23.

HSI saturation decreased in the intravenous group from 1 hour to 8 hours and in the intraperitoneal group it rose, and then decreased, conferring a dependence on diffusion time for intraperitoneal rhodamine to reach maximal saturation, Figure 12. In addition, it appears that HSI saturation measurements depend on the quantity of rhodamine in the system. On the other hand HSV and HSL saturation values appeared unchanged over the course of 8 hours with no difference between the groups. The saturation measurements in these color systems showed no dependence on time for diffusion and thus, no dependence on the amount of rhodamine in the system. Depending on the color system utilized for the purpose at hand, these effects and outcomes should be taken into consideration. However, we can now further characterize *in vivo* Rhodamine 6G over the course of 8 hours according these colorimetric principles and properties.

Hue measures the angle between a vector projected towards 0° and the vector defined by the R, G, and B tristimulus values with 0° = pure red and 120° = pure yellow ultimately arriving back at pure red as 360° is approached (259, 266). More simply hue refers to the pure color (254, 256). Results for hue measurements over the course of 8 hours also produced a pattern similar to the luma measurements, Figure 9. Intravenous rhodamine peaked early and decreased over the course of 8 hours indicating a shift towards pure red over the course of the 8 hours. At 1 hr, intravenous rhodamine had an angle measure of 40.74° and this dropped to 12.56° at 8 hours. In simple terms, the color changed from a red with a hint of yellow to more red throughout the study.

The hue of intraperitoneal rhodamine saw a peak at 3 hours and then decreased over the course of 8 hours. Like luma, hue requires appropriate time for diffusion to occur in intraperitoneal injections in order for the maximal effect to be seen and also depends on the concentration and amount of rhodamine in circulation. Despite the different patterns, the differences in hue at matched time points were not significantly different. Likewise, within each group, the change

over 8 hours was not statistically significant but provided an idea of the range of hues expected with rhodamine administration in vivo.

Calculations for hue in the HSL and HSV system utilize identical formulas (254). In the HSI system the formula takes a more geometric approach but returned results within 1° of the hues already calculated for HSV and HSL. That data was not shown.

After such examinations, we had found that in peripheral blood leukocytes took up Rhodamine 6G equally effectively in both techniques of administration and provided for visual detection. We had found no differences over the course of 8 hours and also gained insight to the colorimetric properties of Rhodamine 6G in vivo for that period of time. Our examination sought to elucidate any difference in the physical properties and thus colorimetric parameters examined. These properties relied on the fact that the images from peripheral blood smears could be captured in color. However, our apparatus only allowed for the collection of black and white images during epi-illuminance intravital microscopy and thus we would not be able to evaluate the same properties. Cranial windows were implanted and leukocytes were observed through the window for the course of 8 hours. Again, there existed no difficulty in locating the cells regardless of the injection technique for the entire period of time Figure 13.

Since the movies captured, and eventually the still images constructed from these movies were in black and white, the tristimulus values would yield equal values of R, G, and B attributes (259). It had previously been pointed out that luma and gray scale had been used interchangeably in published literature (254). Gray scale would seem to be an appropriate term here but the paper will continue to stay with the nomenclature luma for simplicity and consistency. HSL lightness, HSV value, and HSI intensity would return the same values as the luma due to the nature of the formulas and fact that all three tristimulus values have equal contribution. Thus, further graphical

depiction of them or discussion is not provided in the context of visualization through a cranial window. Saturation, regardless of the color system utilized, would produce a value of 0 which remains consistent with the notion that these images are devoid of color. Lastly, hue would also be undefined as the images are achromatic. If an investigator has access to a color epilluminescence intravital microscope then all of these values could again be examined. For the purpose of this study, luma remains the most useful and versatile quantity to examine since it takes into account observer perception and the nature of retinal systems (254, 260). We were able to investigate that quantity and also evaluate both rolling and adhesion of leukocytes through the cranial window to determine if either method of injection produced a difference.

When the images were collected from cranial windows and evaluated for luma of leukocytes, the patterns seen with luma in blood peripheral slides were not found, Figure 13 and 14. Overall, the intravenous injection of rhodamine produced luma through the cranial window that decreased over the course of 8 hours. The leukocyte luma measures from cranial windows did not show an increase up to 3-5 hours prior to decreasing. The intraperitoneal group also decreased over the course of 8 hours and always had lower luma values at matched time points. However, the difference between the groups was not statistically significant. A linear regression showed that the slope of the line for intravenous injection had a slope of -3.2935 luma/hour versus the intraperitoneal group which had a slope of -2.2818 luma/hour, Figure 24. The difference in these slopes was not statistically significant and had a P value of 0.3166 ultimately leading to the conclusion that the change in luma over time did not differ among the two groups.

The rise in the intraperitoneal group up to 3 hours was not observed in luma of leukocytes calculated from cranial windows suggesting that while in peripheral blood smears 3 hours are required for the intraperitoneally applied rhodamine to reach a maximum luma, that it is not

necessary in cranial window observations. Several reasons probably account for this. First of all, the nature of the system plays a factor in the leukocyte luma. In producing the blood smears, the blood is spread directly onto a slide and examined directly. In the cranial windows, the cells are examined through the surrounding endothelial cells of the pial microvasculature, then a layer of isotonic saline, and then a glass window before entering the optics of the microscope. Each transition of medium contributes to some degree of refraction that changes the light emitted from the rhodamine stained cells. In peripheral blood smears, the change in luma from 1 hour to 3 hours in the intraperitoneal group was 16.0484. In terms of luma, this is a very small value and would be unnoticeable to the observer. However, in the studies here, this trend was highly reproducible. As the light refracts, it not only bends but its wavelengths shifts. Depending on the direction of the shift, the luma value could change as the tristimulus values reaching the optics of the microscope would differ. Regardless, refraction and subsequent transmission through several media may account for this loss of detail in collecting the image through cranial windows.

Secondly, in the collection of images with the peripheral blood smears, the images were captured from a live video feed in the software utilized with that microscope. In contrast, the software attached to the epi-illuminescence intravital microscope does not allow for direct photo acquisition. Instead, video footage was captured and a second program was utilized to produce still images for analysis of the tristimulus values. Generally speaking, almost all real channels and storage devices contribute noise and produce errors in data (261). Some errors in data processing through acquisition, multiple file saves, and conversions could account for the loss of intraperitoneal rise to the 3 hour time point observed in peripheral blood smears.

In brief, the question of whether intraperitoneal rhodamine would be as efficacious as intravenous rhodamine in observing leukocytes through a cranial window could begin to be

answered. The studies here showed there was no difference in the luma of the cells observed and that over the course of 8 hours, both injection methods provided nearly equal luma in the leukocytes and allowed for detection of these cells. Cells could be detected through the entire time course in both treatment groups but the question still remained if quantifying these cells in each group would reveal a difference.

LPS was administered to the mice with cranial windows and the number of rolling and adhered leukocytes quantified. At 1 hour, 2 of the mice in the intraperitoneal group had very high levels of rolling suggesting some degree of baseline inflammation or increased susceptibility to LPS induced inflammation. This was the only time point in which a statistically significant difference was observed over the course of 8 hours of quantified rolling, Figure 15. Throughout the day of observation, the level of rolling remained relatively constant in the group administered rhodamine intravenously and after 1 hour, rose steadily in the intraperitoneal group. On the other hand, the number of adherent cells in both groups continued to increase up to 5-6 hours before some slight resolution was observed.

In the intraperitoneal group, after very high counts of rolling at 1 hour, the number of rolling leukocytes dropped back to the same level as in the intravenous group. Then over the next 7 hours, the number of rolling leukocytes rose relatively steadily although not statistically different from the intravenous group, Figure 15. In severe inflammation of the pial microvessels, the number rolling leukocytes can vary greatly, especially at early time points. There are several reasons for such variation. First of all, rolling and adhesion rely on changes in expression of endothelial and leukocyte receptors involved in rolling and adhesions such as selectins and integrins (238). For instance, E-selectin release from vesicles in endothelial cells could vary among animals. The time it takes for this to occur can vary among mice and the variation would

be particularly relevant and more prominent at early time points such as 1 hour. Secondly, steric hindrance from already adhered cells can block sites for other rolling leukocytes which would play a greater role as the time of observation progressed.

However, the concern at hand was whether or not the intraperitoneal injection would underestimate the degree of rolling leukocytes compared to the established method of intravenous injection and provide false negatives in future studies on leukocyte rolling. It was found that in fact, that was not the case as intraperitoneal injection demonstrated greater counts of rolling leukocytes, although not statistically significant from the intravenous group, except at 1 hour. As mentioned, the 1 hour time point had 2 animals in the intraperitoneal group with very high levels of inflammation. That time point also would be most prone to the effects of variation in the rate of changes in expression of proteins necessary to prepare the endothelial cells and leukocytes for rolling. Increasing the number of animals in the experimental groups probably would have eliminated the statistically significant difference observed at 1 hour. However, we were satisfied that the intraperitoneal method yielded sufficient and equal abilities to locate and quantify rolling leukocytes and opted not to invest the time or resources into such an endeavor. Thus, in addition to finding no changes in physical parameters of leukocytes, neither staining method produced any changes or differences in the number of rolling leukocytes observed through a cranial window.

In terms of adhesion, intraperitoneal injection also proved to be as efficacious as the intravenous method of rhodamine application, Figure 16. At 1 hour, there was a statistically significant difference and this time more adhesion was found in the intravenous group, whereas more rolling was found in the intraperitoneal group. A statistically significant difference was also seen at 6 hours in terms of adhesion. At that time point, the intravenously administered rhodamine group scored a lower than expected number of adhered leukocytes. Every effort was made to limit

the amount of light utilized in capturing the images to prevent photobleaching (81, 82). While attempts were made to locate and identify the same vessel and portion of that vessel for examination over the course of 8 hours, a slight shift of the field of view could change the area under observation and consequently affect the number of adhered leukocytes/mm². Some of the videos at 6 and 7 hours had a slight shift in the field of view and probably contributed to some of the variation even though the results were normalized to leukocytes/mm². Typically 3 fields of view are examined in each animal, but to thwart photobleaching and washout of the fluorescent signal, in these experiments the number of views was limited to 1 every hour. Despite the differences, there appears to be no advantage to injecting the rhodamine intravenously as opposed to intraperitoneally since aside from the 1 and 6 hour time points, the number of leukocytes found was not significantly different.

In reference to the statistically significant differences seen in the rolling and adhesions studies, 2 out of 3 times the intraperitoneal group demonstrated higher levels of rolling and adhesion. Thus, intraperitoneal injection did not underscore the number of leukocytes in such a study. Again, increasing the number of animals probably would have eliminated these differences but in examining the sum totality of rolling and adhesion studies the following conclusions were drawn. Intraperitoneal rhodamine, like intravenous application, allowed for visualization adequately over the course of 8 hours. Throughout that time period, there were essentially no significant differences in the number of leukocytes quantified. Other than the one hour time point which was probably most prone to variation, only at the 6 hour time point in adhesion was another difference found. At this time point, intraperitoneal rhodamine animals had a greater mean number of adherent leukocytes which dispelled the fears that intraperitoneal application would not sufficiently stain and underestimate the number of cells present. In short, the intraperitoneal

method of rhodamine application appeared equally efficacious with no substantial differences noted among the two techniques.

For an absolutely precise snapshot of the differences between the injection techniques, blood samples taken at 4 hours were subjected to flow cytometry for analysis. At 4 hours, enough time had been provided for maximal diffusion from the peritoneum to occur. In doing so, it was found that the intravenous method stained $85.88 \pm 1.70\%$ of all leukocytes compared to $73.28 \pm 5.84\%$ when the rhodamine was applied into the peritoneum, Figure 17. This difference did not reach statistical significance although the properties of the stained cells differed. Animals that received intravenous rhodamine had a mean fluorescent value of 450.29 ± 77.58 but intraperitoneally treated animals only had a mean fluorescent value of 119.18 ± 32.54 which did reach statistical significance, Figure 17. The lower fluorescent value indicates that each cell took up less rhodamine compared to cells from intravenously treated mice. Despite the fact that the difference among the overall number of cells was negligible, further evidenced by no changes in rolling and adhesion quantification discussed previously, the change in fluorescent mean suggests the rhodamine/cell ratio in intraperitoneal injection remains lower so that fluorescent activity is diminished. The histogram of the fluorescent signal depicts this as well demonstrating a much flatter pattern compared to a definitive peak in the intravenous group, Figure 17.

The same trend was observed in the geometric mean of the samples, Figure 17. The geometric mean is a weighted average of fluorescent means that skews the value towards the more frequently occurring fluorescent values and is less susceptible to outliers influencing the value (268). The geometric mean in the intravenous group was 308.15 ± 44.21 and in the intraperitoneal group 100.31 ± 16.21 which ultimately reflects the same findings as the fluorescent mean pertaining to the rhodamine/cell ratio. Overall, while intraperitoneal injection proved efficacious

at staining an equal number of cells, it did so with less rhodamine per leukocyte and produces a weaker fluorescent signal. Despite the weaker signal, both visual and mechanical detection of those cells were possible and thus intravenous injection conferred no discernible advantage over intraperitoneal injection aside from the strength of the signal reported by flow cytometry.

Based on the size and granularity of the cells, a distinction between granulocytes and a group composed of lymphocytes and monocytes (agranulocytes) was made (270). On flow cytometry two distinct populations of cells were located, Figure 18. The population with greater forward scatter, and therefore size, but less side scatter or granularity, were defined as lymphocytes and monocytes (agranulocytes) (270). The smaller more granular population was identified as granulocytes (270). In reference to the agranulocytes, among the injection techniques, no statically significant difference existed among the groups despite a near 18% difference in the number of stained cells. Agranulocytes from intravenous mice stained $72.72 \pm 4.40\%$ of the time compared to $54.98 \pm 7.60\%$ in intraperitoneal mice, Figure 19. The fluorescent mean and geometric mean were significantly lower in regards to lymphocytes and monocytes (fluorescent mean 495.62 ± 79.38 IV, 183.77 ± 17.34 IP; geometric mean 316.96 ± 48.21 IV, 100.76 ± 10.91 IP), Figure 19. Again, this probably reflects a lower rhodamine/cell ratio in intraperitoneal mice but overall does not affect the ability to detect the cells.

Like agranulocytes and leukocytes overall staining in general, granulocytes mirrored these findings. There was no significant difference in the number of cells stained with intravenous injection staining $99.83 \pm 0.04\%$ of granulocytes and intraperitoneal injection staining $94.30 \pm 3.41\%$ of granulocytes, Figure 18 and 19. Thus, intraperitoneal injection proved as efficacious as intravenous injection. Interesting here however, is the fact that in both groups, nearly all of the

granulocytes stained compared to only $72.72 \pm 4.39\%$ of agranulocytes in the intravenous group and $54.98 \pm 7.6\%$ in the intraperitoneal group.

Three hypotheses to why granulocytes stain so much more effectively than agranulocytes can be presented. First of all, the intracellular pH of granulocytes, and in particular, the mitochondria may remain closer to physiological pH than lymphocytes. Rhodamine 6G remains positively charged at physiological pH and this positive charge stands as a requirement for mitochondrial staining (240, 241). The intracellular pH of agranulocytes may deviate slightly from physiological conditions outside the cell ultimately affecting the charge status of the rhodamine and thus its ability to stain mitochondria.

Secondly, granulocyte membranes may simply be more conducive to rhodamine diffusion than lymphocytes and monocytes. Axiomatically, if rhodamine cannot enter a cell, it cannot stain mitochondria and thus fewer cells would appear stained if such a barrier existed to diffusion into the cell. Lastly, the number and concentration of intracellular mitochondrial may differ from agranulocytes to granulocytes. Rhodamine stains mitochondria and if a cell were to have fewer mitochondria, it would therefore take up less rhodamine and overall produce a lower fluorescent signal or not even register as a stained leukocyte (240, 241). On the contrary, however, published literature suggests that granulocytes have very few mitochondria since neutrophils, which compose the majority of granulocytes in circulation, rely heavily on glycolysis with low rates of cellular respiration (271). Lymphocytes on the other hand were reported to have higher levels of mitochondria with $6 \text{ mg}/10^9$ lymphocytes (272). However, the study investigating neutrophils utilized human cells and the lymphocyte study examined lymphocytes isolated from pig lymph nodes (271, 272). Neutrophils were reported to have very tightly controlled and regulated mitochondrial membranes to prevent activation of apoptotic proteins (271). The possibility exists

that not the quantity of mitochondria in a given type of leukocyte, but rather the degree to which its mitochondrial membranes discriminate transport and flux across it may alter staining characteristics. The properties of neutrophil mitochondrial membranes may favor Rhodamine 6G uptake and retention compared to agranulocytes.

Granulocytes from mice given rhodamine intraperitoneally also displayed lower fluorescent means and geometric means with differences that were statically significant compared to intravenous samples, Figure 19. The fluorescent mean was 471.24 ± 58.42 in the intravenous group and 184.73 ± 45.11 in the intraperitoneal group. The geometric means were 397.992 ± 42.82 intravenously and 148.53 ± 33.34 intraperitoneally. The difference in fluorescent means and geometric means probably stems from a lower rhodamine to leukocyte ratio with less rhodamine entering the cells in the intraperitoneal mice.

What remains unclear, however, stems from an overall view of this data. We speculated that rhodamine administered through the peritoneum produced lower fluorescent and geometric means because cells took up less rhodamine producing a lower rhodamine/cell ratio. While the flow cytometer detected differences in fluorescent and geometric means, analysis of luma, lightness, value, and intensity showed no discernible difference, especially at 4 hours. Perhaps the sensitivity of the flow cytometer is so great that it can detect this difference that is not perceptible to methods based on human vision. Regardless, both human vision and the flow cytometer were able to detect and identify the cells with equal effectiveness.

While the ability to detect and quantify cells remained unchanged regardless of the method of rhodamine application applied, it remained to be known if the differences seen in the percent of lymphocyte staining, fluorescent mean, and geometric mean could be overcome by increasing the dose administered into the peritoneum. All the studies to this point had been conducted with equal

doses of rhodamine, 0.1 mL. The intraperitoneal dose was doubled to 0.2 mL and flow cytometry repeated at 4 hours.

Overall, leukocytes from intravenous mice stained $79.89 \pm 2.59\%$ compared to $85.62 \pm 2.86\%$ in the intraperitoneal group, Figure 20. More so, the fluorescent mean and geometric means were found to be approximately equal between the two groups, Figure 20. The fluorescent mean was 387.35 ± 44.14 in the intravenous mice and 365.58 ± 80.49 in the intraperitoneal group. The geometric mean (268.08 ± 30.48 IV and 269.44 ± 53.54 IP) also showed essentially no difference. There was no statistically significant difference among these 3 parameters. It appears that increasing the amount of dye in the peritoneum could produce an effect duplicating the traditional intravenous injection. As the amount of dye in the peritoneal cavity is increased, the gradient also increases favoring diffusion of the dye across capillaries and into the vasculature. As more dye enters the vasculature, the gradient shifts proportionally to favor diffusion into the leukocytes for staining. The effect thus increases overall staining percentage, fluorescent mean, and concordantly, geometric mean.

As in the previous experiment, the leukocytes were separated based on their size and granularity to detect differences among the lymphocytes, monocytes, and granulocytes (270). Agranulocytes staining from intravenous mice changed very little from the previous experiment ($70.80 \pm 2.37\%$ versus $72.72 \pm 4.40\%$). No parameters among intravenous mice were changed which demonstrates the consistency of the technique. However, when the intraperitoneal dose of rhodamine was doubled the lymphocyte and monocyte staining changed from $54.90 \pm 7.60\%$ to $79.67 \pm 2.74\%$, Figure 21 and 22.

Fluorescent means increased in intraperitoneal mice given 0.2 mL rhodamine to 288.04 ± 48.60 but while not statistically different than intravenous lymphocyte fluorescent means, they

were lower (397.18 ± 45.59 IV), Figure 22. A similar pattern was observed for the geometric mean with intravenous agranulocytes achieving a geometric mean of 240.51 ± 24.90 while intraperitoneal geometric mean was only 192.55 ± 28.56 , Figure 22. The greater availability of rhodamine in the peritoneum simply could account for this observation.

Granulocyte staining in the intravenous group again achieved near 100% with a score of $99.81 \pm 0.07\%$ compared to $99.79 \pm 0.08\%$ in the intraperitoneal group, Figure 22. Increases were also seen in the fluorescent and geometric mean such that the intraperitoneal group produced higher values (fluorescent mean 370.45 ± 49.42 IV, 485.65 ± 127.79 IP; geometric mean 313.93 ± 39.76 IV, 424.502 ± 109.29 IP Figure 22. A higher concentration of rhodamine in the vasculature would account for the enhanced fluorescence as the diffusion gradient would be shifted to more aptly support diffusion into the leukocytes.

In brief, it seems that the fluorescent mean and geometric mean depend on the amount of available rhodamine in the vasculature. Intravenous administration offers a greater availability and the concentration gradient favors diffusion into the leukocytes ultimately yielding a higher fluorescent and geometric mean with a greater rhodamine/cell ratio. However, when the amount of rhodamine injected into the peritoneum is increased, the fluorescent and geometric means of the leukocytes in general also increases to levels approximately equal and not statistically different from intravenous injection. This suggests that a greater amount of rhodamine in the peritoneum favors diffusion into the vasculature to levels comparable to intravenous injection. In regards to individual groups of cells, when the dose of rhodamine given intraperitoneally was doubled, there again was no statistically significant difference in fluorescent or geometric means between the administration groups in either the lymphocytes and monocytes or granulocytes. It appears that an approximately equal amount of rhodamine entered the cell types in each situation.

Overall, numerous parameters were examined through the course of the study. The study started with properties of light and vision based on the perceptions of the observer. Luma, lightness, value, and intensity all showed no statistically significant difference between the administration techniques. The level of each parameter seemed to increase over the first 3 hours in the intraperitoneal group but when a linear regression was applied to the time period 3 hours to 8 hours, the slopes of lines of best fit between the two groups were nearly identical. The same findings that no significant differences existed were echoed in an examination of HSV, HSL, and HSI saturation as well as hue. Additionally, all of these colorimetric parameters helped to elucidate an understanding of the properties as they related to in vivo rhodamine administration over the course of 8 hours for potential future use such as the development of computer driven algorithms to automate detection of stained cells. When the luma was quantified through a cranial window rather than on a peripheral blood smear, again no statistically significant difference was found among the groups.

Therefore, it became clear that the visual properties of the cells observed did not differ. However, the question remained if the administration technique would affect the quantity of cells examined when exploring rolling and adhesion. The cranial windows were examined and rolling and adhesion quantified. Two mice in the intraperitoneal group demonstrated high baseline inflammation at one hour which produced a statistically significant difference at 1 hour. In terms of rolling, intraperitoneal administration had a higher value but the intravenous group showed greater adhesion at 1 hour. The response to LPS induced rolling and adhesion takes two to three hours to really begin and normalize with consistent values (83). It was concluded that the variation seen at 1 hour were the result of early LPS response as well as initially high inflammation and not the result of the different administration techniques.

Adhesion at 6 hours also showed a significant difference. While a difference was not seen at 5 hours or 7 hours, it again appears that this was due to variation among the animals in the LPS response and not a result of differences in administration technique. Limited views were collected at each time point to prevent photo bleaching and a slight shift in the field of view may also have contributed to this difference. Further, one of the questions the study sought to answer asked whether intraperitoneal injection would underscore the number of cells detected. At the 6 hour time point in adhesion, the intraperitoneal group displayed greater adhesion. Taking all this into account, it was concluded that there was no difference in quantifying rolling and adhesion among the injection methods. Lastly, regardless of the administration technique, at every time point over the course of 8 hours, enough contrast between the cells and the background was observed to satisfy the Weber-Fechner fraction to allow for detection of these cells and in each group an approximately equal number of leukocytes was located.

Lastly, the study examined the flow cytometry for an overall picture at 4 hours after the injections. Regardless of the injection method, there was no statistically significant difference in the overall percentage of leukocytes stained with rhodamine or in the lymphocyte or granulocyte subsets. When equal amounts of rhodamine were injected, there were statistically significant differences in the fluorescent and geometric means of all leukocytes and in the subsets. These findings were attributed this to a difference in the rhodamine/cell ratio based on the amount of rhodamine available in the vasculature for diffusion into the cell. However, the key question of whether the intraperitoneal method would prove as efficacious for identifying cells could be answered. Even with lower fluorescent and geometric means, the cells were located and counted by the flow cytometry to further the findings that intravenous method provided no advantage.

It was decided to explore a higher dose of intraperitoneal rhodamine to see if the result would match the intravenous method in terms of fluorescent and geometric means. When the dose of intraperitoneal rhodamine was doubled, all statistically significant differences in fluorescent and geometric means were erased. Again, it was concluded that these findings were dependent on the amount of rhodamine in the circulation and increasing the intraperitoneal dose favored diffusion into the vasculature.

Based on the findings from the visual analysis of peripheral blood smears and cranial window images, the quantification of the rolling and adhesion, and the flow cytometry studies, the study reached the conclusion that intraperitoneal rhodamine exists as a method as efficacious and reliable as intravenous injection. More so, in conjunction with all the complications that may arise from intravenous injection, it appears that intraperitoneal rhodamine injections stand as a more practical and safer laboratory practice than intravenous injection and the intraperitoneal route should be seriously considered in future investigations and experimental design. Lastly, an overall examination of vivo colorimetric properties of Rhodamine 6G stained cells was conducted and results collected for future investigations.

With a clearer understanding of Rhodamine 6G properties and visualization we hoped to employ this knowledge in our studies of cerebral ischemia. As previously discussed, however, some of our studies moved to a photothrombotic model of inducing ischemia. Due to the potential for the Rhodamine 6G to oxidize and cause further injury in response to light exposure, we reverted to the intravenous injection in visualization of cranial window in photothrombotic stroke. Some speculation as to the mechanism behind the photothrombotic stroke existed and we set out to determine if in fact the stroke demonstrated a complete and permanent occlusion.

The data concerning intravital visualization of pial blood vessels following photochemically induced ischemia reveal that only 15% of vessels after such insult retain blood flow, Figure 25. Visualization through a cranial window revealed stasis of flow in conjunction with large thrombus formations. This was in agreement with another study that demonstrated the rate of flow in capillaries approached 0 $\mu\text{m/sec}$ 10 minutes after the onset of induction of ischemia (273). On the other hand, flow and a lack of occlusions was reported in a second study (274). However, the photochemical element in this study was erythrosin B and activated by a laser instead of Rose Bengal and a cold, white light source as we had employed (274). Further this study examined the vessels 4 hours after the onset of ischemia whereas our examination was approximately 1 hour after the stroke. Although we have not reported that data here, we made multiple examinations of vessels 1 day after the photochemical stroke and found them to still be devoid of flow. Flow began to reappear 7 days after the stroke but we attributed this to neovascularization of scar tissue and not actual effective cerebral blood flow. The data here also indicated that vessels that retained flow were slightly larger than those that were occluded ($48.97 \pm 8.3 \mu\text{m}$ versus $35.58 \pm 3.30 \mu\text{m}$), Figure 26. Although not statistically significant, these findings were not unexpected. Larger vessels have much greater flow rates and shear forces which would help to prevent thrombotic occlusion.

Multiple groups have reported that platelet aggregation and coagulation have no effect on the size of the infarction after a photochemical stroke (274, 275). Here the images observed by intravital microscopy certainly indicated that thrombus formation lead to the blockage of multiple blood vessels. The possibility exists that this microcirculatory dysfunction may not exacerbate the injury induced by this model but this seems counterintuitive to other stroke reports that edema and microcirculatory dysfunction contribute to injury (81, 127, 128). Other studies have also indicated

the observed formation and presence of thrombi (276). The reported study also speculated that platelet activation may contribute to endothelial damage and drive injury progression (276). At this point the findings here indicate that platelet aggregation and thrombus formation occur following a Rose Bengal induced stroke and that blood flow is absent in 85% of vessels. The implications of this in the pathophysiology remain to be determined. However, with such a high percentage of occluded vessels, our laboratory has begun to regard this injury as a permanent occlusion model of cerebral ischemia.

2.5 Conclusion

Intravenous administration of Rhodamine 6G presents multiple risks pertaining to surgery, anesthesia administration, increased mortality, and infection among animals and remains confounded by a high degree of unsuccessful cannulation. Here the study sought to characterize colorimetric properties of Rhodamine 6G in leukocytes over the course of 8 hours and more importantly, examine the efficaciousness of intraperitoneal administration of rhodamine and compared to intravenous injection. Two main questions needed to be answered. Could the cells from both injection methods be equally well detected in terms of quantity? And if so, did the physical differences among the cells vary as a result of the injection technique?

Initially the study looked at peripheral blood smears to begin to characterize the colorimetric properties of Rhodamine 6G administered intravenously over the course of 8 hours and compared these findings to peripheral blood smears from mice administered rhodamine intraperitoneally. When luma, lightness, HSV value, HSI intensity, hue, and saturation (HSV, HSL, HSI) were examined, no differences among the administration groups could be found.

With regard to peripheral blood smears, it appeared that Rhodamine 6G administered intraperitoneally did not differ significantly at 1 hour, although the maximal value of many attributes would peak around 3 hours suggesting a time for maximal diffusion to occur. Luma was examined through the cranial window, as well, and again no difference in the groups was observed. Quantization of rolling and adhesion confirmed that intraperitoneal injection would not underestimate the number of leukocytes present and confirmed the notion that intravenous injection did not differ nor confer any advantage over intraperitoneal injection.

Lastly, the flow cytometer confirmed no statistically significant difference in the number of leukocytes that tested positive for fluorescent dye. However, when the cells were divided into lymphocytes, monocytes, and granulocytes, no difference existed in the overall percentage of stained cells however, intravenous injection scored higher fluorescent and geometric means. Again, the ability to detect the cells was not affected by the administration technique but these physical properties differed with cells from intraperitoneally administered rhodamine generating a lower fluorescent signal. This probably came from a lower rhodamine/cell ratio. However, the rhodamine/cell ratio could be changed to erase any changes in fluorescent and geometric means by increasing the dose of Rhodamine 6G administered into the peritoneum. When the dose injected intraperitoneally was doubled compared to the intravenous injection, no differences in the overall percent of stained cells, fluorescent, or geometric mean was observed.

Taking all of this into account with the known risks of intravenous injection, it was concluded that the risk to benefit ratio strongly favors the utilization, or at the very least, consideration of intraperitoneal injection for administration of Rhodamine 6G in the observation of leukocytes. This is strongly recommended in epi-illuminescence intravital fluorescence

microscopy but should be considered in any study that requires the administration of rhodamine for the detection or tracking of leukocytes.

Lastly, our work with intravital microscopy of Rose Bengal induced cerebral ischemia indicated that the injury essentially constitutes a permanent occlusion. 85% of vessels lacked flow 1 hour after the injury and large thrombus were identified. The mechanisms underlying Rose Bengal stroke were not well reported previously and we were able to provide further insight into the mechanism.

2.6 Works Cited

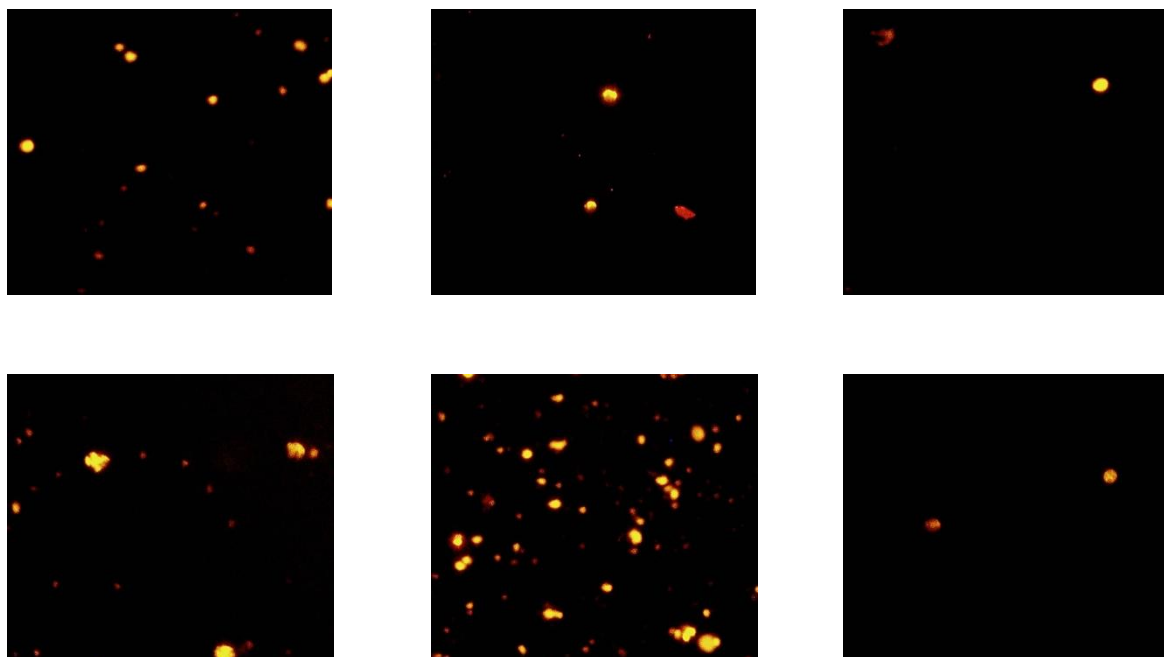
1. Zhang M, Adler MW, Aboot ME, Ganea D, Jallo J, Tuma RF. CB2 receptor activation attenuates microcirculatory dysfunction during cerebral ischemic/reperfusion injury. *Microvasc Res.* 2009;78(1):86-94.
2. AALAS Learning Library Animal Care and Use in Research and Education 2005 [4/17/2012].
3. Zhang M, Martin BR, Adler MW, Razdan RJ, Kong W, Ganea D, et al. Modulation of cannabinoid receptor activation as a neuroprotective strategy for EAE and stroke. *J Neuroimmune Pharmacol.* 2009;4(2):249-59.
4. Zhang M, Martin BR, Adler MW, Razdan RK, Ganea D, Tuma RF. Modulation of the balance between cannabinoid CB(1) and CB(2) receptor activation during cerebral ischemic/reperfusion injury. *Neuroscience.* 2008;152(3):753-60.
5. Jackson L. BD CellQuest Pro Software User's Guide. In: Gautho K, editor. San Jose, California2002.
6. Schreiber WF. Fundamentals of electronic imaging systems : some aspects of image processing. 3rd ed. Berlin ; New York: Springer-Verlag; 1993. xix, 332 p. p.
7. DeMarsh LE, Giorgianni EJ. Color Science For Imaging Systems. *Physics Today.* 1989(September):44-52.
8. Smith AR. Color Gamut Transform Pairs. *SIGGRAPH 78 Conference Proceedings.* 1978:12-9.
9. Joblove GH, Greenberg D. Color Spaces for Computer Graphics. *SIGGRAPH '78 Proceedings on Computer Graphics and Interactive Techniques* 1978:20-5.
10. Haifa BA, Bacarea V, Iacob O, Calinici T, Schiopu A. Comparison between Digital Image Processing and Spectrophotometric Measurements Methods. Application in Electrophoresis Interpretation. *Applied Medical Informatics.* 2011;28(1):29-36.
11. Poynton C. Color FAQ - Frequently Asked Questions Color 2006 [cited 2012 December 15, 2012]. Available from: <http://www.poynton.com/PDFs/ColorFAQ.pdf>.

12. Hunt RWG. The reproduction of colour. 6th ed. Chichester, West Sussex, England ; Hoboken, NJ: John Wiley & Sons; 2004. xxii, 702 p. p.
13. Barnes CD, Eltherington LG. Drug dosage in laboratory animals, a handbook. Rev. and enl. ed. Berkeley,: University of California Press; 1973. 341 p. p.
14. Hanbury A. The Taming of the Hue, Saturation, and Brightness Colour Space. 7th Computer Vision Winter Workshop. 2002:234-43.
15. Li B, Meng MQ. Computer-based detection of bleeding and ulcer in wireless capsule endoscopy images by chromaticity moments. *Comput Biol Med*. 2009;39(2):141-7.
16. Mahmoud-Ghoneim D. Optimizing automated characterization of liver fibrosis histological images by investigating color spaces at different resolutions. *Theor Biol Med Model*. 2011;8:25.
17. van Der Laak JA, Pahlplatz MM, Hanselaar AG, de Wilde PC. Hue-saturation-density (HSD) model for stain recognition in digital images from transmitted light microscopy. *Cytometry*. 2000;39(4):275-84.
18. Levkowitz H, Herman GT. GLHS: A Generalized Lightness, Hue, and Saturation Color Model. *CVGIP: Graphical Models and Image Processing*. 1993;55(No. 4, July):271-85.
19. Goldsby RA, Kindt TJ, Osborne BA, Kuby J. Kuby immunology. 4th ed. New York: W.H. Freeman; 2000. xxv, 670 p. p.
20. Stewart CC, Stewart SJ. Multiparameter analysis of leukocytes by flow cytometry. *Methods Cell Biol*. 1994;41:61-79.
21. Johnson LV, Walsh ML, Chen LB. Localization of mitochondria in living cells with rhodamine 123. *Proc Natl Acad Sci U S A*. 1980;77(2):990-4.
22. Gear AR. Rhodamine 6G. A potent inhibitor of mitochondrial oxidative phosphorylation. *J Biol Chem*. 1974;249(11):3628-37.
23. Fossati G, Moulding DA, Spiller DG, Moots RJ, White MR, Edwards SW. The mitochondrial network of human neutrophils: role in chemotaxis, phagocytosis, respiratory burst activation, and commitment to apoptosis. *J Immunol*. 2003;170(4):1964-72.

24. Dippenaar NG, Brand MD. The isolation of lymphocyte mitochondria and their regulation of extramitochondrial free Ca²⁺ concentration. *Biochem J.* 1982;202(3):731-7.
25. Ramirez SH, Haskó J, Skuba A, Fan S, Dykstra H, McCormick R, et al. Activation of cannabinoid receptor 2 attenuates leukocyte-endothelial cell interactions and blood-brain barrier dysfunction under inflammatory conditions. *J Neurosci.* 2012;32(12):4004-16.
26. Ding S, Wang T, Cui W, Haydon PG. Photothrombosis ischemia stimulates a sustained astrocytic Ca²⁺ signaling in vivo. *Glia.* 2009;57(7):767-76.
27. Frederix K, Chauhan AK, Kisucka J, Zhao BQ, Hoff EI, Spronk HM, et al. Platelet adhesion receptors do not modulate infarct volume after a photochemically induced stroke in mice. *Brain Res.* 2007;1185:239-45.
28. Kleinschnitz C, Braeuninger S, Pham M, Austinat M, Nölte I, Renné T, et al. Blocking of platelets or intrinsic coagulation pathway-driven thrombosis does not prevent cerebral infarctions induced by photothrombosis. *Stroke.* 2008;39(4):1262-8.
29. Lo EH, Dalkara T, Moskowitz MA. Mechanisms, challenges and opportunities in stroke. *Nat Rev Neurosci.* 2003;4(5):399-415.
30. Lo EH, Moskowitz MA, Jacobs TP. Exciting, radical, suicidal: how brain cells die after stroke. *Stroke.* 2005;36(2):189-92.
31. Ishikawa M, Sekizuka E, Oshio C, Sato S, Yamaguchi N, Terao S, et al. Platelet adhesion and arteriolar dilation in the photothrombosis: observation with the rat closed cranial and spinal windows. *J Neurol Sci.* 2002;194(1):59-69.

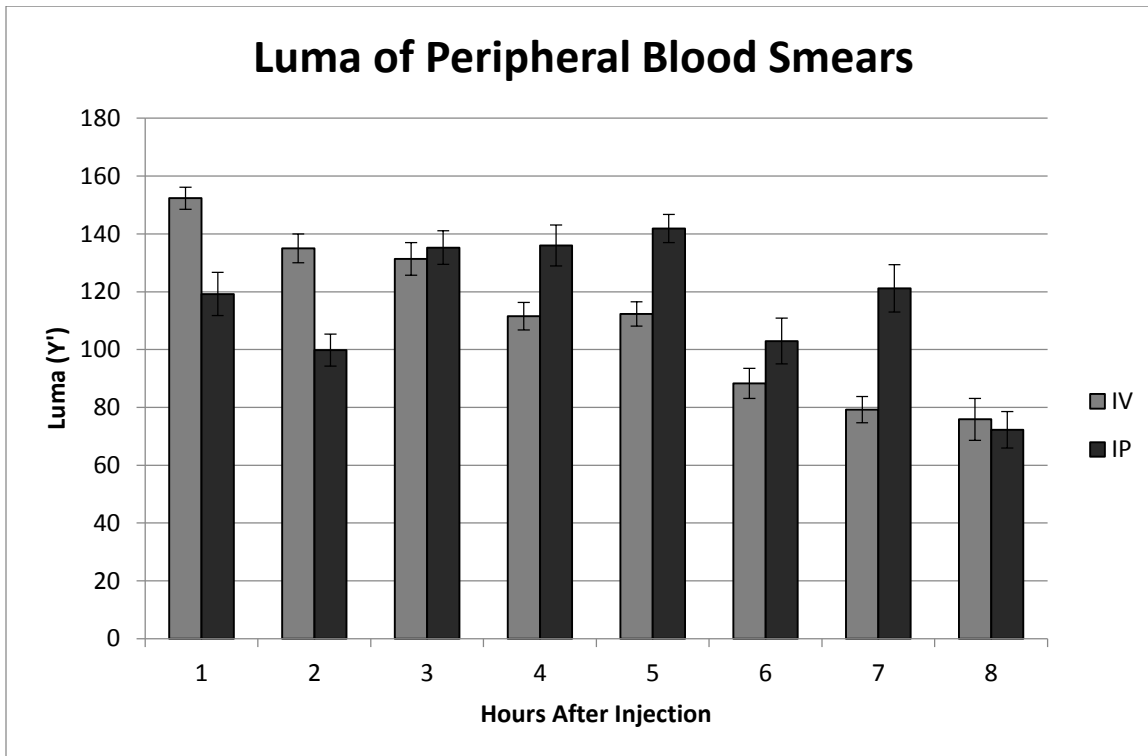
2.7 Figures

Figure 4, Peripheral Blood Smears



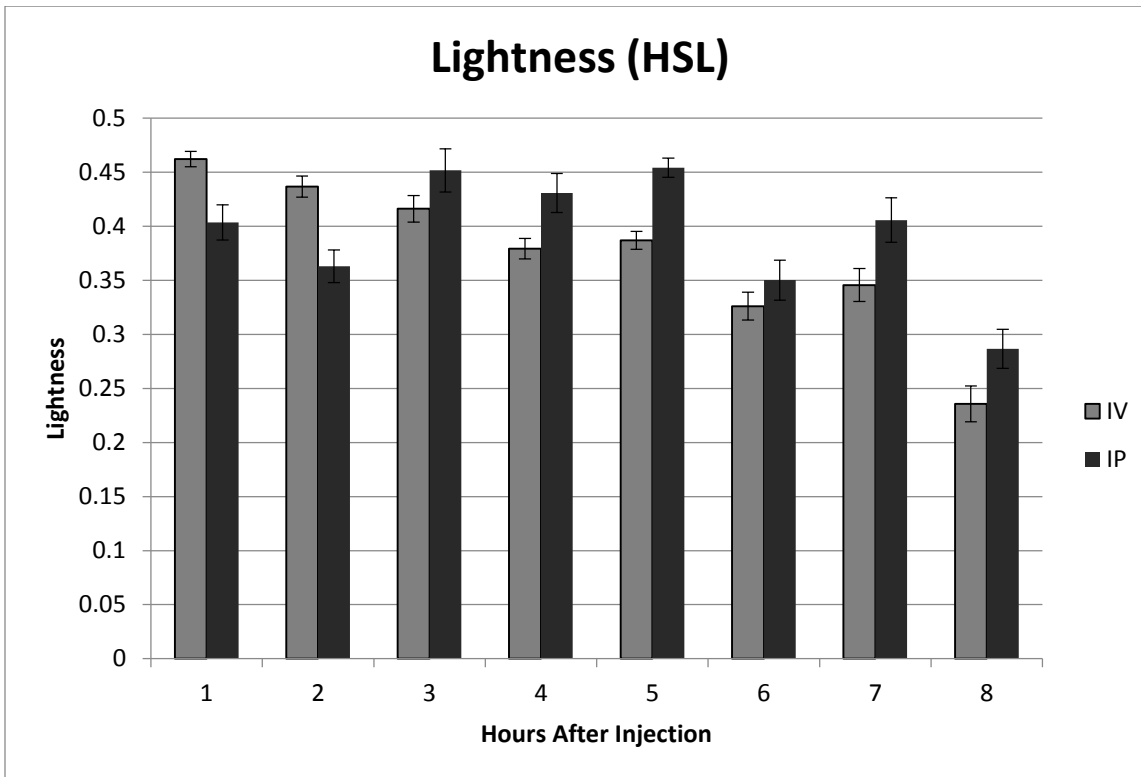
Top row: Fluorescent microscope images from intravenously administered Rhodamine 6G in peripheral blood smears at 1, 4, and 8 hours respectively. Bottom row: Corresponding time points from the intraperitoneal group. All analyzed fluorescent bodies were confirmed to be cells with corresponding light microscopy images to prevent the analysis of artifact.

Figure 5, Luma of Peripheral Blood Smears



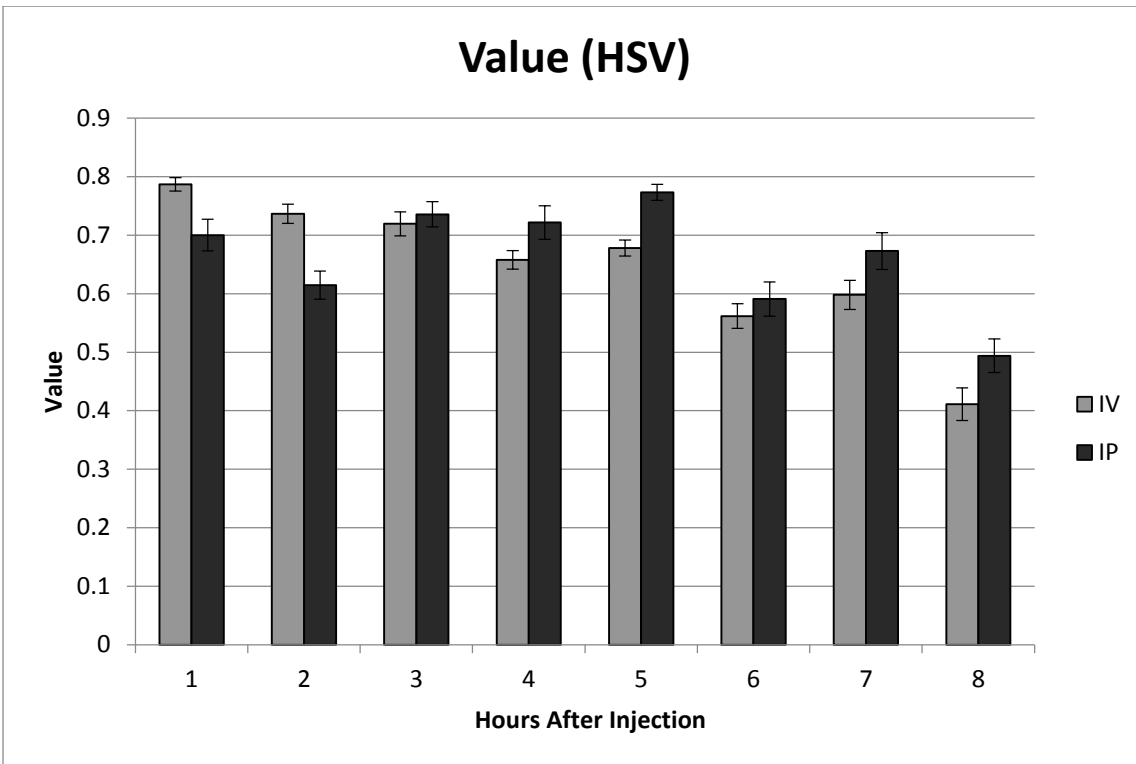
Luma of peripheral blood smears. There was no difference between either group at matched time points. Data expressed as Mean \pm SEM. $p < 0.05$. $n = 2$ mice in each group with at least 5 fields of view with and 10 cells in each view.

Figure 6, Lightness (HSL) of Peripheral Blood Smears



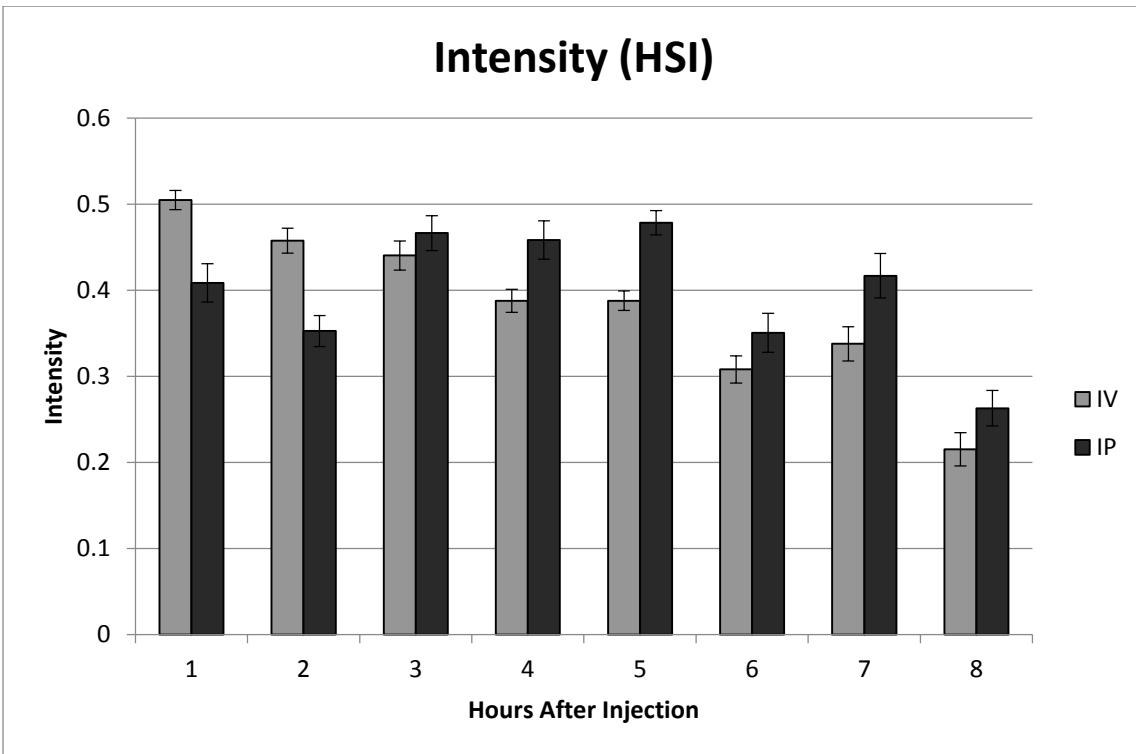
HSL Lightness of peripheral blood smears. There was no difference between either group at matched time points. Data expressed as Mean \pm SEM. $p < 0.05$. $n = 2$ mice in each group with at least 5 fields of view and at least 10 cells in each view.

Figure 7, Value (HSV) of Peripheral Blood Smears



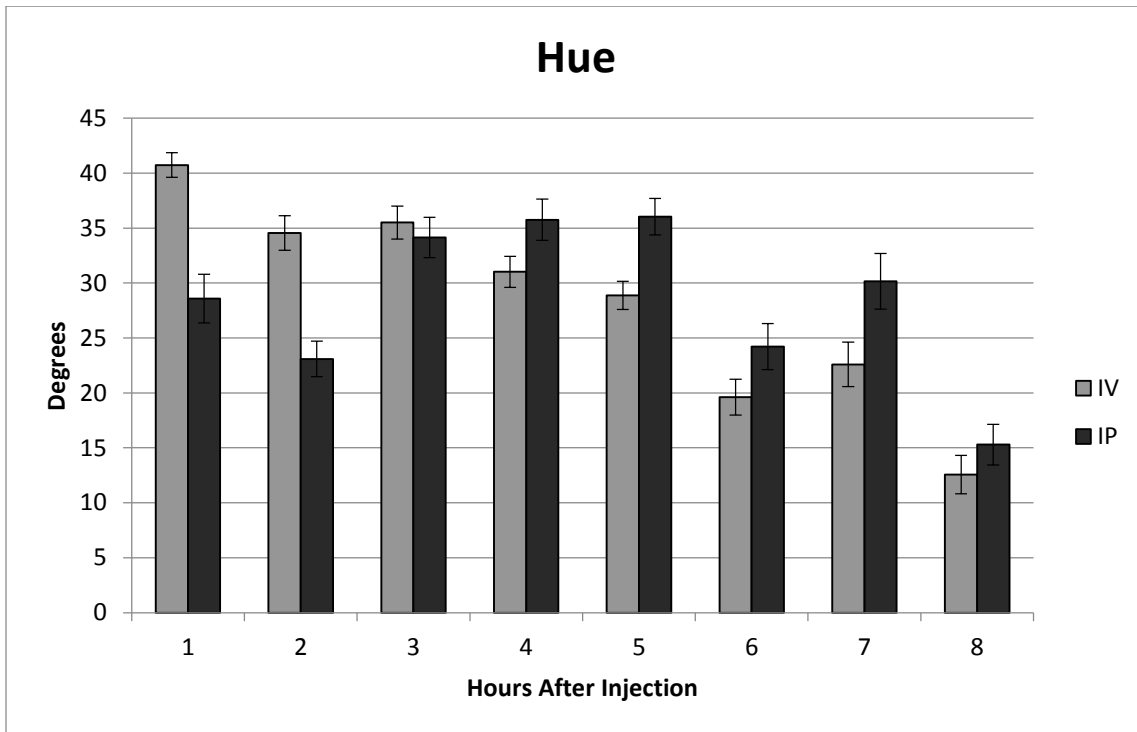
HSV Value of peripheral blood smears. There was no difference between either group at matched time points. Data expressed as Mean \pm SEM. $p < 0.05$. $n = 2$ mice in each group with at least 5 fields of view and 10 cells in each view.

Figure 8, Intensity (HSI) of Peripheral Blood Smears



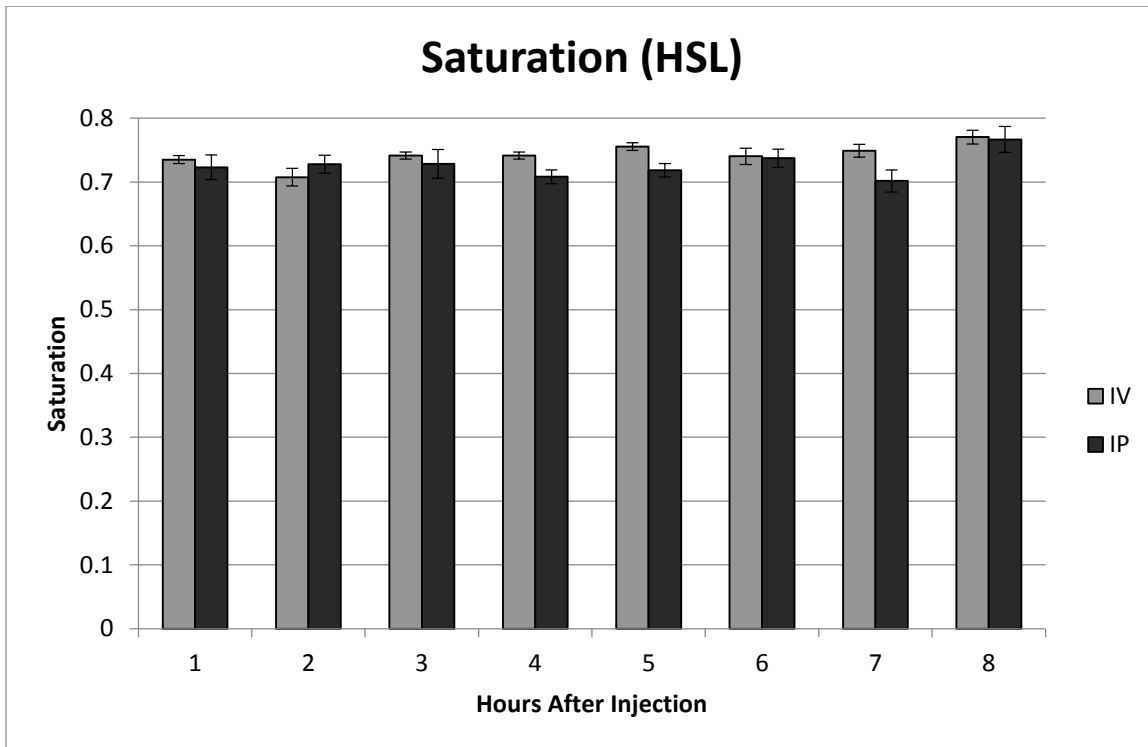
HSI Intensity of peripheral blood smears. There was no difference between either group at matched time points. Data expressed as Mean \pm SEM. $p < 0.05$. $n = 2$ mice in each group with at least 5 fields of view and 10 cells in each view.

Figure 9, Hue of Peripheral Blood Smears



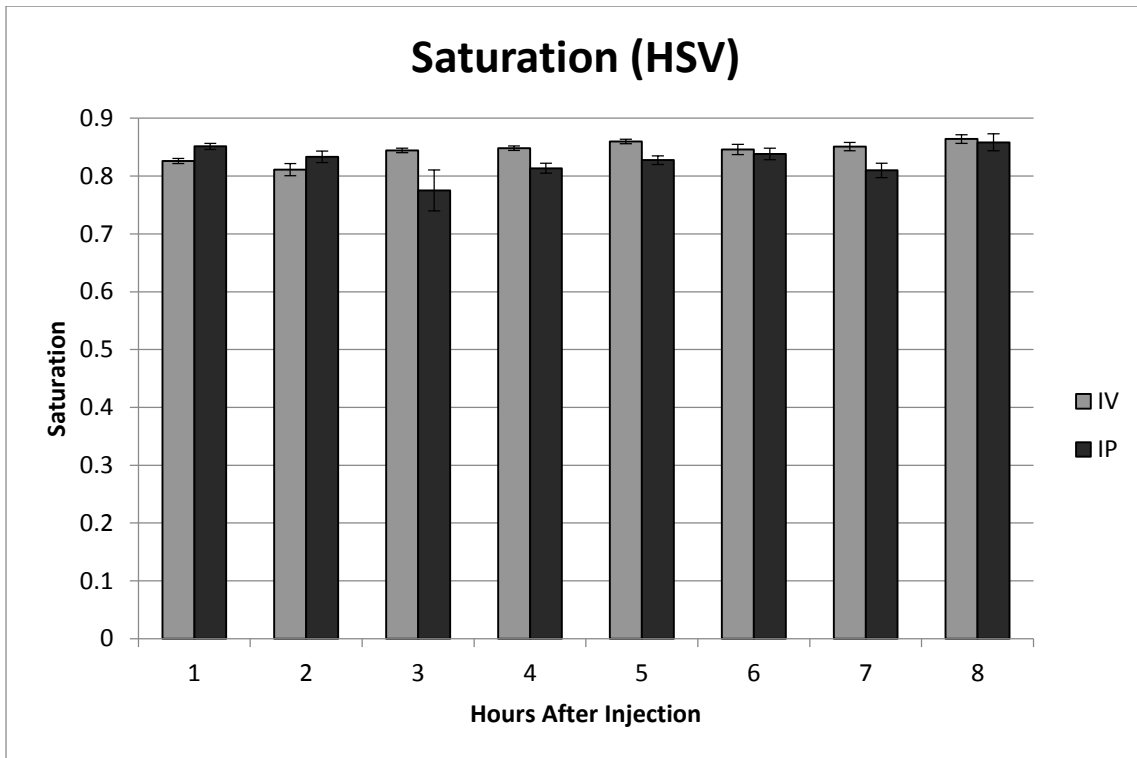
HSV and HSL Hue of peripheral blood smears. There was no difference between either group at matched time points. Data expressed as Mean \pm SEM. $p < 0.05$. $n = 2$ mice in each group with at least 5 fields of view and 10 cells in each view.

Figure 10, Saturation (HSL) of Peripheral Blood Smears



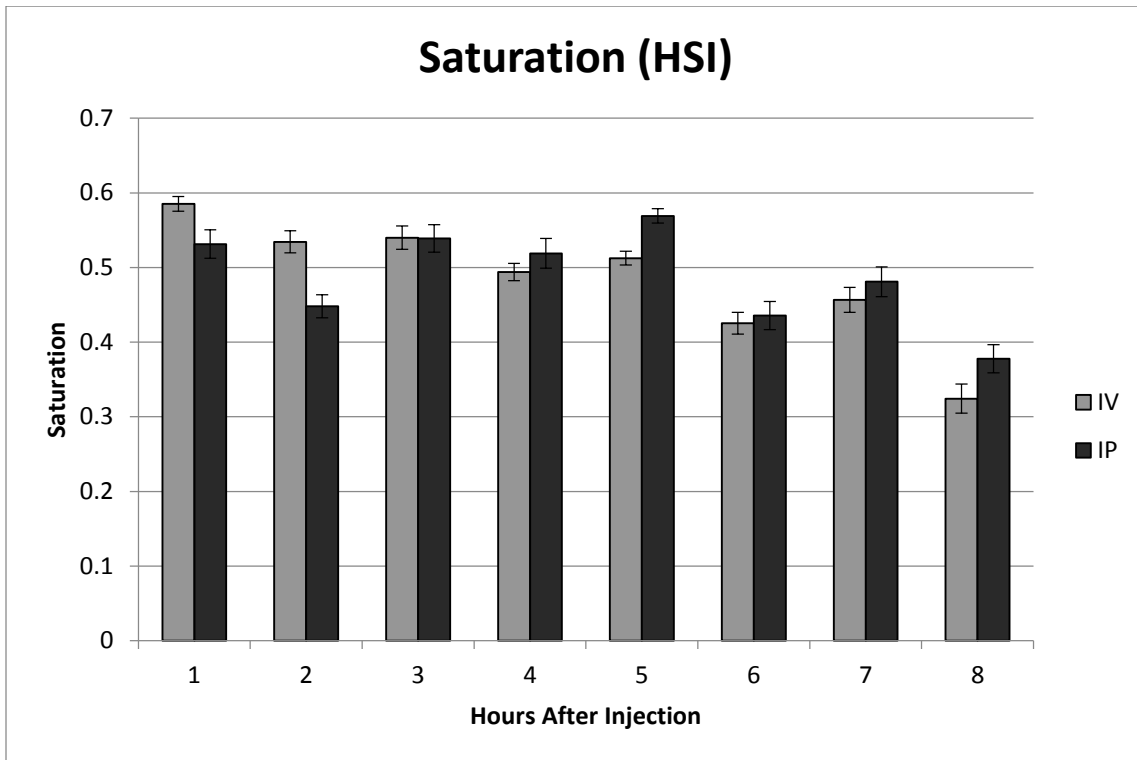
HSL Saturation of peripheral blood smears. There was no difference between either group at matched time points. Data expressed as Mean \pm SEM. $p < 0.05$. $n = 2$ mice in each group with at least 5 fields of view and 10 cells in each view.

Figure 11, Saturation (HSV) of Peripheral Blood Smears



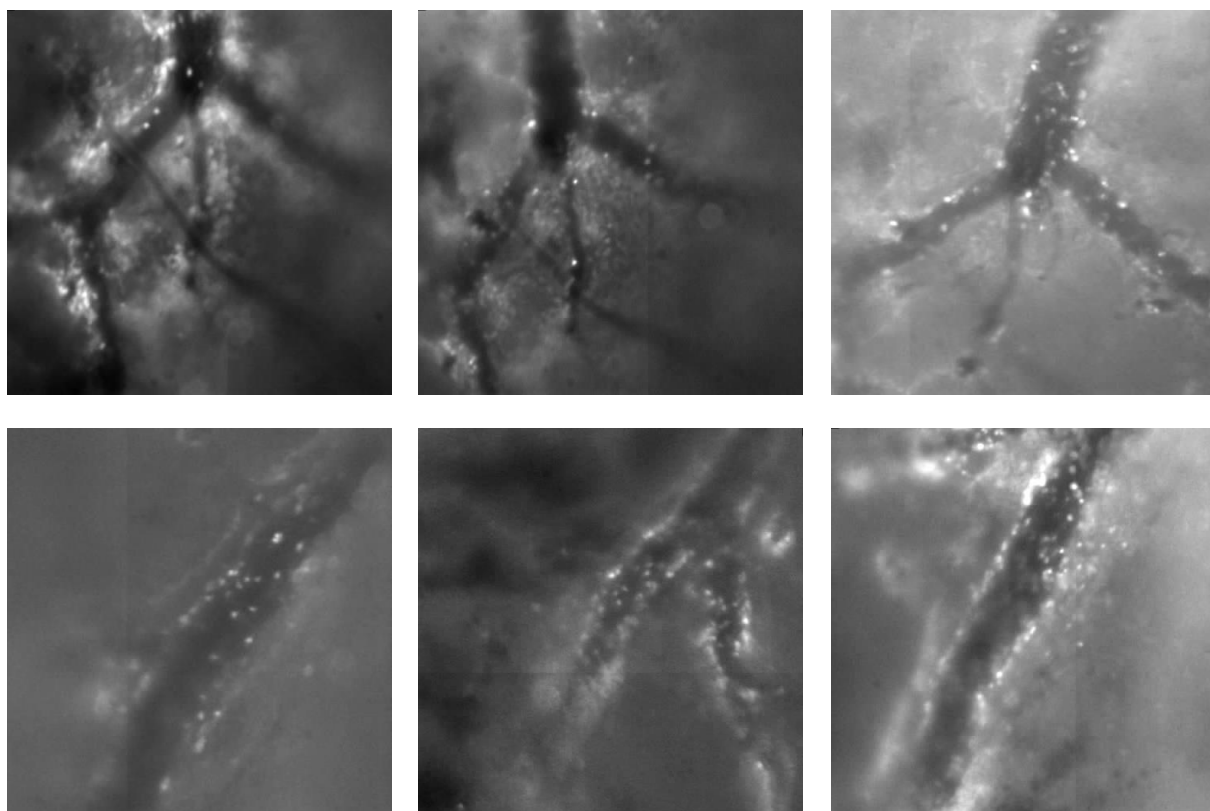
HSV Saturation of peripheral blood smears. There was no difference between either group at matched time points. Data expressed as Mean \pm SEM. $p < 0.05$. $n = 2$ mice in each group with at least 5 fields of view and 10 cells in each view.

Figure 12, Saturation (HSI) of Peripheral Blood Smears



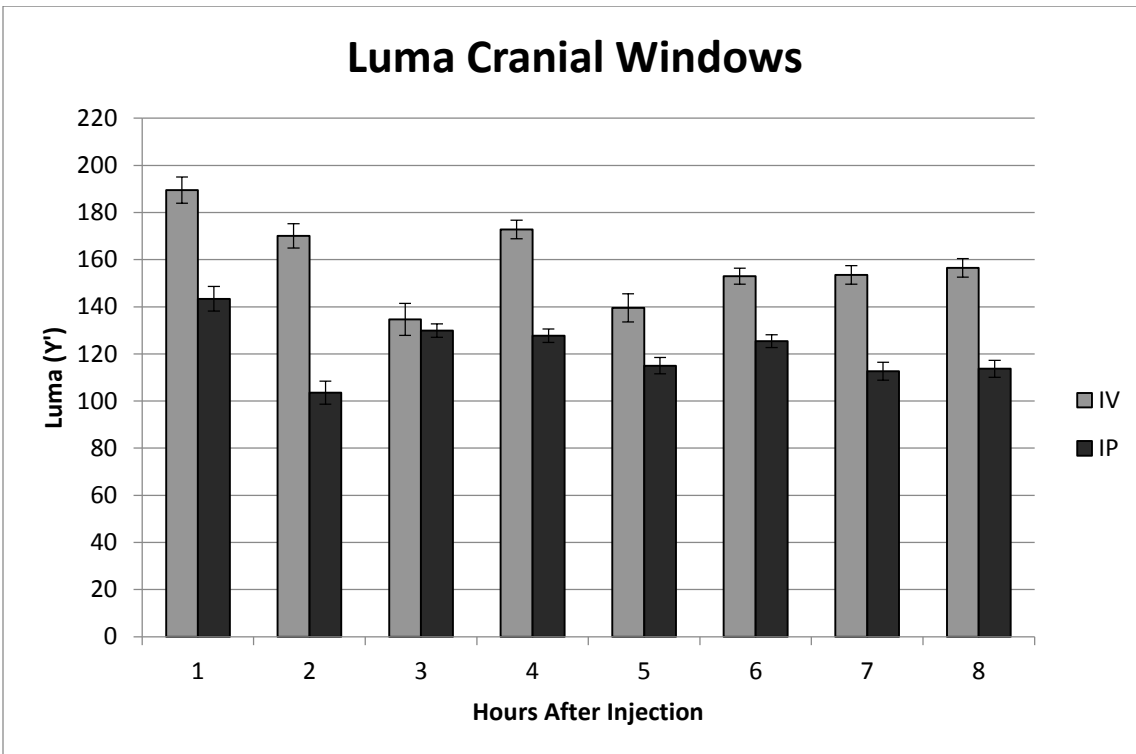
HSI Saturation of peripheral blood smears. There was no difference between either group at matched time points. Data expressed as Mean \pm SEM. $p < 0.05$. $n = 2$ mice in each group with at least 5 fields of view and 10 cells in each view.

Figure 13, Cranial Window Images



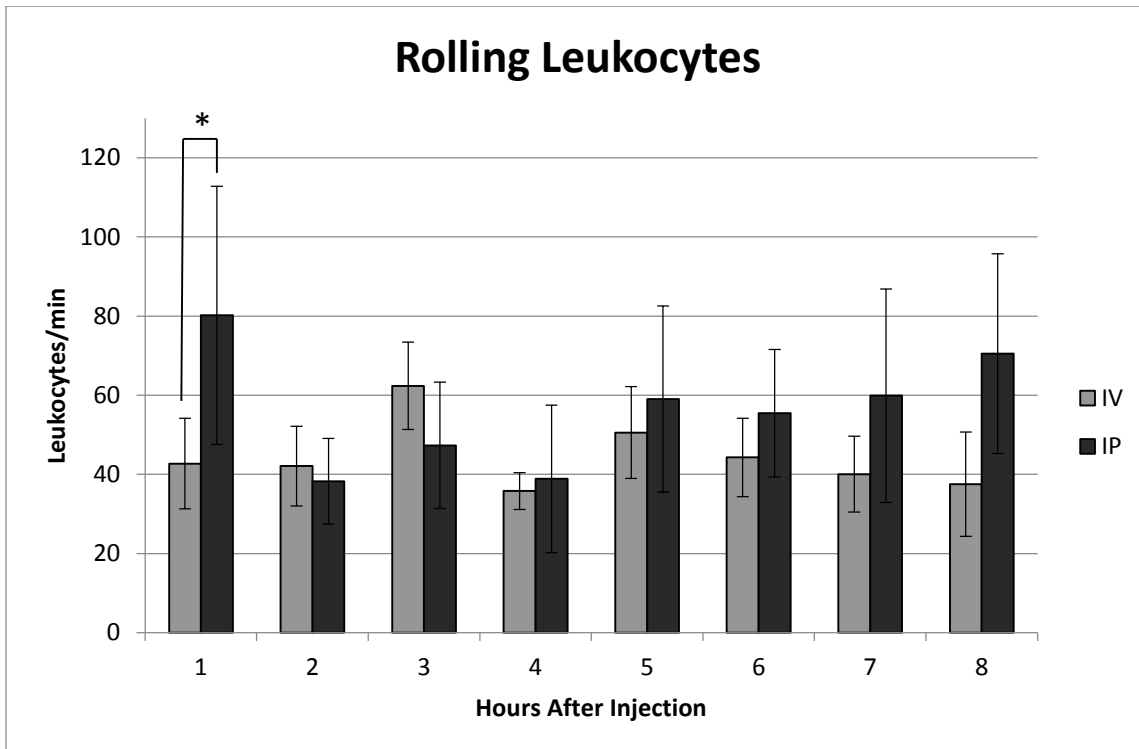
Still images obtained from movies of cerebral blood flow captured by intravital microscopy. Top row: Intravenous administration at 1, 4, and 8 hours respectively. Bottom row: Intraperitoneal administration of Rhodamine 6G at the same time points.

Figure 14, Luma Cranial Windows



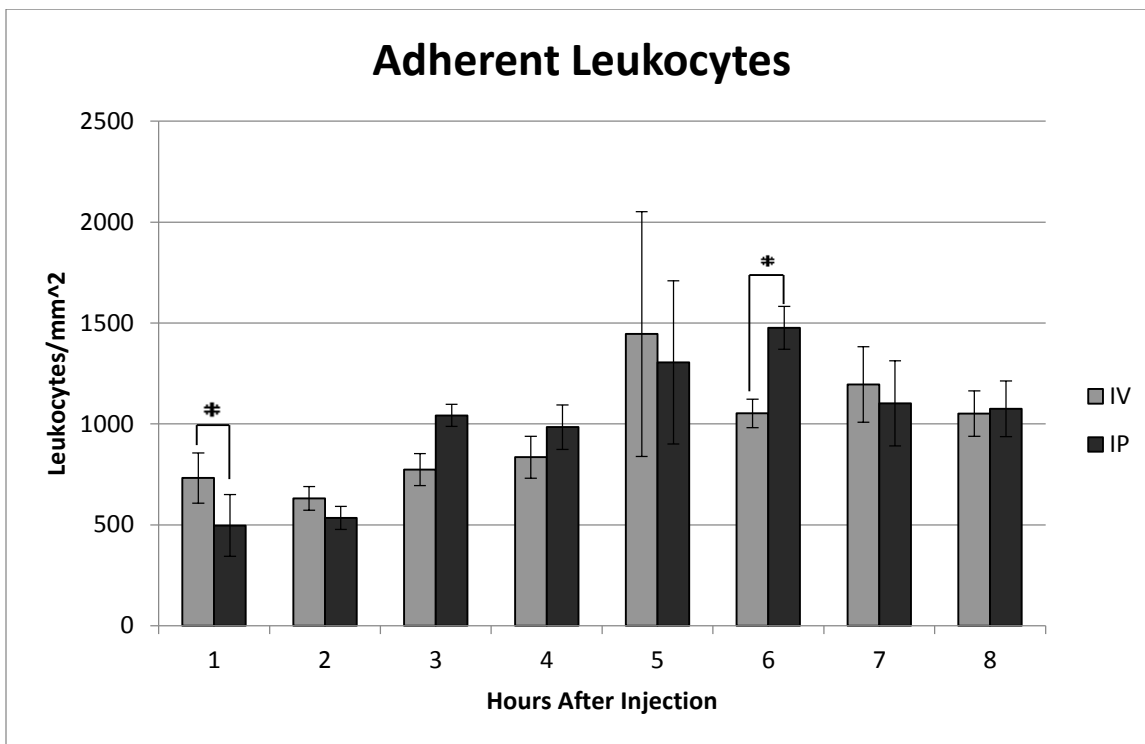
Luma through cranial windows. There was no difference between either group at matched time points. Data expressed as Mean \pm SEM. $p < 0.05$. $n = 3$ mice in each group with 5-15 cells evaluated in each mouse.

Figure 15, Rolling Leukocytes



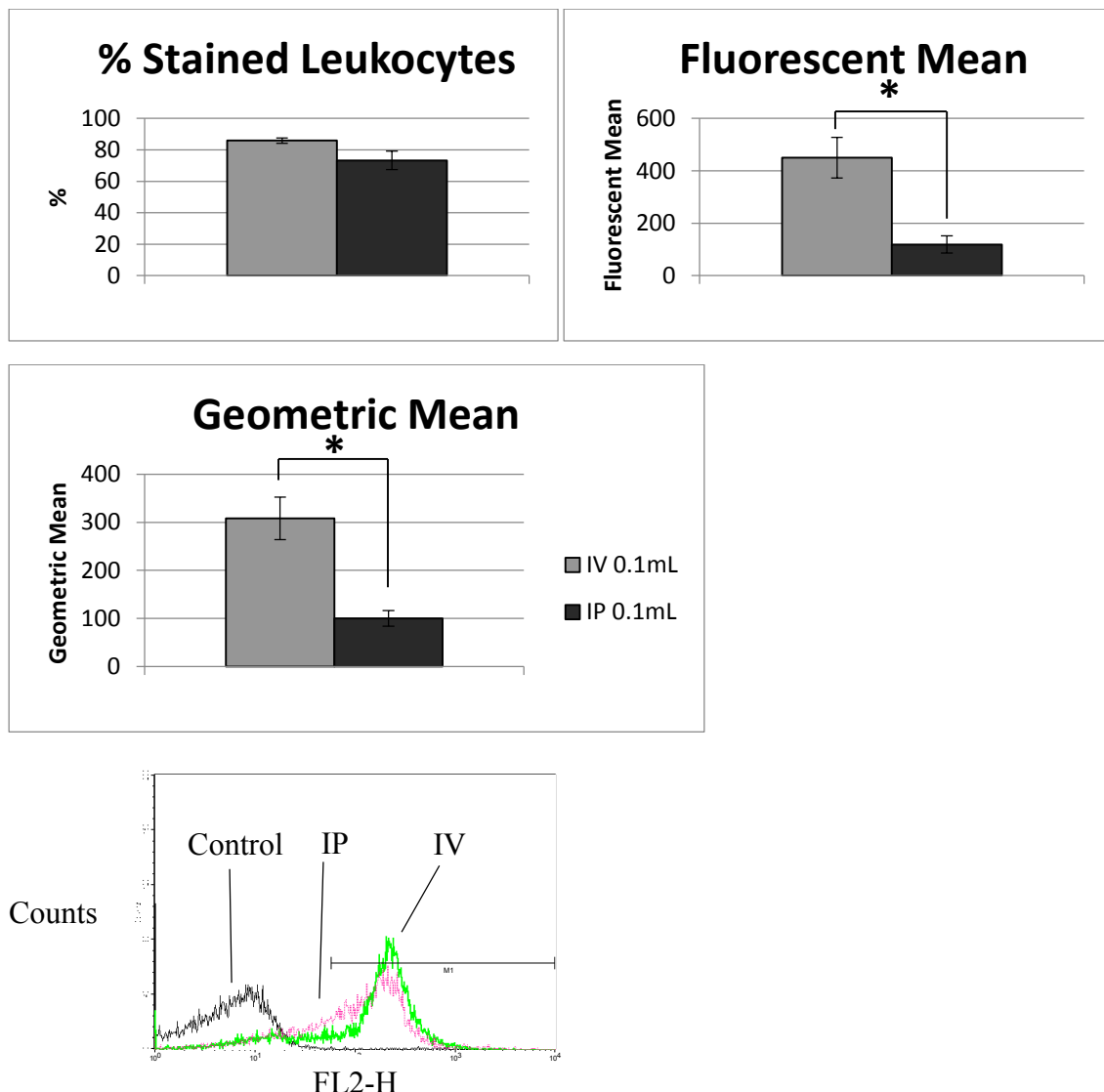
Rolling leukocytes on pial endothelial cells. There was no difference between either group at matched time points except at 1 hour where the intraperitoneal group demonstrated a greater degree of rolling. Two mice had initially high inflammation in this group. Data expressed as Mean ± SEM. $p < 0.05$. $n = 3$ mice in each group

Figure 16, Adherent Leukocytes



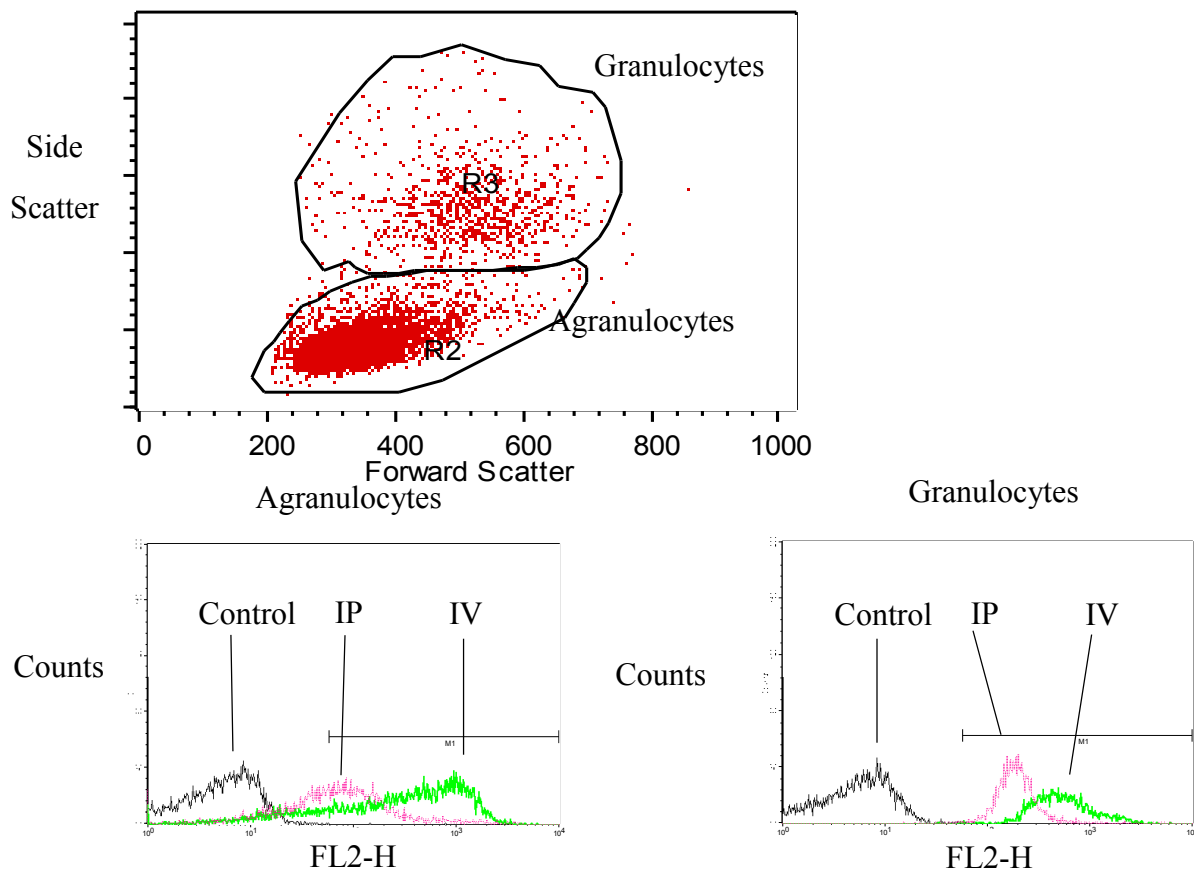
Adherent leukocytes on pial endothelial cells. Statistically significant differences existed at 1 hour and 6 hours between the groups. At 1 hour, the intraperitoneal group showed higher rolling but less adhesion. Two mice in this group had initially high levels of inflammation. Data expressed as Mean \pm SEM. $p < 0.05$. $n = 3$ mice in each group

Figure 17, Flow Cytometry, Overall Leukocytes, Equal Rhodamine 6G Applied



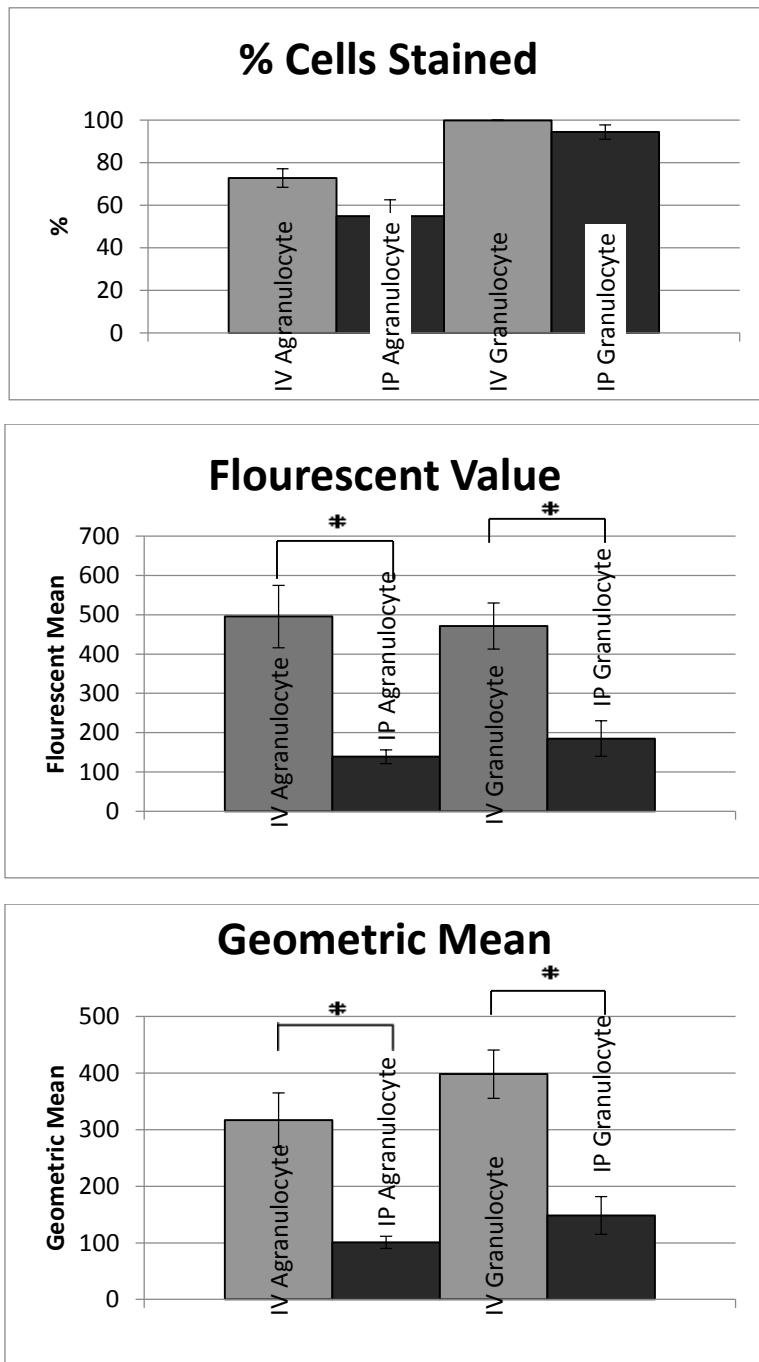
Flow cytometry at 4 hours. 100 μ L of Rhodamine 6G given. Top row: There was no difference in the overall percent of stained cells, however, there was a statistically significant difference among the fluorescent mean. Middle row: a significant difference was also found in the geometric mean. Bottom row: histograms of rhodamine signal versus counts. Data expressed as Mean \pm SEM. $p < 0.05$. $n = 5$ mice in each group

Figure 18, Flow Cytometry, Leukocytes Subpopulations, Equal Rhodamine 6G Applied



Flow cytometry. Top row: Forward scatter versus side scatter used to isolate granulocyte and agranulocyte populations. Bottom Row: Agranulocytes left and Granulocytes right, of rhodamine signal versus counts. n = 5

Figure 19, Flow Cytometry, Leukocytes Subpopulations Quantified, Equal Rhodamine 6G Applied



Flow cytometry at 4 hours

with gating for

agranulocytes and

granulocytes. 100 μ L of

Rhodamine 6G given.

Top row: there was no

difference in the overall

percent of stained cells,

however, there was a

statistically significant

difference among the

fluorescent mean and

geometric mean in both

cell types (middle and

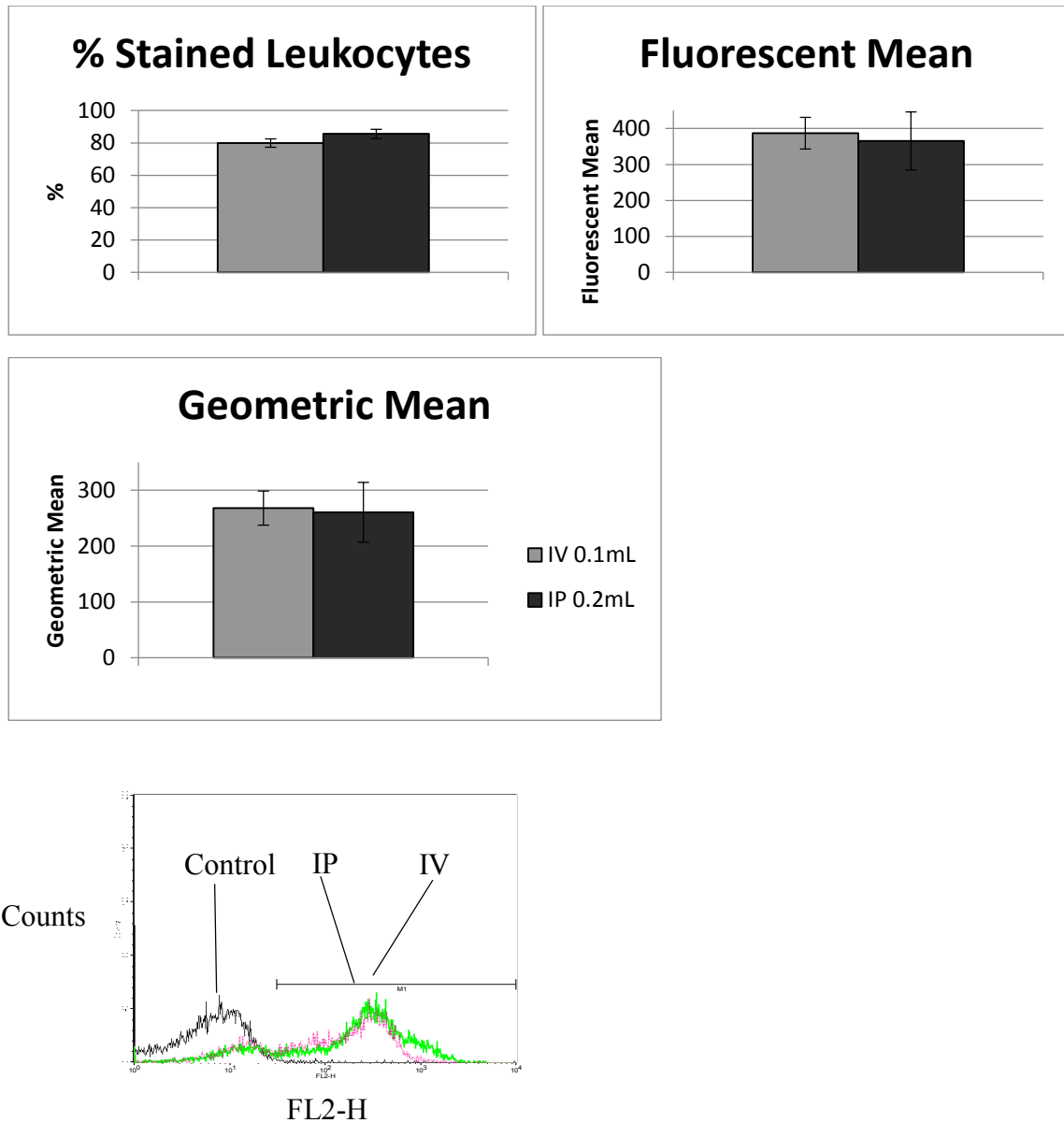
bottom row, respectively).

Data expressed as Mean \pm

SEM. $p < 0.05$. $n = 5$

mice in each group

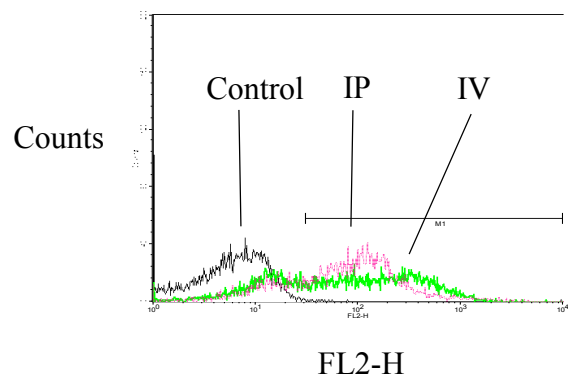
Figure 20, Flow Cytometry, Overall Leukocytes, Increased IP Injection



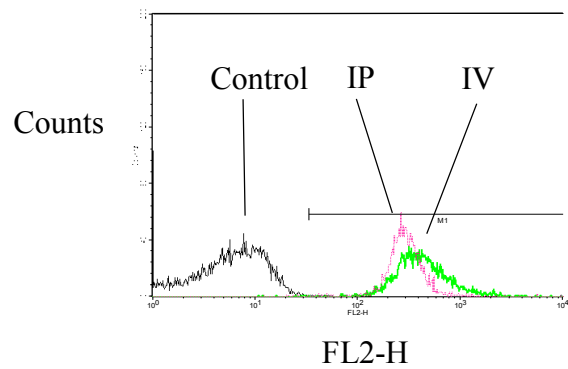
Flow cytometry at 4 hours. 100 μ L of Rhodamine 6G given IV while 200 μ L was given IP. There was no difference among any of the parameters examined. Top row: overall percentage of stained leukocytes and fluorescent mean. Middle row: geometric mean and control histogram. Bottom row: histograms of intensity versus counts. Data expressed as Mean \pm SEM. $p < 0.05$. $n = 5$ mice in each group

Figure 21, Flow Cytometry, Leukocytes Subpopulations, Increased IP Injection

Agranulocytes

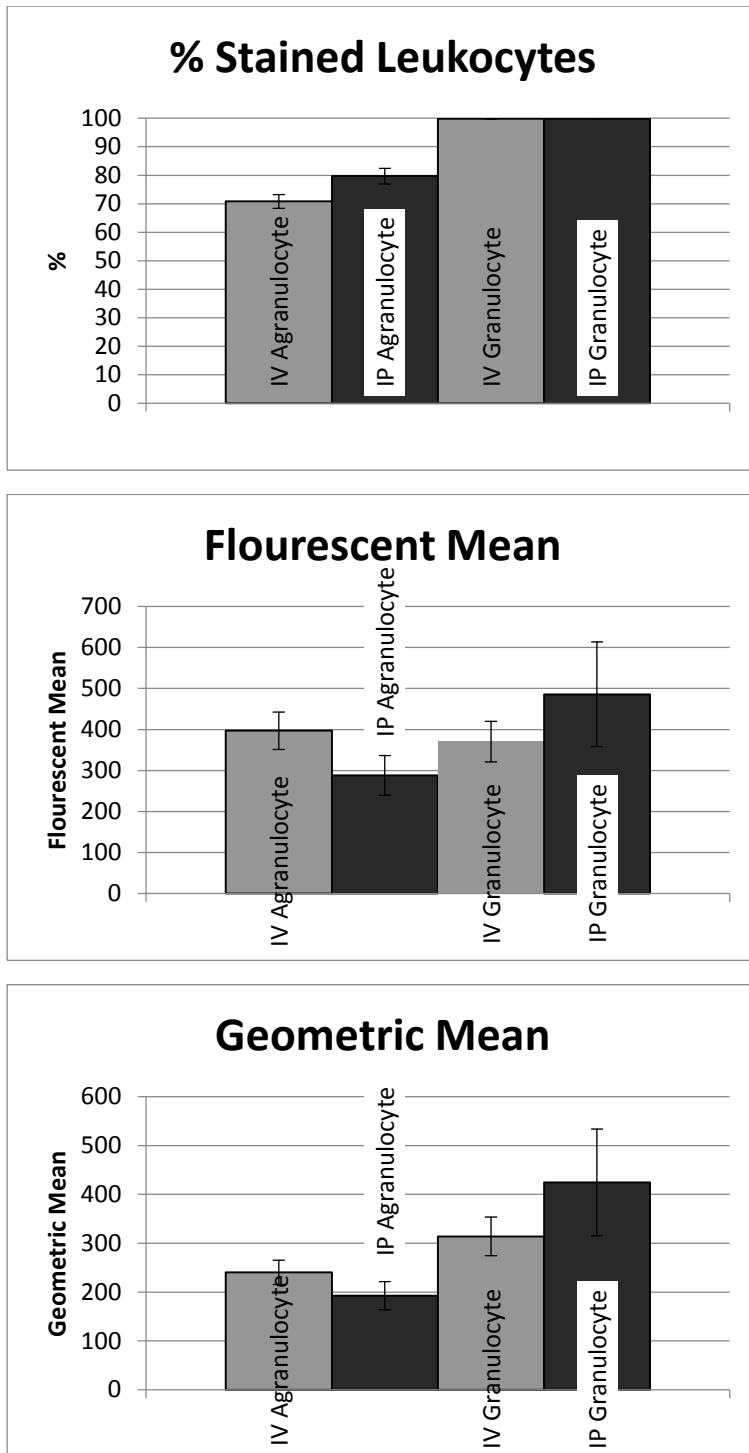


Granulocytes



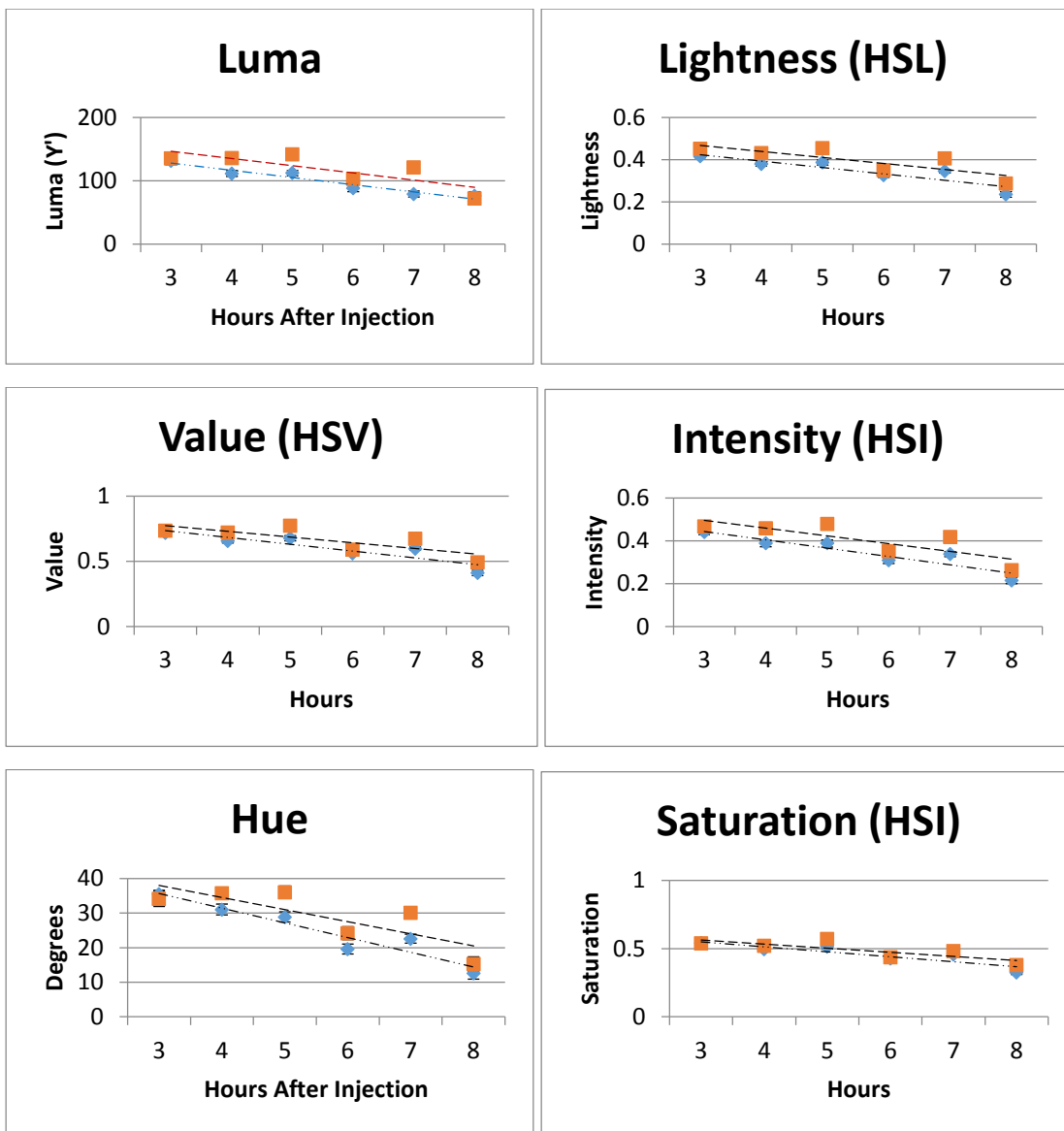
Flow cytometry. 100 μ L of Rhodamine 6G given IV while 200 μ L was given IP. Top row: Agranulocytes: rhodamine signal versus counts Bottom row: Granulocytes: rhodamine signal versus counts. n = 5

Figure 22, Flow Cytometry, Leukocytes Subpopulations Quantified, Increased IP Injection



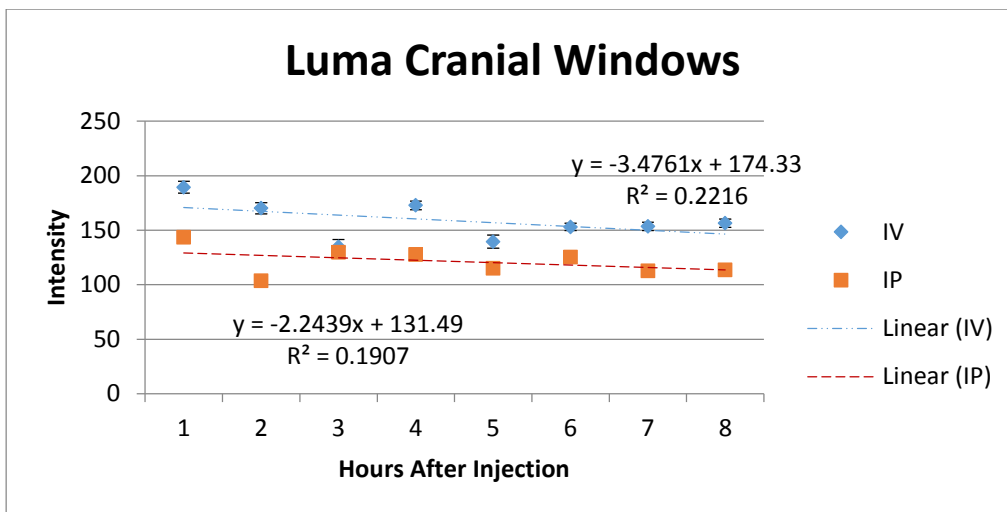
Flow cytometry at 4 hours with gating between agranulocytes and granulocytes. 100 μ L of Rhodamine 6G given IV while 200 μ L was given IP. There was no difference among any of the parameters examined between similar cell types. Top row: overall percentage of stained cells. Middle row: fluorescent mean. Bottom row: geometric mean Data expressed as Mean \pm SEM. p < 0.05. n = 5 mice in each group

Figure 23, Linear Regressions From 3 Hours to 8 Hours



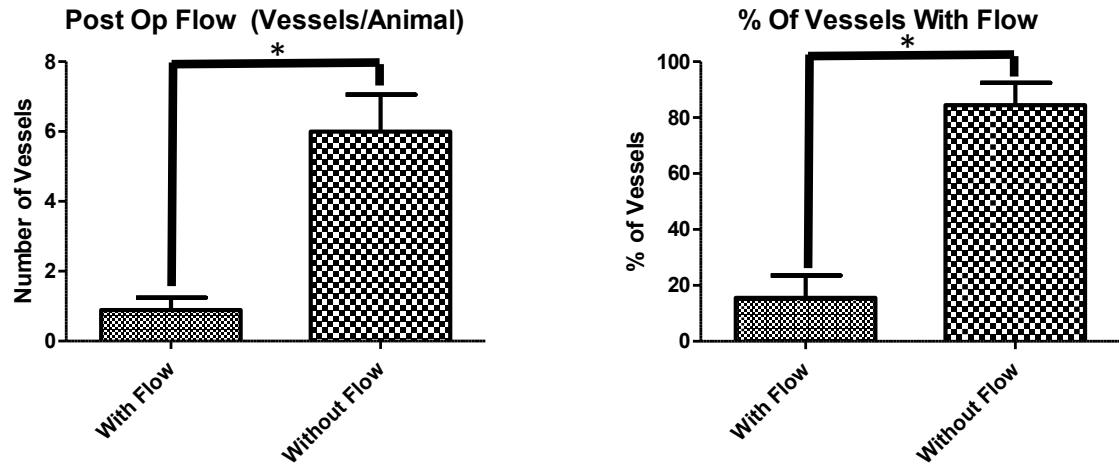
Peripheral blood smear examination of luma, HSL lightness, HSV value, HSI intensity, hue, and HSI saturation demonstrating nearly equal rates of decrease beyond 3 hours when a linear regression is applied. For intraperitoneal injections, these quantities seem to need 3 hours to reach maximum levels and then decrease at a rate equal to the same parameters when examined in intravenous preparations. Other properties studied from the peripheral blood smears seem to be independent of time. Diamonds-IV, Squares IP. Top row: Luma (left) and HSL Lightness (right). Middle row: HSV value (left) and HSI intensity (right). Bottom row: hue (left) and HSI saturation (right). n = 5 mice in each group

Figure 24, Linear Regression of Luma in Cranial Windows



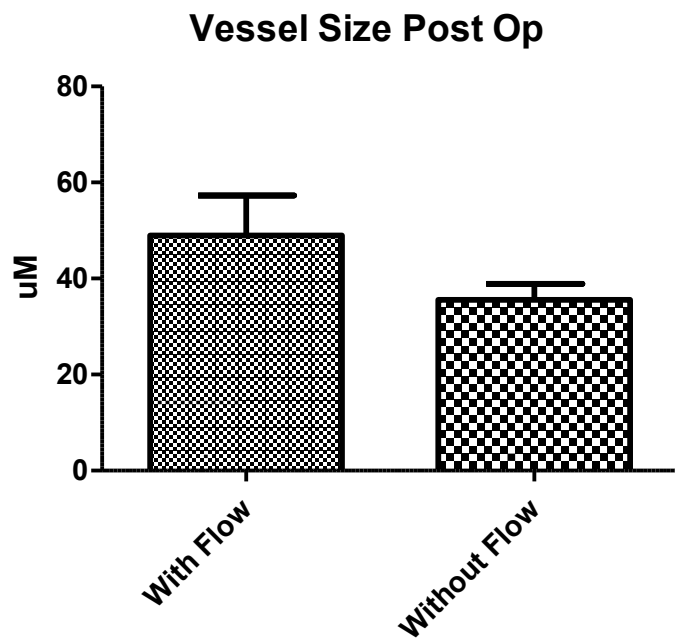
Linear regression applied to Luma calculated through cranial windows shows no significant difference among the slopes. $p < 0.05$. $n = 5$ mice in each group

Figure 25, Blood Flow Following Photochemically Induced Cerebral Ischemia



Left: The number of vessels that had or did not have flow. Right: The percentage of vessels that had or did not have flow. Data expressed as Mean \pm SEM. $p < 0.05$. $n = 9$.

Figure 26, Vessel Size



Vessel size after photothrombosis. Data expressed as Mean \pm SEM. $p < 0.05$. $n = 9$.

CHAPTER 3

MODULATION OF THE ENDOGENOUS CANNABINOID SYSTEM IN TWO STROKE MODELS

3.1 Specific Aims, Rational, and Hypothesis

1. Since the endogenous cannabinoid system is intimately associated with inflammatory response and cerebral ischemia initiates inflammation, we sought to investigate the effect of cerebral ischemia in a CB₁ -/- CB₂ -/- receptor mouse on infarct volume and neurological outcomes in a model of transient ischemia.
2. Determine the effect of CB₁ antagonism in a permanent occlusion model and evaluate the role of serotonergic receptor activation as well.

Based on studies involving single cannabinoid receptor knockout mice, we wanted to know the effect of cerebral ischemia in double knockout animals. More so, our previous studies revealed that SR141716A was protective in a transient cerebral ischemia but that protection could be ablated with 5HT_{1A} antagonists. We wanted to explore this relationship in a permanent occlusion.

We hypothesize that the deletion of both cannabinoid receptors will produce larger infarcts with diminished neurological scores. Additionally, we expect that SR141716A will continue to be protective in the permanent occlusion, and like the transient model, lose efficacy when a 5HT_{1A} antagonist is applied.

3.2 Materials and Methods

3.2.1 Animals

The cerebral ischemia studies were conducted on 7 to 8-week-old male C57BL/6 mice weighing 18-23 grams (Jackson Laboratories, Maine, USA). CB₁ -/- CB₂ -/- receptor mice were obtained from the Center for Substance Abuse Research Breeding Core at Temple University and were also 7-8 weeks old. Studies were conducted in accordance with the guidelines approved by the Institute for Animal Care and Use Committee at Temple University. Animals were maintained on a regular chow diet and had access to food and water ad libitum before and after the procedure.

3.2.2 Middle Cerebral Artery Occlusion and Reperfusion and Cerebral Blood Flow Monitoring

The animals were anesthetized with an intraperitoneal injection of ketamine (100 mg/mL) and xylazine (20 mg/kg) mixed 1:1 at a dose of 1 mL/kg. The skin on the dorsal aspect of the head was resected and the periosteum removed. A mark 2 mm poster and 4 mm lateral to Bregma was placed over the right parietal bone.

Body temperature was maintained at 37°C ± 0.5°C during the period of occlusion by means of 2 heating lamps and a heating pad. The temperature probe was placed into the erector spinae muscles at the base of the neck to more accurately reflect the temperature in the brain. Middle cerebral artery occlusion (MCAO) was achieved by the intraluminal filament method with slight modifications (81, 172, 277). In brief, after securing the animal in place, a midline incision was made on the ventral aspect of the neck. Under an operating microscope, the submaxillary glands were located, separated, and retracted to allow a clear visualization of the trachea and surrounding structures. The right external carotid artery (ECA) was identified, ligated with 6-0

silk suture, and cauterized distal to the bifurcation of the common carotid artery (CCA) into the ECA and internal carotid artery (ICA). Another 6-0 silk suture was tied around the right ICA but not tightened. A third 6-0 silk suture was tied around the right ECA proximal to the point of cauterization. The vagus nerve was separated from the CCA with care taken to not damage it.

A laserPro Blood Perfusion Monitor (TSI, Inc., Shoreview, MN, USA) was utilized to monitor regional cerebral blood flow (rCBF) before ischemia, during MCAO, and after reperfusion. A 1-mm diameter microfiber laser-Doppler probe was placed so that it covered the mark previously indicated on the parietal bone.

Baseline rCBF readings were collected. The second suture placed around the ICA was pulled tight. A microvascular clamp was placed on the CCA. Using a 30-gauge needle, a small incision was placed in the ECA. A blunted 5-0 monofilament nylon suture coated with poly-L-lysine (0.1% in deionized water, Sigma Inc., St. Louis, MO USA) was inserted into the ECA and advanced into the Circle of Willis and finally to the origin of the middle cerebral artery (MCA) (278). Slight resistance upon advancing indicated it was in the proper position. The third suture was secured around the ECA to prevent the suture from dislodging and preclude backflow. The MCAO was considered adequate if rCBF showed a sharp decrease to 25% of baseline levels (279).

After 50 minutes, the nylon suture was withdrawn and the ECA permanently tied and cauterized. Reperfusion was confirmed when pulsations were again observed in the ICA.

3.2.3 Infarct Volume Assessment

Animals were euthanized with an overdose of pentobarbital (200 mg/kg interaperitoneal) 24hr after cerebral ischemia and then the brains were removed. Brains were submerged in cold PBS briefly and then cut into 6 2 mm coronal sections using a mouse brain matrix (Zivic Lab,

Pittsburgh, PA, USA). The brain sections were placed in 2% triphenyltetrazolium chloride (Sigma, Inc) dissolved in saline and stained for 5 minutes at 37°C in the dark. The brain sections were fixed in 4% paraformaldehyde at 4°C for 24hr. Next, the anterior and posterior face of each section was scanned by a flatbed color scanner (Microtek Inc., Carson, CA USA). Images were saved as JPEG files and analyzed with Image-J Software (NIH). The infarct volumes were expressed as mm³ as well as the percentage of overall brain tissue after correcting for edema using the following formulas

$$\text{Infarct Fraction} = \left(\frac{\text{Infarct Volume} + \text{Contralateral Volume} - \text{Ipsilateral Volume}}{\text{Contralateral Volume}} \right) \times 100$$

$$\text{Edema} = \left(\frac{\text{Ipsilateral Volume} - \text{Contralateral Volume}}{\text{Contralateral Volume}} \right) \times 100$$

as described in the literature (81, 82, 172, 280-282).

3.2.4 Neurological Evaluation

The severity of neurological deficits were evaluated 24 hours after the ischemic insult using a five point deficit score. The scale utilized the following criteria adapted from Hata: 0 = normal motor function, 1 = flexion of torso and of contralateral forelimb on lifting of the animal by the tail, 2 = circling but normal posture at rest, 3 = leaning while at rest, 4 = no spontaneous motor activity or lateral rolling (277).

3.2.5 Photothrombotic Cerebral Ischemia

On the day of ischemia, mice were anesthetized with a mixture of ketamine (100 mg/mL) and xylazine (20 mg/mL) mixed (1:1 by volume) at a dose of 1 mL/kg. Mice were maintained at 36.5° to 37.5° C throughout the procedure. 0.1 mL of Rose Bengal (Sigma Aldrich), 10 mg/mL dissolved in 0.9% saline, was injected intraperitoneally. The head was shaved and skin and

periosteum over the right parietal bone removed. The head was secured in place and a cold light source positioned over the bone flap. 5 minutes after the injection of dye, the light source was activated for 20 minutes and temperature monitored (275).

3.2.6 Preparation and Administration of SR14176A and WAY-100635

WAY-100365 (Sigma Aldrich) was prepared 0.3 mg/mL in 0.9% saline and injected at 3mg/kg. SR141716A was prepared to 0.5 mg/mL in Ethanol:Cremaphor:Saline (1:1:18) and injected at 5mg/kg. Injections were intraperitoneal and given 1 hour prior to the photothrombotic injury or 1 hour after the onset (172, 173).

3.2.7 Statistical Analysis

Double knockout studies were subjected to a Student's t-Test. Photothrombosis cerebral ischemia data was analyzed with one way analysis of variance with Bonferroni correction for multiple comparisons. Data is reported as the mean \pm the standard error of the mean. A p-value <0.05 was used for statistical significance.

3.3 Results

3.3.1 Transient Cerebral Ischemia in CB₁ -/- CB₂ -/- Receptor Mice and the Effect on Infarct Size, Figure 27 and 28

Following 50 minutes of cerebral ischemia and 23 hours of reperfusion, Wild Type mice had an average stroke volume of 113.6 ± 11.0 mm³ compared to CB₁ -/- CB₂ -/- receptor mice that had a stroke volume of 91.31 ± 17.78 mm³, Figure 27 and 28. The infarct fraction was found to be 36.10 ± 3.73 % in Wild Type animals and 30.13 ± 5.45 % in CB₁ -/- CB₂ -/- receptor animals,

Figure 28. While CB₁ -/- CB₂ -/- receptor animals tended to have smaller stroke volumes and infarct fractions, the difference was not statistically significant.

3.3.2 Transient Cerebral Ischemia in CB₁ -/- CB₂ -/- Receptor Mice and the Effect on Edema, Figure 29

Calculations of edema following cerebral ischemia and reperfusion showed that Wild Type mice had an edema measurement of 3.54 ± 1.0 compared to CB₁ -/- CB₂ -/- receptor mice who had an edema measurement of 4.06 ± 1.8 , Figure 29. This difference was not statistically significant.

3.3.3 Transient Cerebral Ischemia in CB₁ -/- CB₂ -/- Receptor Mice and the Effect on Clinical Parameters, Figure 30

24 hours after the onset of ischemia, Wild Type mice were found to have lost 5.92 ± 0.71 % of their original body weight, Figure 30. CB₁ -/- CB₂ -/- receptor mice lost 8.27 ± 0.93 % of their body weight. This difference was not statistically significant. However, a statistically significant difference was found in Neurological Scores. The mean Neurological Score for Wild Type mice was 3.53 ± 0.14 compared to 1.90 ± 0.33 in CB₁ -/- CB₂ -/- receptor mice, Figure 29.

3.3.4 Transient Cerebral Ischemia in CB₁ -/- CB₂ -/- Receptor Mice and the Effect Regional Cerebral Blood Flow, Figure 31

During the period of ischemia, CB₁ -/- CB₂ -/- receptor mice tended to have more Cerebral Blood Flow as evaluated by Laser Doppler analysis, Figure 31. Statistical Significance was found at the 5 minute time point where CB₁ -/- CB₂ -/- receptor mice had 33.96 % of baseline blood flow compared to only 17.25 % in Wild Type mice. The overall reduction in blood flow for the entire period of occlusion also reached statistical significance, Figure 30. Wild Type mice had cerebral

blood flow reduced to 17.71 ± 1.78 % of baseline compared to CB₁ -/- CB₂ -/- receptor mice who maintained 27.29 ± 4.05 % of baseline during the occlusion.

3.3.5 Effect of SR141716A and WAY-100365 on Infarct Size in a Permanent Occlusion Model, Figure 32 and 33

The addition of SR141176A before or after the induction of ischemia provided a degree of protection and decreased both stroke volume and infarct fraction regardless of pre or post treatment, Figure 32 and 33. The effect was not attenuated by the addition of WAY-100365. Mice that had received vehicle had an overall stroke volume of 62.85 ± 3.70 mm³ compared to SR141716A pretreatment at 38.67 ± 5.16 mm³, SR141716A post treatment at 43.01 ± 4.55 mm³, and SR141716A with WAY-100365 pretreatment 38.20 ± 9.46 mm³. The difference was statistically significant between the Vehicle group and all other treatment groups but not between treatment groups. Infarct fraction also decreased in treatment groups, Figure 33. Vehicle treated mice had an infarct fraction of 20.45 ± 1.63 % whereas SR141716A given as a pretreatment decreased this to 8.95 ± 3.14 %. The addition of WAY-100365 with SR141716A as a pretreatment produced a mean infarct fraction of 9.34 ± 3.57 %. Post treatment with SR141716A produced infarct fractions of 10.50 ± 2.01 %. Again, the difference between the Vehicle group and all treatment groups was statistically significant.

3.3.6 Effect of SR141716A and WAY-100365 on Edema in a Permanent Occlusion Model, Figure 34

While no statistical significance was reached among the differences, the application of SR141716A tended to increase edema measurements, Figure 34. Vehicle treated mice had edema measurements of 2.27 ± 1.06 while SR141716A had edema measurements of 5.30 ± 1.73 and 5.46

± 1.08 , pre and post respectively. WAY-100365 given with SR14716A as a pretreatment produced edema measurements of 4.17 ± 1.35 .

3.3.7 Effect of SR141716A and WAY-100365 on Clinical Parameters in a Permanent Occlusion Model, Figure 35

Overall, there was no statistical difference among weight loss in the experimental groups although SR141716A pretreatment tended to trend towards a conservation of more body weight, Figure 35. Vehicle treated mice lost 10.23 ± 0.62 % of their original body weight compared to 5.44 ± 3.75 % in SR141716A pretreatment and 10.83 ± 0.90 % in post treatment. The group receiving WAY-100365 lost 9.61 ± 0.86 % of their pre surgical body weight. Neurological Scores did achieve statistical significance between the Vehicle group and the group that received SR141716A as a pretreatment, Figure 33. The Neurological Score for the Vehicle group was 1.65 ± 0.27 , 0.5 for the SR141716A pretreatment group, and 0.96 ± 0.07 for the post treatment group. The group receiving WAY-100365 in addition to SR141716A had a score of 1.2 ± 0.34 .

3.4 Discussion

From the studies on cerebral ischemia in the two models, two surprising results became apparent. First, CB₁ -/- CB₂ -/- receptor mice tended to show a slight degree of protection when compared to Wild Type controls, Figure 27 and 28. More so, this contrasted previous studies in which CB₁ -/- or CB₂ -/- receptor single knockouts demonstrated increased neurological damage (81, 119, 167). The injury in the double knockouts was certainly not worse than the wild type controls. Secondly, in the permanent ischemia model with photochemically induced thrombosis, SR141716A was found to be protective both as a pre and post treatment. WAY-100365, a 5HT_{1A} antagonist, did not attenuate the protective effect of SR141716A. Studies of transient cerebral

ischemia had previously revealed that antagonism of 5HT_{1A} could abolish cannabinoids protective effects (173, 283).

Studies involving the CB₁ -/- CB₂ -/- receptor mice completely contrasted our hypothesis that the lack of CB₁ and CB₂ receptors together would be detrimental and increase infarct fractions and worsen neurological scores. Convincing evidence had been presented that the loss of the CB₁ receptor increased the amount of necrotic brain tissue, decreased cerebral blood flow during the occlusion, and increased excitotoxic injury (167). Belief in a CB₁ protective mechanism centered on the receptors' activation to induce hypothermia and decrease edema after the injury (119, 168). These mechanisms would be lacking in knockout mice. Since CB₁ receptors exist so prevalently in the brain, it seemed likely that the study of cerebral ischemia in CB₁ -/- receptor mice demonstrated convincing evidence (4, 167). However, other laboratories had shown protection in blocking the CB₁ receptor by improving autoregulation of cerebral blood flow and they also speculated a protective effect may stem from enhanced GABA signaling (119, 172).

Less ambiguity surrounded the role of the CB₂ receptor. Our laboratory demonstrated increased neurological damage with greater stroke volumes and poorer neurological scores when a transient ischemia was induced in a CB₂ -/- receptor mouse. Activation of the CB₂ receptor had been shown to decrease leukocytes migration, decrease cytokine production, attenuate adhesion molecules, and prevent rolling and adhesion of leukocytes (34, 82, 94, 97). Without a CB₂ receptor, inflammation following stroke could continue unabated. Thus, the fact that CB₁ -/- CB₂ -/- receptor mice did not demonstrate worse neurological injury, and showed even slightly better outcomes, was a perplexing and interesting result.

The deletion of both known cannabinoid receptors, and the resulting compensatory changes on the entire organism, may lead to several possible explanations for these results. First of all,

deletion of any gene results in untold consequences and compromises in gene expression elsewhere in the organism. The extent to which this imparts an effect remains to be determined. Secondly, compelling evidence exists for a non-CB₁, non CB₂ receptor. This receptor could have been upregulated in the absence of CB₁ and CB₂ receptors. More so, the entire endogenous cannabinoid system could have been altered with greater quantities of endogenous ligands and decreased levels of degrading enzymes. Lastly, the CB₁ -/- CB₂ -/- receptor mice showed increased flow throughout the period of occlusion. It appears that some unknown mechanism may exist to provide CB₁ -/- CB₂ -/- receptor mice with greater compensatory flow during periods of cerebral ischemia. Of course, all of these theories could be contributing to the effect. For example, enhanced levels of endogenous cannabinoid ligands may be exerting an effect at 5HT_{1A} receptors and ultimately increasing flow.

Studies have shown that the CB₁ receptor plays a pivotal role in neuronal development and lack thereof imposes consequences on adult neuronal function (284, 285). The same was true of the CB₂ receptor as CB₂ receptor -/- mice showed behavioral and anatomic differences compared to wild type adults (286). The lack of both receptors in the mice used in this study could have affected development and ultimately the animal's ability to respond or compensate for cerebral ischemia. However, the effects observed here were not detrimental and it appears that the CB₁ -/- CB₂ -/- receptor mice were able to maintain more cerebral blood flow during the ischemic period even through the ischemic core.

The deletion of both receptors could have produced compensatory responses in the endogenous cannabinoid system prior to the injury that proved effective in mitigating damage. First of all, levels of endogenous cannabinoid ligands such as anandamide or 2-AG could have been elevated prior to ischemia. To our knowledge, no studies have evaluated the levels of

endogenous ligands in double knockout animals. Cannabinoid levels have been shown to change after cerebral ischemia although the nature of the study, the timing, and the ligand vary. Multiple reports exist that do in fact confirm the rise in anandamide or 2-AG following cerebral ischemia (158-161, 163). The levels of degrading enzymes for these ligands are also affected after cerebral ischemia and may contribute to the levels and duration of action of these ligands (158, 160).

Interestingly, deletion of one receptor, but not both, failed to induce protection and exacerbated injury. The effect on endogenous ligand concentration may only be a result or compensation if both receptors are lost. Deletion of one receptor does not seem sufficient to induce this protective mechanism, if in fact, this is the mechanism in play. Further testing of endogenous levels of anandamide and 2-AG should be carried out to determine the role, if any, they play. In short, genetic deletion of CB₁ -/- and CB₂ -/- receptors may ultimately impose an effect on concentrations of endogenous ligands at basal levels or in response to ischemia and effect outcomes.

Of course, the hypothesis that an endogenous ligand has increased in concentration, either by enhanced production or diminished degradation, relies on the fact that there exists a receptor for which it may bind. Non CB₁ -/- non CB₂ -/- receptor activity has been identified in a number of reports (5, 10, 25, 102). A potential receptor may be GPR55 (287). To further this theory, binding of such receptors must generate effects like that of the other known cannabinoid receptors, and in particular, should mimic CB₂ receptor activity in quelling inflammation. CB₂ receptor activation has been shown to be protective in cerebral ischemia (81). A yet to be identified receptor may be compensating in this instance for a lack of CB₂ receptor signaling and providing a beneficial effect. Again, this compensatory mechanisms seems to be relevant only when both CB₁ and CB₂ receptors are aberrant. Further, increased concentrations of endogenous ligands may

begin to bind non CB₁ or CB₂ receptors indiscriminately. Anandamide has also been shown to exert activity at the TRPV1 receptor (22, 46, 47). However, capsazepine, an inhibitor of TRPV1 did not abolish the protective effects of other cannabinoid agonists in two stroke studies (173, 283). On the other hand, the 5HT_{1A} receptor was necessary for the protective effects of the cannabinoid agonists in these studies and blockade of such removed the protective effect (173, 283). Genetic knock outs may also provoke a compensation in the expression of any of these receptors.

As the level of endogenous ligands remains unknown in the CB₁ -/- CB₂ -/- receptor mice, as well as the expression of other receptors, any combination of interaction is possible. Increased levels of anandamide and 2-AG may even be allosterically modulating this novel non CB₁ -/- non CB₂ -/- receptor. More so, both CB₁ and CB₂ receptors have been shown to have high levels of tonic activity even in the absence of agonist stimulation (5, 31, 32, 66). While loss of one receptor's basal rate may be detrimental in cerebral ischemia, removal of both may lead to a protective effect or at least prevent injury exacerbation.

At this time, the point at which the protective effect, or lack of exacerbation of injury, occurs can only be speculated. This may be a result of decreased excitotoxicity or diminished inflammation in the reperfusion phase (119). For certain, however, is the fact that during the period of occlusion, CB₁ -/- CB₂ -/- receptor mice had improved blood flow through the ischemic core, Figure 31. Throughout the period of occlusion, CB₁ -/- CB₂ -/- receptor mice had higher levels of cerebral blood flow. A statistically significant difference was found at 5 minutes and when the average decrease in blood flow for the entire 50 minutes was examined, another statistically significant difference was found. The difference throughout the occlusion was approximately 10% greater flow in CB₁ -/- CB₂ -/- receptor mice. It appears that CB₁ -/- CB₂ -/- receptor mice have an ability to provide much better compensation and autoregulation during periods of cerebral

ischemia than matched Wild Type controls. This increased flow most likely accounts for the majority of difference seen both in stroke volume as well as the Neurological Score, Figure 28 and 30. Lastly, CB₁ -/- CB₂ -/- receptor mice had as much edema as Wild Type controls which leads us to reason that the effect is not edema driven, Figure 29.

In brief, despite our predictions that CB₁ -/- CB₂ -/- receptor mice would have much greater stroke volumes and poorer outcomes than Wild Type controls, the mice were no worse than the Wild Type and even had a slight degree of protection. Most likely, this comes from enhanced cerebral blood flow during the occlusion. Augmented flow may stem from higher levels of endogenous ligands, activity at a non CB₁ -/- non CB₂ -/- receptor, or a combination of compensatory mechanisms as a result of genetic deletions. More study in this area is warranted to truly understand the role of the endogenous cannabinoid system in cerebral ischemia and the subsequent inflammation.

As previously stated, our laboratory had found that the endogenous cannabinoid system could be modulated with a CB₁ antagonist, SR141716A, to decrease injury following cerebral ischemia. This effect was reliant on the activity of the 5HT_{1A} receptor. We wanted to examine this same relationship in a permanent occlusion as well.

The model of photochemically induced permanent cerebral ischemia also produced a number of surprising findings. A number of reports from our own laboratory, in addition to outside researchers, had shown that antagonism of the CB₁ receptor provided protection in achieving smaller stroke volumes and infarct fractions (82, 158-160, 172). Thus, the fact that SR141716A, given prior to or after the onset of occlusion, produced a statistically significant difference in stroke volume and infarct fraction, Figure 33, was not entirely surprising. However, of the studies cited, only one had been a permanent occlusion and had been performed in rats (158). To our knowledge,

this is the first report of permanent occlusion and SR141716A yielding a protective effect in mice. Pretreatment with SR141716A also produced a statistically significant improvement in Neurological Score, Figure 35. The surprise did arise when the results of 5HT_{A1} antagonism were studied in regard to SR141716A.

Cannabidiol had been shown to reduce stroke volume in a transient ischemia model and this effect was blocked with WAY-100135, a selective 5HT_{A1} antagonist (283). Cannabidiol is believed to act through a non CB₁, non CB₂ receptor but the study revealed that activation of 5HT_{A1} was necessary for this protection (283). Our laboratory showed similar findings in that antagonism of the CB₁ receptor with SR141716A and activation of the CB₂ receptor with O-1966 provided the greatest degree of protection by increasing flow in cerebral ischemia (172). However, the effect was also lost when WAY-100135, a selective 5HT_{A1} antagonist, was applied (173). In both studies either cannabidiol or SR141716A/O-1966 combination, increased regional cerebral blood flow (173, 283). Again, this effect was lost with the addition of WAY-100135 (173, 283). The protective effect of SR141716A alone with regards to stroke volume was also lost in the presence of 5HT_{A1} antagonists (173). The studies suggested that in transient cerebral ischemia, activation of the 5HT_{A1} receptor was also necessary for the protective effects of cannabinoid agonists to produce effects.

In the study at hand, WAY-100635, a selective 5HT_{A1} antagonist was employed. There is some dispute that in addition to antagonizing 5HT_{A1} more selectively than WAY-100135, WAY-100635 can also activate D₄ receptors (288-290). In the studies here, addition of WAY-100365 to SR141716A as a pretreatment did not affect the stroke volume or infarct fraction 24 hour after the onset of ischemia, Figure 33. This contrasted findings in our own laboratory where in a transient model of cerebral ischemia the protective effect of SR141716A was lost when 5HT_{A1} antagonists

were added (WAY-100135). Previously, studies showed that when 5HT_{A1} was antagonized, cannabinoid driven increases in flow were also prevented (173, 283). The drug combinations utilized in those studies were not employed here. On the other hand, we had established that in the photothrombotic stroke, the injury created a permanent occlusion, Figure 28. The ability of cannabinoids to increase flow may not be relevant in such a model of injury as the occlusion occurs early and remains with no reperfusion.

On the other hand, one of the methods by which CB₁ receptor antagonism could be protective is through enhanced autoregulation of cerebral blood flow in the penumbral region (36, 119, 178). The studies that have examined the increase in cerebral blood flow, and lack thereof when 5HT_{A1} antagonists were applied, measured flow through the ischemic core (173, 283). Our determination of a permanent occlusion via photothrombosis also examined the distal ischemic core. What happens in the ischemic penumbra remains elusive. While 5HT_{A1} antagonism may block the effect of cannabinoid agonists to increase blood flow through the ischemic core, the effects are not known through the penumbral region. It is possible that in this region, autoregulation remains unaffected although it is unlikely since stroke volumes increased with the addition of 5HT_{A1} antagonists. Photothrombosis induced cerebral ischemia has also been shown to have a small penumbral region compared to transient filament models of stroke (179). Thus, enhanced autoregulation by CB₁ receptor antagonists do not seem to provide the mechanism by which SR141716A is protective in a permanent photothrombotic stroke.

On a side note, although statistical significance was not reached, the addition of SR141716A yielded higher levels of edema than in Vehicle mice, Figure 34. Edema is not surprising following the injury as the photothrombotic stroke has been shown to induce both cytogenic and vasogenic edema with the onset of injury (179). The increase in edema with the

SR141716 groups compared to Vehicle groups would support either an increase in flow or a decreased degree of neurovascular coupling. Blockade of the CB₁ receptor has been reported to increase neurovascular coupling and preserve the blood brain barrier (119). Thus, the protective mechanism here probably does not result from enhanced flow or improved coupling of the neurovascular unit.

One possible explanation for the protective effect of CB₁ receptor antagonism with SR141716A may stem from enhanced GABA signaling. Studies have indicated that CB₁ receptor's presynaptic location allows activation of it to decrease GABA release (19, 20, 119, 174, 175). Only one study has examined cannabinoid antagonism directly on GABA release and found no change although the study was carried out in cultured neurons (19). The effect of SR141716A in a post ischemic brain could behave very different as the endogenous cannabinoid system undergoes multiple alterations in response to cerebral ischemia (119). If SR141716A can increase GABA release, it could contribute to mitigating the effect of excitotoxic injury. Increased GABA release has been shown to be protective in ischemia/reperfusion injury by activating Akt signaling and inhibiting JNK, bsl-2, and c-jun phosphorylation and ultimately decreasing inflammation and improving outcomes (175). Cannabinoid activation on astrocytes has been shown to enhance glutamate release and contribute to injury (176). Antagonism of the CB₁ receptor here could also prevent this deleterious effect. In short, SR141716A may exert its protective effects through a modulation of neurotransmitter release.

The effects of SR141716A modulating neurotransmitter release at this point provides the strongest hypothesis for the protective mechanism of the drug. Since the model was shown to be a permanent occlusion and also have a small penumbra region, changes in flow during the procedure and after probably do little to effect the outcome (179). More so, the increase in edema

with SR141716A tends to negate the idea that in this model the CB₁ receptor antagonist improves neurovascular coupling. Unfortunately, the Cannabinoid-GABA axis in ischemia and reperfusion has not been extensively studied. Cannabinoids have been shown to decrease GABA release and increased GABA has been shown to be protective following a stroke (19, 20, 119, 174, 175). The two have not been directly studied together but our study provides convincing evidence that an examination of such interactions should be undertaken. Further the action of WAY-100635 has not been shown to affect GABA release and this further supports this theory of a neurotransmitter driven protective effect.

3.5 Conclusion

In short, here we have undertaken the examination of modulating the endogenous cannabinoid system in two models of cerebral ischemia. In the first model, we employed a transient ischemia and reperfusion model to study the effect of this pathology in CB₁ -/- CB₂ -/- receptor mice. The CB₁ -/- CB₂ -/- receptor mice showed a slight degree of protection and certainly not worsened injury as we had expected. We attribute this finding to modulations in the endogenous cannabinoid systems as a result of compensatory mechanisms following the deletion of both receptors. Increased levels of endogenous ligands, degrading enzymes and in particular, a non CB₁, non CB₂ receptor may contribute to this modulation. More so, these mice demonstrated convincing evidence that they were able to enhance cerebral blood flow during the period of ischemia. Thus, it seems likely that whatever compensatory mechanism is in play, it provides for enhanced autoregulation of neuronal tissue. Also, even without activation of the CB₂ receptor, the neuronal injury did not exceed that of Wild Type mice suggesting a compensatory mechanism in regulation of inflammation as well. Further studies would be needed to truly investigate this relationship.

Also, SR141716A was able to attenuate stroke volumes and infarct fractions in a photothrombotic model of permanent ischemia. The results of this finding were not altered with the addition of WAY-100365. Most likely, the effects of enhanced autoregulation and improved neurovascular coupling that may stem from CB₁ antagonism were not the mechanism in play. Rather, the protective effect most likely stemmed from a neurotransmitter mediate mechanism. Enhanced GABA release via CB₁ receptor antagonism could contribute to the decreased stroke volumes. More studies are warranted in this area to truly comprehend the ischemia-cannabinoid-GABA relationship.

3.6 Works Cited

1. Hata R, Mies G, Wiessner C, Fritze K, Hesselbarth D, Brinker G, et al. A reproducible model of middle cerebral artery occlusion in mice: hemodynamic, biochemical, and magnetic resonance imaging. *J Cereb Blood Flow Metab.* 1998;18(4):367-75.
2. Zhang M, Martin BR, Adler MW, Razdan RK, Ganea D, Tuma RF. Modulation of the balance between cannabinoid CB(1) and CB(2) receptor activation during cerebral ischemic/reperfusion injury. *Neuroscience.* 2008;152(3):753-60.
3. Zhang M, Adler MW, Abood ME, Ganea D, Jallo J, Tuma RF. CB2 receptor activation attenuates microcirculatory dysfunction during cerebral ischemic/reperfusion injury. *Microvasc Res.* 2009;78(1):86-94.
4. Belayev L, Busto R, Zhao W, Ginsberg MD. Quantitative evaluation of blood-brain barrier permeability following middle cerebral artery occlusion in rats. *Brain Res.* 1996;739(1-2):88-96.
5. Tsuchiya D, Hong S, Kayama T, Panter SS, Weinstein PR. Effect of suture size and carotid clip application upon blood flow and infarct volume after permanent and temporary middle cerebral artery occlusion in mice. *Brain Res.* 2003;970(1-2):131-9.
6. Zhang M, Martin BR, Adler MW, Razdan RJ, Kong W, Ganea D, et al. Modulation of cannabinoid receptor activation as a neuroprotective strategy for EAE and stroke. *J Neuroimmune Pharmacol.* 2009;4(2):249-59.
7. Swanson RA, Morton MT, Tsao-Wu G, Savalos RA, Davidson C, Sharp FR. A semiautomated method for measuring brain infarct volume. *J Cereb Blood Flow Metab.* 1990;10(2):290-3.
8. Lin TN, He YY, Wu G, Khan M, Hsu CY. Effect of brain edema on infarct volume in a focal cerebral ischemia model in rats. *Stroke.* 1993;24(1):117-21.
9. Vannucci SJ, Willing LB, Goto S, Alkayed NJ, Brucklacher RM, Wood TL, et al. Experimental stroke in the female diabetic, db/db, mouse. *J Cereb Blood Flow Metab.* 2001;21(1):52-60.
10. Kleinschmitz C, Braeuninger S, Pham M, Austinat M, Nölte I, Renné T, et al. Blocking of platelets or intrinsic coagulation pathway-driven thrombosis does not prevent cerebral infarctions induced by photothrombosis. *Stroke.* 2008;39(4):1262-8.

11. Zhang M, Mahadevan A, Amere M, Li H, Ganea D, Tuma RF. Unique Effects of Compounds Active at Both Cannabinoid and Serotonin Receptors During Stroke. *Translational Stroke Research*. 2012;3(3):348-56.
12. Hillard CJ. Role of cannabinoids and endocannabinoids in cerebral ischemia. *Curr Pharm Des*. 2008;14(23):2347-61.
13. Parmentier-Batteur S, Jin K, Mao XO, Xie L, Greenberg DA. Increased severity of stroke in CB1 cannabinoid receptor knock-out mice. *J Neurosci*. 2002;22(22):9771-5.
14. Mishima K, Hayakawa K, Abe K, Ikeda T, Egashira N, Iwasaki K, et al. Cannabidiol prevents cerebral infarction via a serotonergic 5-hydroxytryptamine1A receptor-dependent mechanism. *Stroke*. 2005;36(5):1077-82.
15. Leker RR, Gai N, Mechoulam R, Ovadia H. Drug-induced hypothermia reduces ischemic damage: effects of the cannabinoid HU-210. *Stroke*. 2003;34(8):2000-6.
16. Lutz B. Molecular biology of cannabinoid receptors. *Prostaglandins Leukot Essent Fatty Acids*. 2002;66(2-3):123-42.
17. Basu S, Dittel BN. Unraveling the complexities of cannabinoid receptor 2 (CB2) immune regulation in health and disease. *Immunol Res*. 2011;51(1):26-38.
18. Bátkai S, Osei-Hyiaman D, Pan H, El-Assal O, Rajesh M, Mukhopadhyay P, et al. Cannabinoid-2 receptor mediates protection against hepatic ischemia/reperfusion injury. *FASEB J*. 2007;21(8):1788-800.
19. Murikinati S, Jüttler E, Keinert T, Ridder DA, Muhammad S, Waibler Z, et al. Activation of cannabinoid 2 receptors protects against cerebral ischemia by inhibiting neutrophil recruitment. *FASEB J*. 2010;24(3):788-98.
20. Díaz-Alonso J, Aguado T, Wu CS, Palazuelos J, Hofmann C, Garcez P, et al. The CB(1) cannabinoid receptor drives corticospinal motor neuron differentiation through the Ctip2/Satb2 transcriptional regulation axis. *J Neurosci*. 2012;32(47):16651-65.
21. Harkany T, Guzmán M, Galve-Roperh I, Berghuis P, Devi LA, Mackie K. The emerging functions of endocannabinoid signaling during CNS development. *Trends Pharmacol Sci*. 2007;28(2):83-92.

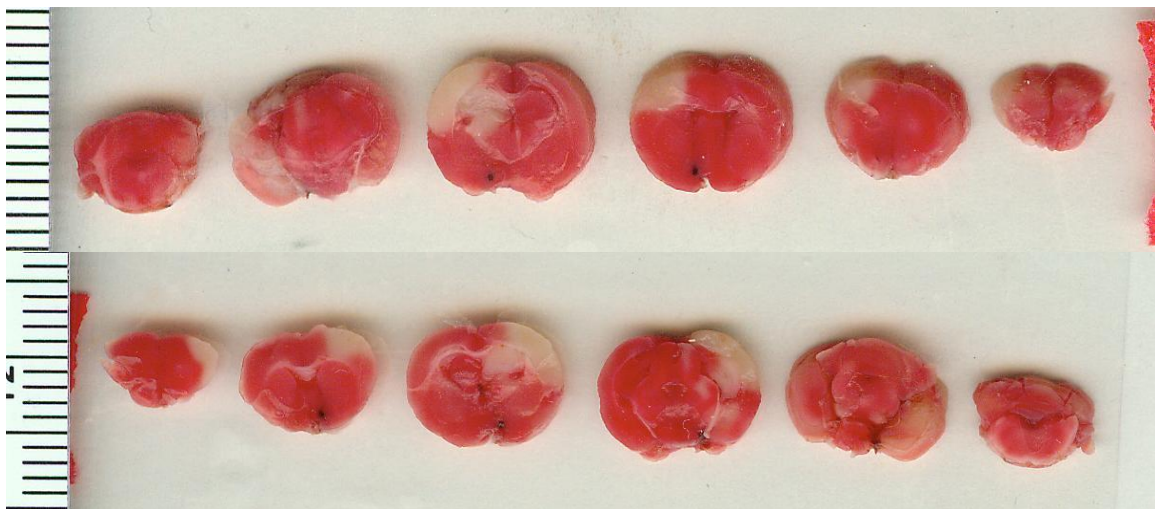
22. Flake NM, Zweifel LS. Behavioral effects of pulp exposure in mice lacking cannabinoid receptor 2. *J Endod.* 2012;38(1):86-90.
23. Berger C, Schmid PC, Schabitz WR, Wolf M, Schwab S, Schmid HH. Massive accumulation of N-acylethanolamines after stroke. Cell signalling in acute cerebral ischemia? *J Neurochem.* 2004;88(5):1159-67.
24. Muthian S, Rademacher DJ, Roelke CT, Gross GJ, Hillard CJ. Anandamide content is increased and CB1 cannabinoid receptor blockade is protective during transient, focal cerebral ischemia. *Neuroscience.* 2004;129(3):743-50.
25. Amantea D, Spagnuolo P, Bari M, Fezza F, Mazzei C, Tassorelli C, et al. Modulation of the endocannabinoid system by focal brain ischemia in the rat is involved in neuroprotection afforded by 17beta-estradiol. *FEBS J.* 2007;274(17):4464-775.
26. Degn M, Lambertsen KL, Petersen G, Meldgaard M, Artmann A, Clausen BH, et al. Changes in brain levels of N-acylethanolamines and 2-arachidonoylglycerol in focal cerebral ischemia in mice. *J Neurochem.* 2007;103(5):1907-16.
27. Schäbitz WR, Giuffrida A, Berger C, Aschoff A, Schwaninger M, Schwab S, et al. Release of fatty acid amides in a patient with hemispheric stroke: a microdialysis study. *Stroke.* 2002;33(8):2112-4.
28. Abood ME. Molecular biology of cannabinoid receptors. *Handb Exp Pharmacol.* 2005(168):81-115.
29. Begg M, Pacher P, Bátka S, Osei-Hyiaman D, Offertáler L, Mo FM, et al. Evidence for novel cannabinoid receptors. *Pharmacol Ther.* 2005;106(2):133-45.
30. Berdyshev EV. Cannabinoid receptors and the regulation of immune response. *Chem Phys Lipids.* 2000;108(1-2):169-90.
31. Puffenbarger RA, Boothe AC, Cabral GA. Cannabinoids inhibit LPS-inducible cytokine mRNA expression in rat microglial cells. *Glia.* 2000;29(1):58-69.
32. Sharir H, Console-Bram L, Mundy C, Popoff SN, Kapur A, Abood ME. The endocannabinoids anandamide and virodhamine modulate the activity of the candidate cannabinoid receptor GPR55. *J Neuroimmune Pharmacol.* 2012;7(4):856-65.

33. Di Marzo V. Targeting the endocannabinoid system: to enhance or reduce? *Nat Rev Drug Discov.* 2008;7(5):438-55.
34. Di Marzo V, Petrosino S. Endocannabinoids and the regulation of their levels in health and disease. *Curr Opin Lipidol.* 2007;18(2):129-40.
35. Niforatos W, Zhang XF, Lake MR, Walter KA, Neelands T, Holzman TF, et al. Activation of TRPA1 channels by the fatty acid amide hydrolase inhibitor 3'-carbamoylbiphenyl-3-yl cyclohexylcarbamate (URB597). *Mol Pharmacol.* 2007;71(5):1209-16.
36. Bouaboula M, Poinot-Chazel C, Bourrié B, Canat X, Calandra B, Rinaldi-Carmona M, et al. Activation of mitogen-activated protein kinases by stimulation of the central cannabinoid receptor CB1. *Biochem J.* 1995;312 (Pt 2):637-41.
37. Bouaboula M, Dussossoy D, Casellas P. Regulation of peripheral cannabinoid receptor CB2 phosphorylation by the inverse agonist SR 144528. Implications for receptor biological responses. *J Biol Chem.* 1999;274(29):20397-405.
38. Bouaboula M, Perrachon S, Milligan L, Canat X, Rinaldi-Carmona M, Portier M, et al. A selective inverse agonist for central cannabinoid receptor inhibits mitogen-activated protein kinase activation stimulated by insulin or insulin-like growth factor 1. Evidence for a new model of receptor/ligand interactions. *J Biol Chem.* 1997;272(35):22330-9.
39. Chemel BR, Roth BL, Armbruster B, Watts VJ, Nichols DE. WAY-100635 is a potent dopamine D4 receptor agonist. *Psychopharmacology (Berl).* 2006;188(2):244-51.
40. Martel JC, Leduc N, Ormière AM, Faucillon V, Danty N, Culie C, et al. WAY-100635 has high selectivity for serotonin 5-HT(1A) versus dopamine D(4) receptors. *Eur J Pharmacol.* 2007;574(1):15-9.
41. Fornal CA, Metzler CW, Gallegos RA, Veasey SC, McCreary AC, Jacobs BL. WAY-100635, a potent and selective 5-hydroxytryptamine1A antagonist, increases serotonergic neuronal activity in behaving cats: comparison with (S)-WAY-100135. *J Pharmacol Exp Ther.* 1996;278(2):752-62.
42. Wagner JA, Járai Z, Bátkai S, Kunos G. Hemodynamic effects of cannabinoids: coronary and cerebral vasodilation mediated by cannabinoid CB(1) receptors. *Eur J Pharmacol.* 2001;423(2-3):203-10.

43. Gebremedhin D, Lange AR, Campbell WB, Hillard CJ, Harder DR. Cannabinoid CB1 receptor of cat cerebral arterial muscle functions to inhibit L-type Ca²⁺ channel current. Am J Physiol. 1999;276(6 Pt 2):H2085-93.
44. Carmichael ST. Rodent models of focal stroke: size, mechanism, and purpose. NeuroRx. 2005;2(3):396-409.
45. Katona I, Sperlágh B, Sík A, Käfalvi A, Vizi ES, Mackie K, et al. Presynaptically located CB1 cannabinoid receptors regulate GABA release from axon terminals of specific hippocampal interneurons. J Neurosci. 1999;19(11):4544-58.
46. Hájos N, Katona I, Naiem SS, MacKie K, Ledent C, Mody I, et al. Cannabinoids inhibit hippocampal GABAergic transmission and network oscillations. Eur J Neurosci. 2000;12(9):3239-49.
47. Varma N, Carlson GC, Ledent C, Alger BE. Metabotropic glutamate receptors drive the endocannabinoid system in hippocampus. J Neurosci. 2001;21(24):RC188.
48. Xu J, Li C, Yin XH, Zhang GY. Additive neuroprotection of GABA A and GABA B receptor agonists in cerebral ischemic injury via PI-3K/Akt pathway inhibiting the ASK1-JNK cascade. Neuropharmacology. 2008;54(7):1029-40.
49. Navarrete M, Araque A. Endocannabinoids mediate neuron-astrocyte communication. Neuron. 2008;57(6):883-93.

3.7 Figures

Figure 27, TTC Staining in Wild Type and Knockout Mice



A.



B.

Panel A: Top Anterior, Bottom Posterior: view of TTC stained slices in Wild Type Mice.

Panel B: Top Anterior, Bottom Posterior: view of TTC stained slices in CB₁ -/- CB₂ -/- receptor mice.

Figure 28, Stroke Size in Wild Type and Knockout Mice

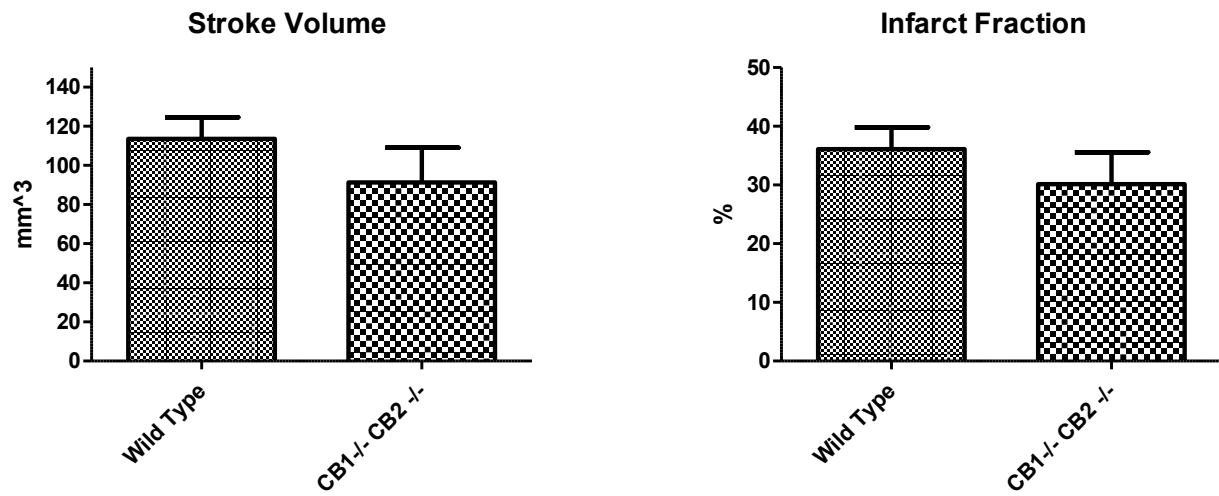


Figure 28. Left: Stroke volume in Wild Type and CB₁ -/- CB₂ -/- receptor mice. Right: Infarct fraction in Wild Type and CB₁ -/- CB₂ -/- receptor mice. Data expressed as Mean \pm SEM. . p < 0.05. n = 20 Wild Type and 5 KO mice.

Figure 29, Edema in Wild Type and Knockout Mice

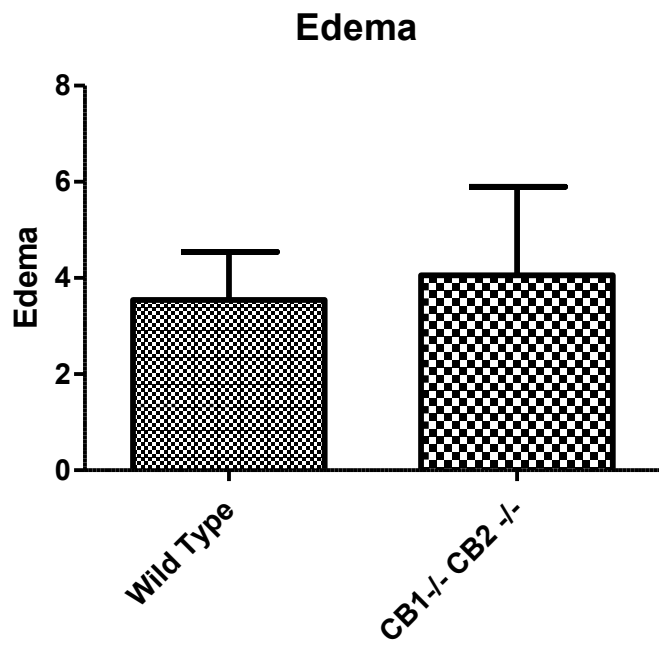


Figure 29. Edema in Wild Type and $\text{CB}_1^{-/-}\text{-}\text{CB}_2^{-/-}$ receptor mice. Data expressed as Mean \pm SEM. . $p < 0.05$. $n = 20$ Wild Type and 5 KO mice.

Figure 30, Clinical Parameters in Wild Type and Knockout Mice

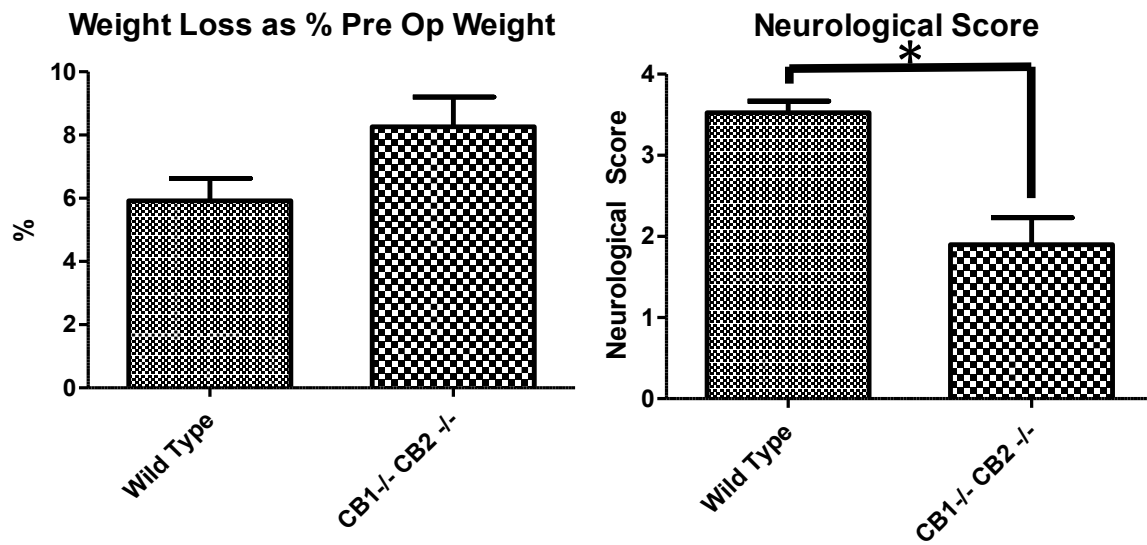


Figure 30: Left Wild Type and $\text{CB}_1^{-/-}\text{CB}_2^{-/-}$ receptor mice weight loss as a percent of pre-operative body weight. Right: Neurological Score of Wild Type and $\text{CB}_1^{-/-}\text{CB}_2^{-/-}$ receptor mice. Data expressed as Mean \pm SEM. . $p < 0.05$. $n = 20$ Wild Type and 5 KO mice.

Figure 31, Blood Flow in Wild Type and Knockout Mice

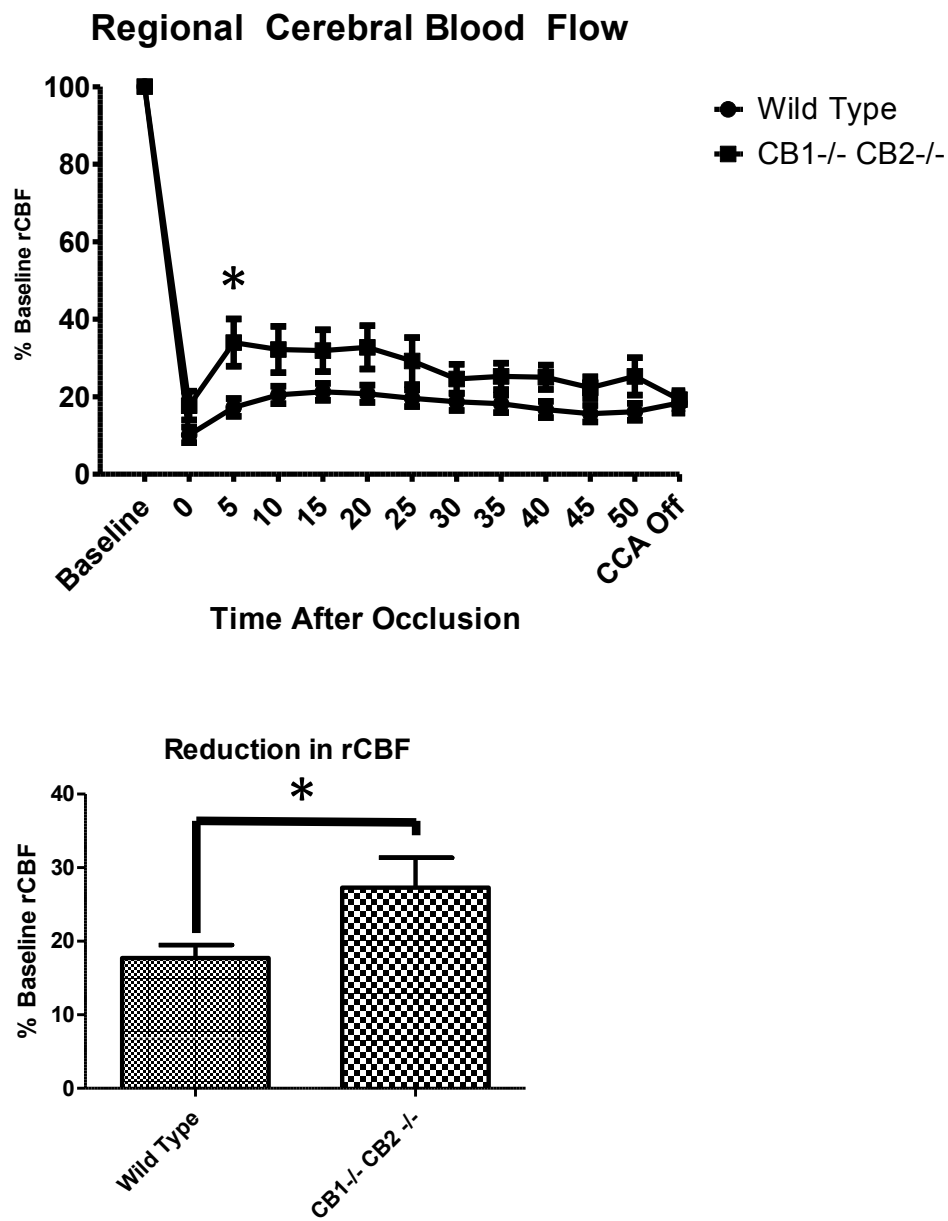


Figure 31. Top: Regional Cerebral Blood Flow between Wild Type and CB₁ -/- CB₂ -/- receptor mice. Bottom: Average Regional Cerebral Blood Flow during period of occlusion. Data expressed as Mean ± SEM. . p < 0.05. n = 20 Wild Type and 5 KO mice.

Figure 32, TTC Staining in Photothrombotic Studies

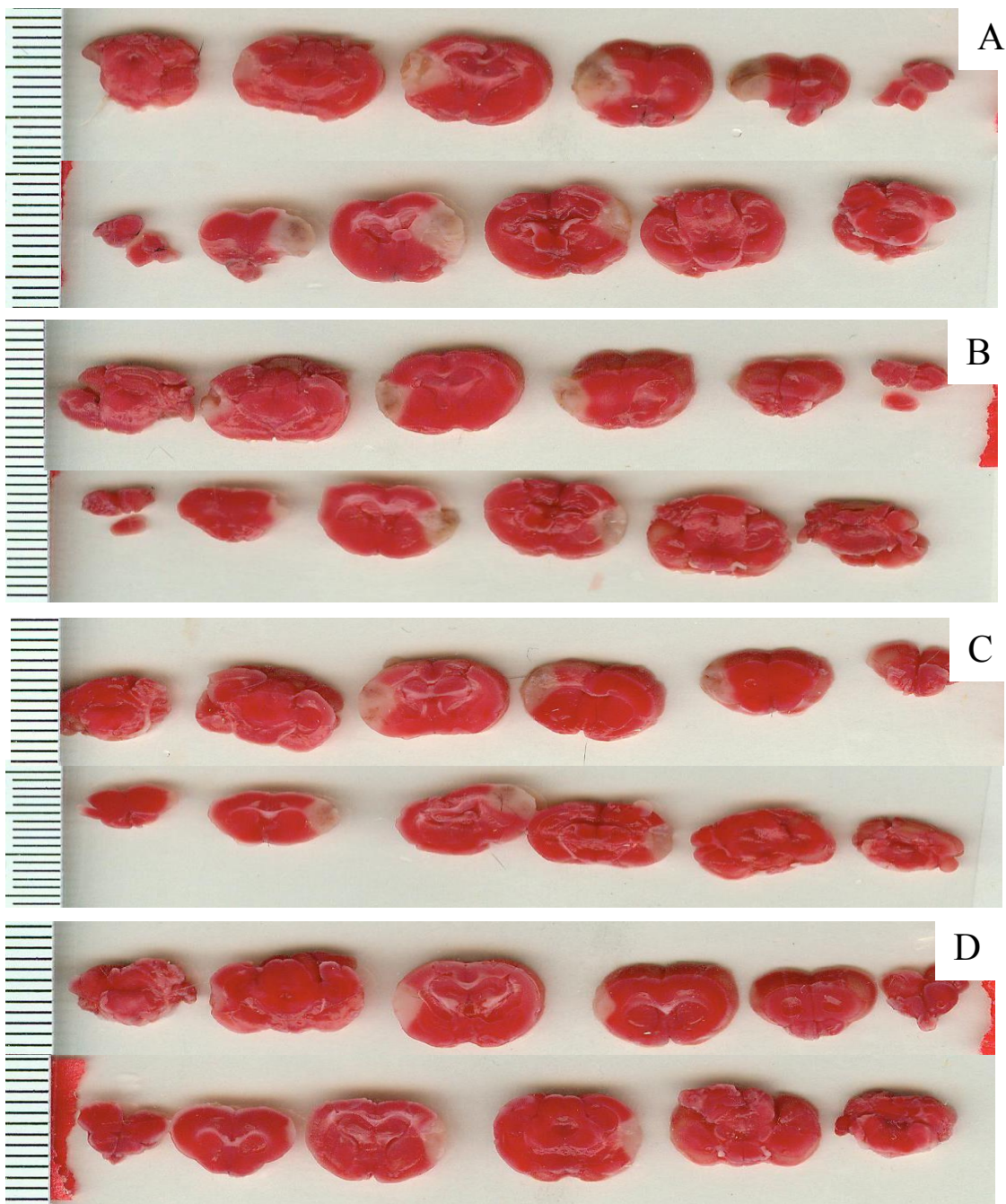


Figure 32. TTTC staining following photothrombotic stroke (24 hours). A: Vehicle Mice. B: SR141716A pretreatment. C: SR141716A post-treatment. D: SR141716A with WAY-100365 pretreatment.

Figure 33, Stroke Size in in Photothrombotic Studies

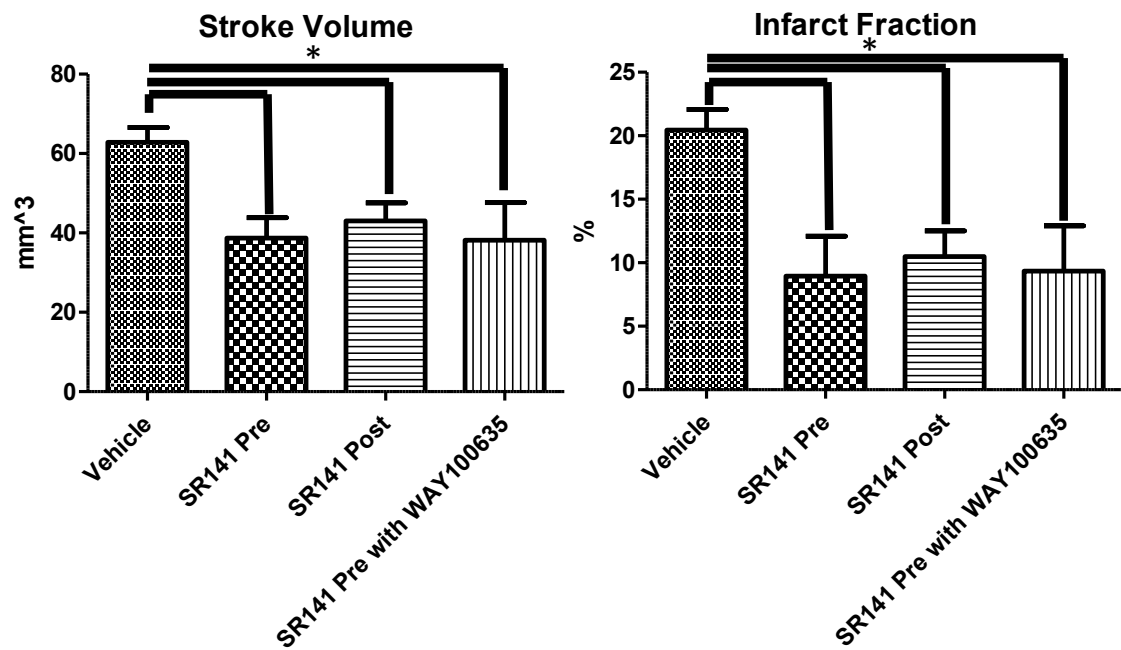


Figure 33. Left: Stroke volume among groups. Right: Infarct fraction among groups. Data expressed as Mean \pm SEM. $p < 0.05$. $n = 5 - 13$ mice in each group.

Figure 34, Edema in in Photothrombotic Studies

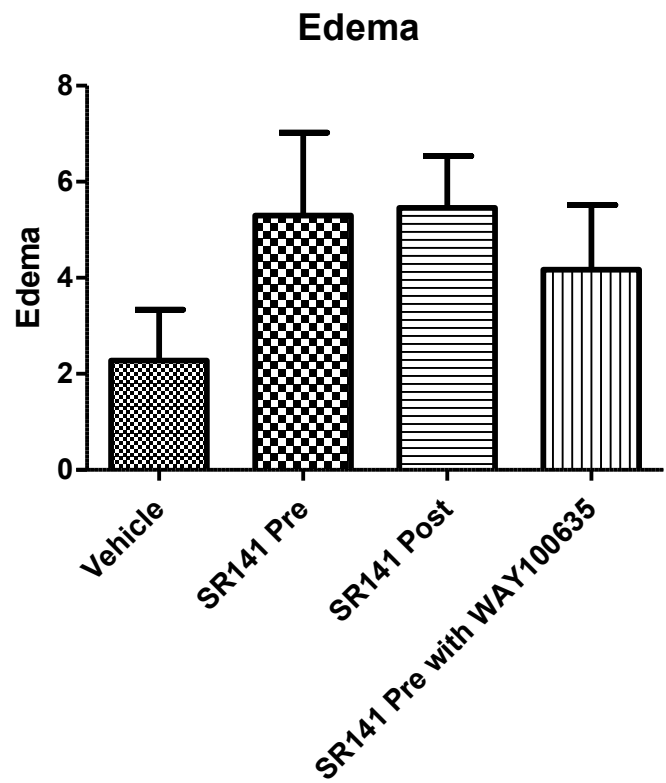


Figure 34. Edema among groups. Data expressed as Mean \pm SEM. $p < 0.05$. $n = 5 - 13$ mice in each group.

Figure 35, Clinical Parameters in Photothrombotic Studies

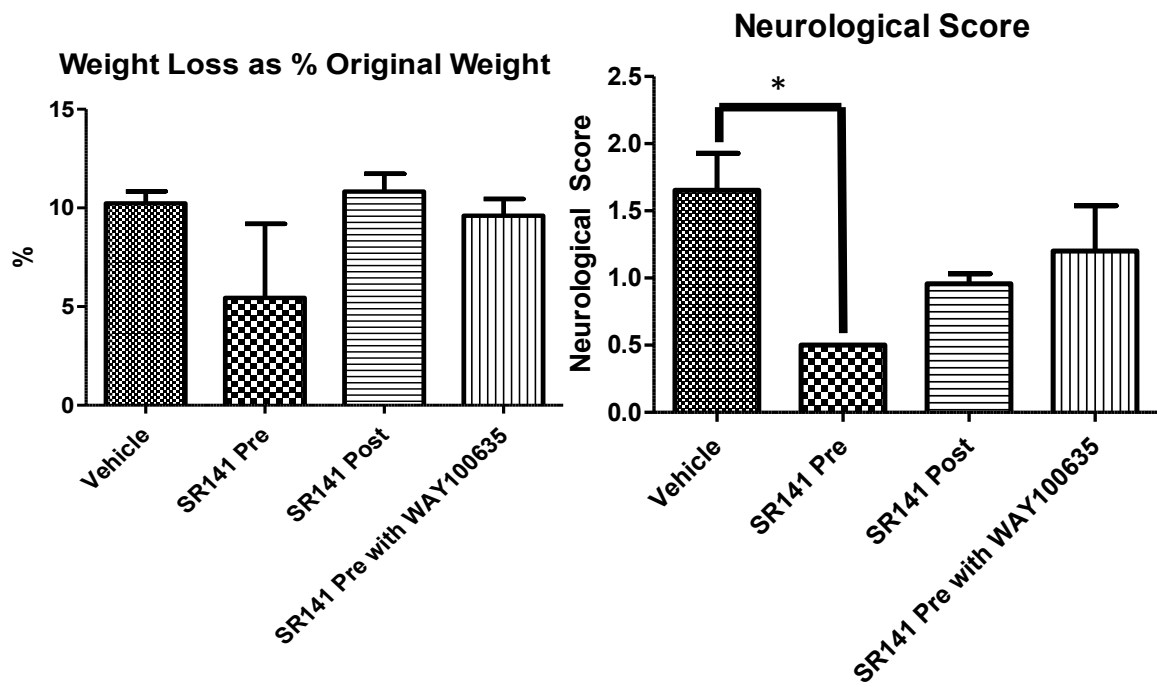


Figure 35. Clinical Parameters. Left: weight loss as a percent of pre-operative body weight. Right: Neurological Score among groups. Data expressed as Mean \pm SEM. $p < 0.05$. $n = 5 - 13$ mice in each group.

CHAPTER 4

UTILIZATION OF THE ENDOGENOUS CANNABINOID SYSTEM TO ATTENUATE INFLAMMATION ASSOCIATED WITH MORPHINE ADMINISTRATION

4.1 Specific Aims, Rational, and Hypothesis

1. Evaluate the use of a highly selective CB₂ agonist, O-1966, in preventing tolerance and hyperalgesia associated with chronic morphine administration.
2. Examine the effect of O-1966 on inflammatory cytokines generated by chronic morphine administration.
3. Determine the functionality and practicality of O-1966 as an adjunct to morphine administration in an acute setting.

Chronic administration of morphine has been shown to be inflammatory in nature and cause the production of IL-6, TNF- α , and IL-1 β . This inflammatory response is thought to contribute to both the development of morphine tolerance and hyperalgesia. Microglial activation is also thought to play a role in the deleterious sequelae. The CB₂ agonist, O-1966, has been shown to reduce these cytokines as well as microglial activation. Here we sought to explore its efficacy in ameliorating the onset of tolerance.

We hypothesize that the use of a CB₂ agonist will prevent the development of tolerance and hyperalgesia in a chronic dosing pattern. Further, we feel this interaction will be mediated by a reduction in inflammatory cytokines. Lastly, in acute interactions, we feel that O-1966 will work synergistically with morphine.

4.2 Materials and Methods

4.2.1 Animals

The morphine studies were conducted on 7 to 8-week-old male C57BL/6 mice weighing 18-23 grams (Taconic Laboratories, New York, USA). Studies were conducted in accordance with the guidelines approved by the Institute for Animal Care and Use Committee at Temple University. Animals were maintained on a regular chow diet and had access to food and water ad libitum through the study. Animals were group housed in 12 hour dark light cycles (Dark 7pm to 7am).

4.2.2 Experimental Groups and Interactions

The drug combinations and experimental groups in the chronic study included: Saline/Saline, Cremophor/Saline, O-1966/Saline, Cremophor/Morphine-100, O-1966/Morphine-100, Morphine-100/O-1966, O-1966/Morphine-32, Cremophor/Morphine-32 where Morphine-100 = morphine sulfate 100 mg/kg and Morphine-32 = morphine sulfate 32 mg/kg. Injections were separated by 15 minutes and performed in the order listed by the “Group Name”. Figure 36 provides a pictorial representation of this experimental design. Acute interactions were indicated in the results and on the appropriate figures and included morphine alone, O-1966 alone, morphine with O-1966 simultaneously, morphine + O-1966 + SR144528 simultaneously, or morphine and O-1966 separated by 15 minutes in varying order.

4.2.3 Measurement of Hot Plate Withdrawal Latency

Nociception and morphine induced antinociception were analyzed by means of a hot plate analgesia meter (Columbus Instruments, Columbus, OH). Mice were placed on a hot plate maintained at $54.0^{\circ}\text{C} \pm 0.5^{\circ}\text{C}$. The latency to hind paw lick, hind paw lift, hind paw flutter, mouse

shuffle, or mouse jump was measured to the nearest 0.1 second. A maximal cutoff of 30 seconds was utilized to prevent injury to the paw tissue. Immediately after the end of the trial, mice were returned to their home cage. Baselines were obtained twice (15 minutes apart). The first testing with medication in the mice occurred two hours after the baseline testing. Each testing period was then separated by 30 minutes and increasing doses of drugs. Latencies obtained following drug administration were reported as Percent Maximal Possible Effect (%MPE). The following formula was utilized to calculate such:

$$\% \text{ MPE} = \frac{(\text{Experimental Latency} - \text{Average Baseline Latency})}{(\text{Maximal Cut Off Time} - \text{Average Baseline Latency})} \times 100$$

This procedure was adapted from Fischer, et al and Ibrahim, et al (190, 228). To calculate hyperalgesia, baselines from Day 1 were compared to Day 7. For chronic testing, hotplate latency was tested on Day 1 and Day 7 as indicated in Figure 36 with appropriate drug combinations as indicated.

4.2.4 Preparation and Dosing of O-1966, SR144528, and Morphine Sulfate

All injections were intraperitoneal and made fresh daily. O-1966 (Organix Laboratories, Massachusetts, USA) was prepared in Ethanol:Cremophor:Saline (1:1:18). It was prepared to 0.1 mg/mL and injected 1 mg/kg twice daily for chronic studies. For acute studies, O-1966 was diluted in Vehicle to the following concentrations: 1.38, 2.75, 5.5, 11.22, 44, 88, and 176 mg/mL and given simultaneously with morphine, 15 minutes after morphine, or 15 minutes prior as indicated.

SR144528 (RTI) was prepared in the same manner and diluted to the same concentrations as O-1966 for the acute study. For the acute study, SR144528 was given with O-1966 simultaneously and intraperitoneally at the same concentrations.

Morphine was dissolved in 0.9% saline. Chronic studies utilized 100 mg/kg or 32 mg/kg as indicated in Figure 36 and was injected twice daily. Morphine dose response curves on days 1 and 7 of chronic studies utilized the following doses: 0.3, 1, 3.2, 10, 32, 100 and 200 mg/kg. For acute studies it was prepared in the following concentrations and paired with O-1966 or SR144528 as indicated: 0.3, 0.6, 1.25, 2.5, 5, 10, 20, and 40 mg/mL. It also was injected intraperitoneally.

Cremophor vehicle was a mix of Ethanol:Cremophor:Saline (1:1:18).

Figure 36 provides a pictorial representation of the dosing and testing regimen.

4.2.5 Quantitative Real Time Polymerase Chain Reaction (qRT-PCR)

The expression of IL-6, TLR-2, TLR-4, MMP-9, TNF- α , and IL-1 β were examined by SYBR-Green real time PCR based technique as described in Adhikary (291). Briefly, immediately following the hotplate testing on Day 7, mice were perfused with 200 mL ice cold 1X PBS. Brain and spinal cords were removed and digested in Tryzol. RNA was purified and collected from the aqueous phase as described in Chomczynski (292). RNA purity and quantity was accessed by spectrophotometric means at 260 nm. cDNA was produced by reverse transcriptase. The 10 μ L of PCR mix contained 4 μ L of diluted cDNA and 6 μ L of Master Mix with primers. Real time PCR was performed using the ABI System and cycling conditions were 95°C for 30 seconds, 55°C for 1 minute, and 72°C for 30 seconds for 40 cycles. The expression of each gene was indicated by the cycle number needed for the cDNA to undergo amplification and ultimately reach threshold. Results were normalized to GAGDH (housekeeping gene).

Primers utilized had the following sequences:

IL-6 Sense 5'-TCC TCT CTG CAA GAG ACT TCC ATCC -3'

 Antisense 5'-GGG AAG GCC GTG GTT GTC ACC -3'

TLR-2 Sense 5'-TCT TGC GCA GTT TGC AGA AG-3'

 Antisense 5'-AGC CCA TTG AGA GGA AAG CC-3'

TLR-4 Sense 5'-GGA CCT TAC CGG GCA GAA G-3'

 Antisense 5'-ACC CCT GGA AAG GAA GGT GT -3'

MMP-9 Sense 5'-AAA ACC TCC AAC CTC ACG GA -3'

 Antisense 5'-GCG GTA CAA GTA TBC CTC TGC -3'

TNF- α Sense 5'-GAC CCT CAC ACT CAG ATC ATC TTC T-3'

 Antisense 5'-CCT CCA CTT GGT GGT TTG CT -3'

IL-1 β Sense 5'- CCC TGC AGC TGG AGA GTG TGG A -3'

 Antisense 5'-TGT GCT CTG CTT GTG AGG TGC TG -3'

GAPDH Sense 5'-GGA GCG AGA CCC CAC TAA CA -3'

 Antisense 5'-ACA TAC TCA GCA CCG GCC TC-3'

4.2.6 Statistical Analysis

Chronic studies were evaluated by comparing ED₅₀ values of Day 1 with Day 7 as a fold increase. Hyperalgesia was compared with a Student's t-test in comparing Day 1 with Day 7 results. PCR analysis was compared with Analysis of Variance. Acute studies were analyzed by

comparing the predicted effect with the achieved effect by the principle of dose equivalence and utilization of a Student's t-test (293). Data is reported as the mean \pm SEM. $p < 0.05$.

4.3 Results

4.3.1 Effect of Chronic Morphine and O-1966 Treatment on the Development of Tolerance,

Figure 37 and Table 1

Experimental groups and combinations are indicated by the two injections separated by a “/” sign. “Morphine-100” implies a dose of 100 mg/kg while “Morphine-32” indicates only 32 mg/kg was given. Day 1 ED₅₀ for the experimental groups were found to be Saline/Saline 7.2 \pm 1.93 mg/kg, Cremophor/Saline 8.0 \pm 2.9 mg/kg, O-1966/Saline 10.7 \pm 2.4 mg/kg, Cremophor/Morphine-100 7.1 \pm 2.0 mg/kg, O-1966/Morphine-100 6.4 \pm 2.3 mg/kg, Morphine-100/O-1966 4.7 \pm 1.8 mg/kg, O-1966/Morphine-32 7.5 \pm 1.7 mg/kg, and Cremophor/Morphine-32 4.0 \pm 1.3 mg/kg. Day 7 ED₅₀s for the experimental groups were found to be Saline/Saline 4.1 \pm 0.6 mg/kg, Cremophor/Saline 12.2 \pm 2.3 mg/kg, O-1966/Saline 9.9 \pm 2.6 mg/kg, Cremophor/Morphine-100 27.8 \pm 10.8 mg/kg, O-1966/Morphine-100 42.0 \pm 16.5 mg/kg, Morphine-100/O-1966 10.7 \pm 3.3 mg/kg, O-1966/Morphine-32 15.6 \pm 8.2 mg/kg, and Cremophor/Morphine-32 8.6 \pm 3.4 mg/kg. Fold changes were thus found to be Saline/Saline 0.57, Cremophor/Saline 1.53, O-1966/Saline 0.93, Cremophor/Morphine-100 3.92, O-1966/Morphine-100 6.56, Morphine-100/O-1966 2.28, O-1966/Morphine-32 2.08, and Cremophor/Morphine-32 2.15.

Table 1, Fold Change in Chronic Morphine Administration

Group	Day 1 ED50	Day 7 ED50	Fold Increase
Sal/Sal	7.2	4.1	0.57
Crem/Sal	8.0	12.2	1.53
O-1966/Sal	10.7	9.9	0.93
Crem/Mor 100	7.1	27.8	3.92
O-1966/Mor 100	6.4	42.0	6.56
Mor 100/O-1966	4.7	10.7	2.28
O-1966/Mor 32	7.5	15.6	2.08
Crem/Mor 32	4.0	8.6	2.15

4.3.2 Effect of Chronic Morphine and O-1966 Treatment on the Development of Hyperalgesia, Figure 38

Day 1 baseline latencies to nociception for the experimental groups were found to be Saline/Saline 20.23 ± 0.51 sec, Cremophor/Saline 19.03 ± 0.29 sec, O-1966/Saline 21.00 ± 0.49 sec, Cremophor/Morphine-100 21.58 ± 0.40 sec, O-1966/Morphine-100 21.5 ± 0.32 sec, Morphine-100/O-1966 19.87 ± 0.30 sec, O-1966/Morphine-32 21.48 ± 0.26 sec, and Cremophor/Morphine-32 17.93 ± 0.40 sec. Day 7 baseline latencies to nociception for the experimental groups were found to be Saline/Saline 18.39 ± 0.40 sec, Cremophor/Saline 18.46 ± 0.50 sec, O-1966/Saline 18.11 ± 0.37 sec, Cremophor/Morphine-100 18.69 ± 0.43 sec, O-1966/Morphine-100 19.42 ± 0.57 sec, Morphine-100/O-1966 20.19 ± 0.31 sec, O-1966/Morphine-32 20.29 ± 0.44 sec, and Cremophor/Morphine-32 19.39 ± 0.40 sec. The only group that reached a statistically significant difference among Day 1 and Day 7 was the group that received Cremophor/Morphine-100 mg/kg.

4.3.3 Results of Chronic Morphine and O-1966 on Inflammatory Gene Expression, Figure

39

All inflammatory genes were compared to the housekeeping gene GAPDH and expressed as a ratio \pm SEM.

Effect on IL-6

After chronic morphine treatment, the ratio of IL-6/GAPDH in the following groups was found to be: Saline/Cremophor 0.37 ± 0.04 , Cremophor/ Morphine-100 0.65 ± 0.26 , O-1966/Morphine-100 0.32 ± 0.03 , and O-1966/Saline 0.58 ± 0.10 . $F(3,3) = 1.23$, $p = 0.36$.

Effect on TLR-2

After chronic morphine treatment, the ratio of TLR-2/GAPDH in the following groups was found to be: Saline/Cremophor 0.52 ± 0.12 , Cremophor/ Morphine-100 0.73 ± 0.33 , O-1966/Morphine-100 0.37 ± 0.08 , and O-1966/Saline 0.38 ± 0.14 . $F(3,3) = 0.73$, $p = 0.56$.

Effect on TLR-4

After chronic morphine treatment, the ratio of TLR-4/GAPDH in the following groups was found to be: Saline/Cremophor 2.02 ± 0.57 , Cremophor/ Morphine-100 1.50 ± 0.47 , O-1966/Morphine-100 1.33 ± 0.24 , and O-1966/Saline 1.68 ± 0.30 . $F(3,3) = 0.49$, $p = 0.70$.

Effect on MMP-9

After chronic morphine treatment, the ratio of TLR-4/GAPDH in the following groups was found to be: Saline/Cremophor 1.05 ± 0.17 , Cremophor/ Morphine-100 0.78 ± 0.12 , O-1966/Morphine-100 0.99 ± 0.13 , and O-1966/Saline 0.79 ± 0.29 . $F(3,3) = 0.53$, $p = 0.67$.

Effect on TNF- α

After chronic morphine treatment, the ratio of TLR-4/GAPDH in the following groups was found to be: Saline/Cremophor 0.56 ± 0.05, Cremophor/ Morphine-100 0.84 ± 0.14, O-1966/Morphine-100 0.76 ± 0.08, and O-1966/Saline 0.59 ± 0.24. $F(3,3) = 0.82$, $p = 0.52$.

Effect on IL-1 β

After chronic morphine treatment, the ratio of TLR-4/GAPDH in the following groups was found to be: Saline/Cremophor 0.16 ± 0.03, Cremophor/ Morphine-100 0.66 ± 0.17, O-1966/Morphine-100 0.16 ± 0.04, and O-1966/Saline 0.09 ± 0.04. $F(3,3) = 8.42$, $p = 0.01$.

4.3.4 Effect of O-1966 on Acute Morphine Administration, Figure 42

In an acute study, morphine administered alone produced an ED₅₀ or 9.1 mg/kg. O-1966 failed to provide enough antinociception to reach an ED₅₀. The administration of morphine and O-1966 simultaneously increased the ED₅₀ to 31.6 mg/kg. However, if SR144528 was added to this combination, the ED₅₀ moved back to 11.8 mg/kg.

4.4.5 Effect of the Order of Administration on Morphine and O-1966, Figure 43

In this acute study, morphine alone produced an ED₅₀ of 11.0 mg/kg. If morphine was administered 15 minutes before O-1966, the ED₅₀ rose to 20.0 mg/kg. However, if O-1966 was administered 15 minutes prior to morphine the ED₅₀ was found to be 47.7 mg/kg.

4.5 Discussion

From the studies at hand, several findings became apparent. First of all, in regards to chronic morphine administration, the order of administration of the compounds was exceedingly

important. If O-1966 was given prior to morphine, the development of tolerance was exacerbated. However, if the morphine was given first, tolerance was attenuated and the fold shift in ED₅₀ reduced to approximately 1/3 of the tolerance fold shift in the reverse order. The application of O-1966 also prevented the induction of hyperalgesia. More so, the application of O-1966 was able to decrease mRNA expression of the proinflammatory cytokine IL-1 β . During acute studies, O-1966 acts as an antagonist of morphine. The effect could be reversed with the selective antagonist, SR144528. However, the order of application was also important in these studies. If morphine was given prior to O-1966, the antagonistic effect was quelled. In short, the findings show an overall reduction in inflammatory cytokine expression and a reduction in tolerance which make this an interesting area for further investigation.

Tolerance is defined as the need to increase the dose of a medication to reach the same level of efficacy (294). Chronic studies revealed a number of interesting findings in regards to the development of tolerance, hyperalgesia, and inflammatory cytokine production, Figures 37, 38, and 39. In the chronic studies performed, mice that received no injections other than saline sensitized slightly over the regimen with an overall reduction in ED₅₀ and a fold change of 0.57, Table 1. This may stem from acclimation as handling the mice all week produced some conditioning. The group that received Cremophor/Saline developed a slight degree of tolerance with a 1.53 fold change in ED₅₀. Cremophor has been shown to be slightly inflammatory on its own and could contribute to inflammation and ultimately a small degree of tolerance (206, 209, 295). O-1966 alone produced essentially no change at all (fold change 0.93) and the addition of the CB₂ agonist most likely quelled any inflammation produced by the Cremophor.

The addition of 100 mg/kg of morphine twice a day with Cremophor vehicle induced a fold change of 3.92. This fold increase indicates that tolerance developed as nearly 4 times more

morphine was needed to achieve 50% of the maximal possible effect on day 7 than on baseline at day 1. Chronic injections of morphine have been shown to lead to the development of tolerance and the mechanisms appears to be intimately linked to the subsequent inflammation (186, 206-209, 213). Morphine administration tends to activate microglia and the inflammatory cytokines released, such as IL-1 β , TNF- α , and IL-6 oppose the action of morphine (186, 207, 209). Glial activation may occur through TLR-4 but studies indicate that glial activation often accompanies the development of tolerance (206-209). As more morphine is introduced, inflammation increases and more proinflammatory cytokines are produced from activated microglia (206, 209, 210, 213). Activated microglial also tend to release excitatory amino acids that facilitate the transmission of pain signals (209, 210). The studies here indicated that by administering O-1966 after morphine had been injected, the tolerance could be attenuated and reduced to only a 2.28 fold increase compared to 3.92 without O-1966, Figure 37, and Table 1.

The most likely explanation for said reduction in the development of tolerance most likely stems from the ability of CB₂ agonists to block microglial activation and the resultant inflammation, Figure 44. Activation of cannabinoid receptors on microglial cells leads to the induction of Mitogen-Activated Protein Kinase Phosphatase-1 and 3 (MKP-1 and MKP-3) to terminate Mitogen Activated Protein Kinase (MAP-K) signaling resulting from TLR-4 activation (28, 29, 296). Activation of the μ opioid receptor by morphine has been shown to activate the signal transduction pathway, akt-ERK1/2, and is attenuated by MKP-1 and MKP-3 (296, 297). Thus, the CB₂ receptor activated by O-1966 administration could be preventing downstream signaling from the μ receptor, Figure 44. Further, activation of the CB₂ receptor was shown to attenuate the production of inflammatory cytokines in chronic morphine therapy (215, 298). Overall activity at the CB₂ receptor was shown to reduce inflammatory cytokine production in

microglial overall (16, 28, 29). Our studies here confirmed this effect by showing a statistically significant reduction in IL-1 β mRNA by O-1966 treatment, Figure 39. CB₂ treatment also tended to decrease IL-6 mRNA production compared to the Cremophor/Morphine-100 mg/kg group but this did not reach statistical significance, Figure 39. We speculate that this reduction in IL-1 β mRNA indicates an overall reduction in protein expression. Decreased protein expression of IL-1 β would help to preclude the development of tolerance since less cytokine would be present to prime microglial cells and also oppose the actions of morphine (54, 210, 298).

However, if the O-1966 was administered prior to the morphine, then the tolerance increased to a 6.56 fold increase. Two possible explanations exist for this finding. First of all, activation of the CB₂ receptor and subsequent activity of MKP-1 or MKP-3 could have prevented downstream signaling of the μ receptor through the akt-ERK pathway (28, 296-298). This could have effectively blocked the downstream activity of the μ receptor. Secondly, Figure 39 shows the results of in vitro GTP γ S binding studies that reveal that O-1966 exists possibly as a non-competitive inhibitor of the μ receptor but certainly as an antagonist as it prevents GTP γ S binding. As increasing doses of morphine are administered in this study, the morphine is unable to displace binding by O-1966. Initially, this seems counterintuitive. If O-1966 acts as a non-competitive inhibitor to morphine at the μ receptor, then why would tolerance develop at all? The expected results would be that animals pretreated with O-1966 would never experience the effects of morphine and behave as naïve animals. However, O-1966's binding of the μ receptor as a non-competitive inhibitor and potential allosteric modulator could facilitate downregulation of the μ receptor. This may occur through increased β -arrestin binding, alterations in phosphorylation, and decreased expression of the receptor (299). Whereas, in the reverse order, morphine preceding O-1966, the activity of the μ receptor to initiate its signal transduction and act locally at ion channels

can commence while the inflammation that it normally would cause was diminished by the CB₂ activation (28, 67, 187, 188, 297, 298).

Lower doses of morphine (32mg/kg) produced lower degrees of tolerance, Figure 37, Table 1. Morphine administered for a week at a dose of 32 mg/kg produced a fold increase of 2.15 compared to 3.92 when 100 mg/kg of morphine was administered. The amount of morphine has been tied to the degree of tolerance that develops (209). O-1966 administered here had little effect and the fold shift was found to be 2.08. It is presumable that some degree of tolerance is unavoidable and that the effects of O-1966 remain best demonstrated in much more severe cases of tolerance. This dose of morphine was also unable to induce a state of hyperalgesia, Figure 38.

With 100 mg/kg of morphine, hyperalgesia developed as the animals' baseline latencies to the hot plate withdrawal tendency decreased after 5 days of morphine administration, Figure 38. Hyperalgesia is defined as a decreased latency and enhanced responsiveness or sensitivity to noxious stimuli (213). The group that received 100 mg/kg of morphine (with Cremophor) was the only group to develop hyperalgesia. Hyperalgesia has been shown to be a result of chronic morphine administration (215, 216). The data here suggest that in fact, high doses of chronic morphine induced hyperalgesia and also that its induction could be blocked with the addition of O-1966. Again, the protective effect of O-1966 arises from its ability to maintain inflammation and reactions in a more quiescent state (54, 206, 298). Our findings of decreased IL-1 β mRNA expression confirm this, Figure 39.

The acute interaction studies further demonstrated that in fact, an interaction between morphine and O-1966 existed, Figure 41, 42, and 43. Figure 41 shows a typical morphine dose response curve. Also of note is the small antinociceptive effect that O-1966 can impart, however, O-1966 never achieves 50% Maximum Percent Effect. This data is also shown in Figure 42 where

morphine demonstrates a linear effect in regards to dose versus Maximum Percent Effect. O-1966 on the other hand shows a more hyperbolic response and an incapability to reach 50% Maximum Percent Effect, Figure 42. The addition of O-1966 to morphine shifts the curve to the right indicating a much higher dose must be utilized to achieve the same level of pain relief, Figure 41. From the projections of morphine and O-1966 in Figure 42, and according to the Theory of Dose Equivalence, expected levels of interaction can be predicted (293). Table 2 illustrates these predictions.

Table 2, Additive and Observed Effects of Morphine and O-1966

Doses: O-1966 and Morphine	Effect Additive	Effect Observed
1.25 + 5.5	25.1	9.8
2.5 + 10.0	47.4	17.2
5.0 + 22.0	88.1	18.2
10.0 + 44.0	100.0	70.4
20.0 + 88.0	100.0	78.0
40.0 + 176.0	100.0	100.0

Of note is the fact that except at the highest dose, the Effect Observed is always much lower than the Effect Additive. This trend was statistically significant. It also shows that the combination of O-1966 and morphine produces a combination that is sub-additive in its analgesic potential (293). Thus, combining O-1966 with morphine decreases the effect of morphine and seems to antagonize its activity in a sub-additive fashion.

The GTP γ S binding studies indicated that O-1966 potentially acts as a noncompetitive inhibitor at the μ opioid receptor, Figure 39. The results suggest that it does antagonize the effects of morphine and prevents binding of GTP γ S. Increasing doses of morphine was unable to increase Percent Saturation in the presence of O-1966. A competitive inhibitor would have shifted the

curve to the right but this effect was not observed, Figure 39. The fact that O-1966 acts as a non-competitive inhibitor seems to suggest that it might allosterically modulate the receptor or may just occupy the binding site.

Interestingly, the addition of SR144528 to the mix of morphine and O-1966 was able to nearly restore the efficacy of morphine in its antinociceptive qualities, Figure 41. In such a situation, two possible explanations can be proposed. The more simplistic explanation is that SR144528 and O-1966 bind at the same location on the μ opioid receptor. SR144528 binds with greater affinity than O-1966 but is unable to induce the same degree of allosteric modulation that O-1966 imposes. Secondly, the interactions of all 3 drugs on intracellular signal transduction could also be in play. The μ opioid receptor activates akt-ERK 1/2 and this signal is opposed by the CB₂ receptor's activation of MKP-1 and MKP-3 (28, 54, 296-298). SR144528 is an inverse agonist at the CB₂ receptor and has been shown to reverse basal activity of the receptor (5, 32, 68). This reversal could contribute to the restoration of akt-ERK 1/2 signaling and improved nociceptive signaling. Figure 42, pictorially demonstrates the effect of the 3 drugs. Each combination was fit to a linear representation of the log of the morphine dose compared to the Percent Effect. The line farthest to the left shows the results of morphine alone with greater Percent Effect through lower doses. The addition of only O-1966 shifts this line to the right indicating higher doses to achieve the same results must be utilized. However, SR144528 can reverse the effect and the line representing this combination nearly returns the same line as the morphine alone.

As previously stated the order of administration of drugs also had importance in the acute studies conducted. Figure 43 illustrates the typical antinociceptive response of morphine. This produced an ED₅₀ of 11 mg/kg. When O-1966 was given 15 minutes prior to morphine the ED₅₀

was 43.7 mg/kg and the curve shifted significantly to the right. As before, the rightward shift indicates that much higher doses of morphine were required to achieve the same antinociceptive effects. Previously, the idea that O-1966 acts potentially as a non-competitive inhibitor of morphine at the μ receptor had been advanced and confirmed through the GTP γ S binding studies Figure 39. Obviously, the injection of O-1966 prior to injecting morphine would create an antagonistic effect since it is a non-competitive inhibitor. More so, it has also been shown that CB₂ activation can block signal transduction from the μ receptor through an MKP-1/3, akt-ERK 1/2 dependent manner (28, 54, 297, 298).

This shift could be attenuated and an increase in ED₅₀ could be limited to only 20 mg/kg if morphine was injected and then 15 minutes later O-1966 was injected, Figure 42. In this scenario, the μ receptor could be activated prior to the antagonistic effect of O-1966 binding it. Additionally, signal transduction through the μ receptor could precede without the competing effects of the CB₂ receptor dephosphorylating akt-ERK 1/2 signaling (28, 54, 296-298). A slight shift occurs and may be the result of O-1996 lingering between injections with some potential to still act as an antagonist. O-1966 is also known to be lipophilic and may deposit into adipose tissue to be released at a later time point and therefore inhibit later morphine injections.

The studies here have revealed some interesting and unexpected findings with regard to O-1966 and morphine treatment. In cases of chronic morphine administration, if morphine were to be administered prior to O-1966, the degree of tolerance could be attenuated from a 3.92 fold increase to a mere 2.28 fold increase, Figure 37, Table 1. However, injections of O-1966 first exacerbated the tolerance effect and generated a 6.56 fold increase, Figure 37. O-1966 was also shown to prevent hyperalgesia and decrease the expression of IL-1 β mRNA, Figure 38 and 39. In acute studies, O-1966 antagonizes the effects of morphine but the antagonism can be reversed with

a CB₂ antagonist, Figure 40. The order of injection is also important as application of O-1966 first tends to necessitate the administration of higher doses of morphine for effective antinociception but could be circumvented if morphine was administered initially.

Thus, while we had an initial hypothesis that the application of O-1966 to a chronic morphine regimen would prevent inflammation and decrease tolerance, the findings that O-1966 could also block the effects of morphine were completely unexpected and novel to us. We were correct in the ability of the drug to limit inflammation, tolerance, and hyperalgesia and discovered an exceedingly important aspect in the order in which the drugs were to be applied.

4.6 Conclusion

The results here are exciting and present the potential for a number of clinical therapeutic interventions in several disease states. Unfortunately, the studies and conclusions here are not without some inherent shortcomings. The GTP γ S binding studies have presented convincing evidence that O-1966 acts as an antagonist and inhibitor at the μ receptor, Figure 40. However, the binding studies were conducted in cultured cell lines which maybe behave very differently than cells *in vivo*. Secondly, the idea that CB₂ receptor activation initiates a signal transduction cascade, possibly MKP-1 or MKP-3, that opposes the action of μ receptor signal transduction through akt-ERK 1/2 has been presented as a possible explanation and confirmed by other researchers (28, 54, 296-298). Unfortunately, we have not investigated this phenomenon ourselves and the use of western blots to detect differences in phosphorylation patterns makes a logical next step in unraveling the interactions between the two drugs.

Shortcomings aside, this work has presented the opportunity for advancing clinical and translational medicine on a number of fronts. In the described experiments we studied the effect

of O-1966 on limiting tolerance to morphine and preventing hyperalgesia through a reduction in inflammatory cytokines. If given after the injection of morphine, O-1966 was effective in these endeavors. In patients with chronic neuropathic pain, presently 66% are receiving little to no pain relief from current medication strategies (185). With the population aging, the number of patients suffering from chronic pain is expected to rise and new strategies must be employed to combat the affliction and improve the quality of life for these patients.

More so, at the onset of the experiment we had no suspicion that O-1966 would non-competitively bind and antagonize μ receptors. Since it does, we propose that O-1966 has the potential to be used as an adjunct pharmacological agent in treating patients with opioid addiction. Opioid addiction continues to present clinical challenges and current therapies are limited (300). Worldwide it is estimated that there are at least 5 million users of opioid based compounds for either medicinal or illicit use (301). Investigation into the use of O-1966 in decreasing cravings and rewarding effects of opioids should be explored more thoroughly.

4.7 Works Cited

1. Fischer BD, Ward SJ, Henry FE, Dykstra LA. Attenuation of morphine antinociceptive tolerance by a CB(1) receptor agonist and an NMDA receptor antagonist: Interactive effects. *Neuropharmacology*. 2010;58(2):544-50.
2. Ibrahim MM, Rude ML, Stagg NJ, Mata HP, Lai J, Vanderah TW, et al. CB2 cannabinoid receptor mediation of antinociception. *Pain*. 2006;122(1-2):36-42.
3. Adhikary S, Kocieda VP, Yen JH, Tuma RF, Ganea D. Signaling through cannabinoid receptor 2 suppresses murine dendritic cell migration by inhibiting matrix metalloproteinase 9 expression. *Blood*. 2012;120(18):3741-9.
4. Chomczynski P, Sacchi N. The single-step method of RNA isolation by acid guanidinium thiocyanate-phenol-chloroform extraction: twenty-something years on. *Nat Protoc*. 2006;1(2):581-5.
5. Tallarida RJ, Raffa RB. The application of drug dose equivalence in the quantitative analysis of receptor occupation and drug combinations. *Pharmacol Ther*. 2010;127(2):165-74.
6. Ballantyne JC, LaForge KS. Opioid dependence and addiction during opioid treatment of chronic pain. *Pain*. 2007;129(3):235-55.
7. Hutchinson MR, Bland ST, Johnson KW, Rice KC, Maier SF, Watkins LR. Opioid-induced glial activation: mechanisms of activation and implications for opioid analgesia, dependence, and reward. *ScientificWorldJournal*. 2007;7:98-111.
8. Watkins LR, Milligan ED, Maier SF. Glial activation: a driving force for pathological pain. *Trends Neurosci*. 2001;24(8):450-5.
9. Kiss L, Walter FR, Bocsik A, Veszelka S, Ozsvári B, Puskás LG, et al. Kinetic analysis of the toxicity of pharmaceutical excipients cremophor EL and RH40 on endothelial and epithelial cells. *J Pharm Sci*. 2013;102(4):1173-81.
10. Raghavendra V, Rutkowski MD, DeLeo JA. The role of spinal neuroimmune activation in morphine tolerance/hyperalgesia in neuropathic and sham-operated rats. *J Neurosci*. 2002;22(22):9980-9.

11. Raghavendra V, Tanga FY, DeLeo JA. Attenuation of morphine tolerance, withdrawal-induced hyperalgesia, and associated spinal inflammatory immune responses by propentofylline in rats. *Neuropsychopharmacology*. 2004;29(2):327-34.
12. Hutchinson MR, Coats BD, Lewis SS, Zhang Y, Sprunger DB, Rezvani N, et al. Proinflammatory cytokines oppose opioid-induced acute and chronic analgesia. *Brain Behav Immun*. 2008;22(8):1178-89.
13. Song P, Zhao ZQ. The involvement of glial cells in the development of morphine tolerance. *Neurosci Res*. 2001;39(3):281-6.
14. Milligan ED, Watkins LR. Pathological and protective roles of glia in chronic pain. *Nat Rev Neurosci*. 2009;10(1):23-36.
15. Eljaschewitsch E, Witting A, Mawrin C, Lee T, Schmidt PM, Wolf S, et al. The endocannabinoid anandamide protects neurons during CNS inflammation by induction of MKP-1 in microglial cells. *Neuron*. 2006;49(1):67-79.
16. Rivest S. Cannabinoids in microglia: a new trick for immune surveillance and neuroprotection. *Neuron*. 2006;49(1):4-8.
17. Romero-Sandoval EA, Horvath R, Landry RP, DeLeo JA. Cannabinoid receptor type 2 activation induces a microglial anti-inflammatory phenotype and reduces migration via MKP induction and ERK dephosphorylation. *Mol Pain*. 2009;5:25.
18. Cussac D, Rauly-Lestienne I, Heusler P, Finana F, Cathala C, Bernois S, et al. μ -opioid and 5-HT1A receptors heterodimerize and show signalling crosstalk via G protein and MAP-kinase pathways. *Cell Signal*. 2012;24(8):1648-57.
19. Tumati S, Largent-Milnes TM, Keresztes A, Ren J, Roeske WR, Vanderah TW, et al. Repeated morphine treatment-mediated hyperalgesia, allodynia and spinal glial activation are blocked by co-administration of a selective cannabinoid receptor type-2 agonist. *J Neuroimmunol*. 2012;244(1-2):23-31.
20. Merighi S, Gessi S, Varani K, Fazzi D, Mirandola P, Borea PA. Cannabinoid CB(2) receptor attenuates morphine-induced inflammatory responses in activated microglial cells. *Br J Pharmacol*. 2012;166(8):2371-85.

21. Färber K, Kettenmann H. Physiology of microglial cells. *Brain Res Brain Res Rev.* 2005;48(2):133-43.
22. Merighi S, Gessi S, Varani K, Simioni C, Fazzi D, Mirandola P, et al. Cannabinoid CB(2) receptors modulate ERK-1/2 kinase signalling and NO release in microglial cells stimulated with bacterial lipopolysaccharide. *Br J Pharmacol.* 2012;165(6):1773-88.
23. Williams JT, Ingram SL, Henderson G, Chavkin C, von Zastrow M, Schulz S, et al. Regulation of μ -opioid receptors: desensitization, phosphorylation, internalization, and tolerance. *Pharmacol Rev.* 2013;65(1):223-54.
24. Katzung BG. Basic & clinical pharmacology. 9th ed. New York: Lange Medical Books/McGraw Hill; 2004. xiv, 1202 p. p.
25. Dhawan BN, Cesselin F, Raghbir R, Reisine T, Bradley PB, Portoghese PS, et al. International Union of Pharmacology. XII. Classification of opioid receptors. *Pharmacol Rev.* 1996;48(4):567-92.
26. Viganò D, Rubino T, Parolaro D. Molecular and cellular basis of cannabinoid and opioid interactions. *Pharmacol Biochem Behav.* 2005;81(2):360-8.
27. Ashton JC, Glass M. The cannabinoid CB2 receptor as a target for inflammation-dependent neurodegeneration. *Curr Neuropharmacol.* 2007;5(2):73-80.
28. Abood ME. Molecular biology of cannabinoid receptors. *Handb Exp Pharmacol.* 2005(168):81-115.
29. Bouaboula M, Desnoyer N, Carayon P, Combes T, Casellas P. Gi protein modulation induced by a selective inverse agonist for the peripheral cannabinoid receptor CB2: implication for intracellular signalization cross-regulation. *Mol Pharmacol.* 1999;55(3):473-80.
30. Bouaboula M, Dussossoy D, Casellas P. Regulation of peripheral cannabinoid receptor CB2 phosphorylation by the inverse agonist SR 144528. Implications for receptor biological responses. *J Biol Chem.* 1999;274(29):20397-405.
31. Sindrup SH, Jensen TS. Efficacy of pharmacological treatments of neuropathic pain: an update and effect related to mechanism of drug action. *Pain.* 1999;83(3):389-400.

32. Ali R, Meena S, Eastwood B, Richards I, Marsden J. Ultra-rapid screening for substance-use disorders: The Alcohol, Smoking and Substance Involvement Screening Test (ASSIST-Lite). *Drug Alcohol Depend.* 2013.
33. Rahimi-Movaghar A, Amin-Esmaeili M, Hefazi M, Yousefi-Nooraie R. Pharmacological therapies for maintenance treatments of opium dependence. *Cochrane Database Syst Rev.* 2013;1:CD007775.

4.8 Figures

Figure 36, Experimental Design for Chronic Morphine Administration

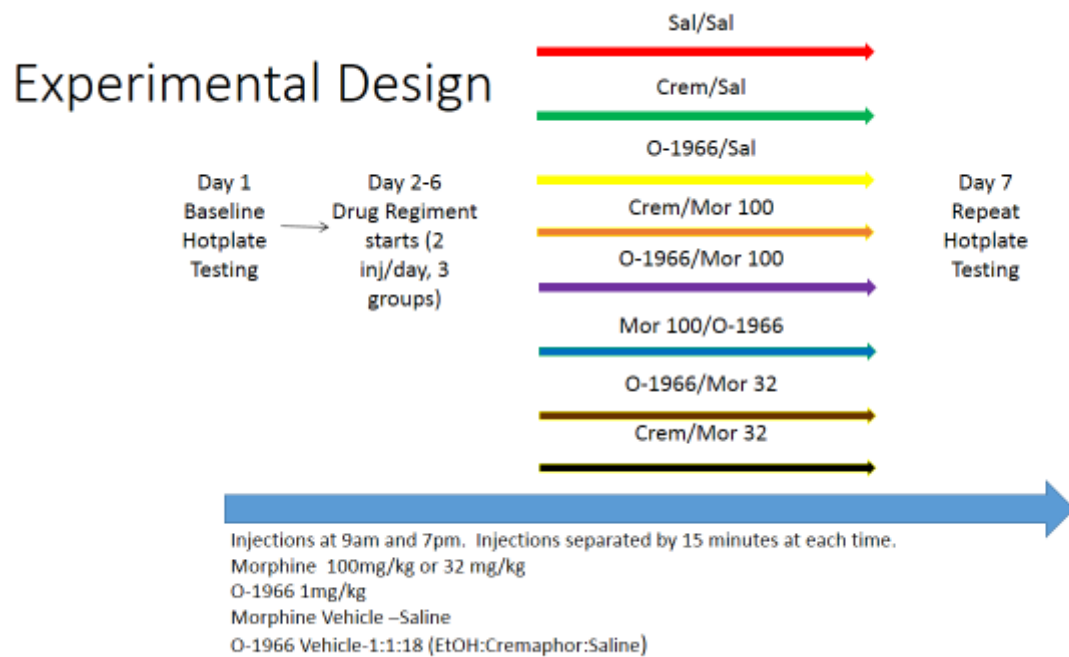


Figure 36. Pictorial representation of experimental design and parameters of chronic morphine studies.

Figure 37, Dose Response Curves From Chronic Morphine Studies

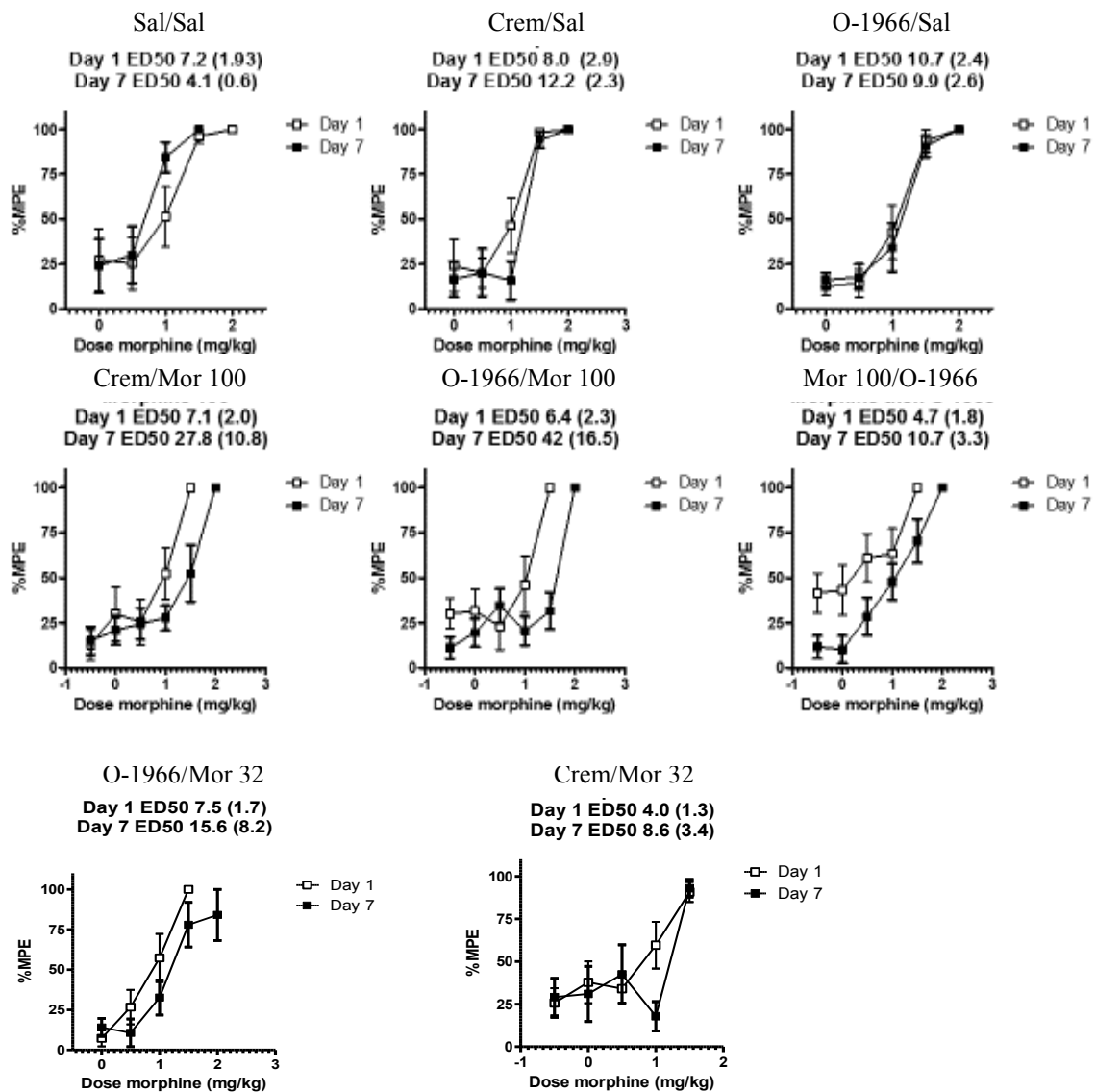


Figure 37, Dose Response Curves from Chronic Morphine Administration Studies. Open Squares—Day 1. Closed Squares—Day 7. ED₅₀ listed with SEM in parenthesis. n = 6-8 animals per group.

Figure 38, Hyperalgesia From Chronic Morphine Administration

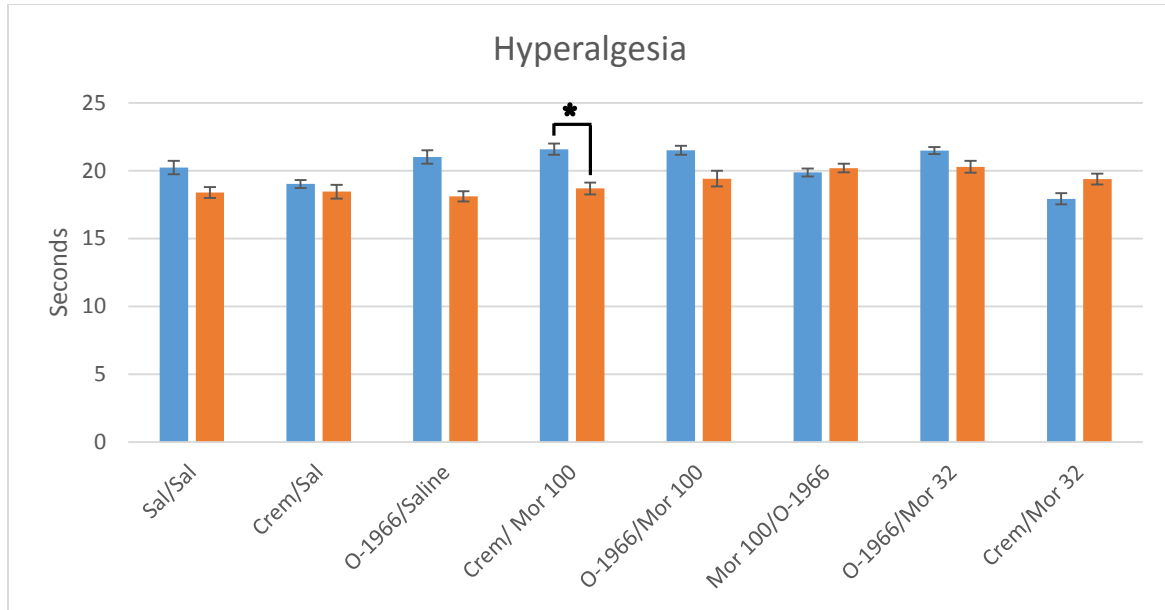


Figure 38, Hyperalgesia From Chronic Morphine Administration. Left bars—Day 1. Right bars—Day 6. Data expressed as mean \pm SEM. $p < 0.05$. $n = 6 - 8$ animals per group.

Figure 39, Molecular Analysis of Chronic Morphine Administration

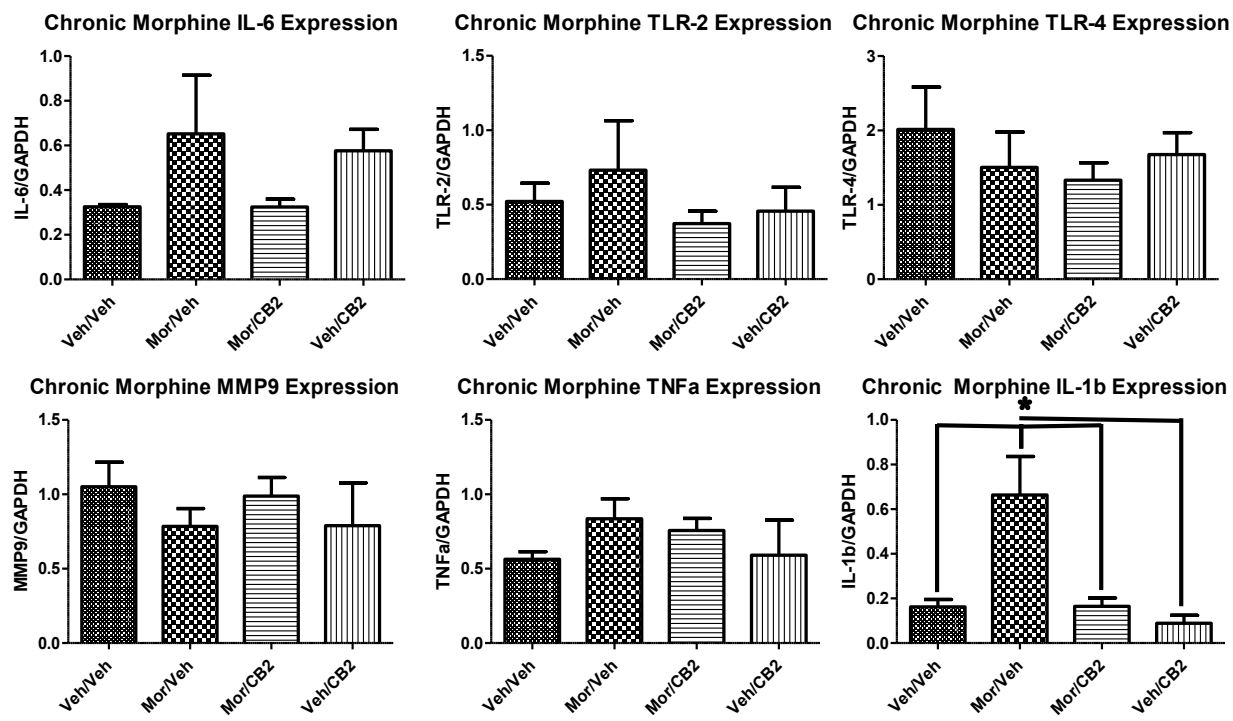


Figure 39, Molecular Analysis of Chronic Morphine Administration. mRNA expression is shown as level of the gene of interest normalized to GAPDH. Displayed as mean \pm SEM. $p < 0.05$. Samples are pooled from 3 mice ($n = 3$).

Figure 40, GTP γ S Binding Study

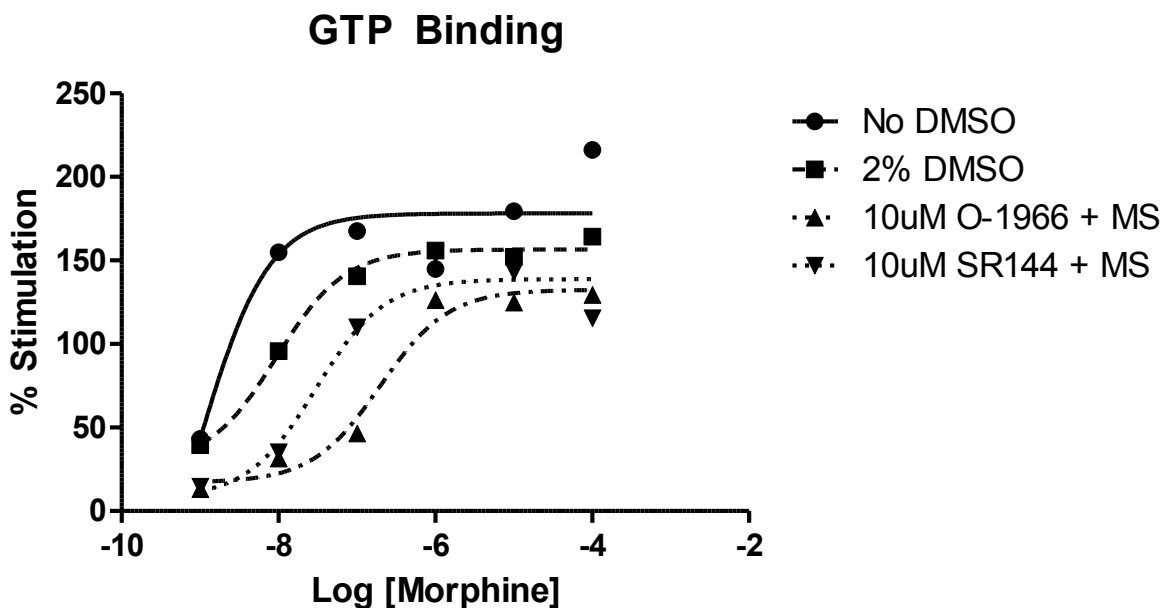


Figure 40, GTP γ S Binding Study. 5 μ g membrane protein. 10 μ g GDP. Incubation at 30°C for 1 hour. O-1966 in the presence of morphine acts as a noncompetitive inhibitor (upward pointing triangles). Regardless of the dose of morphine, it is unable to displace O-1966 and achieve the same percent saturation as morphine alone (squares). SR144528 restores some of the morphine stimulation (downward pointing triangles). Study conducted by Kelly DiMattio from the laboratory of Lee-Yuan Liu-Chen.

Figure 41, Acute Interaction of Morphine and O-1966

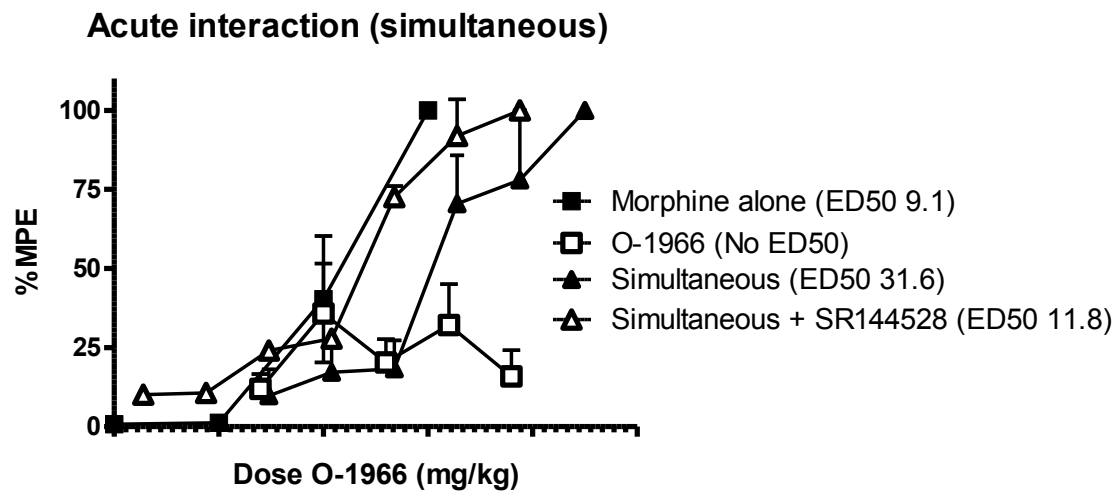


Figure 41, Acute Interactions of Morphine and O-1966. The combination of the two drugs shifts the dose response curve to the right indicating higher doses are needed to achieve the same level of antinociception compared to morphine alone (Closed Triangles versus Closed Squares). SR144528 (Open Triangles) restores the efficacy of morphine. Results displayed as Maximal Percent Effect (MPE) \pm SEM. n = 6-8 mice per group.

Figure 42, Dose Equivalence Theory

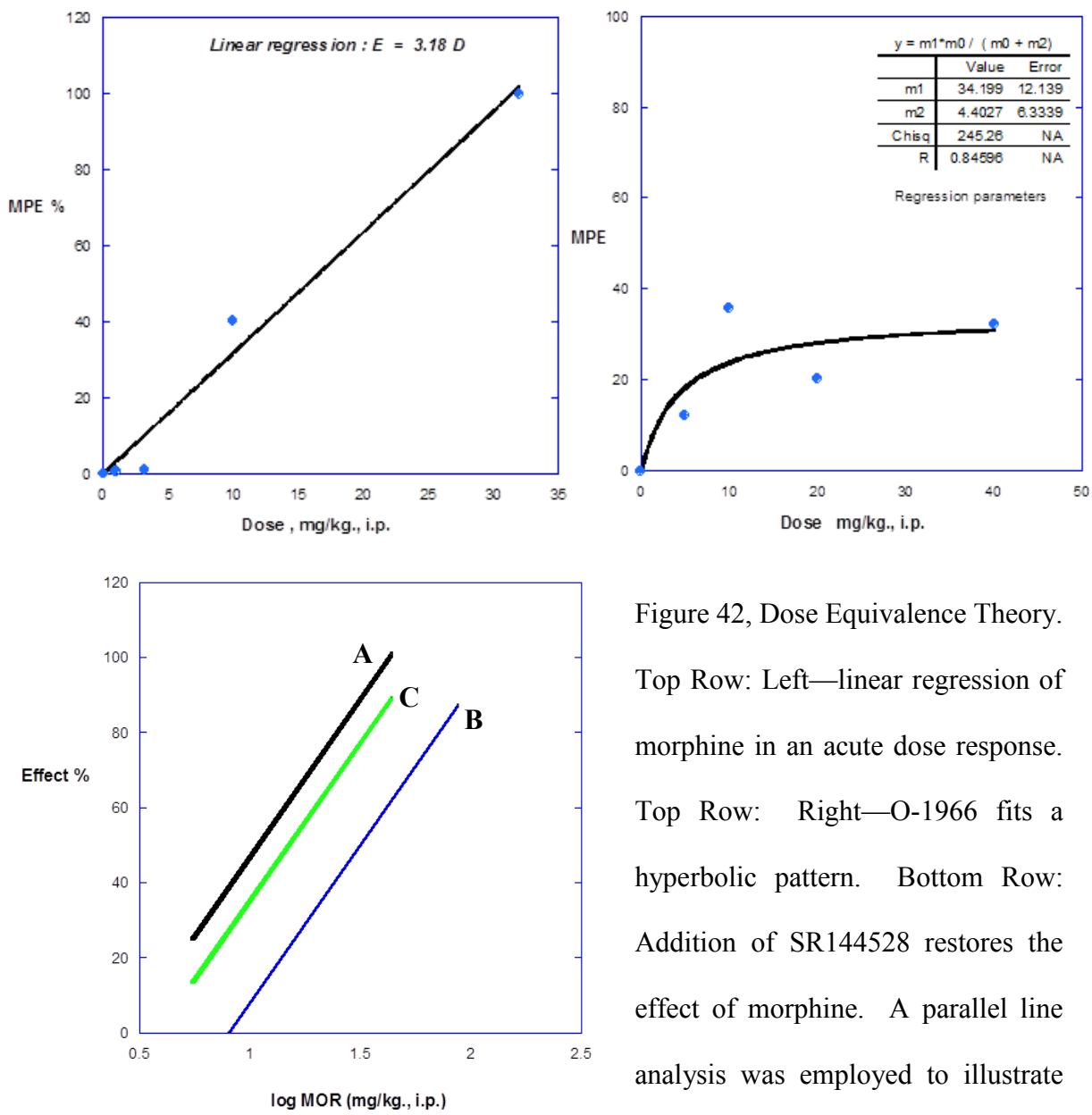


Figure 42, Dose Equivalence Theory.

Top Row: Left—linear regression of morphine in an acute dose response. Top Row: Right—O-1966 fits a hyperbolic pattern. Bottom Row: Addition of SR144528 restores the effect of morphine. A parallel line analysis was employed to illustrate the effect. Line A—morphine, Line B—morphine with O-1966, Line C—morphine, O-1966, SR144528.

Prepared by Dr. Ronald Tallarida.

Figure 43, Acute Morphine and O-1966 Interactions Depends on the Order of Administration

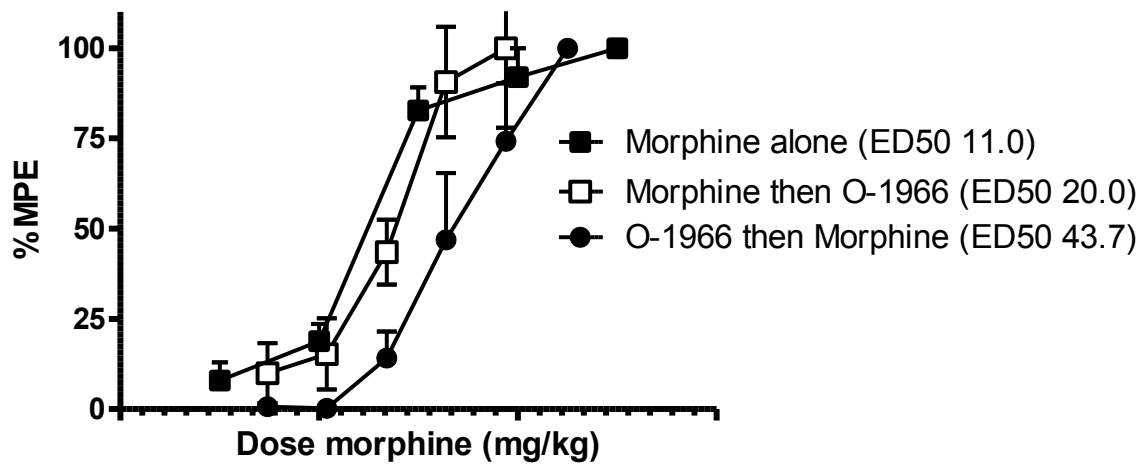


Figure 43. A typical morphine dose response curve (closed squares) compared to administration of O-1966 15 minutes prior to morphine injections (closed circles). The shift to the right implies that higher doses of morphine are required to achieve the same effects. However, morphine injected first, and O-1966 15 minutes later, has a much smaller effect on this shift (open squares). Results shown as Mean Maximal Percent Effect (MPE) \pm SEM. n = 6 – 8 mice per group. ED₅₀ in parenthesis.

Figure 44, Proposed Signaling Pathway

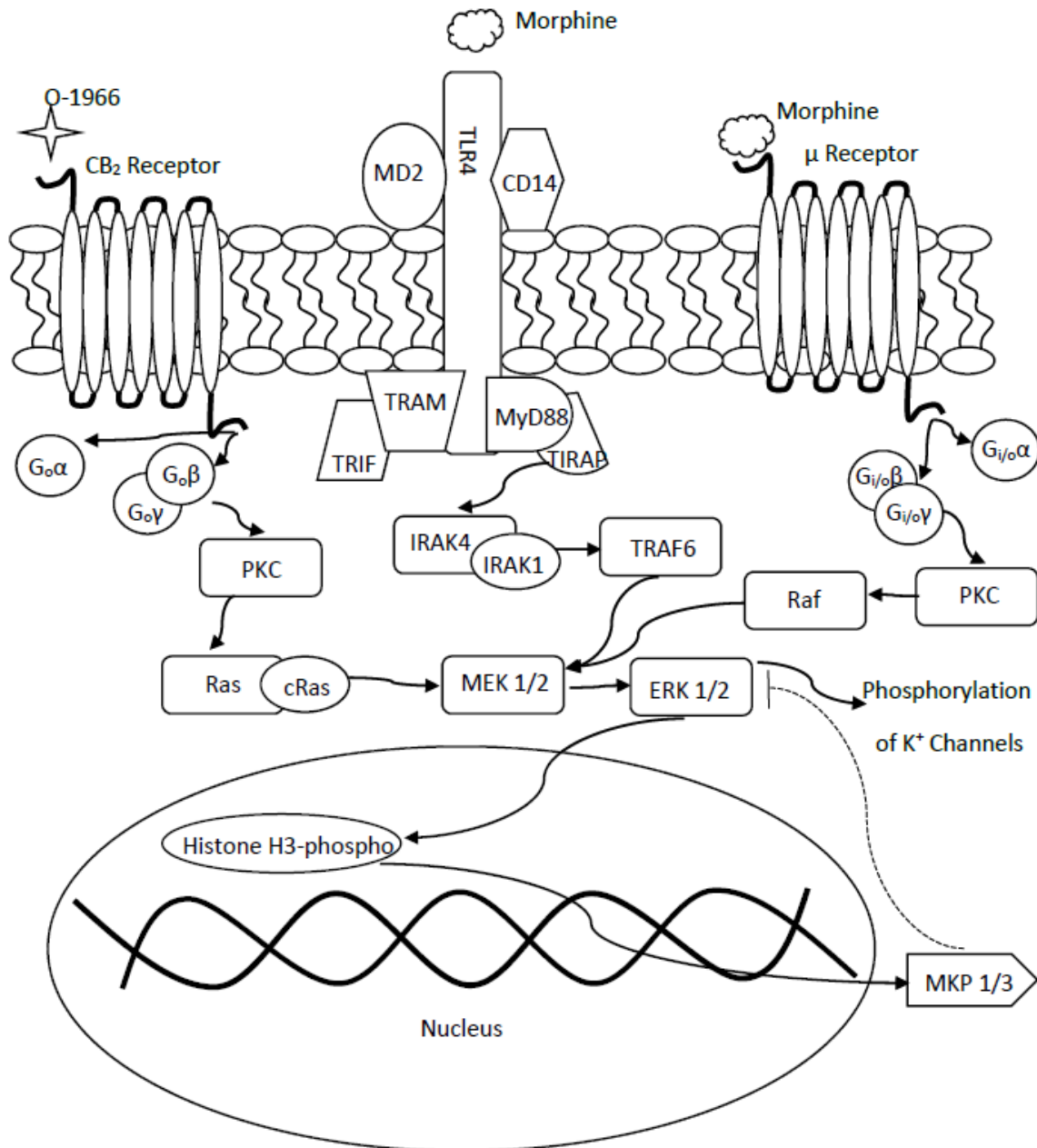


Figure 44, Proposed Signaling Pathway. Activation of CB₂ receptor causes phosphorylation of Histone H3 ultimately causing the production of MKP 1 or 3. MKP 1/3 have been shown to dephosphorylate ERK 1/2. ERK 1/2 may also be activated by CB₂ receptors and may exist as a built in feedback loop. Morphine binding of the μ opioid receptor also activates ERK 1/2. MKP

1/3's dephosphorylation of ERK 1/2 by CB₂ activation may account for the competing and antagonistic effects of O-1966 in the presence of morphine. More so, MKP 1/3 can stop activation of TLR-4 which may undergo activation by morphine. All 3 receptors are present on microglial cells. A small number of recent publications suggest that CB₂ receptors may be found on some neurons.

CHAPTER 5

CONCLUSIONS

5.1 Conclusions

The research at hand set out to accomplish several specific aims amidst the underlying theme that the endogenous cannabinoid system could be modulated to attenuate inflammation in central nervous system injury. By looking at two common pathologies of the central nervous system it became clear how this could be achieved. In addition, to facilitate the progress of the research, work was done to develop and advance two models utilized in the study of central nervous system injury.

First of all, the method of application of Rhodamine 6G was examined by comparing the efficacy of intraperitoneal injection to the traditional intravenous injection. As a corollary, the *in vivo* properties of Rhodamine 6G were examined in terms of visual characteristics over the course of eight hours. Over the course of eight hours, there was no difference in luma, hue, saturation, lightness, value, or intensity in examination of peripheral blood. Multiple parameters however, required three hours to reach a maximal effect if Rhodamine 6G was given intraperitoneally. This demonstrated the time necessary for maximal diffusion to occur. Examination of linear regressions from three hours to eight hours showed the same rate of degradation of the signal in both groups. Visualization through the cranial window also showed no statistically significant difference in luma. Quantification of rolling and adhesion revealed statistically significant difference at two time points but as explained in the preceding chapters, this was most likely the result of artifact.

To garner a very precise picture of what was happening in the two injection methods, flow cytometry was employed. When equal amounts of Rhodamine 6G were injected, there was no statistically significant difference in the overall percentage of stained leukocytes. However, the

fluorescent and geometric means were lower in the intraperitoneal group. This was attributed to a lower rhodamine/cell ratio. Analysis of agranulocytes and granulocytes separately demonstrated the same findings. In contrast, when the amount of Rhodamine 6G injected into the peritoneal cavity was increased, all the differences were avoided. In short, to avoid complications resulting from intravenous injections and ensure delivery of the dye, intraperitoneal application of Rhodamine 6G should be considered as an alternative in experimental design.

Intravital microscopy was also utilized to examine and gain a much better understanding of the stroke occurring in the photothrombotic model of cerebral ischemia. Cranial windows were implanted and the bone flap preserved. The bone flap was later laid back in place and the stroke carried out with Rose Bengal as traditionally performed. After about one hour of the onset of ischemia, the cranial window was visualized. Approximately 86% of the time, there was no flow in the vessels examined. From these findings, we concluded that the photothrombotic stroke existed as a permanent occlusion model of cerebral ischemia. This information would later be employed in conjunction with other stroke studies.

The role of the endogenous cannabinoid system was also examined in cerebral ischemia with a transient ischemia following by reperfusion. However, these studies were carried out in CB₁ -/- CB₂ -/- receptor mice. Based on previous studies, we hypothesized that the injury in these mice would be much more severe. To our surprise, stroke volume and infarct fraction were slightly smaller, although not statistically significant, but certainly not worse. Double knockout mice also had much improved neurological scores demonstrating an ameliorated injury to the brain. Also of interest was the CB₁ -/- CB₂ -/- receptor mice's ability to maintain more regional cerebral blood flow during the period of ischemia. They maintained approximately 10% greater blood flow during the period of ischemia. We attribute this increased flow to the results in stroke size and

neurological function. Multiple reasons as to why CB₁ -/- CB₂ -/- receptor mice demonstrate increased flow have been discussed in Chapter 3 but the findings here underscore the role and importance of the endogenous cannabinoid system in an inflammatory injury like cerebral ischemia and reperfusion.

The photothrombotic stroke was also carried out with an emphasis on flow. Previously, blockade of the CB₁ receptor was shown to be protective and decrease infarct fraction and stroke volume when administered either before or after the onset of cerebral ischemia. However, if administered prior to ischemia, antagonism of the 5HT_{1A} receptor would dissipate this protective effect. In the studies performed here, we confirmed the efficacy of CB₁ antagonism, either pre or post treated, in cerebral ischemia. However, in the pretreatment groups, the 5HT_{1A} receptor was not needed to maintain the protective effect. We concluded that in the photothrombotic stroke, flow was not a factor whereas in the transient strokes it was and thus underscored the importance of the 5HT_{1A} receptor. The protective effect of CB₁ antagonism in photothrombotic stroke most likely arises from enhanced GABA signaling attenuating excitotoxicity and inflammation. Although the connection between ischemia, GABA, and cannabinoids has not yet been clearly established, it yields an enticing avenue for further studies.

The last area of research delved into the inflammation in the central nervous system associated with chronic morphine therapy. Chronic application of morphine generates inflammatory cytokines that leads to tolerance and hyperalgesia ultimately necessitating the need for higher doses of morphine. When a highly selective CB₂ agonist, O-1966, was applied with morphine chronically, the results depended on the order of administration. When the CB₂ agonist was administered first it exacerbated tolerance, however, if morphine was injected and then the

CB₂ agonist, tolerance was roughly cut in half. It also decreased expression of the inflammatory cytokine IL-1 β mRNA and prevented the induction of hyperalgesia.

To fully understand what was occurring, the acute interactions of the drugs was studied as well as GTP γ S binding. GTP γ S binding revealed that O-1966 acted as a non-competitive inhibitor of morphine. Consequently, when administered at the same time as morphine, it antagonized the effect and shifted the dose response curves to the right. The effect could be overcome with a selective CB₂ antagonist. Like in the chronic studies, if morphine was given first, then the CB₂ agonist, there was little effect in the dose response curve of acute studies. The methods in which CB₂ may attenuate tolerance and inflammation as well as interact with the morphine receptor have been reviewed and explored in Chapter 4. Briefly, allosteric modulation of the μ opioid receptor, non-competitive inhibition, or competing intracellular signaling cascades may both contribute to the observed phenomena here.

In summary, both cerebral ischemia and chronic administration of morphine, such as would be used to treat chronic pain, exist as pathologies with inflammatory components intimately tied to their progression and development. The endogenous cannabinoid system plays a role in both disorders. CB₁ -/- CB₂ -/- receptor mice were able to maintain enhanced flow during cerebral ischemia while in photochemical strokes, antagonism of the CB₁ receptor was protective and independent of the actions of the 5HT_{A1} receptor. Use of a CB₂ agonist in chronic morphine therapy also attenuated inflammation and helped reduce the tolerance that developed but only if administered after the morphine injection. Acutely, the CB₂ agonist employed, O-1966, antagonizes the effect of morphine but has revealed an interesting interaction between the two signaling systems.

Unfortunately, we were not able to answer all of the questions that arose from these findings. However, we have shown that in these inflammatory conditions the endogenous cannabinoid system could be utilized to reduce inflammation and preserve function while precluding the progression of the pathology. Much more work needs to be performed to completely understand the meaning of the findings here and to further elucidate the mechanisms in play. The endogenous cannabinoid system has the ability to modulate inflammatory response particularly in central nervous system disorders and the next several years will deliver many exciting results based on this idea. A foundation of understanding exists but the mechanisms need to be fully unraveled. The French novelist Marcel Proust highlighted this notion when he stated, “The voyage of discovery is not in seeking new landscapes but seeing with new eyes”. Surely, new eyes will help to further interpret the mechanisms of the endogenous cannabinoid system so that new therapies can be put into clinical practice and help patients suffering from these horrid afflictions.